Study of Aerosols Characteristics over Central Himalayas

Thesis Submitted for the Degree of

Doctor of Philosophy

In

Physics

T*o*

Kumaun University, Nainital (India)

By

Hema Joshi

Aryabhatta Research Institute of Observational Sciences (ARIES)

Manora Peak, Nainital, 263002, Uttarakhand, India

July 2015

DECLARATION

I hereby declare that the work presented in this thesis is a result of investigation carried out by me at Aryabhatta Research Institute of Observational Sciences (ARIES), Nainital, under the joint supervision of Dr. Manish Naja (ARIES, Nainital) and Prof. H.C. Chandola (Department of Physics, Kumaun University, Nainital). This thesis work is the original work carried out by me and has not been submitted for any award of degree, diploma, associateship or fellowship of any other University or Institute anywhere.

Hema Joshi

Place: Nainital

Date: July 2015

(Hema Joshi)

CERTIFICATE FROM SUPERVISORS

This is to certify that

1. The synopsis of the present thesis entitled "Study of aerosols characteristics over central Himalayas" for the award of the degree of Doctor of Philosophy in Physics has duly been approved by the Kumaun University, Nainital (Letter No. Shodh/Physics/2011, Dated 12-11-2011)
2. The thesis embodies the work of Ms. Hema Joshi herself.
3. Ms. Hema Joshi has worked under our joint supervisions for this thesis as a Research Scholar at the Aryabhatta Research Institute of Observational Sciences (ARIES), Nainital. She has put more than 200 days of attendance at ARIES, Nainital during this period.
4. The thesis has not been submitted anywhere before for award of any degree, diploma, associateship or fellowship of any University or Institute.

10.7.2015

Dr. Manish Naja,

ARIES,

Manora Peak, Nainital

Dr. Manish Naja (Scientist)
Project Manager, ST Radar
ARIES, Manora Peak
Nainital

10/7/15

Prof. H.C. Chandola,

Department of Physics,

Kumaun University, Nainital

Prof. H.C.Chandola
Department of Physics
D S B. Campus
Kumaun University
Nainital-263002

Forwarded

14/7/15

Head & Convener

RDC, Physics Department

Kumaun University, Nainital

Head & Convener
BOS & DC Physics
Kumaun Univ
NAINITAL (U.K.)

Dedicated to

Late Dr. P. Pant

Acknowledgements

I express my sincere gratitude to Late Dr. P. Pant, for his supervision guidance, interest, and encouragement.

I am sincerely thankful to Dr. Manish Naja for his guidance, constant encouragement and full support during the work which resulted in the present thesis. The guidance and support in research and academic work from Dr. H. C. Chandola from Department of Physics, Kumaun University, Nainital is also highly acknowledge.

I would also like to thanks K. Krishnamoorthy, ISRO Headquaters, Bangalaore and S. Suresh Babu, ISRO-GBP (ARFI) Project Manager, SPL, Trivandrum for their encouragements, help and financial support during the work. Special thanks to Director, ARIES and Director Research, Kumaun University, Nainital to carry this work. Special thanks to Brent Holben and S. N. Tripathi for AERONET data and K. P. Singh for Pantnagar data.

Special thanks to Academic Committee, faculty members, engineers and other staff who directly or indirectly helped me. Support from Computer staff, and Library staff of ARIES is also highly acknowledge. I would like to specially acknowledge Kalpana, Manav, Manjul, Nitin, Deepak for their help in data collection. Additionally, I would also like to thanks Ritesh Gautam, Liji David, Mukunda Gogoi, M. R. Manoj, Sobhan Kompalli,

Anish Kumar Nair, Prijith, Manoj Kumar, Binita Pathak, Naseemsa Beegum for fruitful discussions.

I acknowledge my seniors Rajesh Kumar and Narendra Ojha for their help, support and guidance. I also thanks Tapaswini for her nice company. I would also like to thanks my other seniors, batchmates and juniors at ARIES, Manash, Rupak, Sumana, Himali, Neelam, Chavi, Ram Kesh, Brajesh, Akash, Ravi, Devesh, Haritma, Raman, Piyush, Archana, Krishna, Neha, Abhishek, Subhajeet, Arti, Aditi, Aabha, Praveen, Mukesh, Mridweeka, Navdeep, Ashwini, Pankaj, Vinnet, Kuldeep, Sapna, Piyali, Anjasha, Vidushi, Raya, Ekta. Special thanks to Subhash, Rajiv and Sumit. I also acknowledge Pramod, Madhav, Arya, Ranju, and other friends from SPL. The support received at SPL during my stay is also acknowledge.

Finally, but above all I acknowledge my parents who supported me and trusted me so much. My special thanks to my sister and brother for their wonderful company.

This present work has been carried out under ISRO-GBP (ARFI) project.

Preface

The present thesis entitled “Study of Aerosols characteristics over central Himalayas” deals with investigation carried out by the author under the joint supervision of Dr. Manish Naja at ARIES, Nainital and Prof. H. C. Chandola at Kumaun University, Nainital. In view of the crucial role played by aerosols in climate change, radiation budget, and air quality, this work provides a climatological synthesis of aerosols over the central Himalayas using multiyear measurement of aerosols. Such a synthesis is necessary to assess the background variability of aerosols over this region. Here, aerosol measurements are utilized to understand their variability and trends at a high altitude site (Nainital; 29.4^{o}N, 79.5^{o}E, 1958 m amsl) in the central Himalaya and at a low altitude semi urban site (Pantnagar; 29.0° N, 79.5° E, 231 m amsl) in the Indo-Gangetic Plain region, adjacent to Himalayan foothills. The observed data have been used to evaluate the current state of the science chemical transport model known as the Weather Research and Forecasting Model coupled with Chemistry (WRF-Chem) for black carbon aerosols and complemented by space-borne sensors to explain and discuss the surface, columnar, and vertical distribution of aerosols. The roles of meteorological processes such as boundary layer dynamics, convection, regional and long-range transport along with possible sources of aerosols, their seasonality and processes governing the observed concentration or loading are discussed. The present thesis has been divided into six chapters and are summarized below.

The **Chapter 1** introduces atmospheric aerosols, discusses various processes governing their distributions and presents our current state of understanding about aerosols with a focus on the Indian and the Himalayan region. This is followed by a discussion of gap in our knowledge and motivation for this study. Specifically, we discuss how number of aerosol observation sites has increased rapidly in India over the last couple of decades but are still not sufficient to construct a robust spatial and temporal distribution of aerosols. This work attempts to fill this gap through continuous aerosol observations initiated at a high altitude site, Nainital, in the central Himalayas and a semi-urban site, Pantnagar, in the central Himalayas. The observations presented in this work also become a part of the national database on aerosols under the umbrella of Aerosol Radiative Forcing over India (ARFI) project.

The **Chapter 2** describes the observation techniques, data used, analysis methods and models**.** Specifically, the instruments employed for the observations of black carbon (BC), aerosol optical depth (AOD) and number concentration, rainwater sample and meteorological parameters are described. The details of in situ measurements are followed by a discussion of different satellite based measurements used in this work which include the Moderate Resolution Imaging Spectroradiometer (MODIS), the Multi-angle Imaging Spectroradiometer (MISR) and the Cloud-Aerosol Lidar and Infrared Pathfinder Satellite Observation (CALIPSO). The setup of the WRF-Chem model used for BC simulation is also described in this chapter.

The characteristics of aerosol climatology observed at a high altitude site (Nainital) in the central Himalayas are discussed in **Chapter 3.** Since Nainital is located reasonably far from major anthropogenic sources, the aerosol measurements at this site are supposed to provide information about the background levels of aerosols over the northern Indian region against which the urban impacts can be compared. The seasonal variation of both AOD and BC indicate maximum in spring (March-May) at the site and minimum in AOD is observed in winter (December-February), while minimum in BC is observed in summer-monsoon (June-August) season. The winter season shows very low aerosol loadings over the site indicating the presence of pristine environment over the site most of the time. The aerosol load at the site increases significantly in the spring season and is associated with the influence of dust aerosols during spring and early summer-monsoon.

Climatological seasonal mean AOD (500 nm) is observed to be ~0.117, ~0.298, ~0.216, and ~0.153 in winter, spring, summer-monsoon and autumn (September-November) respectively. The percentage enhancements in seasonal AOD with respect to winter are estimated to be ~155%, ~85%, ~31% in spring, summer-monsoon and autumn respectively. The spectral, diurnal, fine and coarse mode variations in AOD are also examined. Fine model aerosols dominate aerosol loading at Nainital in winter (December-February) while the coarse mode dominates in spring and early summer. The volume size distribution of aerosol shows a large increase of more than

300% in the presence of coarse mode of aerosols during April-June. The comparison of AOD observations with the ground based Aerosol Robotic Network (AERONET) data reveals a strong positive relation (0.96) between the two datasets. The spatial variation of AOD obtained from satellite is also examined.

The diurnal variation, amplitude, evolution and seasonal variations of BC are reported. Diurnal variation of BC shows a single afternoon peak at Nainital. Maximum diurnal amplitude is observed during winter (~1.50 μg m^{-3}), followed by autumn (~0.90 μg m^{-3}) and then spring (~0.72 μg m^{-3}). BC amplitude in the summer-monsoon season is lowest (~0.21 μg m^{-3}) with nearly flat pattern. Average BC level is found to be maximum 1.38±0.75 μg m^{-3} in spring, which decreased to the lowest value of 0.67 ±0.51 μg m^{-3} during summer-monsoon season before increasing again to 0.96±0.62 μg m^{-3} in autumn and 1.05±0.76 μg m^{-3} in the winter season. The enhancement in background BC at Nainital, role of different air masses and source apportionment is also discussed. The aerosol observations at Nainital are also used to estimate radiative forcing due to BC aerosols. The ground based number concentration of aerosol concentration is also examined. An episode of dust storm is identified and its influence at the site is assessed. The rainwater chemistry has also been examined at Nainital and is reported. Long-term trends in aerosol optical depth (AOD) and black carbon (BC) at Nainital are examined for the first time and both AOD and BC both shows increasing tendency.

The first time continuous ground based observations of aerosols initiated at a semi-urban low altitude site (Pantnagar; 29.0^{o}N, 79.5^{o}E, 231 m amsl) in the Indo-Gangetic Region (IGP), adjacent to the central Himalayan foothills are reported in **Chapter 4.** The temporal variations are characterized and the role of meteorology (both mesoscale and synoptic) is delineated. The ground based AOD observations are used in conjunction with the satellite retrieved aerosol index to qualitatively understand whether BC is a dominant component of the total and absorbing aerosol load over Pantnagar. Vertical profiles of aerosol extinction coefficient from CALIPSO are used to examine seasonal variation in vertical distribution of aerosols over Pantnagar. The ability of the WRF-Chem model in simulating the observed variations in BC at Pantnagar is also evaluated.

BC levels at Pantnagar shows two peaks (morning and evening) in diurnal variation, unlike those at Nainital. The diurnal amplitude and variations of BC in winter, autumn and spring are strongly governed by the boundary layer evolution. BC concentration observed in winter, spring, summer-monsoon and autumn are 7.9±5.2 μg m^{-3}, 4.8±3.6 μg m^{-3}, 2.8±2.8 μg m^{-3}, and 6.5±4.9 μg m^{-3}, respectively with the annual mean 5.5±4.7 μg m^{-3}. BC exhibits nearly an inverse relation with the mixing layer depth (MLD) in all seasons with the strongest relation in winter (R^2=0.89) and the weakest (R^2=0.33) in monsoon (July-August). The low MLD in winter and autumn leads to high BC, while high MLD in spring contributes to low BC. The lowest BC in summer-monsoon results from a combination of both higher

MLD and extensive rainfall. Similar to BC, CO also shows anti-correlation with MLD. BC-CO correlation indicates the influence of fresh emissions and common combustion sources mainly in winter and autumn, while the site is influenced by aged air-masses and emissions from different combustion sources in the summer-monsoon season. Unlike BC, co-located aerosol optical depths (AOD) and aerosol absorption are highest in spring over IGP, probably due to the presence of higher abundances of aerosols (including dust) above the ABL (in the free troposphere). AOD (500 nm) showed annual peak (>0.6) in May-June, dominated by coarse mode, while fine mode aerosols dominated in late autumn and early winter.

Aerosol Index retrievals from Ozone Monitoring Instrument (OMI) reveals presence of absorbing aerosols. CALIPSO retrieved aerosol extinction confirms that aerosols are confined near the ground and are highest in winter, similar to surface BC observation. While, aerosol extinction shows least vertical gradient in spring and its levels are maximum at higher heights. Aerosols profiles from CALIPSO show highest values close to the surface in winter/autumn, similar to the feature seen in surface BC, whereas at altitudes > 2 km, the extinction is maximum in spring/summer. The WRF-Chem model is used to simulate BC temporal variations and then compared with observed BC. The model captures most of the important features of the diurnal and seasonal variations but significantly underestimated the observed BC levels, suggesting improvements in diurnal and seasonal varying BC emissions apart from the boundary layer processes.

Average observed and modelled BC at Pantnagar during January, May and July are 6.6±2.2 and 2.4±1.2 μg m^{-3}, 5.5±1.8 and 1.6±0.7 μg m^{-3}, and 2.2±1.0 and 1.2±0.5 μg m^{-3}, respectively. Further work in improving BC emission estimates along with finer temporal and spatial resolution in IGP region is strongly suggested.

The **Chapter 5** focuses mainly on the comparison of aerosol characteristics over different regions and role of different processes. The observations at a high altitude site (Nainital) and a low altitude semi-urban site (Pantnagar) are compared in this chapter. The comparison of aerosol characteristics at these two nearby locations of different environments is also important for model evaluation. Few model studies exist for this region but many of them are not able to accurately capture/distinguish the actual magnitude of the aerosol loading or concentration. Hence, they might not be able to resolve the observe features especially when the complex region of the Himalayas is considered. Ground based observations of BC and AOD at both the sites are compared for diurnal, seasonal and annual variations. Role of the boundary layer dynamics, convection is studied and reasons for enhanced levels of aerosols at Pantnagar are examined.

Aerosol loading and BC levels are quite high at Pantnagar throughout the year as compared to those observed at Nainital. The seasonal variation of BC shows maximum in spring at Nainital while maximum in winter at Pantnagar. The percentage enhancement in the seasonal mean BC is found

to be ~652%, ~248%, ~318%, and ~577% at Pantnagar as compared to those at Nainital in winter, spring, summer-monsoon and autumn, respectively. The simultaneous variations of BC at both the sites are studied and the effect of rainfall scavenging is examined. AOD at both the sites show the highest values in spring, while significant differences in AOD are observed in winter. Columnar loading is minimum and quite low in winter representing nearly clean and nearly free troposphere at Nainital while AOD in winter at Pantnagar is significantly higher, typical to what observed at urban, semi-urban location in the IGP. AOD at both the sites shows significant enhancement in spring, indicating the possibility of aerosol direct influence/transport from low altitude IGP locations to high altitude. The observed surface concentrations and columnar loading at both the sites are examined and explained in context to the vertical distribution of aerosols. Further, it is shown that agricultural crop residue burning in northern India significantly affects the aerosol load, radiation budget in the central Himalayas which has implications for the atmospheric thermodynamics in this region. The summary and conclusion of the thesis along with the future scope are discussed in the **Chapter 6**.

List of Publications

1. **Joshi, H.,** P. Pant, M. Naja, Manav Choudhary and K. P. Singh (2011), Impact of Boundary Layer Dynamics on Black Carbon Variation over the Central Himalaya and its Foothills, *Climate change in the Himalayas*, Editors- Vir Singh et al., ISBN 978-81-7387-228-0, pp. 89-105.

2. Kumar, R., M. Naja, S. K. Satheesh, N. Ojha, **H. Joshi,** T. Sarangi, P. Pant, U. C. Dumka, P. Hegde, and S. Venkataramani (2011), Influences of the springtime northern Indian biomass burning over the central Himalayas, *J. Geophys. Res.*, *116*, D19302, doi:10.1029/2010JD015509.

3. Reddy, K., P. Pant, D. V. Phanikumar, U. C. Dumka, Y. Bhavani Kumar, N. Singh, **H. Joshi** (2011), Radiative effects of elevated aerosol layer in Central Himalayas, *International Journal of Remote Sensing*,Vol. 32, Iss. 24.

4. Srivastava, A. K., K. Ram, P. Pant, P. Hegde and **Hema Joshi** (2012), Black carbon aerosols over Manora Peak in the Indian Himalayan foothills: implications for climate forcing, *Environ. Res. Lett.*, 7 014002, doi:10.1088/1748-9326/7/1/014002.

5. Mallik, C., Shyam Lal, Manish Naja, Duli Chand, S. Venkataramani, **Hema Joshi** and P. Pant (2013), Enhanced SO2 concentrations observed over northern India: role of long-range transport, *International Journal of Remote Sensing*, 34:8, 2749-2762.

6. Phanikumar, D. V., K. Niranjan Kumar, K. K. Shukla, **H. Joshi**, M. Venkat Ratnam, M. Naja, and K. Reddy (2014), Signatures of Rossby

wave modulations in aerosol optical depth over the central Himalayan region, *Ann. Geophys.*, 32, 175-180, doi:10.5194/angeo-32-175-2014.

7. **Hema Joshi**, Manish Naja, K. P. Singh, Rajesh Kumar, P. Bhardwaj, S. Suresh Babu, S. K. Satheesh, K. Krishna Moorthy, H. C. Chandola (2015), Investigations of aerosol black carbon from a semi-urban site in the Indo-Gangetic Plain region, *Atmospheric Environment*, ISSN 1352-2310, doi:10.1016/j.atmosenv.2015.04.007.

8. Kishore Reddy, D.V. Phanikumar, **Hema Joshi**, Y. Nazeer Ahammed, M. Naja (2015), Effect of diurnal variation OF aerosols on surface reaching solar radiation, *Journal of Atmospheric and Solar-Terrestrial Physics*, ISSN 1364-6826, doi:10.1016/j.jastp.2015.04.011.

List of Acronyms and Abbreviations

ABC	Atmospheric Brown Clouds
AE	Angstrom Exponent
AERONET	AErosol RObotic NETwork
AGL	Above Ground Level
AI	Aerosol Index
AMSL	Above Mean Sea Level
ANC	Aerosol Number Concentration
AOD	Aerosol Optical Depth
ARFI	Aerosol Radiative Forcing Over India
AWS	Automatic Weather Station
BC	Black Carbon
BL	Boundary Layer
CALIPSO	Cloud-Aerosol Lidar and Infrared Pathfinder Satellite Observation
CWT	Concentration Weighted Trajectories
CO	Carbon Monoxide
DRF	Direct Radiative Forcing
EDGAR	Emission Database for Global Atmospheric Research
GDAS	Global Data Assimilation System
GMT	Greenwich Mean Time
GOCART	Goddard Chemistry Aerosol Radiation and Transport
HTP	Himalayan Tibetan Plateau
HYSPLIT	Hybrid Single Particle Integrated Trajectory Model
IGP	Indo-Gangetic Plain

IMD	Indian Meteorological Department
IMPROVE	The Interagency Monitoring of Protected Visual Environments
INDOEX	Indian Ocean Experiment
IPCC	Intergovernmental Panel on Climate Change
ISRO	Indian Space Research Organization
ISRO-GBP	Indian Space Research Organization-Geosphere Biosphere Programme
IST	Indian Standard Time
LIDAR	Light Detection And Ranging
LT	Local Time
MFRSR	Multi-Filter Rotating Shadowband Radiometer
MICROTOPS	Micro-Processor based Total Ozone Portable Sunphotometer
MISR	Multi-angle Imaging SpectroRadiometer
MLD	Mixing Layer Depth
MODIS	Moderate Resolution Imaging Spectroradiometer
NCEP/NCAR	National Centre for Environmental Research National Centre for Atmospheric Research
NCO-P	Nepal Climate Observatory - Pyramid
OPC	Optical Particle Counter
OMI	Ozone Monitoring Instrument
PBL	Planetary Boundary Layer
PM2.5	Particulate Matter below 2.5 µm
PM10	Particulate Matter below 10 µm
RH	Relative Humidity

SSA	Single Scattering Albedo
TP	Tibetan Plateau
TRMM	Tropical Rainfall Measuring Mission
VMA	Volume Weighted Average
WRF-Chem	Weather Research and Forecast with Chemistry

Contents

Chapter 1

Introduction

The global climate system results as a consequence of balance between the incoming solar radiation and outgoing long-wave (infrared) terrestrial radiation [e.g. *Charlson et al.,* 1991; *Hansen et al.,* 1998; *Seinfeld et al.,* 2004] and an interaction between its subcomponents. It is noteworthy that any process that disturb overall energy balance can cause perturbation in climate or climate change [*Kaufman et al.,* 1997; *Seinfeld and Pandis,* 1998]. In the atmosphere, changes in the greenhouse gas and aerosol content present in the atmosphere affects the radiative balance of the climate system [*Haywood and Ramaswamy,* 1998; *Myhre et al.,* 1998]. The recent estimates of the radiative forcing of the aerosols and gases are shown in Figure 1.1 [*IPCC,* 2013]. Interestingly and more importantly, the quantification of aerosol radiative forcing is more complicated than the quantification of radiative forcing by greenhouse gases due to the high variability of aerosol mass and particle number concentrations in space and time which is mainly due to the much shorter atmospheric lifetime of aerosols compared with the greenhouse gases. It is also reported that aerosols of anthropogenic origin are mainly responsible

for a radiative forcing of climate change via their interaction with radiation and clouds [*IPCC,* 2013]. Additionally, the lack of observations of characteristics and spatio-temporal distribution of aerosols coupled with the multi-faceted impacts on climate makes aerosols one of the least understood components of the Earth's climate [*IPCC,* 2007, 2013 and references therein].

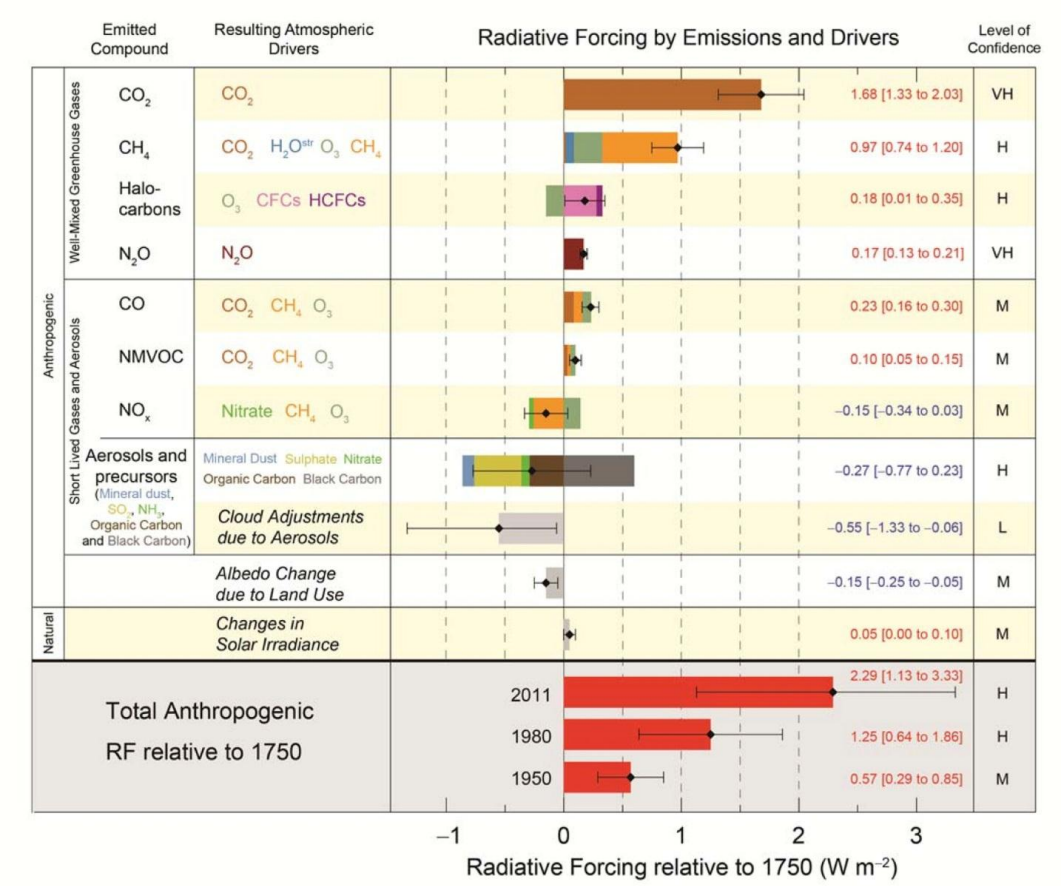

Figure 1.1. *The radiative forcing estimates by various emission in the Atmosphere [Source: IPCC, 2013].*

Atmospheric aerosols affects the earth atmosphere significantly at local, regional and global scale, by scattering and absorbing solar radiation through direct and indirect effects [*IPCC,* 2013]. Aerosols mainly interact with solar

radiation through absorption and scattering and, to a lesser extent with terrestrial radiation through absorption, scattering and emission. These aerosols not only influence the air quality but also affect the radiative forcing [*Russell et al.,* 1999; *Ramanathan et al.,* 2001; *Satheesh and Moorthy,* 2005], radiation budget [*Satheesh and Ramanathan,* 2000; *Moorthy et al.,* 2001], atmospheric warming [*Hansen et al.,* 2000; *Jacobson,* 2001; *Andreae et al.,* 2005; *Lau et al.,* 2006], precipitation and cloud properties [*Rosenfeld et al.,* 2008] significantly.

Aerosols significantly influence via their role in heterogeneous chemistry in the troposphere and stratosphere [Ravishankara, 1997; *Finlayson-Pitts and Pitts, 2000*]. Aerosols also serve as condensation nuclei for cloud droplet formation [*Charlson et al., 1992; Ramanathan et al., 2001*] which depends upon on the chemical composition of aerosols as a function of size. In addition, aerosols also influence the monsoons [*Menon et al.,* 2002] and Himalayan glaciers [*Yasunari et al.,* 2010; *Gautam et al.,* 2009] in a considerable amount. It is reported that aerosol of anthropogenic origin are mainly responsible for a radiative forcing of climate change via their interaction with radiation and clouds.

There exists large uncertainties in their estimates, not only globally but also regionally [*Ramanathan et al.,* 2003] due to non-uniform distributed over globe. Although the model predictions have significantly improved since IPCC second assessment report (IPCC, 1996). Still the most of the present day available models possess high degree of uncertainty associated with their use

and are still not accurate in capturing the actual magnitude of aerosol. The ground based actual measurement thus pose large importance.

1.1. Atmospheric Aerosols

Atmospheric aerosols are defined as particles in solid, liquid or in mixed phase dispersed in atmosphere [*Seinfeld and Pandis, 1998*] and also referred as "particulate matter". The word aerosol was introduced more than 80 years ago as an analogy to the term hydrosol, a stable liquid suspension of solid particles [*Hinds, 1999*]. Atmospheric aerosols include wide range of phenomenon such as fog, haze, dust, smoke, smog and fume [*Seinfeld and Pandis, 1998*]. Aerosols sizes from ~ 10^{-3} to 100 μm [*Junge*, 1963; *Prospero et al*., 1983; *Jaenicke*, 1984]. The aerosol size range as shown in Figure 1.2 is of crucial importance and decides the characteristics of aerosol. It is interesting that sub-micrometer aerosols scatter more light per unit mass and have a longer atmospheric lifetime than larger aerosols. The large aerosols are mainly removed from the atmosphere by gravitational settling, while other scavenging includes rainout and washout processes. The very small aerosols however undergo coagulation and condensation. The detail description regarding different aerosol production mechanism and scavenging is given in later sections. The accumulation mode of aerosols possess larger residence time in the atmosphere. The lifetime of aerosols is typically about a week in troposphere, while lifetime of aerosols is high in stratosphere. The aerosols in troposphere possess high regional characteristics due to relative low lifetime as compared to stratosphere.

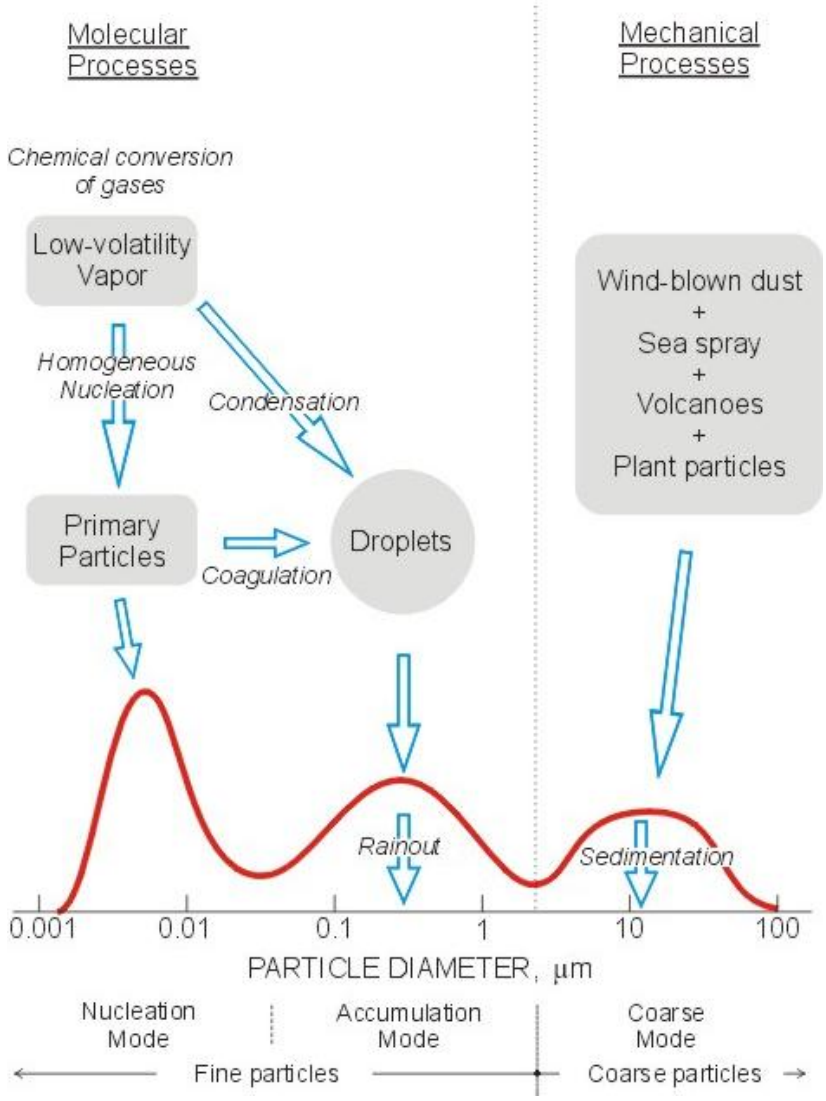

Figure 1.2: *Aerosol size regime, production and removal mechanisms. The size distribution (surface area) of aerosols with respect to the particle diameter in atmosphere is shown.*

It is interesting that aerosols often combine to form mixed aerosols with different optical properties and atmospheric lifetimes different than those of their individual components. Aerosols and clouds also interacts via aerosol-cloud interaction. It is interesting that aerosols are of very crucial importance in cloud formation and serves as an efficient cloud condensation nuclei (CCN). The hygroscopic particles such as sulfate aerosols, act as efficient

CCN and promotes the cloud formation or enhancement in precipitation, while hydrophobic aerosols i.e. soot and dust does not serves as good CCN and might act to suppress rainfall.

1.2. Types and Sources of Atmospheric Aerosols

Atmospheric aerosols can be of natural as well as of anthropogenic origin [*Seinfeld and Pandis, 1998*]. The natural sources includes windborne dust, sea spray, volcanic activities and biomass burning, while anthropogenic activities mainly include fuel combustion, industrial processes, transportation and biomass burning due to crop harvest. There are also common sources i.e. biomass burning, soil dust emissions etc. which can be originated from both the natural and anthropogenic processes.

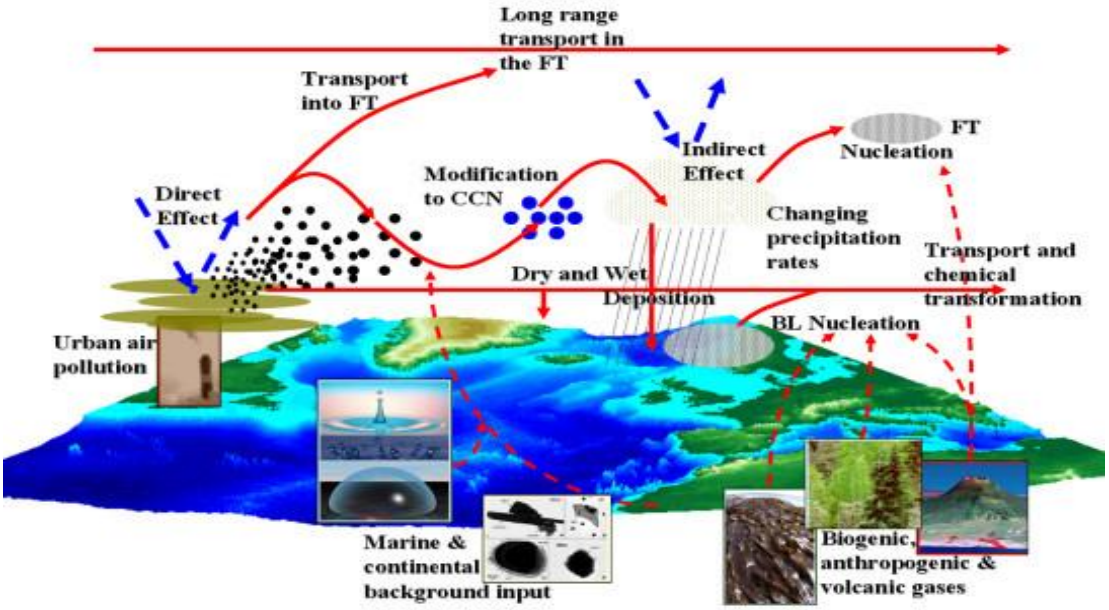

Figure 1.3. *Illustration of aerosol emission, scavenging, direct and indirect effects, transport and chemical transformation and life cycle of aerosols in the atmosphere.*

Interestingly, natural aerosols are present in the higher amount ~ 4 to 5 times larger than anthropogenic ones on a global scale, but regional variations in anthropogenic aerosols mainly change this ratio significantly, especially in the industrialized Northern Hemisphere [*Seinfeld and Pandis, 1998*] and thus anthropogenic aerosols gets more attention as compared to natural ones. These natural and anthropogenic aerosols can be directly emitted from their sources as primary aerosols or can be formed in atmosphere (i.e. through the gaseous precursors) as secondary aerosols. Primary aerosols are those aerosols which are directly emitted into the atmosphere from there sources which mainly includes black carbon, soil dust, sea salt and others, while secondary aerosols mainly include sulphates and nitrates and others mainly produced as a result of chemical reactions in the atmosphere via gaseous precursors, the detail of which is given in later section. These aerosols when emitted in to the atmosphere undergo transport and chemical transformation in addition to the deposition and scavenging (Figure 1.2). The most common types of the aerosols found in the atmosphere are mentioned below.

1.2.1. Dust Aerosols

Soil dust is a major contributor to aerosol loading found all around the globe especially in subtropical and tropical regions due to long-range transport (to over thousands of kilometers) of mineral dust by the general circulation of the atmosphere. The soil dust is one of the major sources of natural aerosols [*Tegen and Fung,* 1994; *Alfaro et al.,* 1997] and the dust thus originating from the soil is mainly of mineral origin. The dust source regions mainly include

deserts, semi-arid desert fringes, dry lakebeds, and also areas in drier regions where vegetation has been reduced or soil surfaces have been disturbed by human activities. The major dust sources are thus in the desert regions of the Northern Hemisphere, while dust emissions in the Southern Hemisphere are relatively small due to far reduced landmass. The mineral dust particles are transported into the atmosphere due to dust and sand storms in arid regions. The dust particle mainly arise when the wind exceeds a value that allows dust particles to be removed from the surface. This minimum wind speed is called the "threshold velocity" and is necessary to mobilize the dust particles. The process of dust and sand uptake from the soil depends on the near-surface dynamics and is controlled by the wind intensity, the soil wetness, the soil texture and the land cover. The production of soil dust aerosols by very high surface wind is shown in Figure. 1.4.

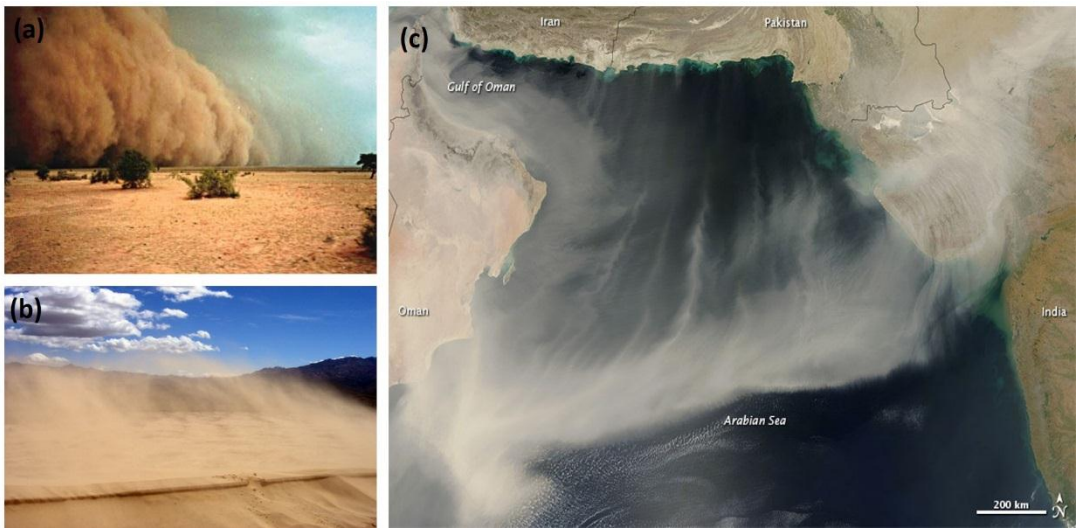

Figure 1.4. *The production of (a) soil dust aerosols by high surface winds (b) uptake of dust from the Desert to the atmosphere (c) A giant dust plume*

stretch across the Arabian Sea from the coast of Oman to India on 20 March 2012, the image is obtained from MODIS Aqua satellite.

The atmospheric lifetime of dust depend upon particle size and altitude to which they are raised. The submicron size particles in the atmosphere (in the troposphere) have higher lifetimes and can stay up to a few weeks, while the particles with the larger size are quickly removed by gravitational settling. The transport of dust from source regions to other far away locations depend upon the wind speed by which the dust loading can be transported to other far away locations. The origin of the dust can be both the natural as well as anthropogenic in origin. It has been estimated that up to 50% of the current atmospheric dust load originates from disturbed soil surfaces, and might therefore be considered anthropogenic in origin [*Tegen and Fung,* 1995]. The dust particles mainly ranges from 0.1 to 100 μm. The particles with radius (r) > 5 μm are found mainly around the source region, while the smaller particles with diameter ranging from 0.1 to 5 μm are transported to the long distances usually ~5000 km [*Arimoto et al.,* 2001; *Prospero et al.,* 2002; *Gong et al.,* 2003; *Maring et al.,* 2003]. Various investigations has reported the influence of Sahara dust at remote locations of Atlantic and Pacific oceans [*Carlson and Prospero,* 1972]. The influence dust is also observed over the Arabian Sea due to mineral dust transport from Arabia and Africa [*Li and Ramanathan,* 2002]. The significant amount of dust is also observed over the North India and over the IGP locations [*Sikka,* 1997; *Washington et al.,* 2003; *Dey et al.,* 2004; *Singh et al.,* 2004; *Jethva et al.,* 2005; *Chinnam et al.,* 2006; *Gautam et*

al., 2009 and others], high altitude of Himalayas [*Hegde et al.,* 2007] and other Oceanic regions [*Kumar et al.,* 2014].

1.2.2. Sea Salt

Sea salt is the most significant single natural source of aerosols. The production rate of seas salts aerosols is about ~ 1000-10, 000 Tg yr^{-1} [*Winter and Chylek*, 1997]. It is found that ~30% of global aerosol burden is attributed to sea salt [*Fitzgerald,* 1991] and Oceans contribute about ~30-75% of seas salt aerosols depending on the region [*Blanchard and Woodcock,* 1980]. The wide range of physical processes generate sea salt aerosols, the most effective of which is by bursting of air bubbles entrained in the ocean surface during white cap formation [*Blanchard and Woodcock*, 1957; *Blanchard*, 1985; *Monahan et al.,* 1986] which strongly depends upon the wind speed. The tearing of drops from wave tops also generate the sea salt aerosols.

The production of sea salt aerosols and its size distribution is very sensitive to wind speed, and salinity, among other factors [*Monahan,* 1968; *Monahan et al*., 1983]. This makes it very difficult to estimates the production rate of sea salt. An example of aerosol production from sea spray at high winds is shown in Figure 1.5. Sea salt particles cover a wide size range (about 0.05 to 10 μm diameter), and have correspondingly wide range of atmospheric lifetimes [*Fitzgerald*, 1991]. Most of the sea salt aerosols are usually above size range

of 1 μm diameter, however a small but significant fraction of sea salt aerosols exist in the sub micrometer fraction [*O'Dowd et al*., 1999].

Figure 1.5. *The sea salt aerosol production from sea spray at high winds*.

Sea salt aerosols may be the dominant contributor to both light scattering and cloud nuclei in those regions of the marine atmosphere where wind speeds are high or other aerosol sources are weak [*Quinn et al*., 1996; *O'Dowd et al*., 1997; *Murphy et al.,* 1998a]. Interestingly, sea salt aerosols are very efficient cloud condensation nuclei (CCN) due to their hygroscopic nature and their characterization is of major importance for aerosol indirect effects [*Feingold et al*., 1999]. The detail regarding production, transport, altitude distribution, size distribution, and wind speed dependence of sea salt aerosols have been extensively studied and documented in the literature [*Woodcock et al*, 1953; 1972; *Lovett*, 1978; *Exton et al*., 1985; *Hoppel et al*., 1990; *Fitzgerald*, 1991; *Moorthy et al*., 1997, 1998; *Moorthy and Satheesh*, 2000; *Satheesh et al.,* 2002; *Vinoj and Satheesh et al.,* 2003]. Over the remote oceanic regions the sea salt aerosols are of crucial importance as the optical properties of marine boundary layer is largely controlled by the concentrations of sea salt aerosol

[*Quinn et al*., 1998]. Over the marine oceanic regions the sea salt aerosols can contribute significantly to the total aerosol loading. Investigation over the tropical Indian Ocean during INDOEX has revealed that the sea salt was single largest natural contributor of aerosol visible optical depth contributing more than 50 % of the natural aerosols [*Satheesh et al*., 1999]. The model simulation of sea salt aerosols are however complicated and are hampered by the dearth of accurate and precise sea salt size and concentration data over the oceans.

1.2.3. Sulphates

Sulphate aerosols are produced by chemical reactions in the atmosphere from gaseous precursors (with the exception of sea salt sulphate and gypsum dust particles). The two main precursors are SO_2 from anthropogenic sources and volcanoes, and DMS from biogenic sources, especially marine planktons. The volcanic eruption also adds large amount of SO2 into the stratosphere where it is converted to sulphate aerosols [*Moorthy et al.,* 1999]. The other origin of sulphates is the industrial activities [*Charlson et al.,* 1992]. The sulphates aerosols are hydrophilic in nature and act as an efficient CCN. Most SO_2 is converted to sulphate either in the gas phase or in cloud droplets that later evaporate. Both processes produce sulphate mostly in sub-micron size regime that are efficient light scatterers, but the size distribution of sulphate in aerosols is different for gas phase and aqueous production. The emitted SO_2 undergo deposition consequently only 46 to 82 % of the SO_2 emitted undergoes chemical transformations and forms sulphate. The sulphate aerosols

are predominantly of submicron range [*Winchester and Bi,* 1984] and due to being in submicron size range can be transported to long distance from their source of origin [*Rodhe and Grandell.,* 1981].

1.2.4. Nitrates

Like the sulphate aerosols nitrate aerosols are also produced by chemical reactions in the atmosphere from gaseous precursors are the end products of a wide variety of reactions in the atmosphere involving trace gases, produced either naturally or anthropogenically. The common precursors for nitrates aerosols are nitrogen oxides, volatile nitrogen bearing acids and gaseous nitrates. Aerosol nitrate is closely tied to the relative abundances of ammonium and sulphate and hence has a strong bearing on agricultural practices and fertilizer usage.

The production of secondary aerosol nitrate is closely tied to the relative abundances of ammonium and sulphate. If ammonia is available in excess of the amount required to neutralize the stronger acid H_2SO_4, gaseous HNO_3 and NH_3 can enter the condensed phase, and their subsequent dissociation yields nitrate (NO_3) and ammonium (NH_4 +) ions. Submicron particles containing nitrate are potentially efficient CCN. The deposition of soluble material on otherwise insoluble dust particles increases their CCN activity. In the presence of acidic accumulation-mode sulphuric-acid containing aerosols, HNO3 deposits on larger alkaline mineral or salt particles which results in an enhanced CCN activity.

1.2.5. Carbonaceous aerosols

Carbonaceous aerosols are the most complex aerosol mixtures which make up a large but highly variable fraction of the atmospheric aerosol concentration. These carbonaceous aerosols are the complex mixture of the elemental carbon and organic carbon. The main sources for carbonaceous aerosols are incomplete combustion of carbonaceous materials, biomass and fossil fuel burning, and the atmospheric oxidation of biogenic and anthropogenic volatile organic compounds (VOC). The total carbonaceous (TC) fraction of aerosols present in the atmosphere mainly constitute the organic carbon (OC) and the Black carbon (also called as soot) [*Cachier*, 1998].

1.2.5.1. Black Carbon

Black carbon is the most absorbing aerosol with strong and wide absorption in the visible and IR range. BC has attained a significant interest due to its dominant light-absorbing characteristics [*Venkataraman et al.,* 2010; *Ramanathan et al.,* 2011]. BC has an atmospheric residence time equal to or longer than that of sulphate [*Ogren and Charlson,* 1984] and therefore similar to the timescale for typical synoptic scale weather features. The primary sources, processes governing fate of BC in atmosphere and its role in climate system is illustrated in Figure 1.6.

Interestingly, BC is mostly inert due to which it is mostly used as a tracer. BC is emitted as primary particles from incomplete combustion processes, such as fossil fuel and biomass burning, and therefore much of atmospheric BC is of

anthropogenic origin. BC retains its basic form at very high temperatures, with a vaporization temperature near 4000K. The total global emissions of black carbon was estimated by *Bond et al.*, [2013] using bottom-up inventory methods which were 7500 Gg yr^{-1} in the year 2000 with an uncertainty range of 2000 to 29,000. The largest global sources of BC are open burning of forests and savannas, however the quantity of BC emitted from these natural fires is very difficult to quantify. It is found that the residential solid fuels (i.e., coal and biomass) contribute ~60 to 80% of Asian and African emissions, while onroad and off-road diesel engines contribute about 70% of emissions in Europe, North America, and Latin America. [*Bond et al.,* 2013]. The best estimate of industrial-era climate forcing of black carbon through all forcing mechanisms was mentioned in *Bond et al.,* [2013] which is +1.1 W m^{-2} with 90% uncertainty bounds of +0.17 to +2.1 W m^{-2}.

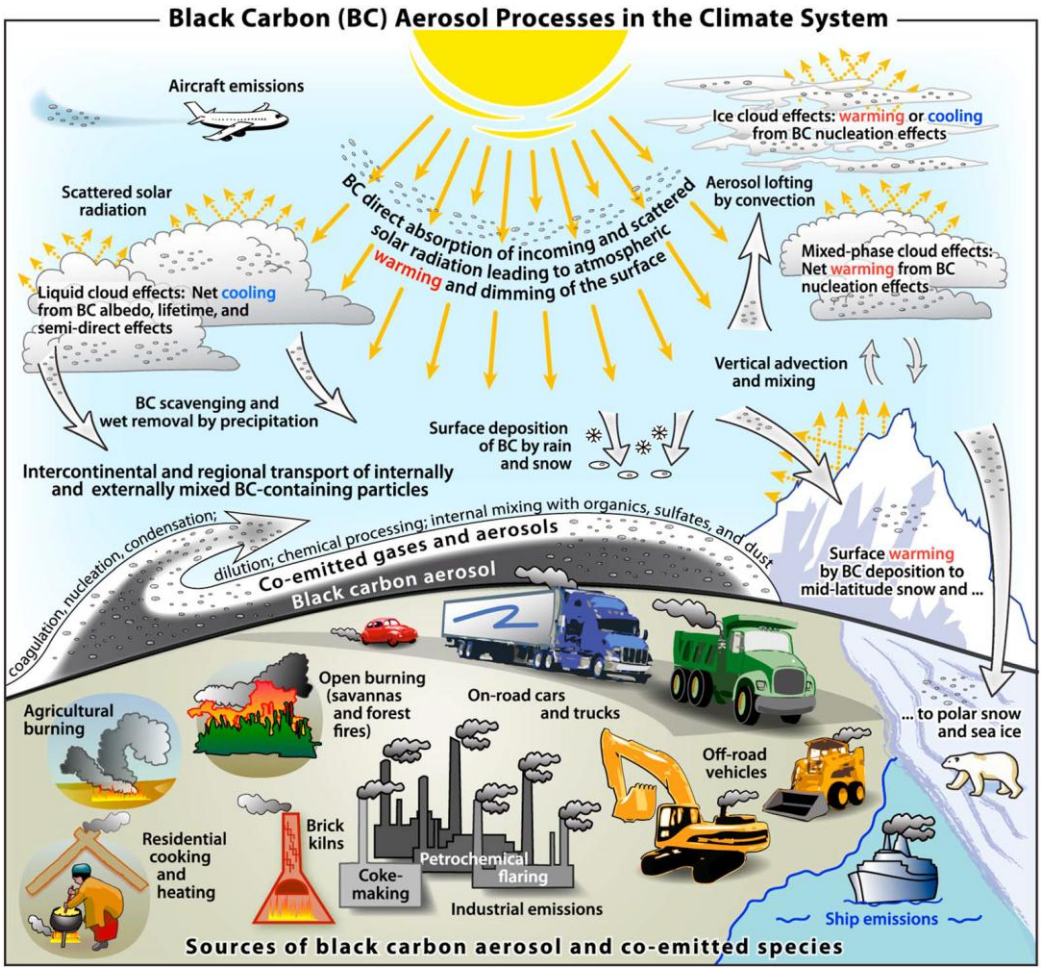

Figure 1.6. *Schematic overview of the primary BC production, sources and processes controlling the fate of BC. The role of BC in climate system is also shown (Source: Bond et al., 2013).*

BC being inert is not degraded under atmospheric conditions and hence wet and dry depositions are the only important sinks of BC. Interestingly, scavenging of BC is far slower than that of OC as being mostly hydrophobic or only weakly hydrophilic. The lifetime of BC is however of the order of days to weeks depending on scavenging and the meteorology [*Reddy and Venkataraman*, 1999; *Babu and Moorthy*, 2001, 2002]. During its short atmospheric lifetime BC can also undergoes the regional and intercontinental

transport and can be transported to remote and clean locations even to Arctic [*Stohl et al.,* 2006]. In context to the short and long wave absorption by atmospheric aerosols, BC is the most significant single species having a high value for the imaginary part of the refractive index over a wide spectral range. The absorption due to BC is quite significant and is second largest after CO2 in producing the atmospheric warming [*Ramanathan and Carmichael,* 2008]. The magnitude of atmospheric heating due to BC could exceed that due to methane, thereby making it an important species contributing in producing atmospheric warming [Jacobson, 2001]. BC has quite a greater effect on the radiation budget than the rather short-lived organic carbon. Due to the large absorption over a wide wavelength range, BC could offset significantly or even reverse the 'white house' effect (brightening of the atmosphere) due to aerosol scattering [*Schwartz*, 1996; *Haywood and Shine*, 1997]. Interestingly, BC can change the sign of radiative forcing from negative (cooling) to positive (warming) [*Haywood and Shine,* 1997; *Heintzenberg et al.,* 1997; *Babu et al.,* 2002]. Significant amount of BC if present in rain clouds can lead to increased absorption of solar radiation resulting in heating and eventually 'burn off' of the clouds [*Ackerman et al*., 2000]. Being mostly in submicron size range, BC is easily inhaled and can be a health hazard [*Horvath*, 1993]. Due to its environmental and climate significances as well as anthropogenic nature of its origin, characterization of BC is attracting considerable interest in the recent years [*Hansen et al*., 2000]. Over India, total BC emission estimate is 0.41 Tg per year; with fossil fuel, biofuel and open burning combustion contribution of 25%, 42% and 33% [*Venkataraman et al.,* 2005]. BC aerosols are found to be

quite high over the IGP region as compared to off IGP regions [*Nair et al.,* 2007].

1.2.5.2. Organic Carbon

Organic Carbon is produced as a primary aerosols and is also produced as a secondary aerosol from gaseous compounds via condensation or gas phase oxidation of hydrocarbons and constitute the largest single component of biomass burning aerosols. The gas-to-particle production processes are the dominant production mechanism of OC. Organic carbon dominates the total carbon for emissions from forest fires, firewood especially when burning is at low temperature. The OC/BC ratio is ≈1 for fossil fuel combustion [*Cachier,* 1998]. The refractive index of OC particle is close to that of sulphates and hence they mainly scatter the solar radiation. The OC aerosols are found to be as much light scattering as sulphate aerosols in a measurement over Atlantic in the haze plume [*Hegg et al*., 1997; *Novakov et al*., 1997]. OC aerosols are quite volatile due to which their sampling is quite difficult as compared to other species. Owing to this the OC aerosols are also least understood. Due to presence of polar functional groups, particularly carboxylic and dicarboxylic acids OC aerosols also participate in cloud droplet nucleation [*Saxena et al*., 1995; *Saxena and Hildemann*, 1996].

1.2.6. Volcanic Aerosols

Volcanoes emission mainly emits primary dust and gaseous Sulphur, the two most significant aerosols. Volcanic emission inject significant amount of burden especially in the stratosphere. Significant amount of aerosols and gases get injected in the stratosphere by volcanic emissions. These pollution load in the stratosphere then gets distributed all over the world along with winds. The aerosols are mainly produced in the stratosphere by the gaseous precursors and have high lifetime and remains in the stratosphere for years. The large injection of volcanic aerosols in stratosphere results in the cooling after eruption.

Figure 1.7. *Photograph of volcanic eruptions. The left image is volcanic emission of Mt. St. Helenes in USA and the right one is Mt. Pinatubo in the Philippines.*

There has been several reporting of volcanic emission adding large amount of aerosols in the stratosphere. In 1982, the erupted volcano, El Chichon, in Mexico was found to inject about 20 Tg of aerosol in to the stratosphere [*Hoffmann and Rosen*, 1983], which includes ~10 megatons of SO_2 [*Hoffman*, 1987]. The eruption of Mount Pinatubo (Figure 1.7) in Luzon, Philippines in June 1991 however, injected approximately 30 million tones of H_2SO_4 aerosols into the stratosphere [*Bluth et al*., 1992] produced large increase in atmospheric aerosol optical depth and extinction [*Hansen et al*., 1992; *Minnis et al*., 1993; *Jayaraman et al.,* 1995; *Moorthy et al.,* 1996]. The global mean cooling was reported due to Mt. Pinatubo. *Robock,* [2000] reported the global mean cooling of ~ 0.4°C at the surface in the year following the eruption. The influence of volcano was observed till ~ 3 years after the eruption. The perturbation in the atmosphere and potential effects of Mt. Pinatubo is well documented in *Brasseur and Granier* [1992], while radiative flux analomities were discussed in detail in *Minnis et al.,* [1993].

1.2.7. Production Mechanisms

Aerosols are mainly produced by mechanical disintegration and gas-to-particle conversion processes. The mechanical disintegration is a direct, (primary process) of aerosol production. The aerosols are produced directly from the bulk of materials and are larger in size in this process. The gas-to-particle production of aerosols however is a secondary process of aerosol production.

The aerosols are formed as a result of chemical reactions between various gaseous species in the atmosphere, followed by nucleation and condensation and thus are smaller in size. The production mechanism of aerosols mainly decides the size range and the shape of produced aerosols and has been shown earlier in Figure 1.2.

1.2.7.1. Mechanical Disintegration

The mechanical disintegration processes is the most common and major process of aerosol production [*Prospero et al*., 1983]. The mechanical disintegration production is also called as "bulk to particle conversion" method and usually produce the particle size greater than 0.1 μm. The production of sea-spray, raising dust, etc. are all example of mechanical disintegration. Anthropogenic primary emissions of aerosols arise mainly arise from industries, transportation, coal combustion, cement manufacturing, and metallurgy [*Cachier*, 1998].

1.2.7.2. Gas-to-Particle Conversion

Aerosols in the atmosphere are also produced by nucleation (condensation) of low volatile gases. The gases or vapors having low vapor pressure in the atmosphere condense on to existing particles, thereby increasing the mass of aerosols. Gases may also condense to form new particles in the air. The former path is favored when the surface area of existing particle is high and the supersaturation of the gases is low. The vapors of highly volatile liquids or

reaction products of certain gaseous species emitted from the Earth's surface condenses either by themselves or on pre-existing particles to give rise to aerosols. The pre-existing aerosols considerably reduce the amount of super saturation required to start condensation. The chemical reactions between various gaseous species also result in products, which are highly volatile in nature and then undergo nucleation or condensation. These reactions are catalyzed by the presence of ultraviolet (UV) radiation from the Sun and presence of water vapor or OH radical. The particles produced from gas-to-particle process are hygroscopic in nature and are efficient CCN.

The major chemical species involved in gas to particle conversion are sulfur, nitrogen, and organic materials. Various sulfur gases can be oxidized to SO_2 which is then oxidized to sulphate (SO_2), the dominant gas phase routes being

$$SO_2+OH+M \rightarrow HSO_3+M \quad (1.1)$$

$$HSO_3+O_3 \rightarrow HO_2+SO_3 \quad (1.2)$$

$$SO_3+H_2O \rightarrow H_2SO_4 \quad (1.3)$$

Over the oceans, the main source of sulphate derives from DMS (dimethyl sulphide). Sulphates are also produced in the vicinity of the clouds, by the combination of water molecules and sulfuric acid molecules.

1.2.8. Transformations of Aerosols

Aerosol transformation processes are very important aerosol microphysical processes, which changes the aerosol particle of one size range to another. The aerosol mass is however not removed from the atmosphere during the transformation, consequently these transformation processes are not the removal processes. The aerosol transformation processes are capable of producing changes in the aerosols number density, size distribution and hence in their optical, radiative and environmental effects. The chief aerosol transformation processes are coagulation, condensational growth, and the processing of aerosols by non-precipitating cloud cycles.

1.2.8.1. Coagulation

Aerosol particles (especially those with diameter < 1 μm) are in constant random motion due to collision with gas molecules. This motion causes aerosol particles to collide and they adhere to each other (coalesce) resulting to larger particles (Figure 1.8). The coagulation is the important process in the atmosphere by which smaller particles shifts towards the larger particle range. It is the main controlling process that limits the particle concentration at the lower end of the aerosol size range (< 0.01 μm). The large number of particles present in the nuclei mode are transferred to the particle in accumulation mode by coagulation [*Pruppacher and Klett,* 1978].

Coagulation is mainly controlled by the diffusion coefficient (μ) of particles which is in turn related to particle mobility (B) through the relation,

$$\mu = BK_BT \quad (1.4)$$

Where , K_B is the Boltzman's constant and T is the absolute temperature.

The particle mobility defined as the average drift velocity of the particle per unit driving force is given by [*Pruppacher and Klett,* 1978] as:

$$B = \frac{(1 + XN_{kn})}{6\pi\eta_a\, r} \quad (1.5)$$

$$\text{Where } X = b_1 + b_2 \exp\left(\frac{b_3}{N_{kn}}\right) \quad (1.6)$$

Here, N_{kn} is the Knudsen number defined as the ratio of the mean free path length of air molecules (λ_a) to the particle radius r, η_a is the coefficient of viscosity of air and b_1 and b_2 are the constants whose values are 1.257, 0.400 and -1.10 respectively. The term ($1+XN_{kn}$) is the Cunningham slip correction factor to account for the slippage of the particle by air molecules while in motion. This term assumes importance when the size of the particle becomes comparable to or less than the mean free path of air molecules. When the two particles of radius r1 and r2 coagulate to form the resultant particle (r) the radius of the resultant particle is given by volume conservation as

$$r = (r_1^3 + r_2^3)^{1/3} \quad (1.7)$$

The rate of coagulation is minimum when two coagulating particles are of same size, thus the rate of coagulation enhances with the polydispersion [*McCartney,* 1976; *Pruppacher and Klett,* 1978].

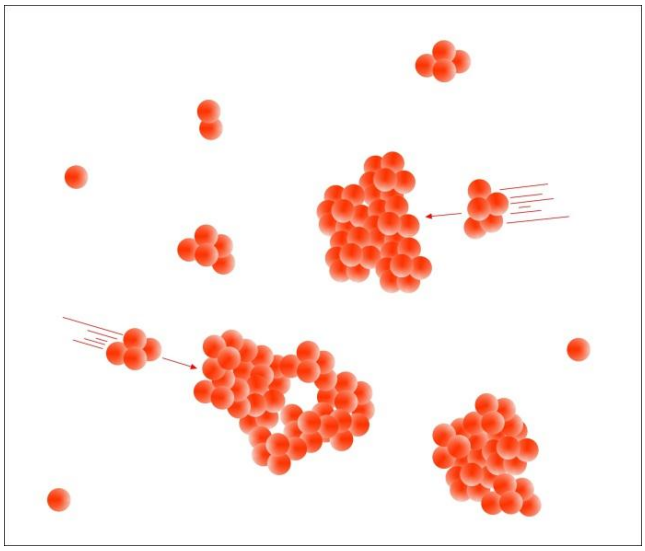

Figure 1.8. *Illustration of coagulation of aerosol.*

1.2.8.2. Condensation

The condensation of vapors (particularly of volatile liquids) present in the atmosphere on the surface of aerosols make them to grow in size (Figure 1.9). Most of the aerosols present in the sub-micron range (< 1μm) provides large amount of surface area for condensation to occur and act as efficient condensation nuclei in the atmosphere. The rate of condensation ultimately depends on the aerosol size and concentration and diffusion coefficient of vapor. The condensation rate (J) of a vapor on an aerosol is described by using the Fuchs-Stugin equation [*Hegg*, 1990] as:

$$J = 4\pi\mu_v rF(N_{kn})A_{(p-p_0)} \tag{1.8}$$

where μ_v is the diffusion coefficient of the vapor in air, N_{kn} is the Knudsen number and p and p_0 are respectively the bulk vapor partial pressures and partial pressure at the particle surface. Here, $F(N_{kn})$ is a coefficient correcting

for molecular effects and the coefficient A is for correcting the inter facial mass transport limitations.

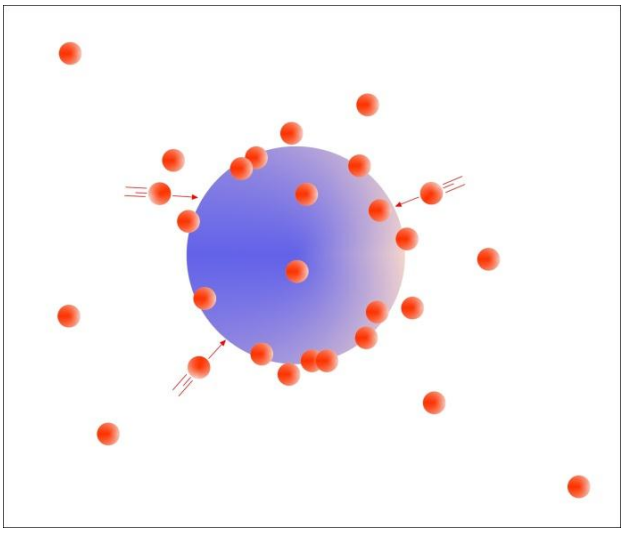

Figure 1.9. *Illustration of the condensation of aerosol particles during gas-to-particle condensation.*

1.3. Sinks of Aerosols

Aerosols are removed from the atmosphere by two main processes: dry and wet processes. The dry processes are also called as dry deposition or sedimentation, while the wet processes involves the rain out and wash out processes [*Pruppacher and Klett*, 1978]. Dry removal processes include sedimentation and impaction onto surfaces. Sedimentation refers to settling of aerosols due to the Earth's gravitational attraction. Sedimentation is significant only for aerosols with diameters greater than a few micrometers. It is estimated that ~10% to 20% of the mass of aerosols is removed from the atmosphere by sedimentation. Small aerosols, for which sedimentation over

large distances is ineffective, can impact on to obstacles if they are brought close to a surface by winds relative to the surface or by turbulent air motion. For particles in the form of spheres with diameter D (> *l*, mean freepath), the terminal settling velocity v_s of a particle in still air is given by Stokes equation

$$v_s = \frac{D^2 g}{18\mu}(\rho_p - \rho) \tag{1.9}$$

where g is the acceleration due to gravity, μ the dynamic viscosity of air, ρ_p the density of the particle, and ρ the density of the air.

Wet removal, however involves washout and rainout and is the main process which limits the residence time of aerosols in size range of 0.05 to 3 μm. The wash out processes are also called as precipitation scavenging, while the rainout processes are called nucleation scavenging. The wash out scavenging is the below cloud scavenging and involves removal of aerosol from the atmosphere by the falling raindrops. The wash out process removes only those aerosols which are pushed away by the air steam of falling raindrops and not all the particles in the air path of a raindrop are removed from the atmosphere. The efficiency of collection depends on both the raindrop size and particle size [*Pruppacher and Klett*, 1978]. Depending on the collection efficiency of the raindrops, many particles merge with the falling drops and are removed from the atmosphere. The rain out mainly describes the removal of a cloud condensation nuclei. This process takes place within the cloud and is also referred as in cloud scavenging. Several studies has reported the in-cloud and

below cloud scavenging of aerosols [*Wang et al.,* 1978; *Flossmann* et al., 1985; *Goncalves et al.,* 2002, 2003].

1.4. Mixing State of Aerosols

Aerosols, when once emitted into the atmosphere undergo various chemical processes during its atmospheric residence time, which sometimes changes the chemical composition thus the mixing of the aerosols. Atmospheric aerosols can exist in different mixing state depending upon how the constituent chemicals are distributed among the particles. Aerosols can be externally or internally mixed. External mixture refers to non-homogeneity in the chemical composition of individual particles. In an external mixture, particles from different sources remain separated, i.e., not attached to each other. In contrast, in internally mixed aerosols the various chemical components are mixed within a single particle. It has also been suggested by aerosols can also form core-shell type mixing when one component forms coating over another component [*Jacobson,* 2001]. The greater the time aerosol resides in the atmosphere in aged airmasses greater the possibility of the internal mixing. The nature of mixing affects optical and physical properties of aerosols, and plays a crucial role in the aerosol radiative forcing.

1.5. Transport of Aerosols

Aerosols get transported from their source region to distant locations by means of prevailing winds by the airflows they encounter during the time they spend

in the atmosphere. The mesoscale or synoptic scale air mass type influences the aerosol concentration and properties significantly [*Smirnov et al.,* 1995]. The transport of the aerosols can be of regional, intercontinental and global scales. Aerosols when get transported to the free troposphere, can stay there for a long time and can also undergo long range transport. The long range free tropospheric transport of aerosols can bring aerosols from polluted locations to clean Himalayan sites or marine regions. Long-range transport of continental air even over the oceans has been observed and documented in several field experiments [*Carlson and Prospero,* 1972; *Prospero et al*., 1981; *Merrill et al*., 1985; *Whelpdale et al*., 1988; *Andreae et al*., 1988; *Prospero,* 1999]. Transport of aerosols from South Africa to regions over the Atlantic and Indian Oceans has also been observed [*Tyson et al*., 1996]. Large-scale transport of dust from Africa to south Indian Ocean, from West Asia to Arabian Sea, from China across the Pacific, from Australia over to Indian Ocean has also been reported [*Moorthy and Satheesh,* 2000; *Satheesh and Srinivasan,* 2002].

1.6. Residence Time

The lifetime of atmospheric aerosol depends on their properties i.e. size, chemical composition, etc. and on altitude range. The aerosols in the atmospheric boundary layer (lower troposphere), possess the less life or residence time which is usually less than or about a week, depending on aerosol properties and meteorological conditions. In the free troposphere, the

typical particle lifetime is more as compared to boundary layer on average. During this time, particle can easily be transported to a long distance. The stratosphere however has the maximum lifetime of aerosols usually in years, due to the lack of precipitation. Smaller particles in atmosphere are efficiently removed by coagulation with other particles and have very short lifetime. Similarly, the large particles spend only a short time in the atmosphere due to the sedimentation. The particles in the accumulation mode have the longest lifetime (7–10 days on average), as both the brownian diffusion and sedimentation are less important for this size range. These particles are removed from the atmosphere predominantly by wet deposition.

There are several concepts about characterizing the time, which aerosol particles spend in the atmosphere i.e. relaxation time, residence time, and lifetime. Residence time of aerosols indicates the time up to which they remain airborne, which is influenced by various processes like wet and dry deposition and transformation. It is a measure of the time the particle spends chemically in the atmosphere and its spatial and temporal variation. In addition, the residence time also reflects the time the aerosol particle spends in a certain size bin. If the aerosol particle is moved to another size bin by coagulation, cloud incorporation or evaporation, its influence on atmospheric processes changes. *Jaenicke*, [1984] has formulated the residence time of aerosols and developed a semi-empirical relationship as follows:

$$\frac{1}{t_R} = \frac{1}{1.28\times10^8}\left(\frac{r}{0.3}\right)^2 + \frac{1}{1.28\times10^8}\left(\frac{r}{0.3}\right)^{-2} + \frac{1}{t_{wet}} \qquad (1.10)$$

where t_R is the residence time (s), t_{wet} the wet removal time (s) and r the particle radius (μm).

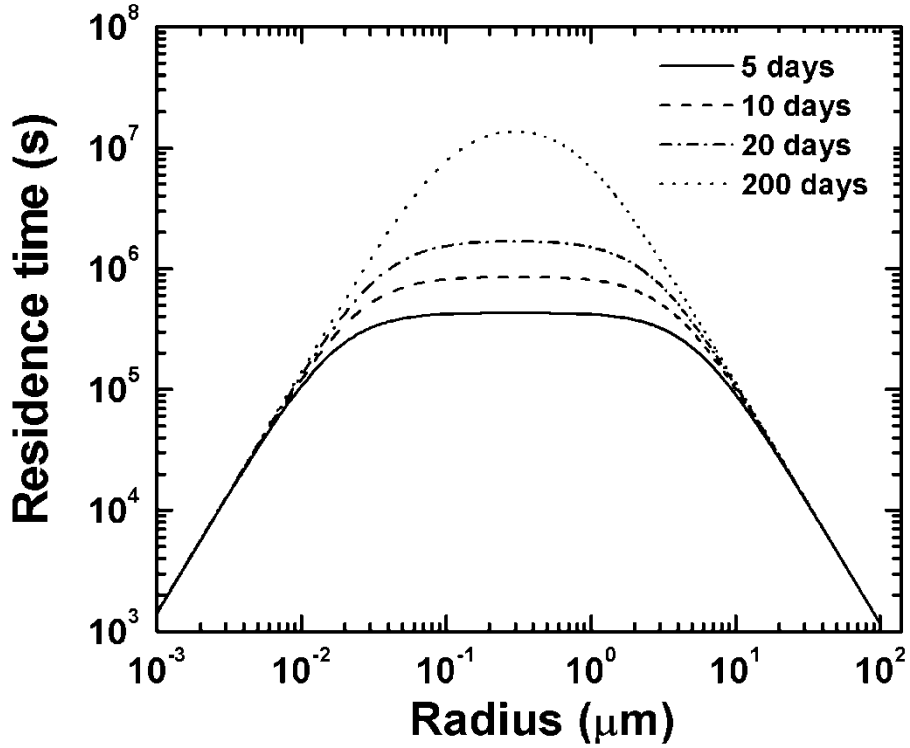

Figure 1.10. *The residence time estimates of atmospheric aerosols for different wet removal times as a function of their radius.*

The residence time of aerosols as a function of their radius are shown for various wet removal times (Figure 1.10). The residence time for very large and very small particles is rather short due to large settling velocities of the large particles and high mechanical mobility of the small particles. The possible horizontal displacement of aerosols when estimated based on the residence time by this method shows ~ 8 km for aerosols with r ~ 0.001 μm and ~ 8000 km for those in the radius range 0.1-1.0 μm [*Jaenicke*, 1984]. These estimates are important particularly in the perspective of known horizontal transport of aerosols and subsequent modifications in the aerosol characteristics at locations far away from their sources [*Prospero*, 1979; *Tegen and Fung*, 1994].

1.7. Vertical Distribution of Aerosols

Aerosols produced near the Earth's surface from the emission sources are transported upwards in the atmosphere by convective eddies. Aerosol in higher regions are however distributed to larger horizontal distances by the prevailing winds. The vertical distribution of aerosols shows a rapid decrease of particle size. The vertical distribution of aerosol concentration depends on turbulent diffusion and gravitational fall. Convection leads to vertical transport of warmer air. Turbulent motion is the random motion of air parcels of different sizes and is caused by wind shear which together with the inertia of the air causes instabilities in air stream leading to the formation of eddies, which move in all directions relative to the mean wind. These eddies cause rapid transports vertically. The vertical flux of aerosols is expressed as

$$F = -K_t \frac{\partial n}{\partial z} + V_t n \tag{1.11}$$

At steady state,

F = 0,

$$-K_t \frac{\partial n}{\partial z} + V_t n = 0 \tag{1.12}$$

Solving,

$$n = n_0 \exp(-V_t z / K_t) \tag{1.13}$$

where n is the number density at altitude z, n_0 is the surface density, V_t is the settling velocity and K_t is the turbulent diffusion coefficient.

1.8. Aerosol Interaction with Radiation

Aerosols absorb and scatter radiation in both the solar (short-wave) and the terrestrial thermal infra-red (longwave) spectra. The interaction of aerosols with radiation is mainly studied and determined by the scattering, absorption, and extinction coefficients ($\sigma_{sc,ab,ex}$), optical depth (τ), single scattering albedo (ω), scattering phase function ($P(\theta)$), and asymmetry parameter (g).

1.8.1. Scattering, Absorption and Extinction

Both scattering and absorption removes flux from a given beam of light, but scattering does not produce net change in the internal energy states of molecules, however, absorption does produce changes in the energy states. The refractive index of the particle must be different from that of the surrounding medium for scattering to occur [*McCartney*, 1976].

Scattering can be broadly classified into, Elastic and Inelastic scattering. In elastic scattering, the wavelength of the scatter radiation is at the same wavelength as that of the incident radiation while in the inelastic scattering, the wavelength of the scattered radiation is different from that of the incident radiation. The elastic scattering is of two types, the Rayleigh and Mie scattering depending upon the size of particle relative to the wavelength of the incident radiation. The intensity distribution of Rayleigh and Mie scattering is shown in Figure 1.11. Rayleigh scattering occur when the particle diameter is far smaller than the wavelength. Rayleigh scattering is inversely proportional to the fourth power of the wavelength with equal

amount of fluxes in forward and backward direction. The scattering by air molecules is mainly Rayleigh.

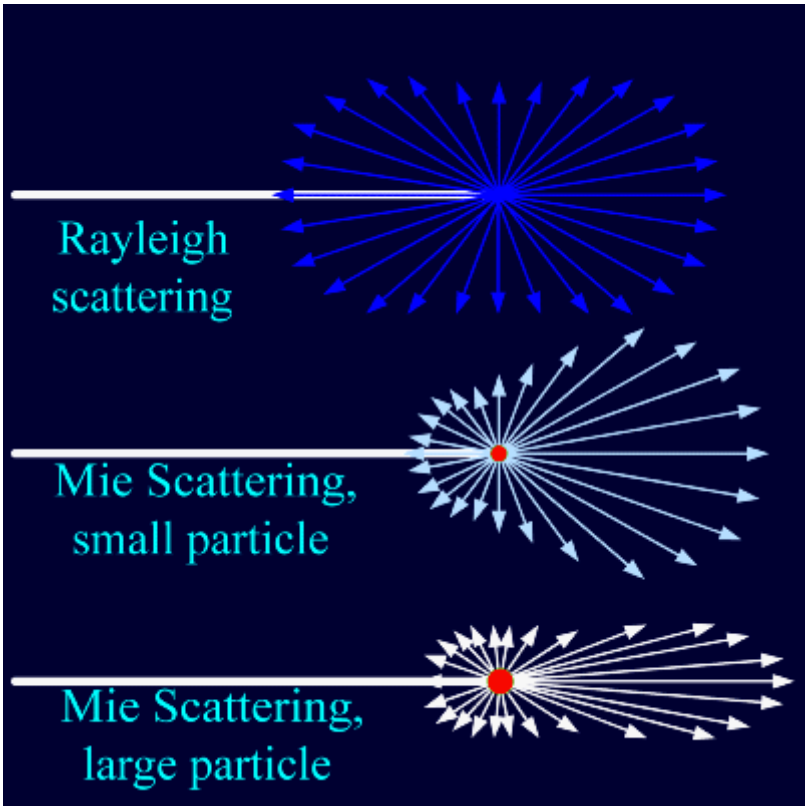

Figure 1.11. *The intensity distribution pattern of Rayleigh and Mie scattering.*

On the other hand, when particle size is comparable to the wavelength of the incident radiation Rayleigh theory becomes inadequate to explain the scattering phenomenon. As the particle size increases, the scattering no more becomes symmetric and more radiation is scattered in the forward direction than in the backward direction. Mie scattering is highly anisotropic with forward scattering being most dominant over the back scattering. The scattered intensity has a much weaker dependence on wavelength. The aerosols mainly undergo Mie scattering.

The aerosol–radiation interaction involves scattering and absorption of radiation and several terms are used to define the amount of interaction. The amount of scattering and absorption can be measured in terms of scattering and absorption coefficients. If the particle does not absorb any of the flux then only scattering occurs and the attenuation is expressed in terms of the total scattering coefficient (β_{sc}). If the particle also absorbs a significant amount of the flux, the two processes are additive and produce an extinction coefficient (β_{ex}), which is the sum of scattering coefficient and absorption coefficient (β_{ab}).

$$\beta_{ex} = \beta_{sc} + \beta_{ab} \tag{1.14}$$

The energy associated with β_{sc} directly propagates, while that of β_{ab} does not propagate directly from the beam. Instead, it raises the temperature of the medium.

The scattering / absorption / extinction coefficient ($\beta_{sc,ab,ex}$) of aerosols are measured as the fraction of radiant flux lost from a collimated beam per unit thickness of aerosol due to scattering/ absorption/ extinction, and are given in units of reciprocal of length. For mono-disperse aerosols consisting of N spherical particles per unit volume, the scattering / absorption / extinction coefficient is given by

$$\beta_{sc,ab,ex} = \pi r^2 Q_{sc,ab,ex}(\xi, \lambda, r) N \tag{1.15}$$

where $Q_{sc,ab,ex}$ is the scattering / absorption / extinction efficiency, ξ is the refractive index of the particle, λ is the wavelength of the radiation and r is the radius of the particle. For poly-disperse aerosols having a number size distribution given by n(r) within the radius r_1 and r_2, the scattering / absorption / extinction coefficient is given by

$$\beta_{sc,ab,ex} = \int_{r_1}^{r_2} \pi r^2 Q_{sc,ab,ex}(\xi, \lambda, r) n(r) dr \tag{1.16}$$

The extinction coefficient (β_{ex}) is the fraction of energy removed, per unit path length from an incident wave having unit energy flux density, by a collection of particles in suspension characterized by the particle size distribution and unit path length.

Here, Q is the efficiency factor which is related to total scattering cross section σ_p as follows

$$Q = \frac{\sigma_P}{\pi r^2} \tag{1.17}$$

$$\sigma_p = \int_0^{4\pi} \sigma_p(\theta) d\psi \tag{1.18}$$

Here, σ_p is the total scattering cross section, σ_p (θ) is angular scattering cross section, $d\psi$ is the solid angle.

The angular scattering cross section (σ_p (θ)) of a particle is defined as that cross section of an incident wave, acted on by the particle, having an area such that the power flowing across it is equal to the scattered power per steradian at an observation angle θ. The total scattering cross section (σ_p) is defined as

that cross section of an incident wave, acted on by the particle having an area such that the power flowing across it is equal to the total power scattered in all directions [*McCartney*, 1976]. Values of the total scattering cross section cover a wide range greater than the corresponding range of geometric cross sections.

1.8.2. Aerosol Optical Depth (τ_p)

The aerosol optical depth (AOD,τ_p) is the integrated aerosol extinction coefficient (β_{ex}) over the total path length of unit cross-section traversed by the radiation of wavelength λ, through the atmosphere. AOD describes the attenuation of radiation by a column of aerosol having unit cross sectional area and is given by the following equation:

$$\tau_p = \int_0^z \beta_{ex}(\lambda, z)dz \tag{1.19}$$

where z is the altitude to which the integration is carried out usually the top of the atmosphere. AOD tells about the optical state of the atmosphere and is a parameter of foremost importance in atmospheric radiation budgeting, atmospheric corrections to satellite imageries and for estimating aerosol radiative forcing.

1.8.3. Single Scattering Albedo (ω)

Single scattering albedo (SSA) is a very important parameter of aerosols to measure the effectiveness of scattering over absorption [*McClatchey et al*., 1972]. SSA is a dimensionless quantity defined as a ratio of scattering coefficient to extinction coefficient, defined as below:

$$\omega = \frac{\beta_{sc}}{\beta_{ex}} \tag{1.20}$$

SSA varies between 0 and 1. It is 0 for a perfectly absorbing aerosol, and 1 for a pure scatterer. The value of ω for BC at visible wavelengths is about 0.2, whereas it is ~1 for a sulphate aerosol. It is reported that SSA values in the northern hemispheric varies from 0.85 to 0.95 [*Hansen et al*., 1997].

1.8.4. Scattering Phase Function

The scattering phase function P(θ) describes the angular distribution of scattered radiation with respect to the incident radiation. It is defined as the ratio of the energy scattered per unit solid angle in a given direction (θ) with respect to the incident direction, to the average energy scattered per solid angle in all directions. The integral of the phase function is normalized to unity, so that

$$\frac{1}{4\pi}\int P(\theta)d\theta = 1 \tag{1.21}$$

$$\text{and } P(\theta) = \frac{\beta_{sc}(\theta)}{\frac{1}{4\pi}\int_0^{4\pi}\beta_{sc}(\theta\ )d\psi} \tag{1.22}$$

The phase function for an isotropically scattering medium is 1.

1.8.5. Asymmetry Parameter, g (λ)

The asymmetry parameter g (λ) describes the shape of the phase function. Or in other word, it describes the amount of forward and backward scattering by aerosols and is a function of particle size distribution. It is a useful parameter for characterizing the phase function, independent of scattering angle. It is given by the average of the cosine of the scattering angle over the total solid angle weighted by the phase function and is given as

$$g(\lambda) = \frac{\int \cos(\theta) P(\theta) d(\cos(\theta))}{\int P(\theta) d(\cos(\theta))} \tag{1.23}$$

It is a measure of the deviation of the scatterer from being isotropic and describes how much forward /backward scattering dominates. Theoretically, the asymmetry parameter can vary between –1 and +1. For particles with isotropic scattering properties, the average intensity in the forward and backward directions is equal, and hence g (λ) is 0. The asymmetry parameter of the cloudless atmosphere ranges from 0.1 (very clean) to 0.75 (polluted) while for a cloudy atmosphere, its value ranges from 0.8 and 0.9 [*Zege et al.,* 1991].

1.9. Chemical Characteristic of Aerosols

Aerosol due to different production mechanism and thus resulting to different size i.e. fine mode (Aitken or nuclei mode, accumulation mode) and coarse mode. Because of the different sources of the fine and the coarse particles, their chemical compositions also tend to be different. Coarse mode of aerosols generally comprised of soil elements over the continent and sea salt elements over the oceans. Over the land , major elements found in coarse fraction are Si, Al, Fe, K, Ti, Mn and Sr and these are often in the same ratio as they are found in the Earth' s crust material. [*Finlayson-Pitts and Pitts,* 1986]. However in the marine regions, aerosols characteristic of sea salt are found dominating. Most of the element found in coarse mode over the land or sea are involatile and relatively chemically inert; however few elements such as Cl, this is not true.

The fine particles on the other hand mainly arise from the gas-to-particle conversion and combustion, their chemical composition is however expected to be quite different that of the soil and ocean derived coarse particles. The major chemical components of fine particles are nitrate, sulphate, organic and elemental carbon and ammonium ions. The chemical composition of fine mode aerosols also contains a variety of trace metals from the combustion sources. Both the relative absolute concentration and relative proportion of these species in the particle depend on a number of factors such as the nature of emission, photochemical activity (solar activity) and meteorology (relative humidity).

The products expected from gas-to-particle conversion of SO^2, NO_x and NH^3, i.e. SO_4^{-2}, NO_3^- and $NH4^+$ are all found at significant concentrations in the fine particle phase [*Finlayson-Pitts and Pitts,* 1986]. There are also the variety of potential sources of the trace metals found in ambient particulate matter. These include the combustion of coal and oil (including gasoline), wood burning, waste incineration, and metal mining and production. There are also the natural sources of metals, such as windblown dusts, sea salts, forest fires, volcanic emissions, and emissions from vegetation. The elemental composition of aerosols has been related to their sources and it has been suggested that certain elements or ratio of elements may serve as tracers for various sources [*Rahn and Lowenthal,* 1984; *Shah et al.,* 1985]. Both in situ and filter extraction methods has shown that the sulphate may exist as H_2SO_4, $(NH_4)HSO_4$ or $(NH4)_2SO_4$ depending upon the available ammonia. The filter based analysis of chemical composition of aerosol by anion and cation analysis is most common. The method of study of chemical composition of aerosols, however depends upon the chemical component to be measured.

Interestingly, the aerosols and gases present in the atmosphere not only have a myriad of effects as discussed earlier, but can also change the composition of rainwater. While, aerosols and gaseous pollutants are scavenge due to rain, the scavenging of atmospheric pollutants in turns also affects chemical composition and pH of rainwater. Raindrops while falling, forms a complex chemical mixture with aerosols and gaseous pollutions before reaching to ground [*Chate and Devara,* 2009]. It is, thus crucial to study the influence of

pollutants (aerosols and gaseous) to rainwater by elaborating rainwater chemistry. Rainwater chemistry deals with the complex interaction between cloud dynamics and microphysical processes as well as series of rainout and washout atmospheric chemical reactions. The chemistry of precipitation reflects quality and quantity of emissions added to the atmosphere from natural and anthropogenic sources and helps in evaluating relative importance of different sources and estimating future possible acidification or buffering. The processes controlling the composition of rain are complex and influenced by both natural and anthropogenic sources.

1.10. Brief Overview of Aerosol Studies Over India

Over the Indian region, strong seasonal variations in aerosols are observed along with large spatial and temporal variations [*Moorthy et al.,* 2001]. In addition, the increase in aerosols emissions have also been reported over Indian region [*Ramachandran and Jayaraman,* 2003; *Streets et al.,* 2009; *Moorthy et al.,* 2013a; *Kurokawa et al.,* 2013]. Although recent studies of aerosols have significantly improved our understanding of physical, chemical, and optical properties of atmospheric aerosols, still uncertainties regarding their effects on the atmosphere and climate, are still high. The substantial uncertainties in the climate impact of aerosols, despite extensive studies in the last decades are pointed out recently in an elaborate way [*IPCC,* 2013].

Aerosols over the IGP region undergo strong seasonality in terms of the loading as well as aerosol type [*Singh et al.,* 2004; *Jethva et al.,* 2005; *Lau et*

al., 2008]. Aerosols as well as the gaseous emissions are high over the IGP region throughout the year. During spring and summer seasons, dust aerosols are transported from the northwestern arid regions to the IGP [*Middleton,* 1986; *Prospero et al.,* 2002; *Agnihotri et al.,* 2011]. Seasonal mineral dust is transported mainly from the Thar Desert in pre-monsoon season [*Hegde et* al., 2007]. Dust, when mixed with BC, plays a different role, as it leads to enhanced absorption ever greater than what observed solely due to BC in IGP [*Gautam et al.,* 2011].

Recent studies has reported increased warming, accompanied by earlier snow melt and retreat of high mountain glaciers over Himalayas [*Jain,* 2008] and Tibetan Plateau (TP) regions [*Flanner et al.,* 2009; *Menon et al.,* 2010]. In context to Himalayas, it is reported that BC received by the Himalayas and Tibetan Plateau (HTP) has increased by 41% from 1996 to 2010 [*Lu et al.,* 2012]. South Asia and East Asia are the main source regions, accounting for 67% and 17% of BC transported to the HTP on an annual basis [*Lu et al.,* 2012]. It is reported that the high concentration of BC over this region heats the atmosphere via so-called Elevated Heat Pump (EHP) and may lead to atmospheric water cycle feedback during the pre- and early monsoon seasons [*Lau et al.,* 2006]. The EHP modifies the energy balance between the atmosphere and the land over northern India and the Himalayas-Tibetan Plateau (TP) region, potentially changing the precipitation pattern of the Indian monsoon [*Lau et al.,* 2006, 2008; *Lau and Kim,* 2006] and accelerating the spring melting of Himalayan snowpack [*Lau et al.,* 2010].

However, calculating the full effect of BC emissions on global climate is complex due to myriad of effects (direct, indirect, semi-direct and snow-albedo effect) and source types (industrial, diesel, stoves, open biomass burning, etc.). The present day models also underestimate the actual ground based BC, thus the exact emission of BC are uncertain. The uncertainties associated with the exact emission of BC, its aging in atmosphere, exact transport and removal by precipitation is also high and these uncertainties directly propagates directly into the global model simulations as a result, estimates also poses significant uncertainties [*Bond et al.,* 2014].

The direct observations of these high BC concentrations in the atmosphere during pre-monsoon seasons have also been detected at the Nepal Climate Observatory Pyramid (NCO-P) in the form of brown clouds [*Bonasoni et al.,* 2008, 2010; *Marinoni et al.,* 2010] consisting of absorbed anthropogenic aerosols BC as well. BC concentrations of only 10 ng g^{-1} or more can significantly reduce snow albedo [*Hansen and Nazarenko* 2004, *Flanner et al.,* 2009], and thus even the small amount of BC reached/present in the Himalayas might be significant.

In India, systematic measurements of aerosols have been investigated extensively since the 1980's at different distinct geographical regions under I-MAP (Indian Middle Atmosphere Programme) and ISRO-GBP (Indian Space Research Organization, Geosphere Biosphere Programme) [*Moorthy et al.,* 1999]. The aerosol characteristics over few selected sites were initiated during I-MAP in the nineties. In the initial years, the attention was more on the

composite aerosol characterization and microphysics of aerosols which then later gradually shifted to more detail aerosol characterization of aerosol radiative implications, chemical nature and long-range transport. The regional efforts by the ISRO-GBP in 1998 also recognized the possible importance of BC aerosols to the climate system and pursued it in Aerosol Climatology Effects (ACE) Project [*Moorthy et al.,* 1999] and the aerosol monitoring program continued after I-MAP as part of the ACE (Aerosol Climatology and Effects) project of ISRO-GBP. Under the ACE program network of MWR (Multi Wavelength Solar Radiometer) systems was also setup to study aerosol optical depth over the distinct geographical regions over Indian.

In addition, in order to characterizing spatial heterogeneity of aerosols, road/land, LC-I was conducted during 2004 under the ISRO-GBP over Central/Peninsular India [*Moorthy et al.,* 2004]. The campaign was further continued as another campaign LC-II, in which aerosols with concurrent measurements from a network of eight stations spread across the Indo-Gangetic Plains was conducted, in order to study temporal changes, effects of long-range transport, mesoscale processes and local emission of aerosols [*Pant et al.,* 2006; *Dumka et al.,* 2006; *Nair et al.,* 2007]. The INDOEX campaign was however conducted from 1996 to 1998 [*Satheesh and Ramanathan,* 2000; *Ramanathan et al.,* 2001]. INDOEX campaign demonstrated the crucial importance of BC aerosols. It was found that despite contributing a mere 11% to the optical depth, BC could contribute as high as 60% to the radiative forcing of aerosols. The large difference in the tropical aerosol forcing at the

top of the atmosphere and Earth's surface was also reported [*Satheesh and Ramanathan,* 2000].

ICARB (Integrated Campaign for Aerosols, gases and Radiation Budget) campaign was conducted during 2006 over the oceanic regions and was the largest multi-instrumental, multi-platform field experiment ever conducted over these regions [*Moorthy et al.,* 2008]. The experiment revealed the latitudinal and longitudinal gradients of aerosols over oceans, significant advection from the East Asian regions into the Bay of Bengal (BoB), and more absorbing nature of aerosols over BoB compared to the Arabian Sea [*Nair et al.,* 2008]. The spatial synthesis was also reported over the oceanic regions [*Moorthy et al.,* 2008; *Babu et al.,* 2008]. In addition the vertical profiles of BC were also reported [*Satheesh et al.,* 2008]. The presence of elevated aerosol layers was also reported over most of the Indian region during the premonsoon season. The elevated aerosols layers were characterized by high extinction. The extinction coefficients were higher (up to 3 times) than near the surface. A substantial fraction (as much as 50 to 70%) of aerosol optical depth was contributed by aerosols above the clouds. Additionally the meridional gradient in the aerosol induced heating of the lower atmosphere was also reported.

The ARFI and ICARB are two major extensive national projects covering the detail aerosols characterization over the land and ocean regions of India. The ARFI project mainly focuses over establishing the network of observatories and aims at generating regional aerosol database, radiative forcing maps and

climate impact assessment. At present, the ARFI project has more than 33 stations of aerosol observation over the Indian region. The ICARB, on the other hand mainly focuses on the mega-field experiments, focusing on specific themes that feed to ARFI. Recently, realizing the importance of aerosols over the Himalayan region, Ganges Valley Aerosol Experiment (GVAX), was also conducted at Nainital in June 2011 for nine months [*Kotamarthi,* 2011]. The project was a joint collaboration under the ISRO and U.S. Department of Energy. In the campaign, the Atmospheric Radiation Measurement (ARM) Climate Research Facility, deployed its portable laboratory, the ARM Mobile Facility (AMF), to Nainital. Detail aerosol characterization was made utilizing multiple instruments. The aerosol absorption, radiative forcing, CCN activities and the role of boundary layer was studied along with other parameters in elaborate way over the Himalayan site [*Manoharan et al.,* 2014; *Dumka et al.,* 2014, 2015; *Gogoi et al.,* 2015 and others]. The campaign at Nainital provided useful information regarding aerosol characterization but the observations were limited for only nine months. The importance of long term continuous datasets of aerosols can't be ruled out at the site.

1.12. Scope and Significance of Present Study

The continuous increase of BC and other aerosols over northern India and southern slopes of Himalayas has attracted the global scientific interest in the view of climate implications. Aerosols from IGP can be transported to high altitude by enhanced convection and uplifting along the slopes of Himalayas and can have myriads of effects, once reached to Himalayas. Despite significant scientific interest, there are not much measurements of BC over the

Himalayas. The actual ground based observations of BC are also limited over the Himalayas in view of the topographic changes, although the number of observation sites has bit improved, yet the long term data set of BC over Himalayan region are very limited. Thus in the present study long term BC datasets from the high altitude site, Nainital in central Himalayas are extensively used for BC climatology and trend analysis. The multiyear climatological synthesis and trend of AOD over the central Himalayas are also reported. In addition, aerosol characterization from a low altitude semi urban location at Pantnagar, in the Indo-Gangetic Plain region, adjacent to Himalayan foothills are also made and reported. The possible sources of aerosols, their seasonality and processes governing the observed concentration or loading are discussed. An attempt has also been made to simulate surface BC from WRF-Chem and is compared with the ground based measurement of BC. Further, aerosols characteristics over the different environments is also studied and the other associated processes are discussed in detail.

Chapter 2

Measurement Techniques and Data Analysis

The science of aerosol measurement has significantly advanced over the past several years. From simple gravimetric measurements of airborne dusts in the early 1900s to the state-of-the-art instruments that can perform near instantaneous size and chemical composition measurements, the advances are indeed exciting and promising with wide implications. Aerosol measurements from both the ground based and satellite datasets are discussed here along with different data analysis tools.

2.1. Ground Based Measurements

2.1.1 Columnar Measurement of Aerosol Optical Depth

Ground based Aerosol Optical Depth measurements were carried out using hand held, portable multiband Sunphotometer MICROTOPS-II (Solar Light

Company, USA). It contains five different interference filters at 380nm, 440nm, 500nm, 675nm, and 870 nm wavelengths and provides AOD corresponding to these channels (Figure 2.1). The first MICROTOP-Sunphotometer (Serial number: 8429) is used to measure AOD at these five channels while another MICROTOP- Ozonometer (Serial number: 8438) with five channel is used for the retrieval of columnar Ozone, Water vapor and AOD at 1020 nm wavelength. The three channels of the MICROTOP-Ozonometer are utilized for the retrieval of columnar Ozone in UV wavelengths, while one for columnar water vapor at 940 nm and another for columnar AOD at 1020nm. AOD is determined assuming the validity of the Bouguer-Lambert-Beer law. The optical depth due to Rayleigh scattering is subtracted from the total optical depth to obtain AOD. AOD value at each wavelength is calculated based on the channel's signal, its extra-terrestrial constant, atmospheric pressure (for Rayleigh scattering), time and location. Solar distance correction is automatically applied. All optical thickness calculations are based on the Bouguer-Lambert-Beer law and AOD is determined using :

$$\mathrm{AOD}_{\chi} = \frac{\ln(V_{0\lambda}) - \ln(V_{\lambda} * \mathrm{SDCORR})}{M} - \tau_{R\chi} * \frac{P}{P0} \qquad (1)$$

Where λ references the channel's wavelength, ln (Vλ) is the AOT calibration constant, Vλ is the signal intensity in [mV], SDCORR is the mean Earth-Sun distance correction, M is the optical airmass, $\tau_{R}\chi$ is the Rayleigh optical

thickness, and P and P0 are station pressure and standard sea level pressure respectively.

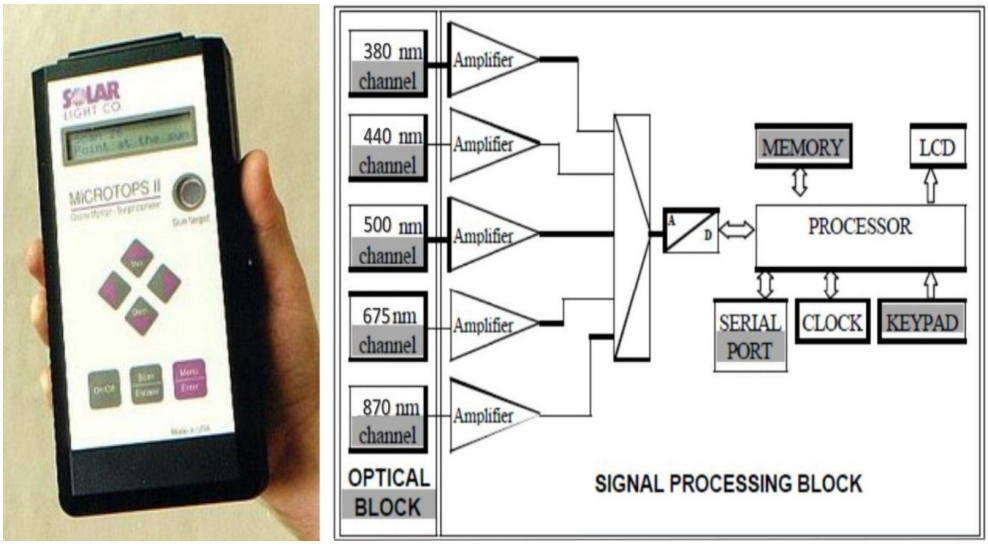

Figure 2.1: *Image of the instrument MICROTOP Sunphotometer (Left) and schematic diagram of AOD measurement by MICROTOP Sunphotometer (right).*

Cloud contamination has been avoided in measurements and data has been collected only when the region of sky of ~10° around the Sun was free from clouds. The data has been taken at half hour intervals during daytime) with a minimum of three consecutive observations at a time (within a short span <20 s). Out of these three successive observations, the one with minimum AOD at 500 nm was used for further analysis, to ensure better pointing of MICROTOP toward the Sun, as the minimum AOD correspond to maximum pointing

accuracy [*Morys et al.,* 2001; *Porter et al.,* 2001; *Ichoku et al.,* 2002]. Further details of MICROTOPS II, its calibration and performance are given in *Morys et al.,* [2001].

Each MICROTOP is equipped with accurately aligned optical collimators, with a full field view

of 2.5°. Instrument is integrated with the Internal baffles eliminate internal reflections. The individual channels are fitted with a narrow-band interference filter and a photodiode suitable for the particular wavelength range. The collimators are encapsulated in a cast aluminium optical block for stability. A sun target and pointing assembly is permanently attached to the optical block and laser-aligned to ensure accurate alignment with the optical channels. The image of the Sun is centered in the bull's-eye of the sun target assembly, at the same time all optical channels are oriented directly at the solar disk. The radiation captured by the collimator and bandpass filters radiate onto the photodiodes, producing an electrical current that is proportional to the radiant power intercepted by the photodiodes. The signals are first amplified and then converted to a digital signal by a high resolution A/D converter and are processed in series with 20 conversions per second. The filters used in all channels except 380 nm have a peak wavelength precision of ±1.5 nm, and a full width at half maximum (FWHM) band pass of 10 nm. The 380 nm channel has the wavelength precision of ± 0.4 nm, and a full width at half maximum (FWHM) band pass of 4 nm FWHM. The filters used in all channels have a peak wavelength precision of ±1.5 nm, and a full width at half maximum (FWHM) band pass of 10 nm.

2.1.2. AOD and Other Parameters From AERONET

Aerosol observation from AERONET (Aerosol Robotic NETwork) has been initiated by NASA's EOS and expanded by federation with many non-NASA institutions [*Holben et al.,* 1998, 2001]. The CIMEL sun/sky radiometer of AERONET takes measurements of direct Sun and diffuse sky radiances at eight spectral channels within the range from 340 to 1020 nm. AERONET was operational at Nainital during 2008-2009. The direct Sun measurements were made once every 15 min at 340, 380, 440, 500, 675, 870, 940, and 1020 nm. The uncertainty in AOD retrieval under cloud free conditions is less than ±0.01 for λ>440 nm and less than ±0.02 for shorter wavelengths. Here, we have used Level 2 quality assured data, which are pre and post field calibrated, automatically cloud cleared and manually inspected. The further detail regarding instrumentation, retrieval algorithms, data acquisition, etc. are well documented in *Holben et al.,* [2001], *Eck et al.,* [1999] and *Dubovik et al.,* [2000].

2.1.3. Black Carbon Measurement

Continuous measurements of BC mass concentration (also referred as 'BC') have been carried out using a seven-channel (0.37-0.95μm) aethalometer from Magee Scientific, USA. Aethalometer works on the principle of continuous filtration and estimation of optical absorption by using optical transmission [*Hansen et al.,* 1984]. Aethalometer measures light attenuation through a quartz filter and compute absorption coefficient by measuring the

difference in light transmission through particle laden sample spot and a particle-free reference spot of filter. The absorption measurements by Aethalometer at 0.88 μm wavelength is considered to be true measurement of BC in atmosphere, as BC is principal absorber of light at this wavelength [*Bodhaine,* 1995] and reported in earlier works [*Favez et al.,* 2009; *Cheng et al.*, 2010 and references within].

Generally, portable aethalometer (model AE-42) is used at Nainital and rack mount (model AE-31) is used at Pantnagar (Figure 2.2). During few occasions, portable aethalometer is used at Pantnagar mainly due to some technical problem in rack mount aethalometer. Both the instruments have been inter-compared by keeping them side by side with adjacent inlets at same heights. The comparison between two instruments reveals the correlation coefficient (R^2) of 0.9 (Figure 2.3).

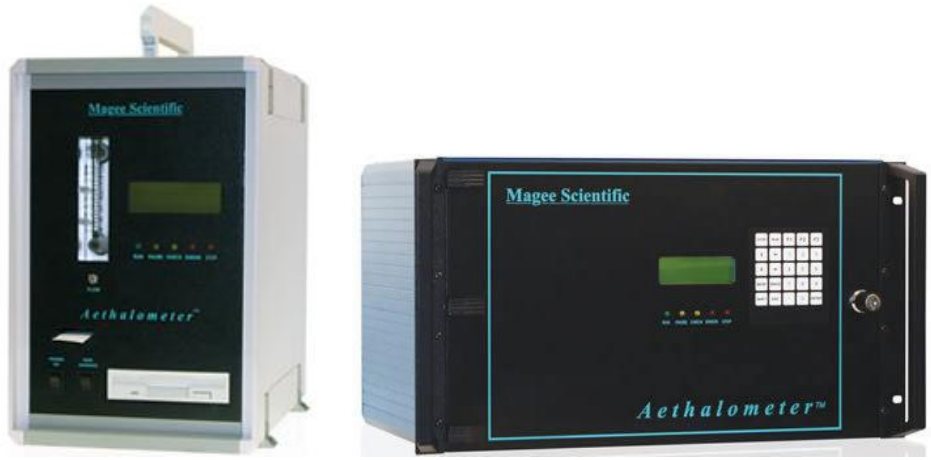

Figure 2.2: *Portable (model AE-42) and rack mount (AE-31) Aethalometers.*

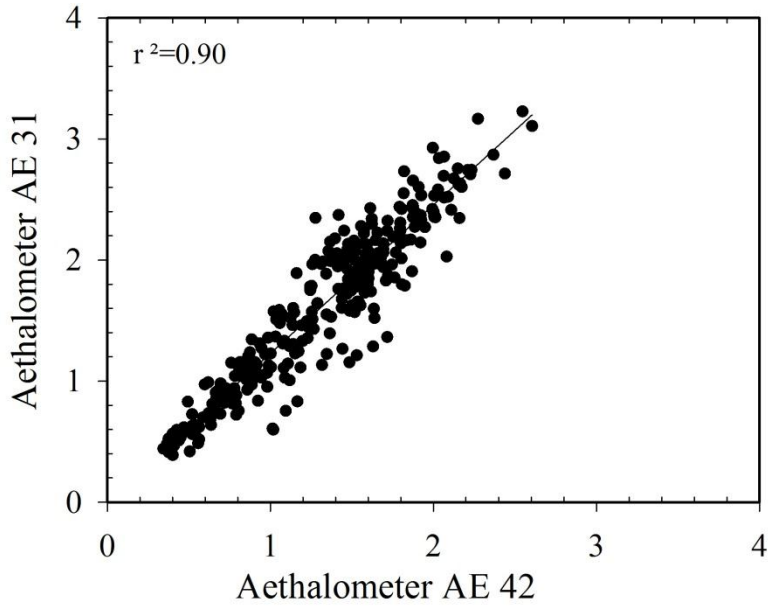

Figure 2.3: *Intercomparison between two aethalometers (AE-31 and AE-42) operated simultaneously. .*

The air samples are drawn into aethalometer through the inlet port using an internal pump. The flow rate is monitored by an internal mass flow meter and is stabilized electronically to the set-point value entered in software. The sample is collected on a quartz fiber filter tape within the instrument, and performs a continuous optical analysis (Figure 2.4), while the sample is collecting. During this process, the tape does not move. This method of BC measurement has also shown agreement with other analytic techniques and has been widely used [*Babu and Moorthy*, 2001; *Moorthy et al.*, 2004]. Although optical attenuation technique has been widely used but it is found that filter-based absorption techniques suffer from various systematic errors that need to be corrected.

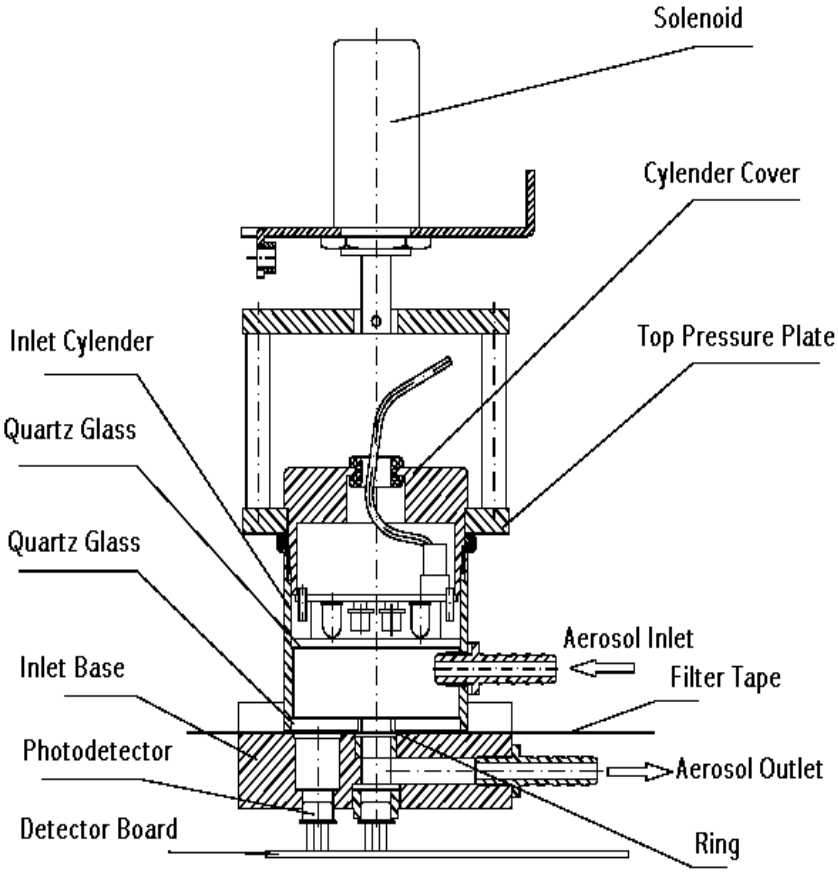

Figure 2.4: *Schematic diagram of optical analysis head of Aethalometer.*

Uncertainties in Aethalometer technique arises from multiple scattering effects in filter tape and from shadowing effects [*Weingartner et al.,* 2003; *Arnott et al.,* 2005]. In the present study, corrections for these are done following *Weingartner et al.,* [2003] and *Moorthy et al.,* [2007]. The maximum uncertainty for BC can reach 20% (ranging from ~40 to 60 ng m^{-3}), with higher percentage error for low mass concentrations [*Moorthy et al.,* 2007]. Additional details of instrumentation, methodology and uncertainty are discussed in a number of studies [*Hansen et al.,* 1984; *Nair et al.,* 2007].

The errors in the BC estimations are assumed to be about 50 ng m^{-3} about 2 to 5% of measured values and the errors can be up to 30% [*Müller et al.,* 2011]. However the BC measurements suffers from two main errors, first due to multiple scattering on quartz filter (C-factor) and the second due to the deposition of scattering material along with BC on filter tape called 'shadowing effect'(R-factor) [*Weingartner et al.,* 2003; *Arnott et al.,* 2005; *Sheridan et al.,* 2005; *Corrigan et al.,* 2006; *Hitzenberger et al.,* 2006]. The C-factor in the present case is 1.9 [*Dumka et al.,* 2010], and as the site generally receives the aged aerosols so the shadowing effect is negligible [*Weingartner et al.,* 2003; *Dumka et al.,* 2010]. Several others has also reported error budget in detailed [*Babu and Moorthy,* 2002, *Weingartner et al.,* 2003; *Arnott et al.,* 2005; *Sheridan et al.,* 2005 and *Corrigan et al.,* 2006].

BC measurement at Nainital have also been corrected for temperature and pressure to the measured BC concentration M_{B*} in accordance to the *Moorthy et al.,* [2004] in order to account for different pressure and temperature at the high altitude location in contrary to the standard value (standard temperature (T_0 = 293 K) and pressure (P_0 = 1013 hpa)), assumed in the BC mass concentration calculation. The corrected BC mass concentration M_B is expressed as follows

$$M_B = M_{B*}\left[\frac{P_0 T_1}{P_1 T_0}\right]^{-1} \qquad (2)$$

Where P_1 T_1 represents ambient pressure and temperature

2.1.4. Aerosol Number Concentration Measurement

The number concentration of composite aerosols at Nainital is carried out using optical particle counter (OPC), Grimm Series 1.108, Aerosol Spectrometer (Grimm Technologies, Inc., Douglasville, Ga) (Figure 2.5). The instrument measures number concentration at 15 channels (0.30 µm, 0.40 µm, 0.50 µm, 0.65 µm, 0.80 µm, 1.0 µm, 1.6 µm, 2.0 µm, 3.0 µm, 4.0 µm, 5.0 µm, 7.5 µm, 10.0 µm, 15.0 µm, and 20.0 µm) corresponding to particle in different size ranges. The continuous measurements of particles in the air are measured in one of two basic modes, particle counts and mass mode. The scattered signal from the particle passing through the laser beam is collected at approximately 90° by a mirror and transferred to a recipient-diode. The signal of the diode is feed, after a corresponding reinforcement, a multi-channel size classifier (Figure 2.6). A pulse height analyzer then classifies the signal transmitted in each channel. The ambient air is aspirated at a rate of 1.2 liters per minute via an isokinetic probe connected to the instrument kept in environmental housing.

The sample passes through the sample cell, past the laser diode detector and is collected onto the main dust filter (standard: external bottle filter, optional: 47-mm PTFE filter). The entire sample is collected on the optional PTFE filter, which can then be analyzed gravimetrically for verification of the reported aerosol's mass. The pump also generates the necessary clean sheath air, which is filtered and passes through the sheath air regulator back in to optical chamber. This is to ensure that no dust contamination comes in contact with the laser-optic assembly. This particle free airflow is also used for the reference-zero tests during the self-test. All particulate in the air passes the sampling inlet and enters vertically into the optical measurement cell.

Figure 2.5: *The optical particle counter (OPC). Top panels are the weather housing to keep the instrument, while lower panel shows the spectrometer.*

During the measurement process all particles are categorized in their proper size and as being larger than the largest size channel can only be categorized as such (i.e. particles classified with diameter > 32 um will be reported as such regardless of how much larger actually are). Practical experience has shown that very few particles above 10 μm are in the ambient air and rarely anything above 20 μm has been found (as count) over a 24h collection time.

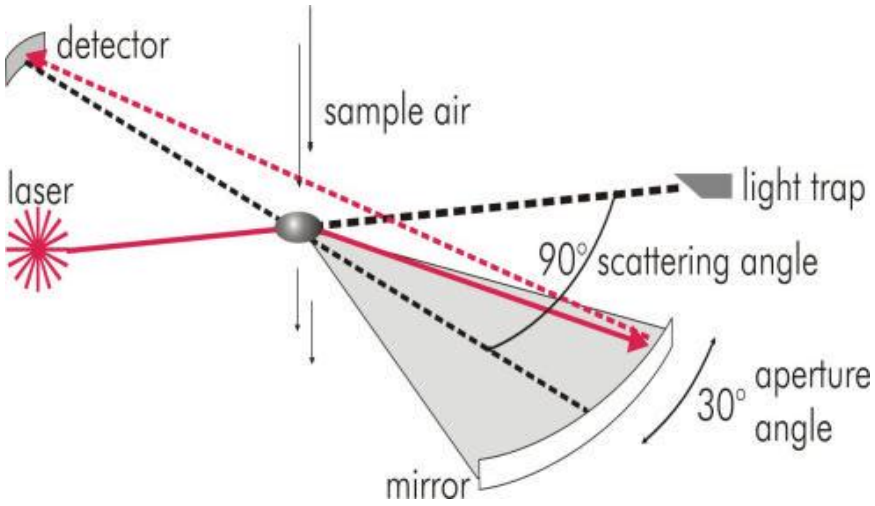

Figure 2.6: *The schematic of principle of measurement used in Optical Particle Counter (OPC).*

The sample air is not heated to avoid loss of volatile compounds before measurement. High humidity can cause an error in the dust monitor readings because water molecules and nuclear condensation can be misread as solid particles. For such a case the measurement unit requires a special dehumidifier. This has been done here by using a special dehumidification system build into the weather housing which does not heat or change the sample. The relative humidity is constantly monitored. If the value is below 65% the dehumidification system remains inactive. However above 65% relative humidity part of the already sampled air coming from the outlet of the dust monitor is fed through a silica gel drying cartridge. The air leaving the cartridge is filtered and lead via a tube to the top of the sample pipe in a mixer. Here the sample air is mixed with clean dry air in a ration 1:1. This will lower the dew point and prevent unwanted condensation.

2.1.5. Measurement of Meteorological Parameters

Continuous measurements of all the meteorological parameters like solar radiation, air temperature, pressure, relative humidity, wind speed, wind direction, and rainfall have been made using automatic weather station (AWS) (Campbell Scientific Inc., Canada, and Astra Scientific, India). Surface wind speed and wind direction data from AWS setup by Indian Meteorological Department was also used for Pantnagar. In absence of the observed meteorological parameters, data from space borne sensors have been used. The data from Global Data Assimilation System (GDAS; ftp://gdas-server.iarc.uaf.edu/gdas1/) was used every 6 hours at the spatial resolution of 1° x 1°. The rainfall data is taken from the Tropical Rainfall Measuring Mission (TRMM) at a spatial resolution of 0.25°x0.25° around observation site. More details of these are described in chapter 3 and chapter 4 for respective observation sites.

2.2. Satellite Measurements of Aerosols

The satellite based measurement from Moderate Resolution Imaging Spectroradiometer (MODIS:Terra and Aqua) and Multi-angle Imaging SpectroRadiometer (MISR) is also utilized in the study. The twin Moderate Resolution Imaging Spectroradiometer (MODIS) aboard the Terra and Aqua satellites were launched under NASA Earth Observing System (EOS) program to obtain daily remote measures of aerosols over the land and ocean, and to better understand the global aerosol budget. The Terra satellite was first launched on December 18, 1999 for observation at morning when it crossed the equator during the daytime at about 10:30 AM local time. The Aqua satellite was launched on May 4, 2002 for observing in the afternoon, and crossed the equator during the daytime at about 1:30 PM local time. The MODIS aerosol products, provide the ability to monitor spatial and temporal

characteristics of the aerosol field globally, over both land [*Kaufman et al.,* 1997] and ocean [*Tanré et al.,* 1997], using seven well calibrated spectral channels (0.47–2.1 μm). Radiance data are acquired by MODIS in 36 spectral bands, spanning 405 – 14,385 nm wavelengths, which range from the visible (VIS) through the near-infrared (NIR) and midinfrared (MIR) up to the thermal infrared (TIR) regions of the electromagnetic spectrum. They are acquired in one of three spatial resolutions at nadir: 0.25 km (bands 1 – 2: VIS), 0.5 km (bands 3 – 7: VIS-MIR), and 1 km (bands 8 – 36: VIS-TIR). These MODIS aerosol products have been comprehensively validated over land on a global scale [*Chu et al.,* 2002; *Remer et al.,* 2005; *Levy et al.,* 2007] by observations through the Aerosol Robotic Network (AERONET) [*Holben et al.,* 1998].

Additionally, data from MISR (Multi-angle Imaging SpectroRadiometer) aboard the Terra satellite (launched in December 1999) in a sun-synchronous orbit are also examined. The satellite utilizes the change in reflection at different view angles to distinguish different types of atmospheric particles (aerosols), cloud forms, and land surface covers. MISR instrument views the entire Earth's surface every 9 days, with repeat coverage between 2 and 9 days depending on latitude [*Diner et al.,* 1998, 1989; *Kaufman et al.,* 1998]. MISR acquires data in four spectral channels (blue, green, red, and near-infrared) with nine cameras pointed at fixed angles to observe reflected and scattered sunlight in four wavelength bands providing five viewing angles (0, 26.1, 45.6, 60.0, and 70.5 degrees). This unique design enables it to retrieve

tropospheric AOD, and aerosol size distribution over both land and ocean at a spatial resolution of 17.6 km [*Diner et al.,* 1998].

These satellite datasets are mainly used to characterize the spatial variation of the aerosols. The spatial variation of columnar AOD from MISR (MIS) at 555 nm and MODIS Terra (MOD) and MODIS Aqua (MYD) both at 550 nm are utilized. The spatial variation of AOD from MODIS Terra and Aqua were available at 1x1 degree resolution for Level 3 and 10 km for Level 2 while MISR data were available at 0.5 x0.5 degree resolution for Level 3 and 17.6 km for Level 2. The MISR Level 3 products are global or regional maps of select parameters from the Level 2 products and associated covariances reported on various geographic grids depending on the data product. The Level 3 datasets are used for regional analysis while Level 2 data are utilize to characterize aerorol loading at a particular site in the present study.

2.3. Aerosol Vertical Profiles From CALIPSO

CALIPSO mission was developed as part of the NASA Earth System Science Pathfinder (ESSP) program in collaboration with the French space agency CNES, with the goal of filling existing gaps in observing the global distribution and properties of aerosols and clouds [*Winker et al.,* 2003] in the troposphere and lower stratosphere. CALIPSO was launched together with the CloudSat satellite in April 2006 in the A-train constellation of satellites [*Stephens et al.,* 2002]. The satellites of the A-train are in a 705 km sun synchronous polar orbit, giving a 16-day repeat cycle, with an equator-crossing time of about 13:30 local solar time. CALIOP is the first polarization lidar to provide global atmospheric measurements of aerosol and clouds

around a solid-state Nd:YAG laser which produces simultaneous, coaligned, pulses at 1064 nm and 532 nm. The elastic backscatter observation are utilized at 532 and 1064 nm channels [*Winker et al.,* 2009]. The laser generates optical pulses which are about 20 nsec long (~6 meters) with nominally 110 mJ of energy at each of the two wavelengths and the output pulse energy at each wavelength is measured by energy monitors. The angular divergence of the transmitted laser beam is reduced by a beam expander to produce a beam diameter of ~70 meters at the Earth's surface. The laser pulse repetition frequency of 20.16 Hz produces footprints every 335 m along the ground. The instrument operates continuously, acquiring 1.7 million laser shots every 24 hours and providing observations during both day and night portions of the orbit. CALIPSO also carries two passive infrared and visible imagers sensors.

The retrieval algorithms for Level 2 data products require the assumption of an extinction- to-backscatter ratio (lidar ratio) to calculate profiles of particle backscatter and extinction coefficients from the Level 1 product of attenuated backscatter. A look-up table with lidar ratios at 532 and 1064 nm for six types of aerosol (dust, smoke, clean marine, polluted continental, clean continental, polluted dust) is applied for aerosol observations [*Omar et al.,* 2009]. Aerosol types and thus lidar ratios are assigned according to the geographical location of the measurement and the detected integrated attenuated backscatter and approximate particulate depolarization ratio. The six aerosol types are represented by aerosol models with a prescribed bi-modal size distribution (fine and coarse mode) and a characteristic complex refractive index for each mode and wavelength [*Omar et al.,* 2009]. The models are mainly based on the analysis of Aerosol Robotic Network (AERONET) observations, with some adjustments to generate lidar ratios that are in agreement with observations [*Winker et al.,* 2009; *Omar et al.,* 2009]. The lidar ratios follow directly from the aerosol models by Mie scattering calculations except for the mineral dust. The dust aerosol layers has

been classified in CALIPSO algorithm as those that having volume depolarization ratio greater than 0.075 [*Omar et al.,* 2009; *Mielonen et al.,* 2009].

The vertical profiles of aerosol extinction coefficient (532 nm) from CALIPSO [*Winker et al.,* 2009] version-3, 5-km horizontal resolution datasets are examined. The extinction coefficients are derived using the Hybrid Extinction Retrieval Algorithm (HERA) [*Young and Vaughan,* 2009]. The version-3 data products are latest which incorporate and address a number of factors contributing to the uncertainty in aerosol extinction retrievals. These products also provided the uncertainty associated with measurement and are used in present study.

Further accurate measurement of aerosol and cloud heights and the retrieval of extinction coefficient profiles are derived from the total backscatter measurements. The discrimination between ice clouds and water clouds and the identification of non-spherical aerosol particles is done by depolarization measurements. Additionally the various other information like the aerosol size and type of aerosols as smoke, dust, polluted dust etc. is also obtained from the ratios of the signals obtained at the two wavelengths. The daily CALIPSO images are also utilized in the present study.

2.4. HYSPLIT model for Back-Air Trajectories and Mixing Layer Depth

The airmasses, arriving at the observation sites have been investigated by examining back–air trajectories. These trajectories are calculated using Hybrid Single-Particle Lagrangian Integrated Trajectory (HYSPLIT) [*Draxler and*

Rolph, 2003; *Draxler and Hess*, 1998] model and employing NCEP/NCAR global reanalysis data. The trajectories are calculated at higher height than the actual altitude of the observation site in order to avoid the collision of trajectories with the surface. Further, mixing layer depth (MLD) estimation has also been done for different months using GDAS meteorological data as input in HYSPLIT and is calculated from the potential temperature profile by identifying the height of an elevated inversion at each grid point. The height at which the potential temperature first exceeds the value at the ground by 2 K is identified and assigned as MLD. Site specific details of trajectory setup are given in Chapter 3 and Chapter 4.

2.5. WRF-Chem Model Simulations

We have used version 3.6 of the Weather Research and Forecasting Model [*Skamarock et al.*, 2008] coupled with chemistry [*Grell et al.*, 2005] for simulating diurnal and seasonal variation in BC mass concentration at Pantnagar. The model domain is centered at Pantnagar (79.5^{o}E, 29.0^{o}N) and has (100, 100, 37) grid points in (longitude, latitude, vertical) directions. The horizontal grid spacing is 10 km and the model top is located at 50 hPa. The initial and lateral boundary conditions for the meteorological fields are obtained from the National Center for Environmental Predictions (NCEP) Final Analysis (FNL) fields available every 6h at a spatial resolution of 1^{o}x1^{o}. The resolved scale cloud physics is represented by WRF single moment 5-class scheme [*Hong et al.*, 2004] and sub-grid scale effects of convective and shallow clouds are parameterized according to the Grell 3D ensemble scheme [*Grell and Devenyi*, 2002]. For surface processes, the model setup uses the

Noah Land Surface model [*Chen and Dudhia,* 2001] and MM5 similarity scheme [*Beljaars,* 1994]. The vertical sub-grid scale fluxes due to eddy transport in the planetary boundary layer (PBL) and the free troposphere are parameterized according to the Yonsei University (YSU) boundary layer scheme. Rest of the model physics set-up is same as used by *Kumar et al.,* [2012] except that analysis nudging is applied above the planetary boundary layer.

Aerosol processes are represented by the GOCART bulk aerosol scheme [*Chin et al.,* 2002]. The GOCART model simulates five major tropospheric aerosol types including black carbon, sulfate, organic carbon, dust and sea-salt, assuming externally mixed aerosols. The GOCART model does not have an aerosol thermodynamics module. The emissions of sea-salt (four size bins) and dust aerosols (five size bins) are calculated online within the model. Anthropogenic emissions of BC, OC and SO_2, PM2.5 and PM10 are taken from Emission Database for Global Atmospheric Research (EDGAR) available at a spatial resolution of 0.1^o x 0.1^o [*Janssens-Maenhout et al.,* 2012]. The spatial distribution of anthropogenic BC emissions is shown in Figure 1c along with location of Pantnagar. Daily varying emissions of BC and other trace species from biomass burning are taken from the Fire Inventory from NCAR version 1 (FINN v1) [*Wiedinmyer et al.,* 2011] and distributed vertically in the model following the online plume-rise module [*Freitas et al.,* 2007]. Note that FINN v1 accounts only for open biomass burning and the residential biomass burning is included in anthropogenic emissions. The initial and boundary conditions for chemical fields are taken

from the Model for Ozone and Related Tracers-4 results. The simulations are conducted for January, May and July representing the winter, spring and summer/monsoon season. Each simulation started on the first day of the month and ran through the month. The model results are stored every hour for comparison with the observations.

2.6. Source Apportionment Studies

The multiyear long term BC mass concentration measurements at Nainital is used for source apportionment of BC and thus used to infer the spatial pattern of the potential sources of BC. Major pathways of BC reaching the receptor site and source/receptor study has been carried out that includes trajectory clustering and Concentration Weighted Trajectory (CWT) analysis. The high and moderate BC concentration sources are then identified by concentration weighted trajectory (CWT) method developed by *Seibert et al.,* [1994]. In this method, concentration values at receptor site are assign to corresponding backward trajectories, by assigning the measured concentration uniformly to all segments of its trajectory, using calculated mean as a weight for residence time of each grid cell. The trajectory calculation function is taken from Hybrid Single Particle Lagrangian Integrated Trajectory Model (HYSPLIT), [*Draxler and Hess,* 1998]. The measured BC concentration was assigned to the corresponding trajectories for cluster analysis, the nearest trajectories were combined according to angle distance by Ward's hierarchical method thus the direction, from which the air masses are reaching the site are identified. The average concentration to corresponding trajectories are assigned and calculated as follows:

$$Cij = \frac{1}{\sum_{l=1}^{M} \tau_{ijl}} \sum_{l=1}^{M} cl\ \tau_{ijl} \qquad (3)$$

where C_{ij} is average weighted concentration in the ijth cell

l is the index of trajectory

M is the total no of trajectories

c_l is concentration observed on arrival of corresponding trajectory l

τ_{ijl} is the time spent by the l^{th} trajectory in the ij^{th} cell

High values of C_{ij} is the indication of high concentration at receptor site which on average indicates that the air parcel traveling over corresponding ij^{th} cell would be contributing more to the observed high concentration at receptor site. By and large the uncertainty in analyzing the trajectory depends on the assumption in trajectory calculation.

2.7. Aerosol Scavenging: Rainwater Chemistry

Precipitation samples were collected by bulk precipitation sampler (Figure 2.7) and analyzed in collaboration with Indian Institute of Tropical Meteorology (IITM), New Delhi. Automatic rain collector consists of a polypropylene funnel (200 mm in diameter) connected to the bottle.

Figure 2.7: *Photograph of rainwater collector called Bulk Collector*

The sample bottle as well as funnel which are the part of collection gadgets has been cleaned twice in a day in the morning and evening, using triple distilled water to avoid dry deposition of gaseous and particulate species and to ensure quality control. Prior to interpretative analysis, data was screened to ensure analytical data quality, standardization and considering blank measurements. Collected samples of rainwater have been stored in small polythene bottles, which were cleaned by triple distilled water. Thymol (~5mg) was added to these samples for preventing biological degradation. All samples were refrigerated at 4^{o}C in the laboratory till the analysis was done.

Concentrations of F^-, Cl^-, NO_3^- and SO_4^{2-} were determined by Ion Chromatograph (DIONEX-2000, USA) using analytical column Ion Pac-AS15, anion micro-membrane suppressor ASRS-II, 38 mM sodium hydroxide/potassium hydroxide as eluent and triple distilled water as regenerator (Figure 2.8). After calibration through standards in the morning, at least three times standards were injected to see the variations of the radicals. In order to ensure the accuracy and precision of results, sometimes replicate samples were analysed at every 10th injection. The pH values of the samples were measured with the help of Elico make (model L1-120) digital pH meter. One of the fundamental and widely used tests to judge the acidity (or basicity) of an aqueous solution is to check the pH which is a negative decimal logarithm of the hydrogen ion activity in a solution, expressed as:

$$\mathrm{pH} = -\log_{10}\left(a_{H+}\right) = \log_{10}\left(\frac{1}{a_{H+}}\right) \qquad (4)$$

Where $a_{H}+$ is the activity of hydrogen ions in units of mol/l (molar concentration).

Figure 2.8: *Ion Chromatograph (Dionex, Model-2000)*

Conductivity was measured with a digital conductivity meter calibrated against a reference KCl solution. Pinch of (50-75 mg) thymol was then added to the samples to prevent bio-degradation and then the samples were kept in a refrigerator at 4^{o}C until the completion of all the analyses.

Chapter 3

Aerosol Optical Depth and Black Carbon over a High Altitude Site in the Central Himalayas

Aerosols emissions are reported to be increasing in India during recent years [*Streets et al.,* 2009; *Moorthy et al.,* 2013a; *Kurokawa et al.,* 2013]. Ground based aerosol observations over the Indian region has revealed increase of aerosol loading by 2.3% per year since 1985 [*Moorthy et al.,* 2013a]. The increase in aerosols emission is however not uniform, at some places aerosol emission has been reported to increase sharply while at other places increase is lesser or no increase has been reported. In addition, south Asian region is also believed to be one of the hot spots of BC aerosols [*Koch and Hansen,* 2005; *Lawrence and Lelieveld,* 2010] as well. These aerosols not only have a significant role in Asian monsoon, climate change, air quality, radiation budget, precipitation and amount of rainfall etc. but can also affect the

rainwater chemistry. In context to Himalayas, enhancement in aerosol load especially black carbon (BC) is very crucial. Enhanced BC extending up to the Himalayan glacier region, is significant and is found responsible for glacier retreats [*Menon et al.,* 2010] as it causes the decreases in snow surface albedo [*Flanner et al.,* 2009; *Yasunari et al.,* 2010]. The evidence of increased warming, accompanied by earlier snow melt and retreat of high mountain glaciers have been observed over Himalayas and Tibetan Plateau (TP) region [*Ramanathan et al.,* 2007; *IPCC,* 2007]. This rate of retreat has been reported to increase over western and central Himalayas in recent decades [*Raina and Sangewar,* 2007; *Jain,* 2008]. It is also reported that deposition of BC over snow and ice over the Polar and Himalayan regions would modify the albedo of snow [*Flanner et al.,* 2009]. It is found that coatings of snow on BC particles further enhances solar radiation [*Mikhailov et al.,* 2006].

Although the number of ground based stations has increase in recent years, still the numbers of ground based observations over the Himalayan region are sparse. Most of the present studies focused to either urban/semi-urban landmass or oceans adjacent to densely populated coastal belt and ground based observations from the high altitude regions in Himalayas are very less. Many ground based aerosol monitoring sites are established under Aerosol Radiative Forcing Over India (ARFI), Indian Space Research Organization, Geosphere Biosphere Programme (ISRO–GBP) project. Considering the importance of aerosols studies from a high altitude region of the Himalayas, the ground based observations were initiated at Mohal (31.9◦N, 77.11◦E,

altitude 1154 m amsl) in the Kullu valley [*Kuniyal et al.,* 2006], Hanle (32.78°N, 78.96°E, ~4250 m amsl) in western Himalayas [*Babu et al.,* 2011]. In the same sequence, a remote high altitude site at Aryabhatta Research Institute of Observational Sciences (ARIES), Nainital (29.4^{o}N; 79.5^{o}E, 1958m amsl) in the central Himalayas was also setup [*Sagar et al.,* 2004]. Variations in AOD (2002-2005) [*Dumka et al.,* 2009] and BC (2004-2007) [*Dumka et al.,* 2010] have been reported at this site.

Here, long-term changes (2005-2012) in BC and AOD are studied and utilized for source apportionment studies and climatological synthesis. In addition, aerosol number concentration data have been used to examine diurnal, seasonal variations and have been utilized to examine the influence of dust at the site. Data from Aerosol Robotic Network (AERONET) and space-borne sensors are also used. The rainwater chemistry is studied at Nainital. Thus the detail characterization of aerosols at the high altitude site, Nainital are made and presented in this chapter.

3.1. Observing Site and General Meteorology

The location of the observational site ARIES, Nainital (29.4^{o} N, 79.5^{o} E, 1958 m amsl), a high altitude site in the central Himalayas is shown in Figure 3.1. The clean and transparent night made the present site suitable for astronomical observations also. The observing site is located at a mountain top and has a unique topography. The high Himalayan Mountains are in north and northeast

side of the site while southwest region has low elevated plain regions merging to the Indo-Gangatic Basin. The observation site is ~2 km due south from main town of Nainital. The observation site is away from major anthropogenic activities and no industries are located in the main town of Nainital. Few small scale industries are located at low elevated nearby cities, Haldwani (423 m msl) and Rudrapur (209 m msl) at a distance of 20-40 km (aerial) from the site due south. The main town of Nainital is spread in an area of ~11.73 km^2. The total population of Nainital district is about 0.9 million. The mega city and country capital Delhi is located at a distance of ~225 km due southwest of the site.

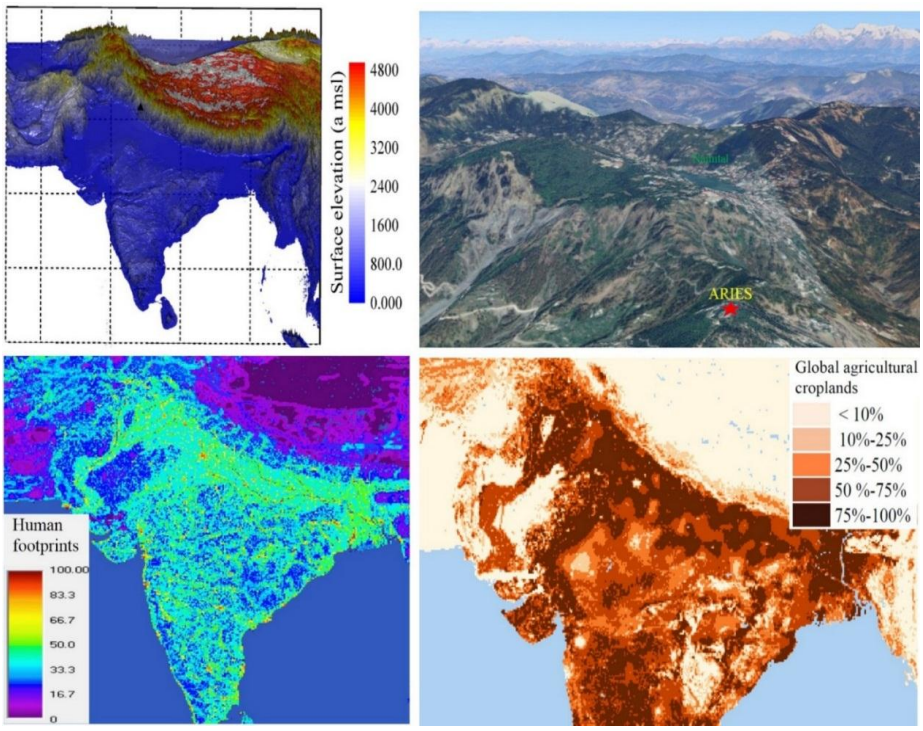

Figure 3.1: *Location of the observational site ARIES, Nainital (29.4 ^oN; 79.5 ^oE; 1958 m amsl) in the central Himalayas (a) the topography map of India (b) the zoomed topographic image of the region with marking of ARIES,*

Nainital. The high altitude Himalayas are also shown in the back. (c) The influence due to human footprints and (d) the agricultural cropland distribution is also shown.

Surface observations of meteorological parameters like temperature, wind speed, wind direction relative humidity and solar radiation are made using Automatic Weather Station (Campbell Scientific Inc., Canada, and Astra Scientific, India). The average meteorological temperature at the site is observed to be maximum during May-June (T_{max} ~ 31^{o} C) and minimum during January-February (T_{min} ~ -1.5^{o} C) (Figure 3.2) with annual mean temperature ~ 15^{o} C. The site also receives snowfall during few days. The relative humidity is maximum during monsoon season. The average humidity is ~95 % in July-August and remains moderate in all other months (38-55 %), with annual average RH ~ 62%. The site receives maximum rainfall during July to September ~83% of the annual rainfall. The rainfall in July–August month alone constitutes ~72% of the annual rainfall.

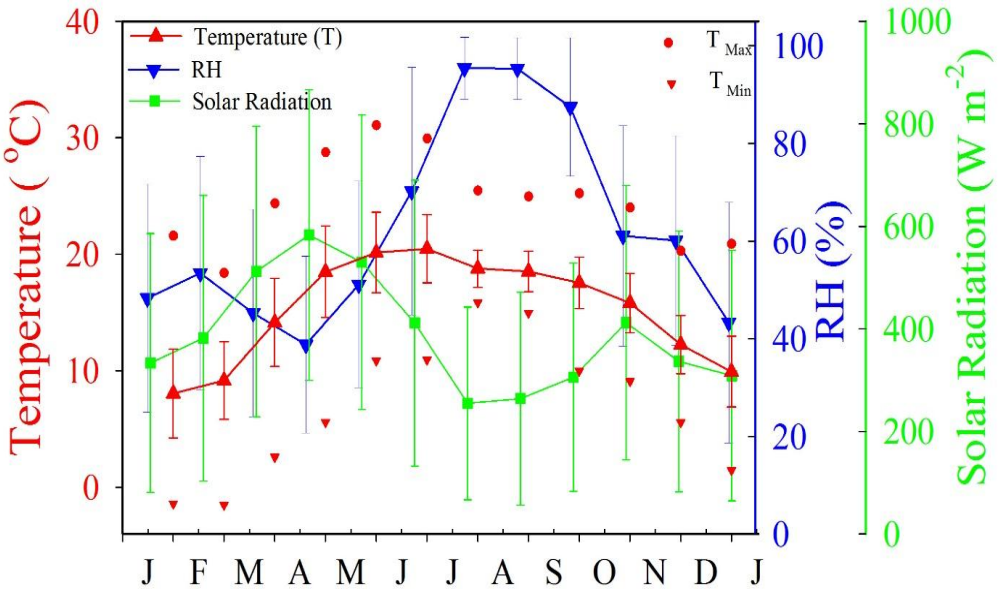

Figure 3.2: *Mean temperature, maximum and minimum temperature (°C), Relative Humidity (RH %) and solar radiation (W m^{-2}) during 2007-2012 at Nainital. Vertical bars are one standard deviation.*

Local surface winds are northwesterly during winter and southwesterly during summer. Solar radiation (0700 hrs to 1700 hrs) is minimum in July-August months due to prevalent cloudy and rainy conditions and is maximum in April. In addition, synoptic winds at 700 hPa are also examined and shown for different seasons i.e. winter (December-February), spring (March-May), summer-monsoon (June to August) and autumn (September to November) in Figure 3.3. The more detail discussion of the site and prevailing meteorological conditions can also be found in *Kumar et al.*, [2011].

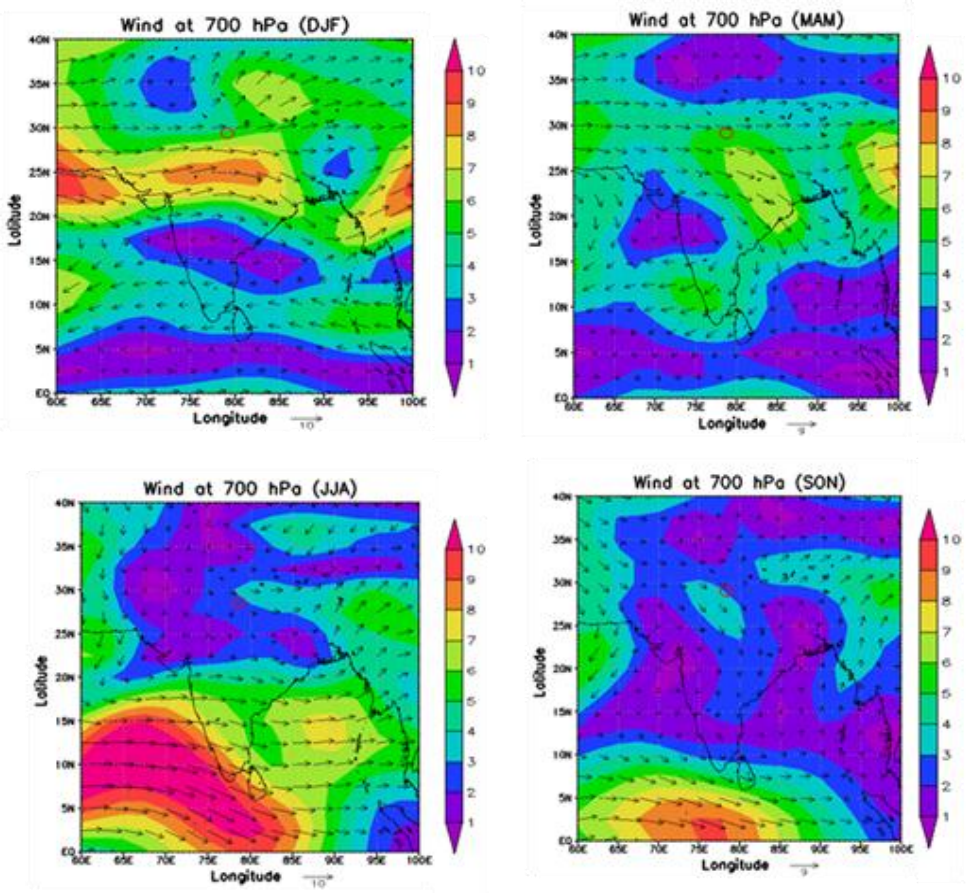

Figure 3.3: *Synoptic wind pattern at 700 hPa during four seasons in year 2009. Here, DJF, MAM, JJA, SON corresponds to winter (December to February), spring (March to May), monsoon (June to August) and autumn (September to November) seasons respectively. The observing site Nainital is shown by circle*

3.2. Daily, Seasonal and Annual Variations of Aerosol Optical Depth

The long term (2005-2012) data of aerosol optical depth (AOD) at Nainital are first examined for daily, seasonal and annual variations. AOD observations are taken using Microtops II Sunphotometer during full clear sky day conditions.

These data are converted to hourly AOD values and are then further used to calculate daily, monthly, seasonal and annual mean. AOD observation shows day to day variations. AOD increase each year after March and reach maximum in the month of May-June and then decreases, while lowest AOD is observed in December-January month. AOD value at shorter wavelength generally reaches above value of 0.4 during April-June month and shows higher standard deviation, while AOD at higher wavelengths shows less standard deviation during these months (Figure 3.4).

Table 3.1: *Climatological mean AOD at different wavelengths during year 2005-2012 at Nainital.*

Months	AOD380	AOD440	AOD500	AOD675	AOD870
January	0.14±0.08	0.11±0.07	0.11±0.06	0.08±0.04	0.08±0.04
February	0.17±0.07	0.15±0.07	0.14±0.07	0.10±0.05	0.10±0.06
March	0.28±0.18	0.24±0.14	0.22±0.12	0.17±0.09	0.16±0.08
April	0.38±0.21	0.32±0.17	0.29±0.16	0.21±0.13	0.21±0.12
May	0.42±0.16	0.43±0.19	0.38±0.17	0.29±0.12	0.26±0.12
June	0.38±0.17	0.37±0.14	0.33±0.13	0.26±0.10	0.23±0.11
July	0.26±0.17	0.21±0.13	0.19±0.11	0.14±0.09	0.13±0.08
August	0.14±0.07	0.15±0.10	0.14±0.09	0.12±0.06	0.11±0.05
September	0.26±0.10	0.21±0.08	0.18±0.08	0.15±0.06	0.13±0.04
October	0.23±0.10	0.18±0.08	0.15±0.07	0.12±0.06	0.11±0.06
November	0.15±0.08	0.15±0.08	0.13±0.07	0.10±0.05	0.08±0.05
December	0.20±0.12	0.11±0.06	0.10±0.05	0.09±0.05	0.11±0.10

Long-term (2005-2012) monthly average AOD value shows maximum in May in all five channels that is followed by June (Table 3.1). Monthly mean AOD at 500 nm is below 0.2, except during spring and early summer. The maximum AOD is found for the month of May when AOD (500 nm) reaches 0.38±0.17,

while AOD at 440 nm and 870 nm is found to be 0.43±0.19 and 0.26±0.12 respectively. The data statistics of AOD (500 nm) from hourly data reveals that AOD below 0.2 constitute 68 % of the data, while AOD up to 0.3 constitutes 83% (cumulative frequency) of the data, or in other word AOD data between 0.2-0.3 constitutes 15% of the data, while data between 0.3- 0.4 constitutes 8% while data above 0.4 constitutes 9% of the data.

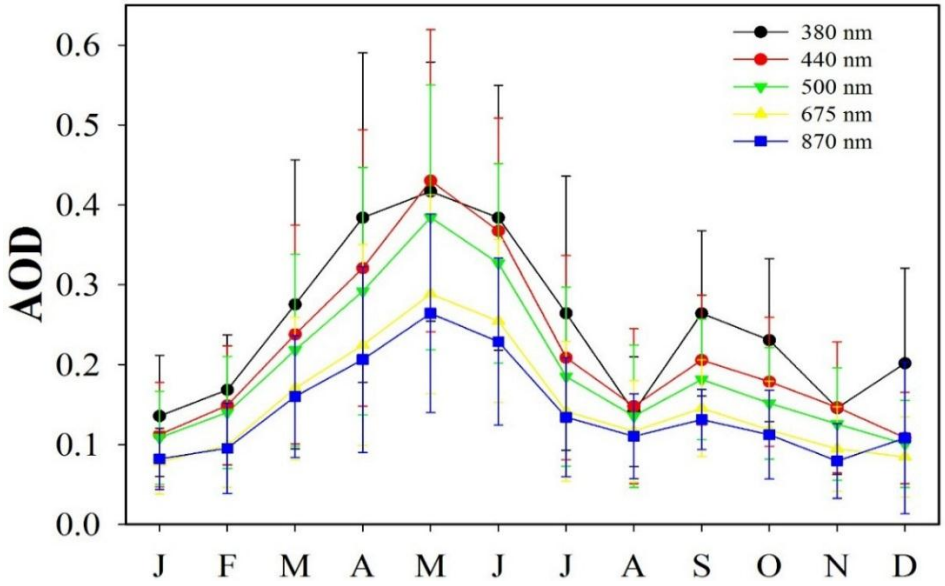

Figure 3.4: *Seasonal variation in monthly mean AOD at different wavelength at Nainital during 2005-2012.*

Monthly mean AOD as well as median AOD at 500 nm is shown in Figure 3.5. Monthly mean AOD is greater than 0.2 during March–June months. Monthly mean and median AOD shows less variation for some months while shows more variation for some other months. Mean AOD (500 nm) is low ~0.10 during January and December month. AOD increases in February (0.14±0.07) as compared to January month. The columnar abundance of

aerosols increases after the February month. AOD enhancement accelerates in the month of March 0.23±0.12 and continues till May-June month. Enhancement in AOD observed in the month of March, April, May and June month are estimated with respect to the February month which are found to be ~56%, ~108%, ~174% and ~133% respectively, while these enhancements with respect to the January month are much rapid ~101%, 169%, 253%, and 201% for the month of March, April, May and June respectively.

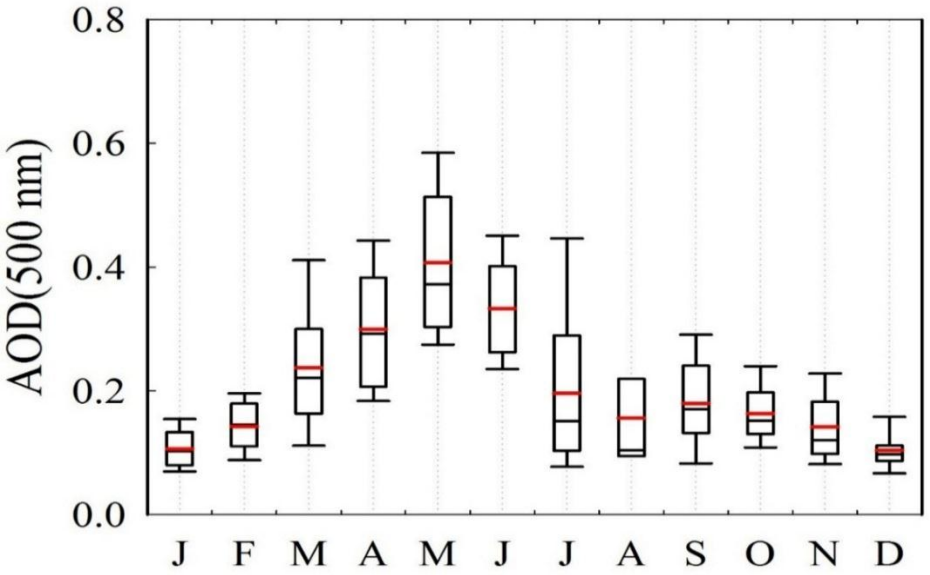

Figure 3.5: *Seasonal variation in AOD at 500 nm at Nainital during 2005-2012. The box plot shows the Mean AOD by thick dark red line within box and median is shown by black line within box. The lower and upper edges of the boxes represent the 25th and 75th percentiles. The whiskers below and above are 10th and 90th percentiles while the data point outside the box represents 5th and 95th percentiles.*

Seasonal mean AOD at 500 nm is observed to be ~0.117, ~0.298, ~0.216, and ~0.153 in winter, spring, summer-monsoon and autumn respectively. The annual AOD (500 nm) varies from ~0.08 to ~0.26 during different years with mean AOD of ~0.15 (climatological). The mean annual (climatological) AOD at the wavelength of 380 nm, 440 nm, 550 nm, 675 nm and 870 nm are 0.25±0.17, 0.21±0.15, 0.19±0.14, 0.14±0.11, and 0.14±0.10 respectively. AOD values are maximum in spring and lowest in winter. The percentage enhancement in seasonal AOD with respect to winter is estimated, which reveals the percentage enhancement of ~155%, ~85%, ~31% in spring, summer-monsoon and autumn respectively. The observed AOD at Nainital exhibit seasonal as well as the wavelength dependent characteristics. AOD at 380, 440, 500, 675 and 870 nm wavelength increases to 112%, 168%, 155%, 161% and 121% percentage respectively in spring as compared to the winter. The percentage enhancement in summer-monsoon is observed to be ~56%, ~96%, ~85%, ~96%, and ~66% respectively as compared to winter.

Seasonal variation of AOD reaches lowest in winter and increases after winter mainly due to biomass burning, enhanced anthropogenic activities and transport of dust. Biomass burning activities in the entire northern India region enhances the surface as well as columnar loading significantly. The dust loading in May–June month further exaggerates the columnar loading of aerosols. Aerosols from the IGP region are also uplifted due to convective turbulent mixing in spring which might transport aerosols to the high altitudes regions of adjacent Himalayas. The present of elevated level of aerosols have

also been reported over different location in India during this season. The columnar loading of aerosols reduces as soon as marine air masses arrives at the site mainly due to aerosol scavenging. It is interesting that AOD reduces as soon as the arrival of monsoon, however lowest AOD is not observed in the summer-monsoon rather it is observed lowest in winter season. The growth of aerosols due to the high humidity might be possible reason for the same. It is reported that more precipitation in the summer-monsoon could increase the water vapour content in the atmosphere consequently increase in AOD is observed due to high relative humidity [*Yoon.,* 2006; *Deng et al.,* 2012]. Aerosols can easily absorb moisture and grow during this period.

3.3. Spectral and Diurnal Variation of Aerosol Optical Depth

Spectral variation of AOD for each month has been examined over the period and is shown in Figure 3.6. Spectral variation shows that AOD at lower wavelength is higher and AOD at higher wavelength is lower. The observed spectral pattern i.e. decrease in AOD with wavelength, is consistent with the Mie scattering theory of aerosol particles. It is examined that spectral variation shows less variation from November to February month.

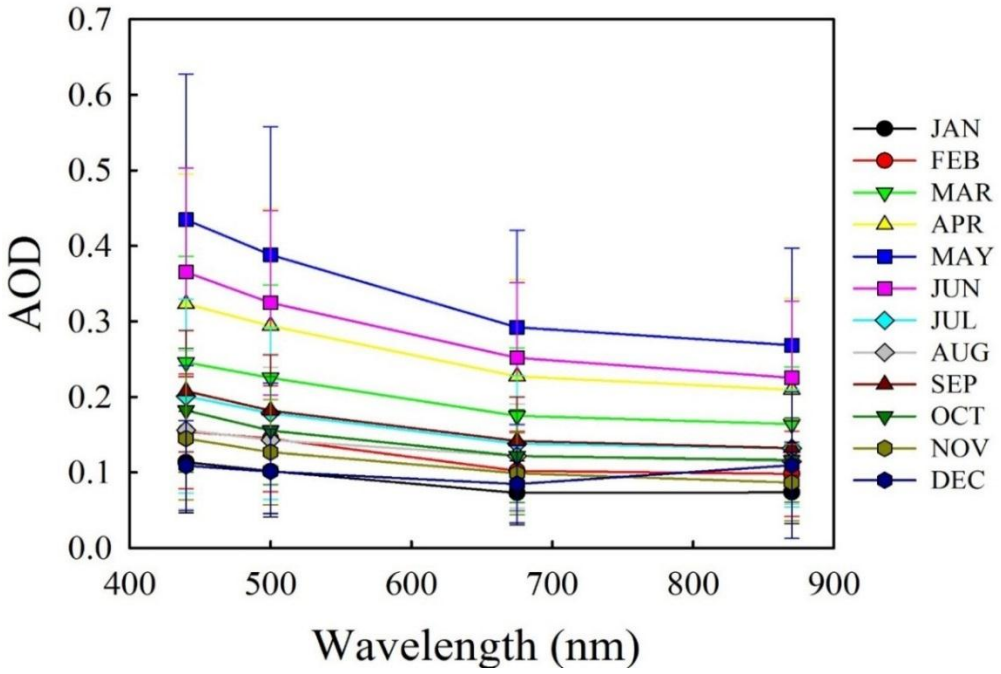

Figure 3.6: *Spectral variation in AOD for different months during 2005-2012 at Nainital. The error bars represents one sigma deviation.*

The spectral variation shows large variation from March which continues till the month of June. AOD at the lower wavelength is found to be above 0.3 from April till June month and is below 0.3 during other months, while AOD at the higher wavelength is above 0.2 from April till June month, and is below 0.2 in other months. The increase spectral variation both at the lower as well as the higher end during the April to June month indicate the increase in the both the small size aerosols as well as the large size aerosols at the site. The standard deviations of AOD spectra at the lower wavelength are large which indicate large day to day variability in the fine aerosols as compared to the coarse mode aerosols.

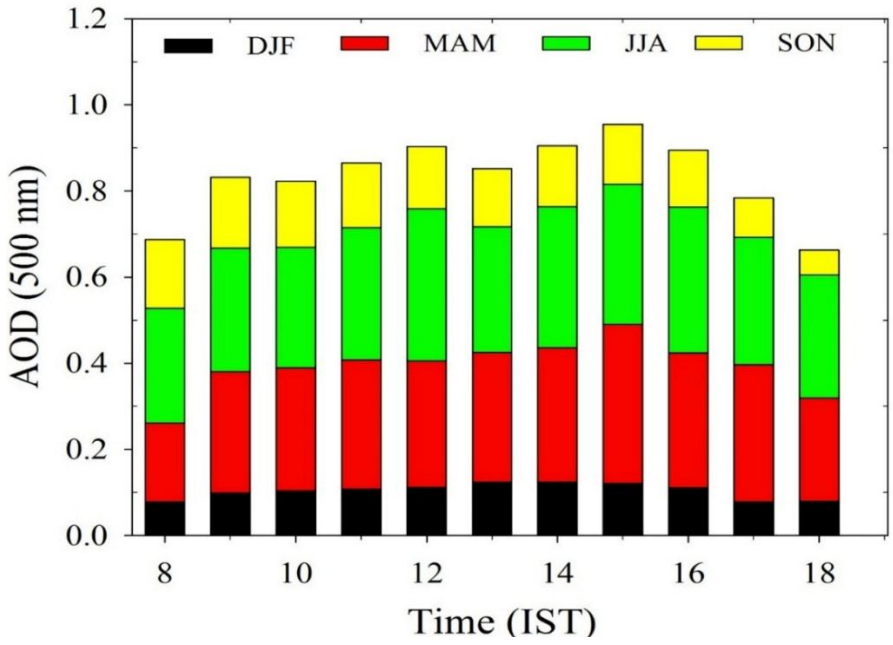

Figure 3.7: *Diurnal variation of AOD at 500 nm during different seasons (2005-2012) at Nainital.*

Figure 3.7 shows average (2005-2012) diurnal variation in AOD (500 nm) during four seasons. Since AOD is a columnar characteristics and not a surface characteristics so the diurnal variation in AOD are not quite sharp as compared to the diurnal variations in the surface characteristics which are directly influenced by the boundary layer characteristics.

3.4. AOD Characterization Utilizing AERONET Data

Aerosol RObotic NETwork (AERONET) was operational at ARIES during 2008-2011 and this dataset is used in addition to ground based AOD data from

MICROTOP. The instrument possess the radiometer which makes two basic measurements, either direct sun or sky, both within programmed sequences. The direct sun measurements are made in eight spectral bands requiring approximately 10 seconds during daytime starting at an air mass of 7 in the morning and ending at an air mass of 7 in the evening at eight spectral band 340, 380, 440, 500, 670, 870, 940 and 1020 nm. Channel at 940 nm is used for determining column water abundance while rest of channels are used for AOD measurements. AOD is calculated from the spectral extinction of direct beam radiation. AERONET data set is also utilized for the fine mode and coarse mode of aerosols along with the size distribution, SSA and other parameters.

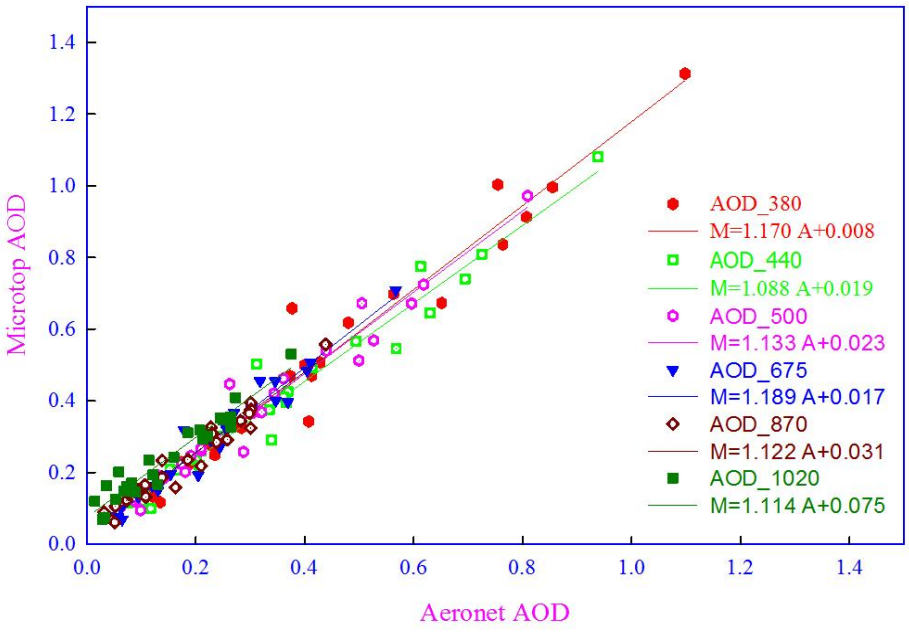

Figure 3.8: *Correlation of AOD measured with AERONET and MICROTOP at Nainital during year 2008.*

AOD at six wavelengths, five of which i.e. 380 nm, 440nm, 500nm, 675nm and 870 nm are obtained from the MIRCOTOP (Serial no: 8429) while AOD

at 1020 nm is obtained from the second MICROTOP (Serial no: 8438). Correlation of level 2 AOD data from AERONET with that from MICROTOP is shown in Figure 3.8. Daily average AOD measurements during same day are used for the comparison. AOD shows good correlation between two instruments and (R^2) have been found to be ~0.96, 0.96, 0.96, 0.95, 0.96, and 0.92 for 380 nm, 440 nm, 500 nm, 675 nm, 870 nm, and 1020 nm wavelength, respectively. A good correlation between AERONET and MICROTOP data indicate that data from both the instruments are in well agreement with each other.

Fine and coarse mode of aerosols are further studied using AERONET data. These coarse and find mode of AOD are based on *O'Neill et al.,* [2003] and are extracted based on the facts that the aerosol particle size distribution is effectively bimodal. Temporal and monthly mean variation of fine and coarse mode of aerosols is shown in Figure 3.9. It is examined that coarse mode of aerosols usually shows similar seasonal variation as shown by the angstrom exponent. Coarse mode of aerosol usually shows low as compared to the fine mode of aerosols, but coarse mode shows large enhancement even greater than the fine mode of aerosols (Figure 3.9**)** usually from March-June, while fine mode of aerosols is usually higher from October-February months and most of the total AOD is contributed by fine mode of aerosols, while from March-June most of the total AOD is contributed by coarse mode of aerosols. Association of total AOD with the fine and coarse mode is also studied.

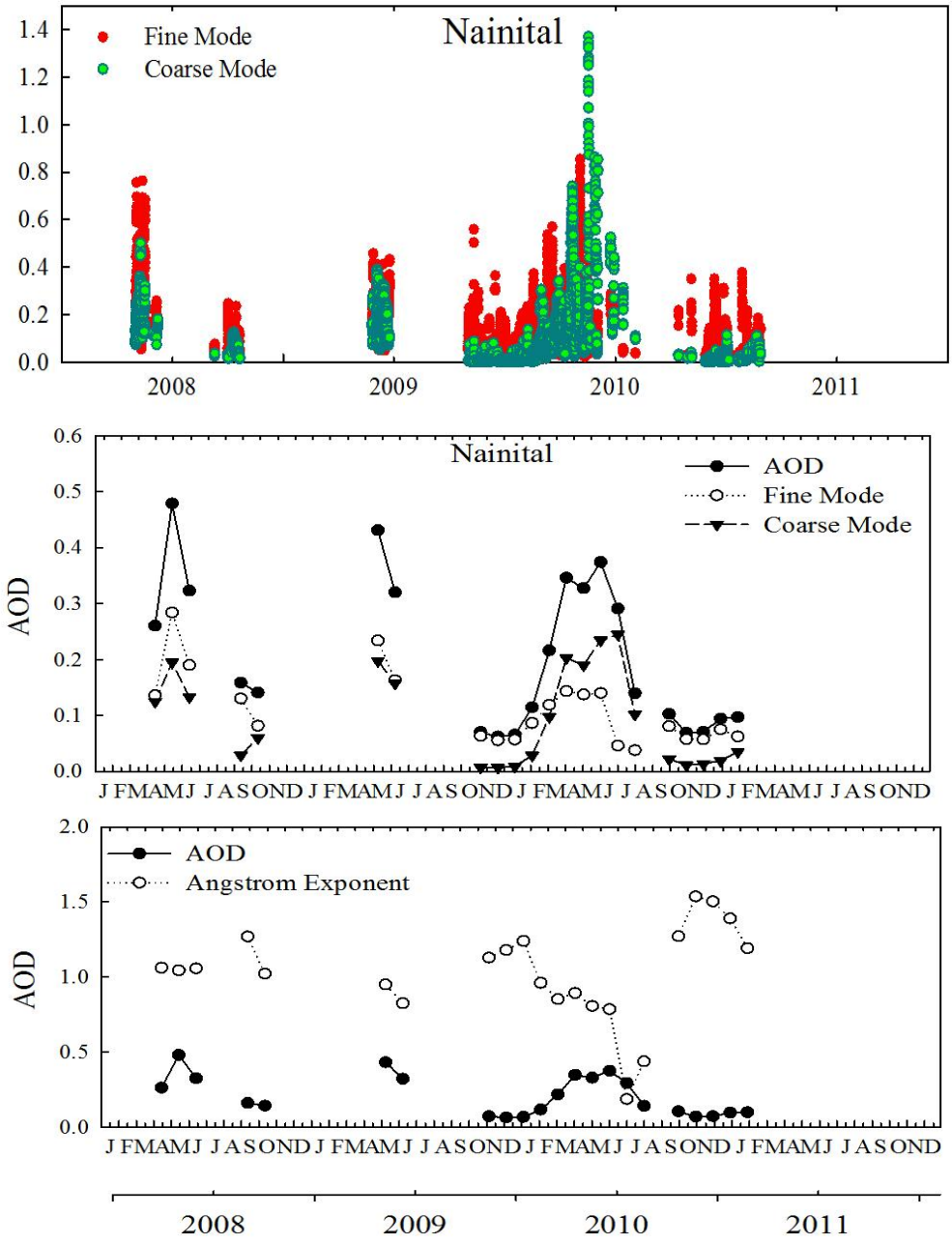

Figure 3.9: *Temporal (upper panel) and monthly variation of fine and coarse mode of aerosols during year 2008-2011. The lower panel shows the*

simultaneous variation of AOD and angstrom exponent during the observation period at Nainital.

The variation in angstrom exponent is also examined, which determines whether the aerosol loading is dominated by fine mode or coarse mode particles. The angstrom exponent (AE), is characterized by the logarithms of aerosol optical depth and wavelength as follows:

$$AE = -\frac{d\ln(\tau(\lambda))}{d\ln(\lambda)} \quad (1)$$

Here, AE is calculated for wavelength range from 440 to 870 nm, utilizing a linear fit of τ versus λ on a logarithmic scale. Seasonal variation in AE (440-870 nm) shows a clear and distinct change in aerosol size which is different from AOD. Seasonal variation of angstrom exponent shows high values from November to February month (Figure 3.9) which then decreases afterwards. Monthly mean angstrom exponent shows value greater than 1 during this time indicating the presence of fine mode of aerosols while angstrom exponent is low from March to June month. Angstrom exponent is observed to be lowest for the month of June which indicates the presence of coarse mode of aerosols.

Seasonal association of AOD with fine and coarse mode of aerosols is shown in Figure 3.10, which reveals high correlation of total AOD with fine AOD in winter (0.89) and autumn (1.0) followed by summer-monsoon (0.60), and

minimum in spring (0.36). Correlation of total AOD with coarse mode revels minimum correlation in winter (0.20) while in spring, summer-monsoon and autumn correlation is ~0.73, 0.93 and 0.81 respectively. The high fine mode correlation and low correlation in coarse mode during winter implies that most of the columnar aerosols loading possess fine mode of aerosols. While in spring season correlation of coarse mode of aerosols is high as compared to fine mode aerosols which indicate the dominance of dust load during this season. Aerosol swells in presence of high humidity in monsoon due to which aerosols are present in coarse mode during summer-monsoon. In autumn, the numbers of data points are quite less to infer any conclusion. Further detail investigation regarding the identification of episodic enhancement in fine and coarse mode is given in later section.

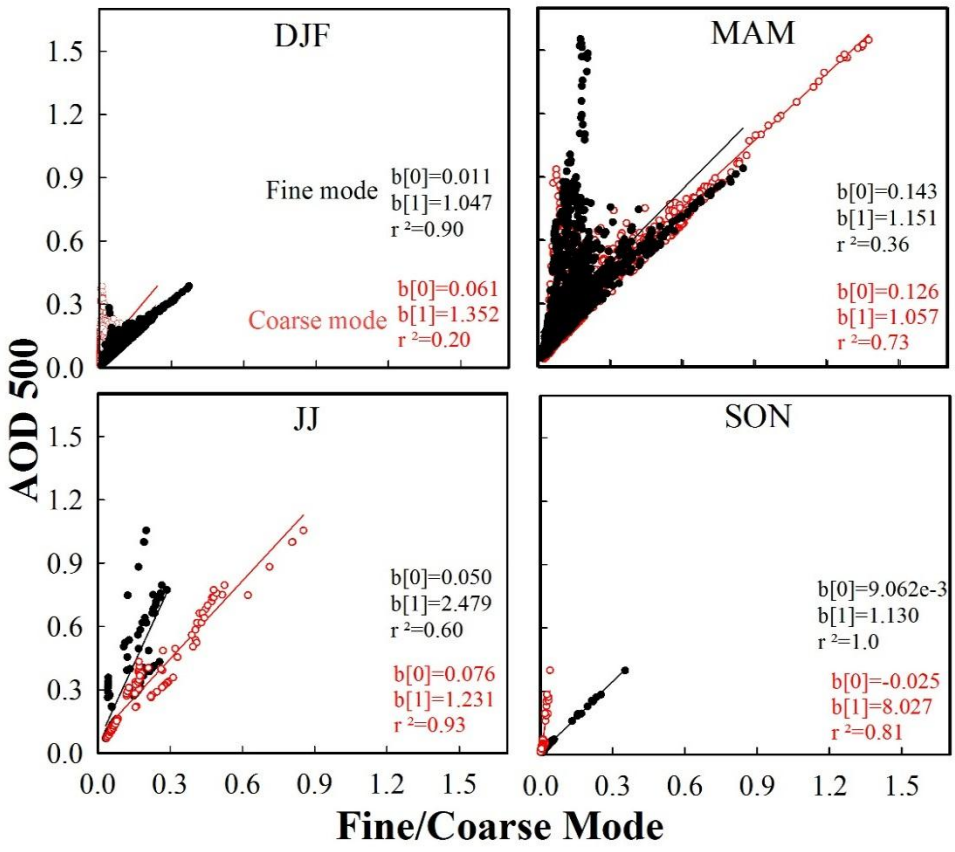

Figure 3.10: *Correlation of AOD at 500 nm with fine and coarse mode aerosol during the observational period at Nainital.*

3.4.1. Size Distribution of Aerosols at Nainital

AERONET data has also been used to study size distribution of aerosols at Nainital. Seasonal variation of volume size distribution of aerosols is shown in Figure 3.11. Size distribution of aerosols shows low value from November to February and fine mode of aerosol is bit higher in these month and coarse mode is low. Fine and coarse mode of aerosols enhances in the month of March. Enhancement in fine and coarse mode peak in the volume size distribution accelerates from April to June. Although enhancement in fine

mode is also seen during this period, but enhancement in coarse mode is quite high as compared to fine mode. The maximum peak in fine mode and coarse mode is seen in the month of May followed by April. The enhancement in the volume concentration of coarse mode with respect to the fine mode of aerosol is found to be ~ 300% and ~367 % in May and June respectively.

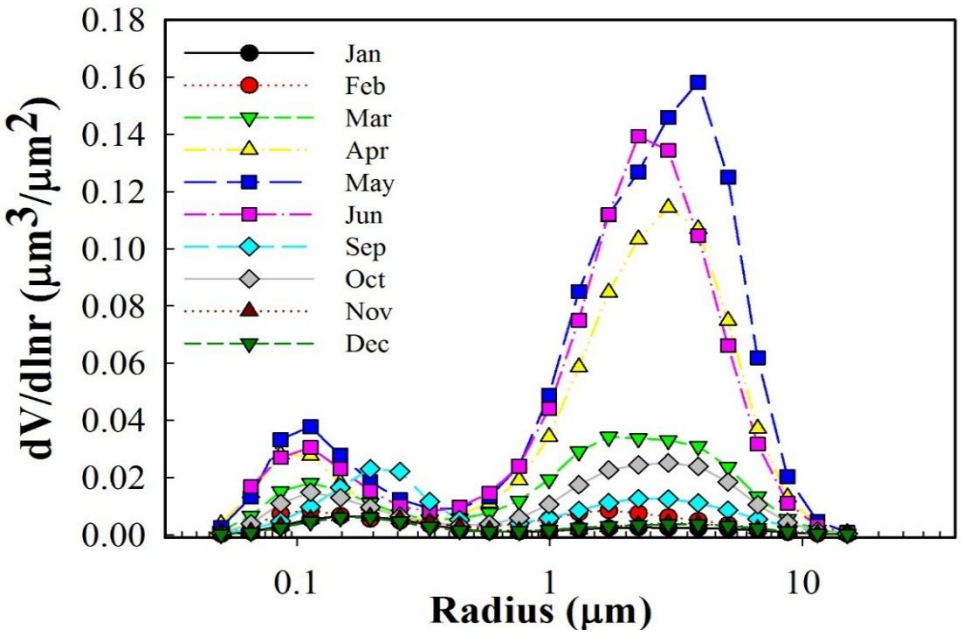

Figure 3.11: *Seasonal variation of aerosol columnar volume size distribution over Nainital using AERONET measurements during the period 2008–2011.*

3.5. Trend in AOD Variations at Nainital

Long term AOD observations (2005-2012) at the high altitude site Nainital are used for determining trend in aerosol loading at the site. The clear sky and filtered hourly AOD values are used to calculate monthly mean AOD.

Monthly mean AOD values are then smoothed (Figure 3.12). The linear trend in AOD shows slightly increasing trend with the trend of 0.0008-0.001 per year. The slight increasing trend is observed over the site indicate that the aerosol loading might have increased over the site during 2005-2012.

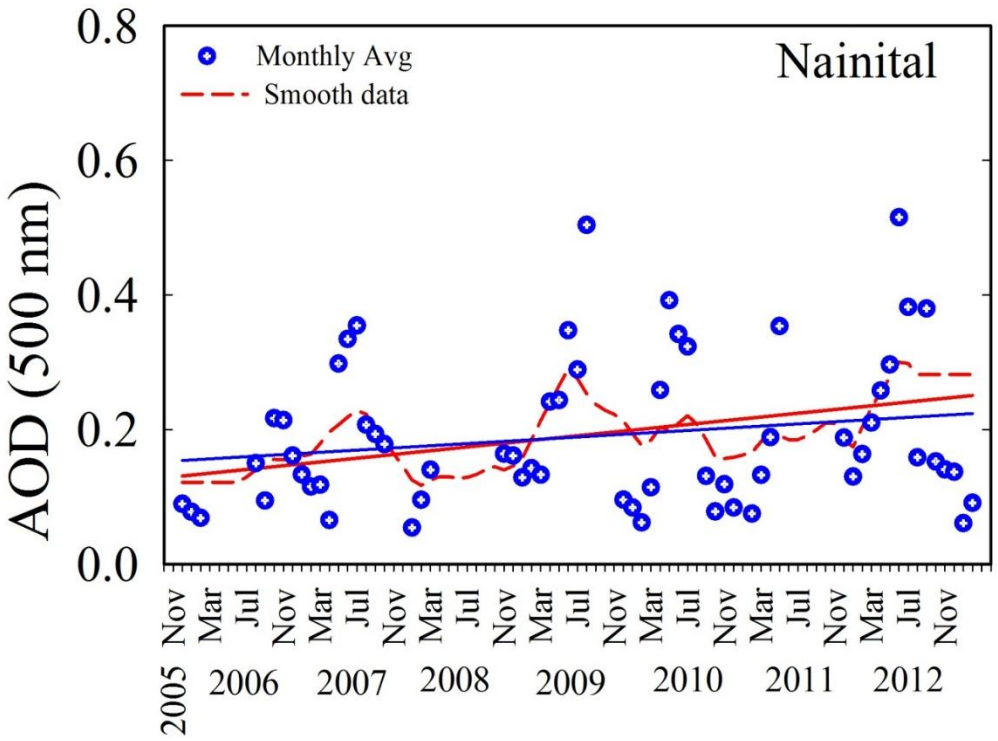

Figure 3.12: *AOD trend at 500 nm wavelength at Nainital from year 2005 to 2012.*

It has been reported that AOD is increasing at a rate of 2.3% per year and the rate of increase was more rapidly (~4%) during the last decade [*Moorthy et al.*, 2013a]. The concern was also aroused over the rising AOD trend and it was mention that AOD at several Indian locations would double if the present increase might continue in next few decades as a result of which aerosol-induced lower atmospheric warming might also increase by a factor of two. It

was also reported that AOD over the central India was undergoing increase at a higher rate as compared to the northern India or southern India. Increasing AOD trends over some stations were more pronounced as compared to the other stations. The major fraction of this increased aerosol loading was also reported to be of anthropogenic origin.

In another study by *Ramachandran et al.*, [2012], aerosol seasonal and annual trends were estimated using MODIS data over different locations in India and showed that AOD increases at some locations while some of the locations show decrease in AOD. Aerosols trends over most of the major cities in India show positive trend. A slight negative trend in annual mean AOD was found over four locations i.e. Shimla, Chandigarh, Dehradun and Trivandrum. Aerosol trends were higher for the locations in west and south India. Although the satellite data also cover the pollution load pretty well, however satellite measurement at different location always have some offset with the ground based data and both measurement differ by some amount, considering this the ground based observations are important for representing aerosols trends.

3.6. AOD Characterization Utilizing Satellite Datasets

The satellite based measurement from Moderate Resolution Imaging Spectroradiometer (MODIS:Terra and Aqua) and Multi-angle Imaging SpectroRadiometer (MISR) are utilized in the study. Ground based data is mainly used to characterized columnar loading at Nainital, while data sets

based on satellite data are mainly used to characterized the spatial variation of aerosols. Spatial variation of columnar AOD from MISR (MIS) at 555 nm and MODIS Terra (MOD) and MODIS Aqua (MYD) both at 550 nm are shown in Figure 3.13 for winter (December to February: DJF) and autumn season (September to November: SON) season.

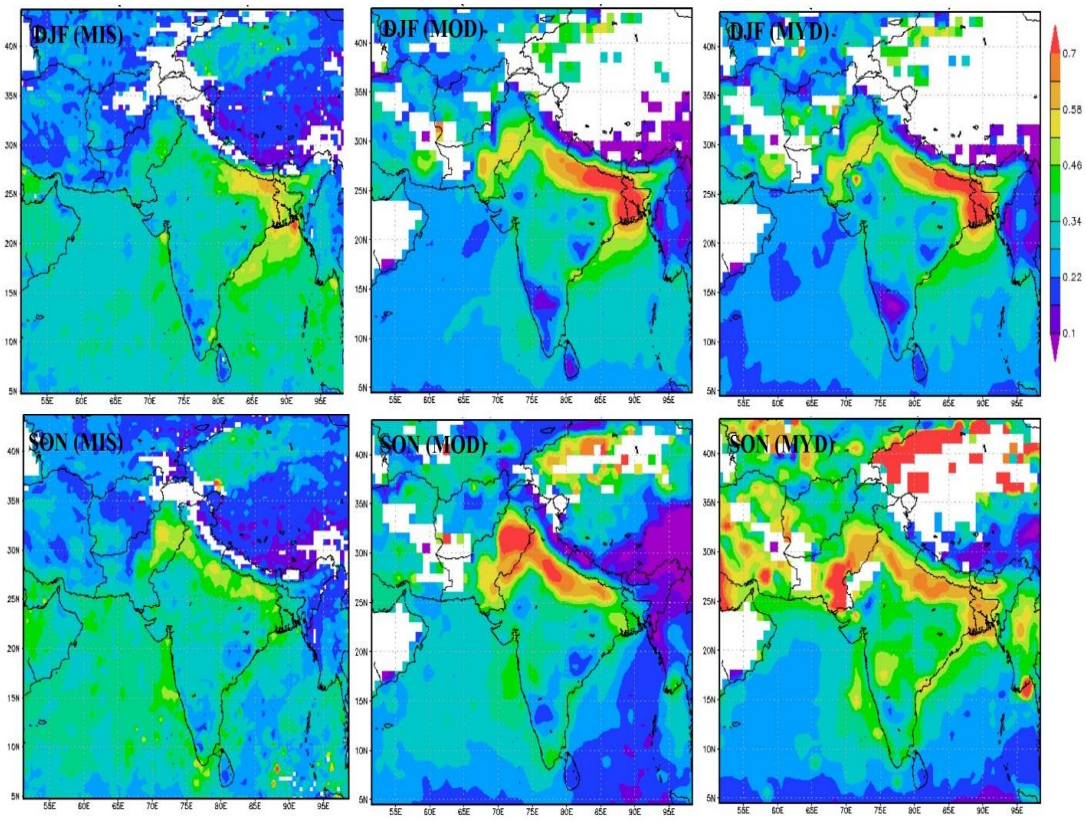

Figure 3.13: *Seasonal (winter and autumn) variation of columnar AOD from MISR (MIS) at 555 nm and MODIS Terra (MOD) and MODIS Aqua (MYD) both at 550 nm.*

Spatial variation of AOD although shows higher AOD along the entire IGP region during both of this season as compared to other Indian region, the spatial distribution of high AOD locations are important. In winter, high

loading is observed over the regions of Bihar and Bangladesh and adjacent regions towards the Bay of Bengal, while in Autumn season the high loading is observed towards the northern Indian region along the Arabian Sea. Aerosol loading is distributed from the IGP regions of Pakistan to northern Indian regions adjacent to the regions of Pakistan and relatively less AOD is observed over the eastern regions of IGP over the regions of Bihar and Bangladesh and adjacent regions. Although the observed pattern of spatial gradient is nearly same in all the datasets, however magnitude of aerosol loading is observed to be less from the MISR as compared to what observed from the MODIS Terra and MODIS Aqua both of which shows nearly similar spatial gradient with nearly similar magnitude. Aerosol loading over the northern Indian regions in winter is usually less as compared to the autumn season.

In autumn season, the regions of Pakistan and Panjab also undergoes the biomass burning due to crop harvesting each year which might be a reason of high AOD along these regions in autumn. While high AOD over the eastern regions of Bihar and Bangladesh and adjacent regions might possibly be due to the role of meteorology. The high magnitude of wide spread aerosol loading over the entire IGP and adjacent regions is observed in spring. The spatial gradient of AOD also shows moderate levels during summer-monsoon which are not lowest levels. These high loading in winter influences the aerosol characteristics at the regions in IGP while may or may not influence high altitude nearby locations, while the high loading in IGP in spring not only affects the locations in IGP but also directly influence the aerosol

characteristics at high altitude clean sites. Aerosol loading in spring also exhibits the multiple elevated layers as reported at few other locations. The presence of aerosols has also been confirmed even to the high altitude clean Himalayas in this season. Aerosols are transported to the high altitude Himalayas along the slope of the Himalayas during this season [*Gautam et al.,* 2011], where the aerosols are found to be accumulated. The knowledge of vertical structure of the aerosols is of foremost importance mainly in spring.

3.7. Black Carbon Variation at Nainital

Long term (2005-2012) BC mass concentrations data at a high altitude location at Nainital (29.4 N; 79.5^{o} E; 1958 m amsl) in central Himalayas are examined and utilized here for detail climalotogical study. BC diurnal, monthly and seasonal variations are described in detail with an aid of meteorology and air mass trajectories. Figure 3.14 shows frequency distribution with binning average of 1 µg m^{-3} of entire data set during four seasons. The data statistics of BC reveals that 50% of BC lies below 1 µg m^{-3} while BC from 1 µg m^{-3} to 2 µg m^{-3} constitute 42.9% of data, and BC above 2 µg m^{-3} constitutes only 6.7 % of data (Figure 3.14). The distribution of data shows high BC in spring season, while minimum in summer-monsoon. Data distribution is sharp in summer-monsoon and more skewed towards lower BC indicating dominance of low BC during most of the days, while in other season it is slow.

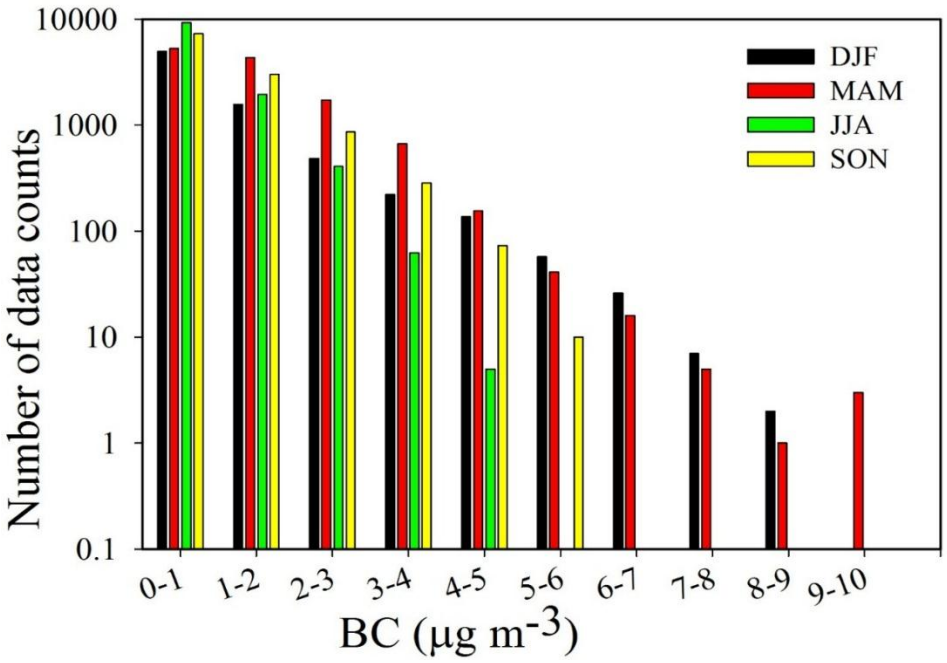

Figure 3.14: *Data statistics of climatological BC mass concentration during different seasons at Nainital (29.4^o N; 79.5^o E; 1958 m amsl) during 2005-2012. Data has been binned using the hourly BC data at a 1 μg m^{-3} bin size.*

3.7.1. Diurnal Variation in BC

Average (2005-2012) diurnal variations in BC show afternoon peak at Nainital (Figure 3.15). It is observed that diurnal variations are well pronounced from October to March resulting in a single afternoon peak at Nainital, which starts reducing after April months and more-or-less flat diurnal variation is observed till September. In order to characterize the magnitude of enhancement in BC peak in these monthly diurnal variations, amplitude of these diurnal variations are calculated.

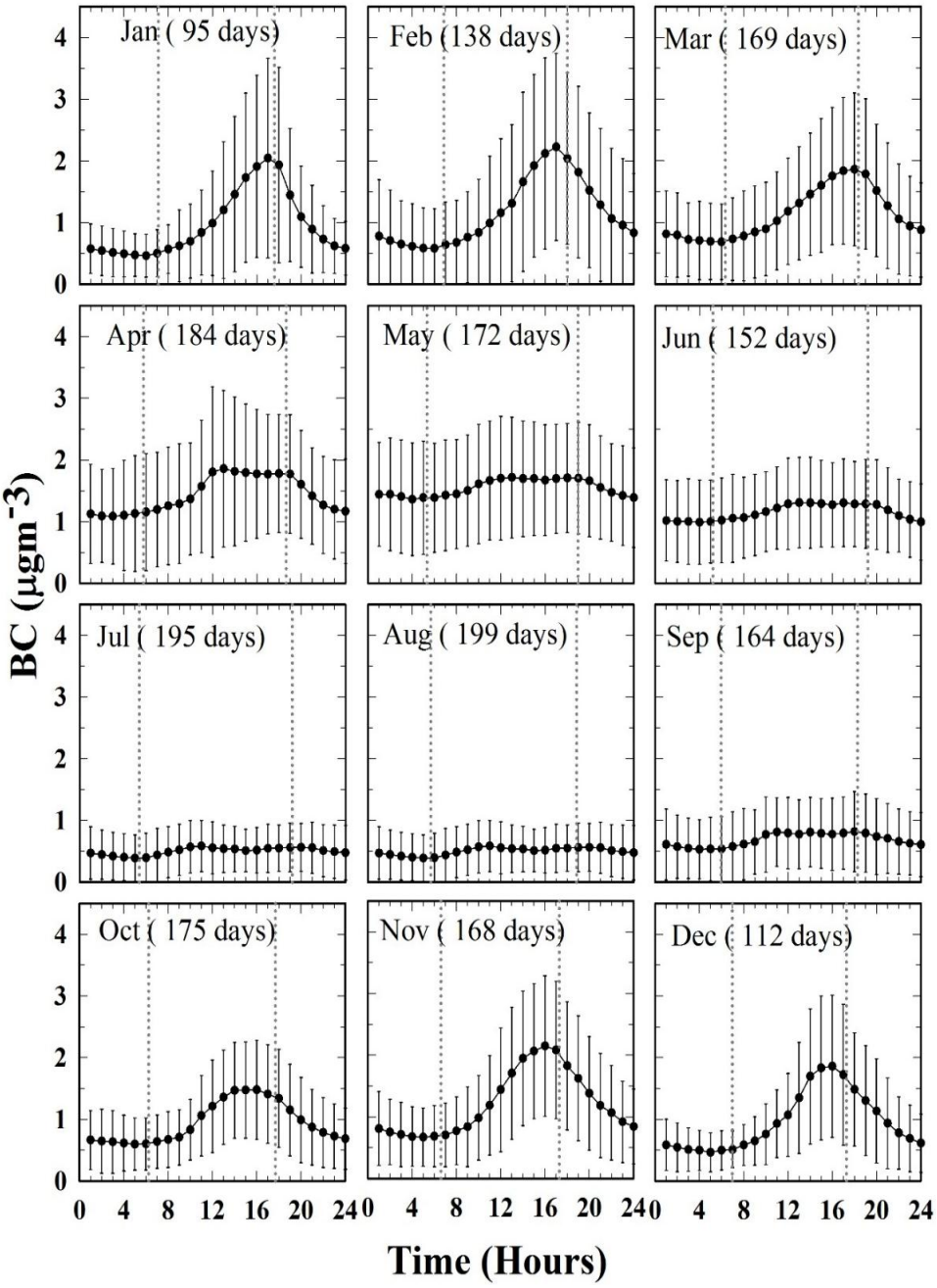

Figure 3.15: *Average (2005-2012) diurnal variation in BC mass concentration at Nainital for different months. Total numbers of days of observations are shown in bracket for each month. The time mentioned here is local time in Indian Standard Time (IST).*

BC amplitudes are calculated for each month by calculating the difference of the maximum and minimum BC and are mention in Table 3.2. BC amplitude is high in February (~1.65 µg m^{-3}) followed by January (~1.58 µg m^{-3}), while for November, December months BC amplitude is ~1.48 µg m^{-3} and ~1.40 µg m^{-3} respectively. Nearly flat pattern is observed in July–August month when BC amplitude is ~0.19 µg m^{-3} and ~0.22 µg m^{-3} respectively. BC amplitude again builds in October month when BC amplitude is observed to be ~0.88 µg m^{-3}.

Greater amplitude from November to February is mainly due to the lower boundary layer height during this time. As a result BC concentration is low on an average during nighttime as most of BC along with other pollutants resides in the valley region below the observing site and close to earth surface. BC along with other aerosols uplift slowly after the sunrise from nearby valley regions to nearby high altitude locations. The uplifting is maximum during the daytime, when the boundary layer is evolved maximum. As a result of this uplifting BC along with other aerosols are transported to mountain top at the present location and results in a peak during afternoon hours (1400 hrs to 1800hrs).

It is observed that BC is mainly transported from the valley regions to this site during daytime, due to the site being in the top of mountain. This enhances the daytime levels of BC at the site, while the nighttime values of BC remains low especially during November to February month as most of the pollutants resides below the location of site in valleys. It is interesting that level of

nighttime BC is sufficiently low from December to January months at Nainital. BC levels, especially nighttime starts increasing after February due to enhancement in the anthropogenic activities.

Table 3.2: *Monthly mean (2005-2012) BC mass concentration (µg m^{-3}) alongwith standard deviation at Nainital. Median, Maximum, data count, Daytime (1400 hrs to 1700 hrs) BC, Nighttime BC (0000 hrs to 0300 hrs) values are also shown along with the percentage increase in BC with respect to nighttime BC. BC amplitude is calculated by the difference of maximum and minimum BC.*

Months	BC	median	Max	Count	BC Amplitude	BC Nighttime	BC Daytime	% Increase
January	0.97±1.02	0.62	7.08	1829	1.58	0.53±0.39	1.90±1.52	258
February	1.19±1.24	0.73	8.32	3031	1.65	0.69±0.79	2.08±1.49	201
March	1.14±0.98	0.82	6.45	3869	1.18	0.76±0.66	1.76±1.16	132
April	1.45±1.02	1.18	12.25	4123	0.77	1.10±0.81	1.78±1.02	62
May	1.56±0.91	1.37	6.97	4221	0.35	1.41±0.90	1.69±0.90	20
June	1.16±0.69	1.02	4.47	3380	0.32	1.00±0.68	1.29±0.70	29
July	0.50±0.41	0.39	3.49	4445	0.19	0.43±0.40	0.53±0.37	23
August	0.45±0.33	0.36	4.31	3854	0.22	0.36±0.27	0.48±0.32	33
September	0.69±0.57	0.51	3.90	3645	0.29	0.57±0.52	0.79±0.60	39
October	0.96±0.70	0.75	5.46	4730	0.88	0.64±0.49	1.43±0.80	123
November	1.22±0.96	0.91	5.59	4529	1.48	0.74±0.54	2.03±1.11	174
December	0.97±0.85	0.73	5.76	2601	1.40	0.54±0.38	1.72±1.11	219

The level of early morning and nighttime BC shows quite significant enhancement in April-May months leading to the maximum BC in April-May month. This is mainly due to biomass burning that begins in April and can also be seen sometimes on local scale at few kilometres away from the site. The peak biomass burning over entire South Asia is reported to occur during April –May month [*Streets et al.,* 2003; *Venkataraman et al.,* 2006; *Adhikary et al.,* 2007]. Over India, northern India experiences the intense biomass burning during April–May month. Enhancement in BC as well as AOD has been reported by *Kumar et al.,* [2011] at the present site Nainital where enhancement in BC and AOD were estimated to be 1802 ng m^{-3} (~145%) and 0.3 (~150%) respectively during high fire activity period.

Soon after the arrival of marine airmasses during southwest monsoon, BC reduces abruptly. The scavenging of BC alongwith other aerosols occurs during southwest monsoon by both rainout and washout processes and is maximum in the July-August month, consequently BC reduces to minimum value in July-August months.

Table 3.2 also shows monthly mean values of BC mass concentration. BC is maximum in May month with mean 1.56±0.91 µg m^{-3} and median 1.37 µg m^{-3}. Mean and median BC for April are 1.45±1.02 µg m^{-3} and 1.18 µg m^{-3} respectively. Mean and median BC is observed to be minimum in August,

followed by July when BC is observed to be 0.45±0.33 µg m^{-3} and 0.50±0.41 µg m^{-3} with median ~0.36 µg m^{-3} and ~0.39 µg m^{-3} respectively.

BC diurnal variations are also studied for different seasons i.e. winter (December, January and February), spring (March, April and May), summer-monsoon (June, July and August) and autumn (September, October and November) (Figure 3.16). Maximum amplitude is observed during winter (~1.50 µg m^{-3}), followed by autumn (~0.90 µg m^{-3}) and then spring (~0.72 µg m^{-3}). BC amplitude in summer-monsoon is lowest (~0.21 µg m^{-3}) with nearly flat pattern (Table 3.3). Further, maximum BC levels during afternoon are observed in winter (~2.02 µg m^{-3}) followed by spring (~1.78 µg m^{-3}) and autumn (~1.51 µg m^{-3}).

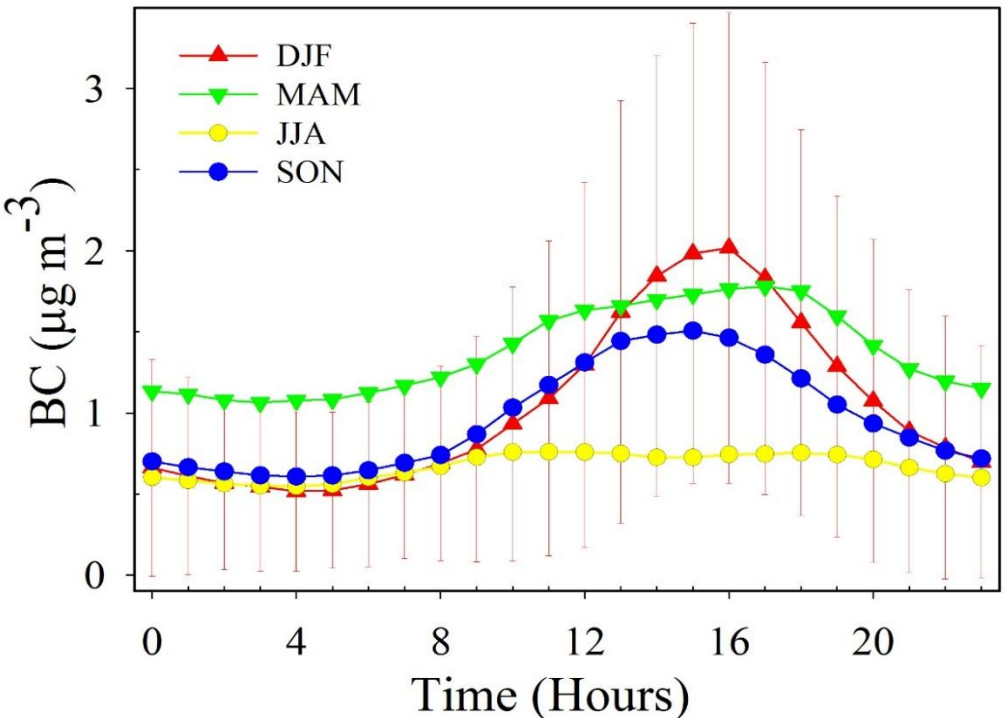

Figure 3.16*: Average diurnal variation in BC during different seasons winter (DJF), spring (MAM), summer-monsoon (JJA) and autumn (SON). The time is local time in Indian Standard Time (IST).*

Table 3.3: *Seasonal mean BC, maximum, nightime, daytime BC, and BC amplitude at Nainital.*

Seasons	BC	BC (Max)	BC Nightime	BC Daytime	BC Amplitude
DJF	1.05±0.76	2.02	0.6±0.59	1.92±1.39	1.50
MAM	1.38±0.75	1.78	1.1±0.84	1.74±1.03	0.72
JJA	0.67±0.51	0.76	0.57±0.54	0.73±0.60	0.21
SON	0.96±0.62	1.51	0.65±0.52	1.45±1.0	0.90

3.7.2. Monthly, Seasonal and Annual Characteristics of BC

Long-term (2005-2012) temporal variations in BC (from hourly data) are shown in Figure 3.17. BC shows day to day variability. BC enhances each year during April –May month which repeats nearly from year to year. BC concentration (hourly) reaches well above 6 μg m^{-3} during these months. BC also enhances sometimes during January-February months, although the number of such events are very few.

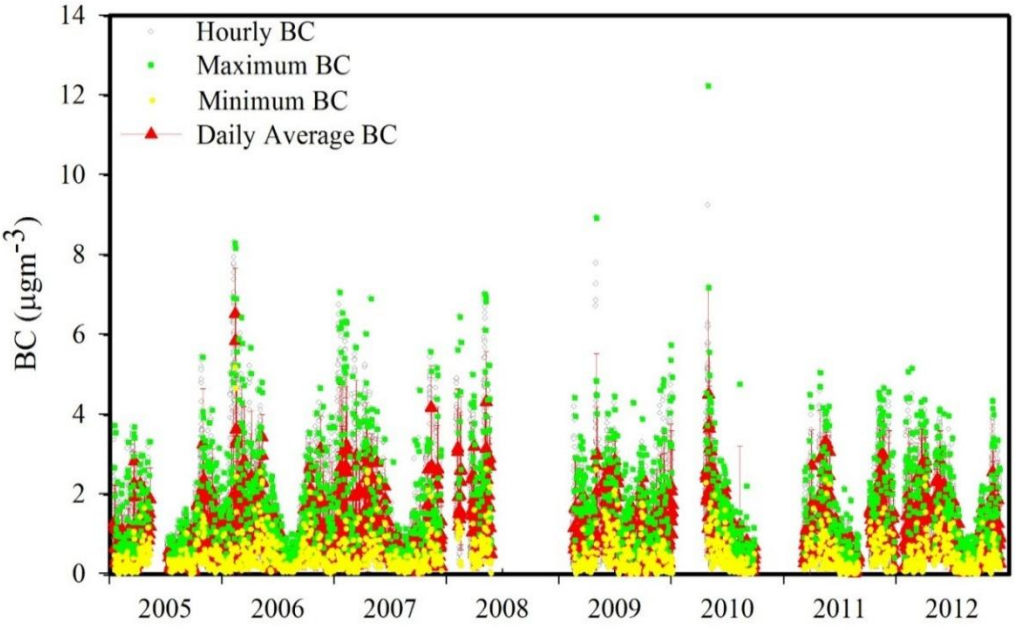

Figure 3.17: *Temporal variation of BC mass concentration at Nainital from 2005 to 2012.*

BC during the entire observation period is averaged to determine daily and monthly mean for climatological view and is shown in Figure 3.18. The enhancement in the month of April-May, especially in nighttime can be clearly seen. The early morning low is visible especially in December to February month. The negligible afternoon peak in July-August month can also be seen with low concentrations in the morning and evening hours.

BC climatological seasonal mean are also calculated. BC is found to be maximum 1.38 ± 0.75 µg m^{-3} in spring, which decreased to lowest value 0.67 ± 0.51 µg m^{-3} in monsoon before increasing to 0.96± 0.62 µg m^{-3} in autumn and 1.05 ± 0.76 µg m^{-3} in winter season (Table 3.3).

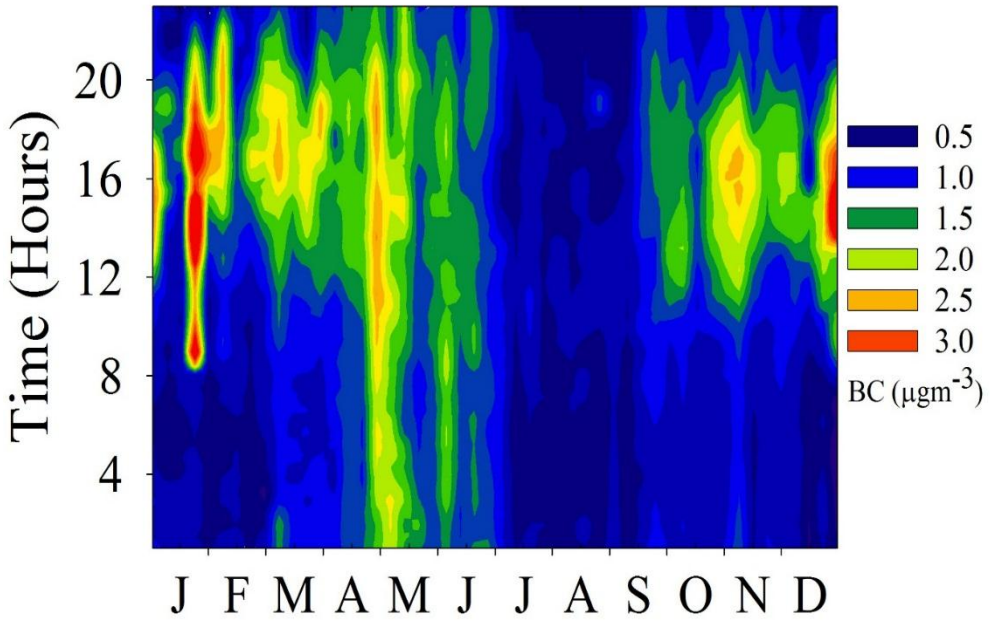

Figure 3.18: *Average (2005-2012) diurnal and seasonal variations in BC at Nainital.*

3.7.3. Daytime and Nighttime Variation in BC at Nainital

Daytime (1400-1700 hrs) as well as the nighttime (0000-0300 hrs) BC is also studied at the site. Seasonal variation of nighttime BC reveals low concentration normally in December-January months and high concentration in April-May months. The maximum nighttime concentration is observed for May month, while minimum concentration of BC is observed for August month. Seasonal variation of daytime BC is quite different from the seasonal variation of nightime BC. The daytime (1400-1700 hrs) BC shows high concentration from November to February and then decreases afterwards and is minimum in July-August month (Figure 3.19). Seasonal variation of daytime BC resembles to the seasonal variation of BC at any low altitude site but the magnitudes of BC are different. This will be discussed in Chapter 5.

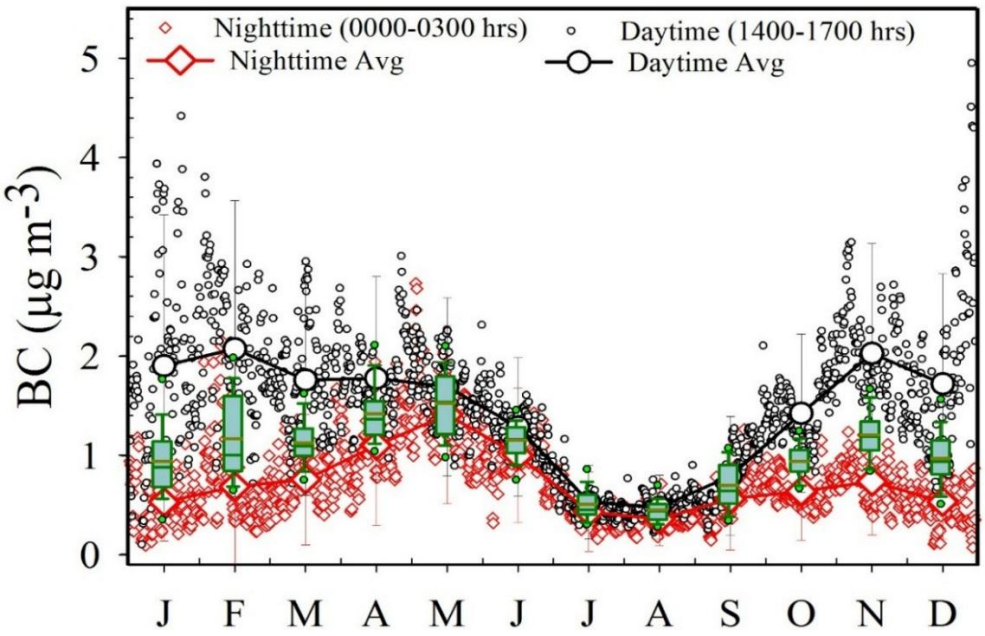

Figure 3.19: *Seasonal variation in BC mass concentration at Nainital. Hourly and monthly mean BC for daytime (1400 hrs-1700 hrs) as well as for nighttime (0000 hrs-0300 hrs) is also shown. Monthly BC are shown by box plot. Mean BC is shown by thick dark yellow line within box and median is shown by green line within box. The lower and upper edges of the boxes represent the 25th and 75th percentiles. The whiskers below and above are 10th and 90th percentiles while the data point outside the box represents 5th and 95th percentiles.*

The monthly mean BC during the daytime and nighttime are calculated and are mentioned in Table 3.2. BC during nighttime indicate the background BC at Nainital and is also referred as background BC, while BC during daytime is mainly due to the influence from valley. Nightime BC is nearly comparable during December and January with BC mass concentration of 0.54±0.38 µg m^{-}

^{3} and 0.53±0.39 µg m^{-3}, which gradually increases February onwards. BC concentration then increases sharply in April 1.10±0.81 µg m^{-3} and May 1.41±0.90 µg m^{-3} month. Nighttime (background) BC in May enhances to ~166% as compared to the background concentration of BC in January. BC then decreases and reach minimum in August 0.36±0.27 µg m^{-3}, followed by July 0.43±0.40 µg m^{-3}, due to scavenging as a result of arrival of marine air masses. Nightime BC slightly increases as soon as the influence of monsoon decreases. Nightime BC concentration in October and November is observed as 0.62±0.44 µg m^{-3} and 0.74±0.54 µg m^{-3} respectively.

Maximum daytime value is observed for February 2.08±1.49 µg m^{-3} followed by November 2.03 ±1.11 µg m^{-3}. Daytime BC shows decreases after February and is 1.78±1.02 µg m^{-3} and 1.69±0.90 µg m^{-3} in April and May months respectively, which further decreases and shows minimum in August 1.78±1.02 µg m^{-3}, followed by in July 0.53±0.37 µg m^{-3}. Daytime BC starts building up after the withdrawal of monsoon and BC again increases significantly after September. The percentage enhancement is found to be maximum in January ~258% followed by December ~219%.

The contribution of black carbon (BC) to the total aerosol optical depth (AOD) and subsequently to the direct radiative forcing (DRF) at Nainital was estimated [*Srivastava et al.,* 2012]. Measurements of the chemical composition of aerosols, from July 2006 to May 2007 along with BC was used to deduce the aerosol optical parameters. BC alone was used in the optical model to deduce the optical parameters solely for BC aerosols. The derived aerosol optical

parameters were used independently in a radiative transfer model to estimate the DRF separately for composite and BC aerosols. The average BC was found to be 0.98 (±0.68) μg m^{-3} during the entire observation period, which contributed <3% to the total aerosol mass and ~17% to the total AOD at Manora Peak. The mean surface forcing was found to be -14.0 (±9.7) and -7.4 (±2.1) W m^{-2}, respectively for composite and BC aerosols whereas mean atmospheric forcing was about +14 (±10) and +10 (±3) W m^{-2} for these aerosols. The results suggested that BC aerosols exert relatively large surface heating (~ 45% higher) as compared to composite aerosols and contribute ~70% to the total atmospheric forcing at site. Such a large warming effect of BC was crucial in context to Himalayas.

3.8. Influence of Airmasses and Source Apportionment

The influence of factor affecting BC mass concentration has been examined. The main factors are the role of boundary layer dynamics and influence of seasonally changing air masses. The role of boundary layer dynamics has already been discussed in the previous section. The role of seasonally changing air masses is investigated in this section. The air masses has been examined for which 5 days back air trajectories are calculated using HYSPLIT (Hybrid Single Particle Lagrangian Integrated Trajectory Model) by utilizing the 1°x1° degree meteorology data from GDAS. Seasonally changing air masses over the entire observation period from 2005 to 2012 at Nainital are shown in Figure 3.20. In winter most of the time the air masses arriving from the high altitude western regions, which reduces in spring. The air masses in summer-monsoon arrives from south-west and south-east regions and

influence of marine air masses are experienced in this season. The influence of air masses from south-west reduces in autumn, while the influence from the south-east region is seen in autumn. The western airmasses (long range) might influence BC level in winter at the observation site, while the influence of regional pollution could be in spring.

These air mass pathways from different directions are investigated in more precise way for which back air trajectories are clustered by splitting whole data according to angular distance resulting to a final number of clusters [*Ashbaugh et al.,*1983,1985; *Stohl,* 1996], having similar length and curvature [*Moody and Samson.,*1989]. Air mass pathway during different season are classified to different numbers of clusters. The multiyear long term BC data at Nainital is used for source apportionment of BC and also used to infer the spatial pattern of the potential sources of BC.

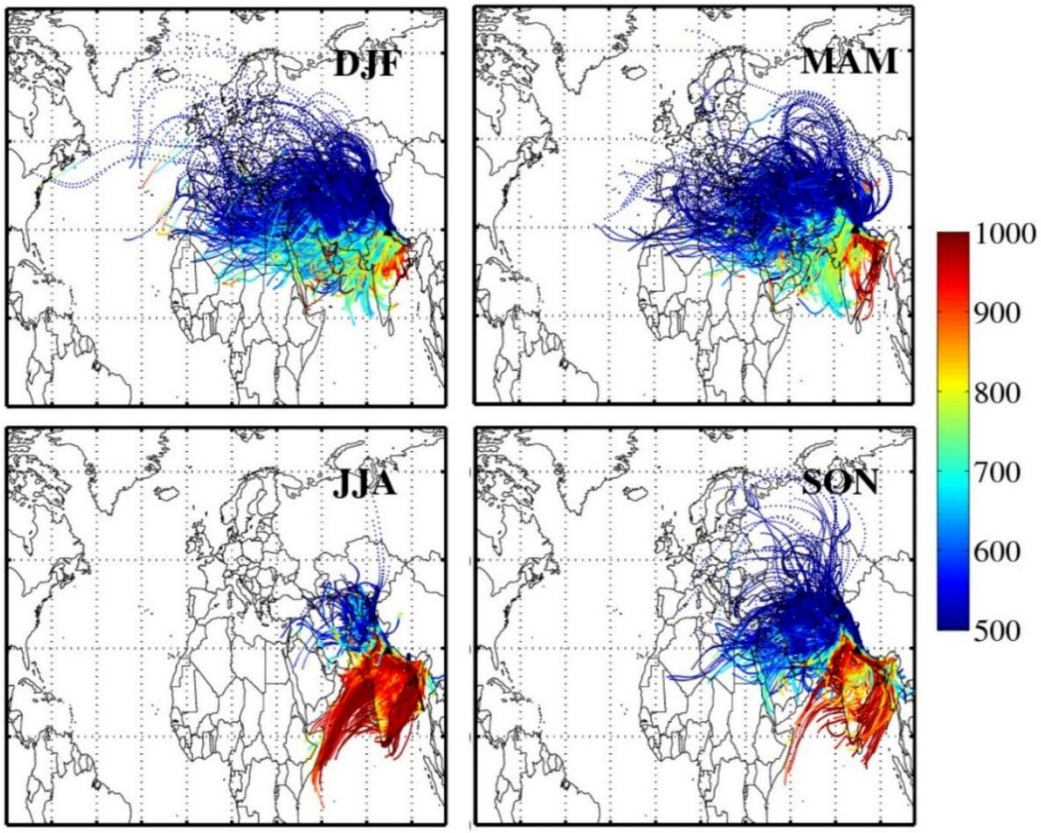

Figure 3.20: *The five days back air trajectories at 500 m AGL at ARIES, Nainital (29.4^o N; 79.5^o E; 1958 m amsl). The color scale represents the pressure along the air trajectories and thus representing the height attained by the air masses before arrival to the observing site. The observing site is also shown in figure with a black triangle.*

The major pathways of BC reaching the receptor site are studied utilizing trajectory clustering and Concentration Weighted Trajectory (CWT) analysis. The high and moderate BC concentration sources are then identified by CWT method developed by *Seibert et al.,* [1994] as discussed in Chapter 2.

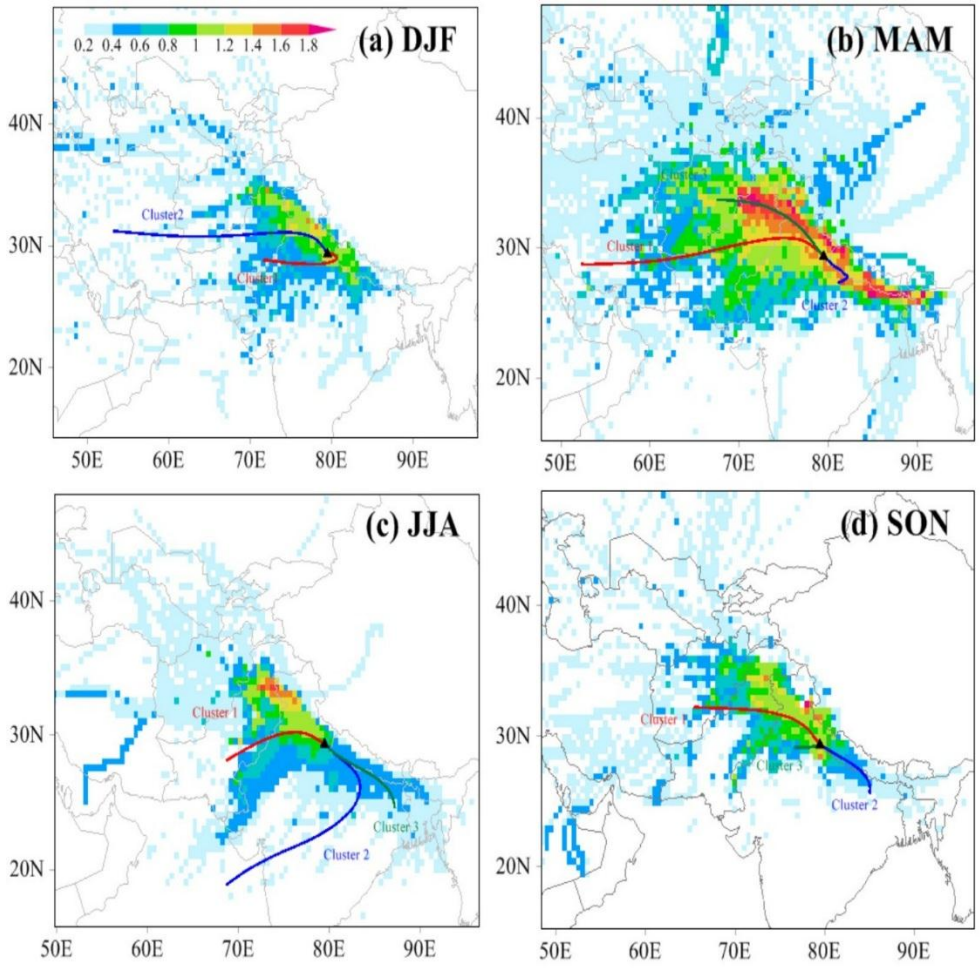

Figure 3.21: *Climatological CWT analysis along with the cluster analysis for different seasons at the receptor site (a) winter (December - February), (b) spring (March- May), (c) monsoon (June - August) and (d) autumn (September - November). The colour scale shows the BC mass concentration in µg* m^{-3}.

In winter seasons two major pathways are identified as cluster 1 and cluster 2 (Figure 3.21). These pathways have major airflow from the west and northwest direction respectively. Here we have distinguished the two directions as northwest and west just to differentiate the air masses arriving from long range and distant locations of Africa and Europe with that from the

air masses which are mainly of continental origin from west. Origin of air masses during all seasons is predominantly from the west, over Middle East/central Asia, except during monsoon season for which a transport from the south is dominant. Air masses from west (W) and northwest (NW) contribute 38.4% and 61.6% of air masses respectively (Table 3.4) with BC contribution of 0.96±0.54 μg m^{-3} and 1.02±0.68 μg m^{-3} respectively. The higher concentration of BC was contributed from northwest direction which passes through the IGP region and then arrives to the observing site (Figure 3.21). The spatial distribution of BC also shows high BC along the IGP site north toward the location.

*Ta**ble 3.4:** Percentage Contribution of different clusters and BC mass concentration (mean and standard deviation) from them.*

Season	Cluster	Direction	Trajectories (%)	Mean	St Dev
DJF	Cluster 1	W	38.4	0.96	0.54
	Cluster 2	NW	61.6	1.02	0.68
MAM	Cluster 1	W	42.2	1.21	0.75
	Cluster 2	SE	18.7	1.44	0.73
	Cluster 3	NW	39.1	1.52	0.71
JJA	Cluster 1	NW	27.7	1.02	0.53
	Cluster 2	SW	8.6	0.46	0.37
	Cluster 3	SE	63.7	0.53	0.42
SON	Cluster 1	NW	47.6	1.09	0.61
	Cluster 2	SE	29.4	0.66	0.57
	Cluster 3	W	23.0	1	0.59

In spring season air mass arrives mainly from three main pathways west (W), northwest (NW) and SE directions which constitute air mass of 42.2%, 39.1% and 18.7% (Table 3.4). Maximum BC was contributed from north-west direction in spring as well and BC was observed to be 1.52±0.71 μg m^{-3}. The

air masses arriving through the location south-east of the observing site located in IGP contribute 1.44±0.73 μg m^{-3} while from west contributes 1.21±0.75 μg m^{-3}. It is interesting that the spatial distribution of BC shows wide spread around most of the north Indian sites and shows maximum distribution of BC as compared to other seasons.

In summer-monsoon, the marine airmasses arrives through the large part of the continent before arriving to the observational site. The air masses which originates from the Arabian Sea and Bay of Bengal both passes through the vast continental region and then arrives collectively from south east direction, while some of the air masses originating from the continental location from west are also seen. The air pathways from west (W), south-west (SW) and south-east (SE) contributes air mass of ~27.7%, ~8.6% and ~63.7% respectively. BC contribution of 1.02±0.53 μg m^{-3}, 0.46±0.37 μg m^{-3}, and 0.53±0.42 μg m^{-3} was found from NW, SW and SE direction respectively.

The air mass pathways during autumn are mainly from NW, SE and W direction which contribute air mass of ~47.6%, ~29.4% and ~23.0 % respectively. BC contribution from these directions are 1.09±0.61μg m^{-3}, 0.66±0.57 μg m^{-3} and 1.0±0.59 μg m^{-3} respectively. Air mass arriving from north-western direction which passes through the IGP region and then arriving to the observed location contribute higher BC at the observed site.

3.9. BC Mass Concentration and Aerosol Number Concentration

The number concentration of aerosols (N_C) is available at 15 different channels (0.30 µm, 0.40 µm, 0.50 µm, 0.65 µm, 0.80 µm, 1.0 µm, 1.6 µm, 2.0 µm, 3.0 µm, 4.0 µm, 5.0 µm, 7.5 µm, 10.0 µm, 15.0 µm, and 20.0 µm) corresponding to particle in different size ranges. The size range has been classified in three main classes; fine (0.3-1.0 µm), coarse (1-10 µm) and ultra-coarse or giant modes (10-20 µm) for convenience.

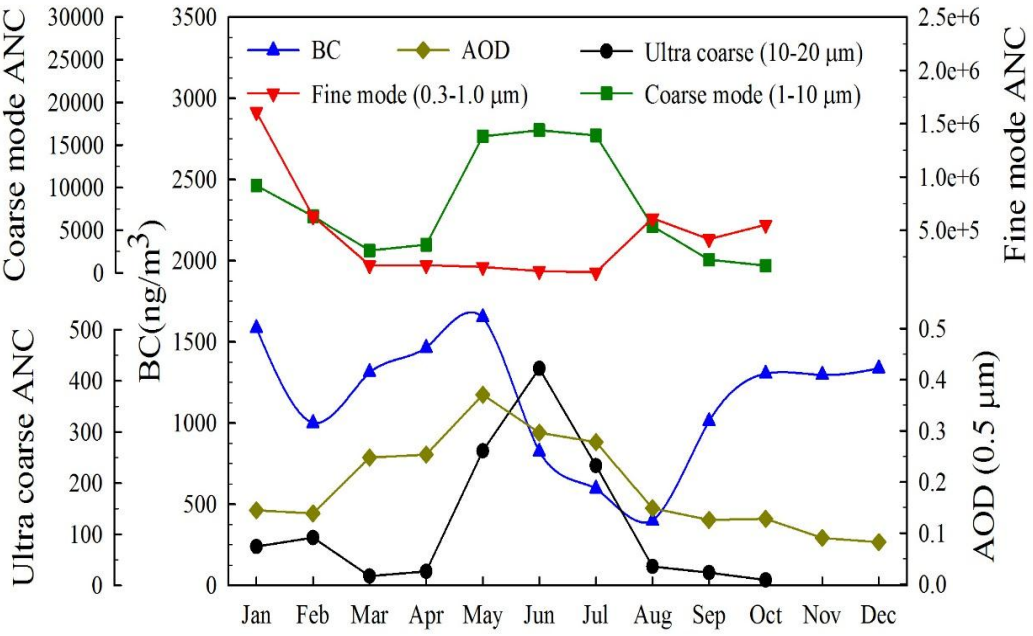

Figure 3.22: *Seasonal variation in BC, aerosol number concentration (Fine, Coarse and Ultra Coarse mode) and AOD (500 nm) at Nainital.*

Seasonal variation of fine mode (0.3-1.0 µm) shows high concentration in January which reduces from March-June and again increases as soon as monsoon withdraws. While seasonal variations in coarse mode and ultra-

coarse mode aerosol number concentration are slightly. Coarse mode aerosol increases at site from May-July while ultra-coarse mode shows sharp peak in June month. The increase in coarse mode of aerosols in general is mainly due to the build-up of dust and other aerosols at the site, while the sharp enhancement in ultra-coarse mode of aerosol in June is mainly due to build-up of dust load. Dust aerosols in the month of June mostly originate from the desert regions most of which comes from Thar Desert. Interestingly, coarse mode of aerosols shows high from May-July, while ultra-coarse mode shows maximum in June, while BC decreases after May.

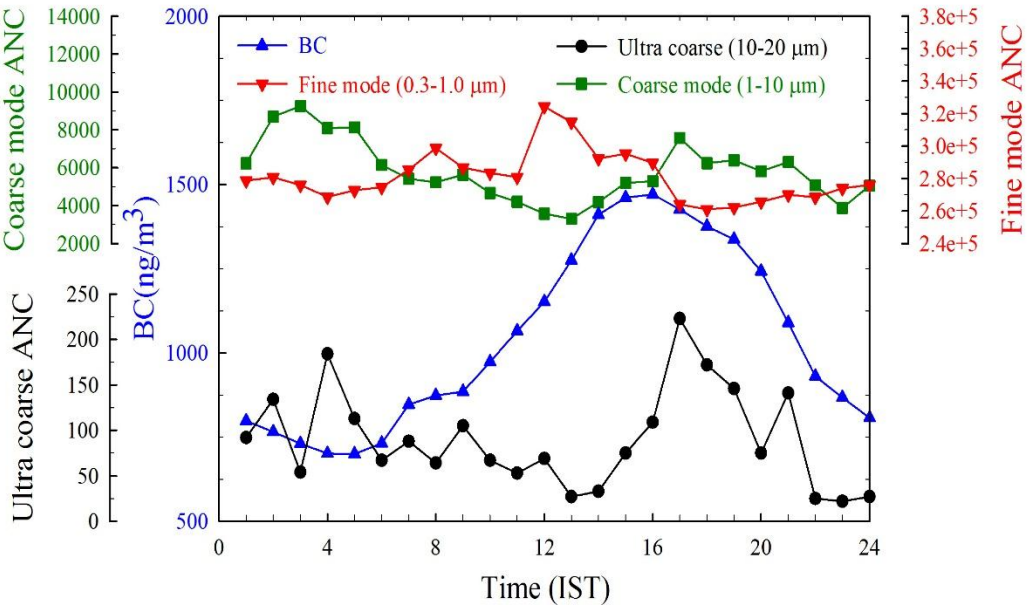

Figure 3.23: *Diurnal variation in BC and aerosol number concentration (Fine, Coarse and Ultra Coarse mode) at Nainital.*

Diurnal variation in N_C are also examined and is shown in Figure 3.23. Diurnal variations in N_C are not very clear as those observed for BC. Fine mode and ultra-coarse mode show a slight tendency of day time higher values, which is similar to that of BC. Coarse mode shows a tendency of two peaks.

3.10. Trend in BC Mass Concentration

Long term (2005-2012) BC data is used to determine BC trend at Nainital. Figure 3.24 shows monthly mean, smoothed data and de-seasonalized BC variations from 2005 to 2012. Trend in BC is found to be 21 ng m^{-3} per year. Although much of the studies are carried out reporting the trends in aerosol optical depth using the ground and satellite based AOD. However, study based on BC trends over Indian location is very scanty due to the lack of long term ground based observations. In contrast to the present study, long term trend in BC was reported to show negative trend at Trivandrum [*Moorthy et al.*, 2011].

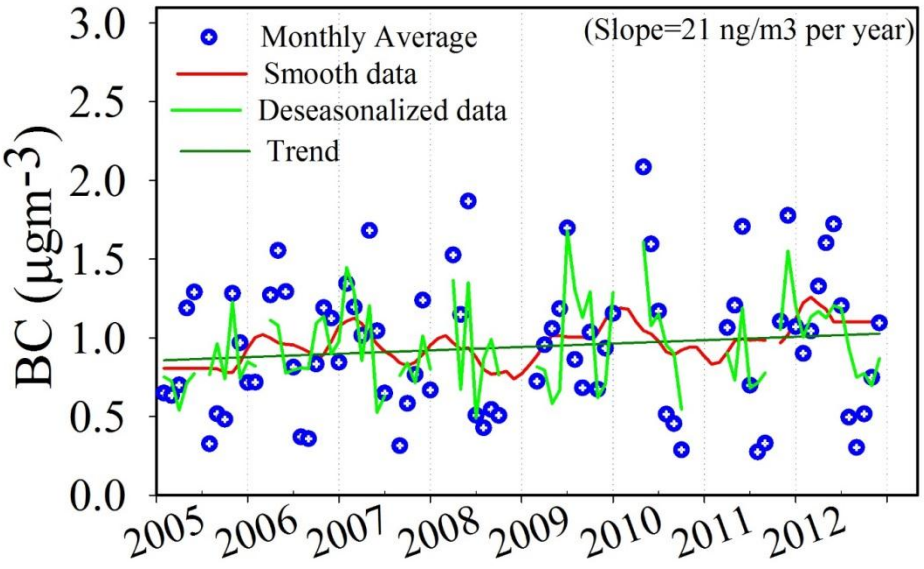

Figure 3.24: *Trend in BC mass concentration at Nainital from 2005 to 2012.*

3.11. Episodic Enhancement of Aerosols at Nainital

It is important to note that northern Indian region often experiences the influence of the dust. The maximum frequency of these dust storms occurs in April–June [*Sikka,* 1997; *Dey et al.*, 2004; *Prasad and Singh*, 2007]. Over South Asia, dust storms mainly originate from the Thar Desert [*Washington et al.*, 2003; *Gautam et al.*, 2009] under the hot and dry conditions as a result dust is transported from the Thar Desert to downwinds locations towards east or IGP region [*Sikka*, 1997]. The influence of which is experienced at several places in northern India. Previously, the influence of the dust from Thar Desert has also been observed over Nainital [*Hegde et al.*, 2007].

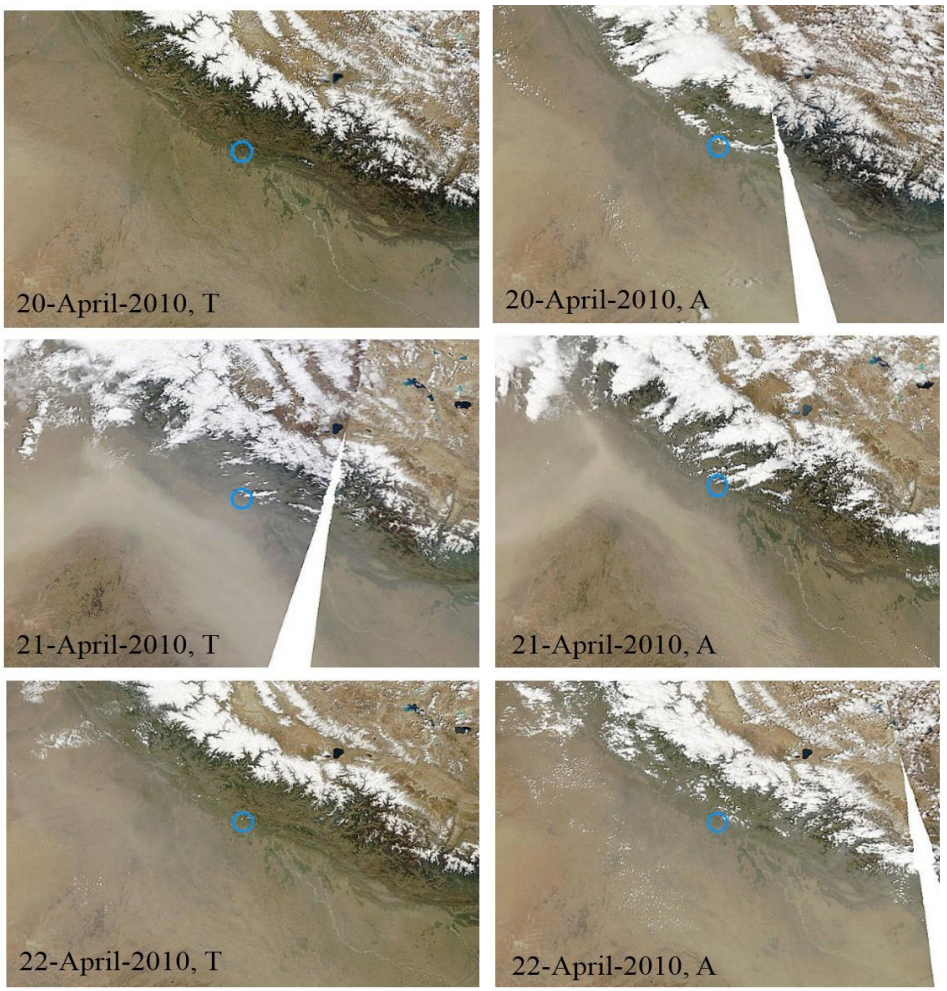

Figure 3.25: *The satellite captured natural color image by Moderate Resolution Imaging Spectroradiometer (MODIS) aboard Terra (T) and Aqua (A) from 20 April 2010 to 22 April 2010. The observing site Nainital is shown is shown inside the circle.*

Dust aerosols introduce large amount of coarse mode of aerosols and also changes the scattering and absorbing properties of aerosols and thus the radiative forcing. The data from the ground based instruments and the satellite observations are used to study an event (18-24 April 2010) of dust storm. The ground based AOD from MICROTOP and AERONET are used for the columnar characteristics of aerosols, aerosol number concentration has been

studied using the data from Optical Particle Counter (OPC) data at different channels. The satellite captured natural color image by Moderate Resolution Imaging Spectroradiometer (MODIS) aboard Terra (T) and Aqua (A) from 20 April 2010 to 22 April is shown in Figure 3.25. The higher intensity of dust storm can be seen on 21 April 2010.

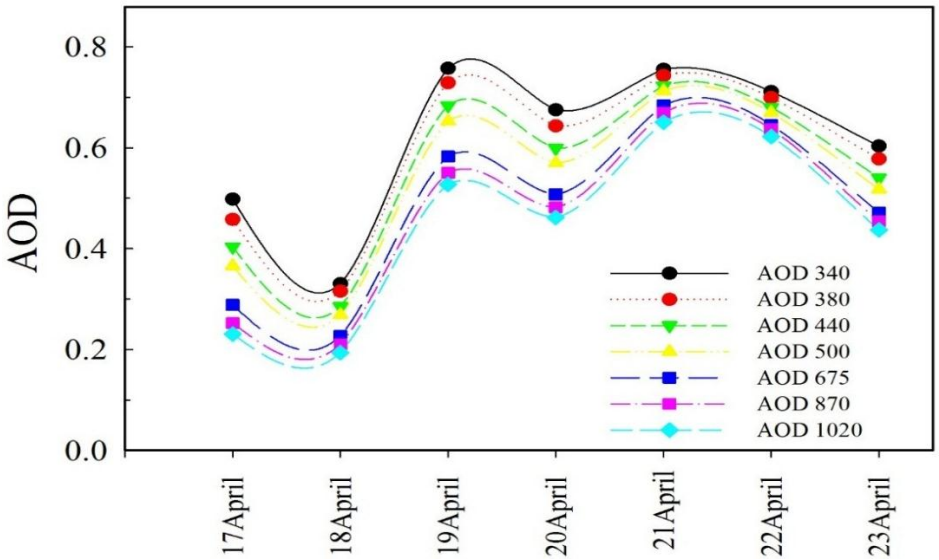

Figure 3.26: *Daily average aerosol optical depth (AOD) variation at Nainital from 17 April 2010 to 23 April 2010 obtained from the AERONET data during the dust episode period.*

Figure 3.26 shows AOD variation at different wavelength during 17-23 April, 2010. The temporal variation of AOD with its fine and coarse mode components along with daily average AOD and angstrom exponent is shown in Figure 3.27. AOD is observed to be lower on 18 April 2010 and maximum on 21 April 2010. Coarse mode of AOD contributes a significant proportion of AOD while fine mode of aerosols contribute less to total AOD during these

days of dust events. Fine mode AOD usually remains below 0.2, while coarse mode AOD reaches up to 0.7 during the dust episodes. Coarse mode of aerosol enhances by 160% on 19 April as compared to its value on 18 April. Total AOD was found to be maximum ~0.71 on 21 April 2010. Coarse mode AOD was also found to be maximum ~0.59 on 21 April 2010. Slight decrease in AOD is observed on the next day on 22 April 2010, while AOD decreases sharply after 23 April 2010. Angstrom exponent (AE) was low both on 21 April 2010 (~0.15) and one 22 April 2010 (~0.14).

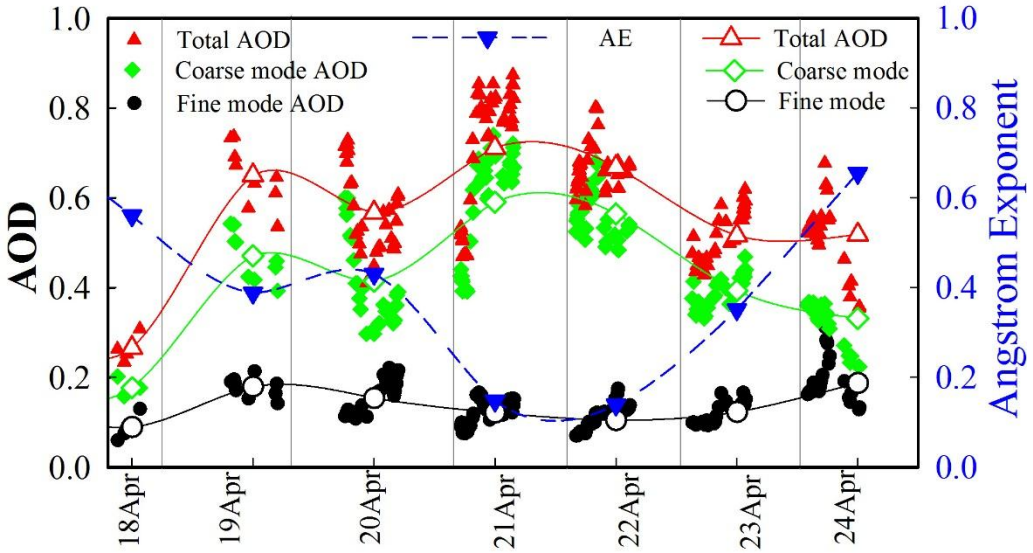

Figure 3.27: *Daily variation of Total AOD, coarse and fine AOD during 18-24 April 2010 at Nainital. The daily average angstrom exponent is also shown.*

Ground based aerosol number concentration data from OPC is also examined during 17-22 April 2010 (Figure 3.28). It is observed that fine mode of N_C shows day to day variability unlike that in coarse mode and giant (ultra-coarse) mode. However, fine mode of aerosols does not enhancement or variability from 20-22 April while coarse mode and giant mode of aerosols

shows rapid enhancement. Maximum concentration of N_C was observed on 21 April 2010 both in coarse and giant mode.

N_C in coarse mode varies from minimum value of 1.5 x10^6 m^{-3} to maximum value of 39.3 x 10^6 m^{-3}, while N_C in giant mode of aerosols varies from 12 x 10^3 m^{-3} to 208 x 10^3 m^{-3}. Fine mode of aerosol does not show much variability. Average concentrations showed significant enhancement during 21 and 22 April, both in coarse and giant mode (Table 3.5).

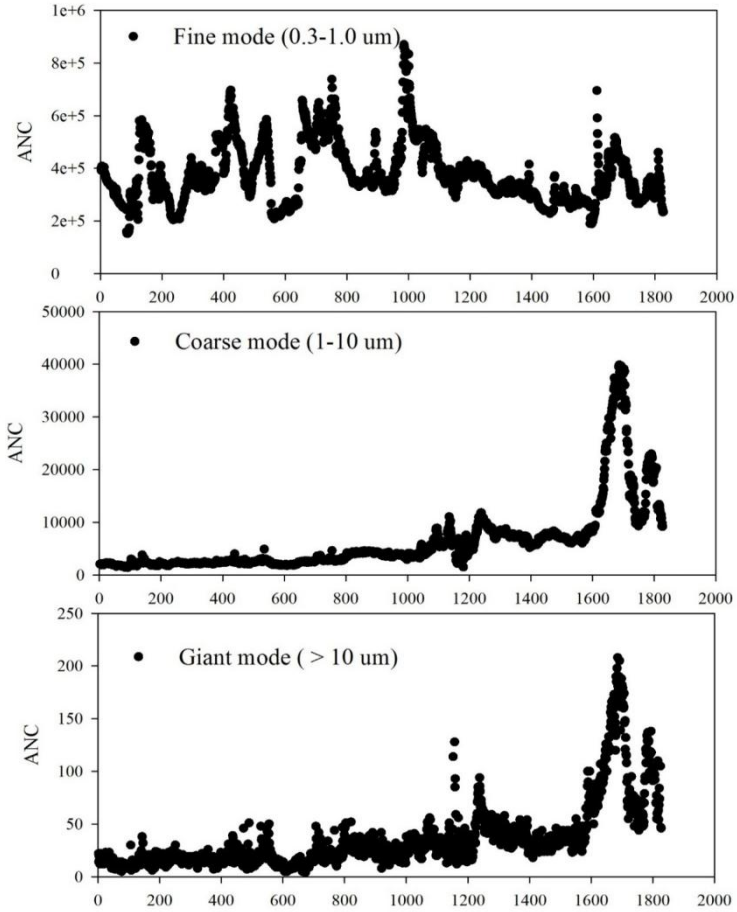

Figure 3.28: *Temporal variation of aerosol number concentrations in fine (0.3-1.0 µm), coarse (1-10 µm) and giant mode (<10 µm) from 14 April 2010 to 22 April 2010.*

Table 3.5: *Aerosol number concentration (m^3) in fine mode (0.3-1.0 um), coarse mode (1.0-10 um) and giant mode (above 10 um) during 19-22 April 2010. Daily mean with standard deviation, maximum and minimum N_C is also shown.*

	Fine mode (0.3-1.0 um)			Coarse mode (1.0-10 um)			Giant mode (above 10 um)		
Date	Average ($x10^8$)	Max ($x10^8$)	Min ($x10^8$)	Average ($x10^6$)	Max ($x10^6$)	Min ($x10^6$)	Average ($x10^3$)	Max ($x10^3$)	Min ($x10^3$)
19-Apr	4.8±0.9	8.3	3.4	5.2±1.6	11	3.2	31.6±7.3	56	13
20-Apr	3.4±0.4	4.3	2.6	7.1±2.0	11.8	1.5	40.3±16.4	128	12
21-Apr	3.1±0.8	7.0	1.9	13.0±10.1	39.9	6	65.3±45.9	208	23
22-Apr	3.3±0.5	4.6	2.3	18.1±8.0	39.1	9.2	91.3±37.0	188	44
Average	3.5±0.9	8.3	1.9	10.5±8.1	39.9	1.5	55.2±37.8	208	12

Back air trajectories corresponding to the dust storm days are also examined. Air-masses are observed to be more exposed to Thar desert region on 21 April, 2010 when compare with their exposure on 17 April, 2010 (Figure 3.29) and confirming that the source region has been Thar desert for this episode.

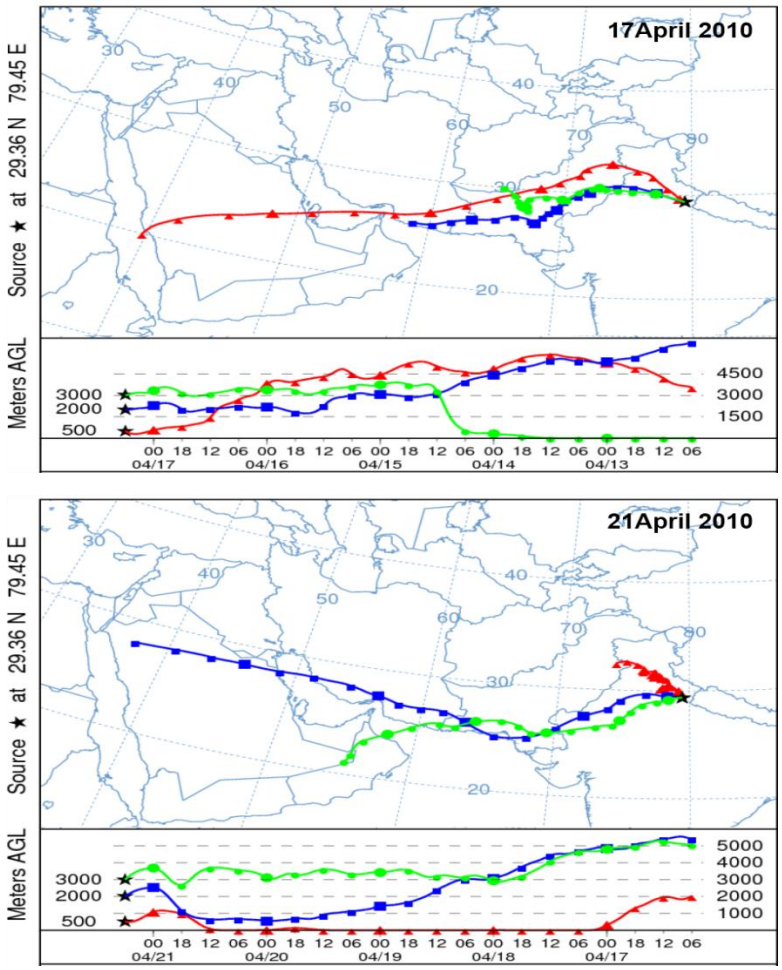

Figure 3.29: *Back air trajectories ending at 06 GMT on 17 April 2010 and 21 April 2010.*

Further, vertical profiles of aerosols are also examined for which data from CALIPSO has been utilized. The total attenuated backscattered profile was available for 20 April 2010 and is shown in Figure 3.30 alongwith the satellite track. The aerosol subtype profile shows the presence of dust and polluted dust over the site. The dust aerosols extending at a height of about ~5 km are seen on 20 April 2010 from the daytime profile of CALIPSO.

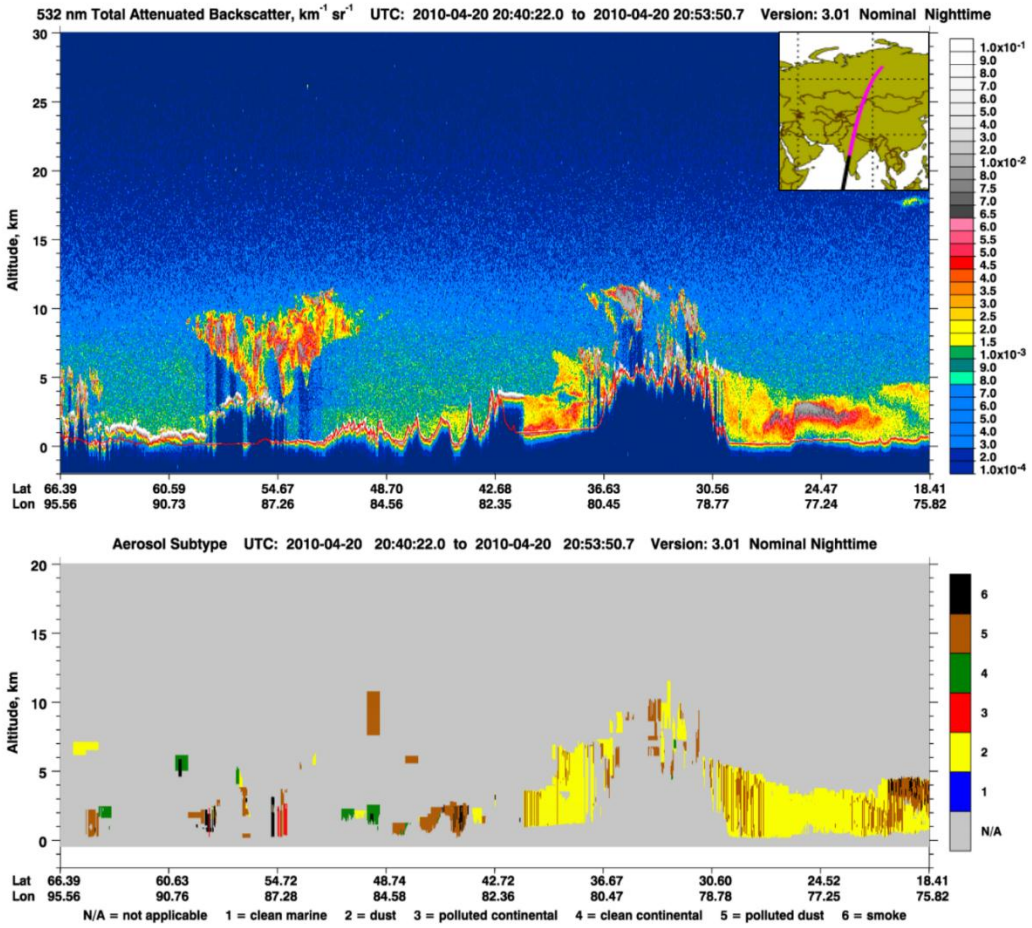

Figure 3.30: *CALIPSO derived image Lidar level1 (version 3.01) identifying the desert dust aerosol along the overpass of the trajectory on 20 April 2010. The total attenuated backscattered at 532 nm is shown in the upper panel.*

The impact of this dust storm has also been reported by *Kumar et al.,* (2014) by utilizing WRF model in which significant increase ~50 % in AOD and decrease in Ångström exponent ~70% has been observed in local to regional scale. The model simulations showed that dust particles warmed the atmosphere while cooling was reported at the surface and the top of the atmosphere.

3.12. Study of Precipitation Chemistry Over the Central Himalayas

The rain plays important role in the aerosol scavenging. The aerosols and other pollutants present in the atmosphere are not only scavenged from the atmosphere with rain, but also affect the chemistry and composition of rainwater. Therefore, in addition to the aerosol characterization studies at Nainital, attempt was also made to study the rainwater chemistry at Nainital. Rainwater samples were collected at Nainital during the monsoon season of 2012 and were analysed for pH and rainwater components and discussed here.

3.12.1. pH, Conductivity and Composition of Rainwater

Figure 3.31 shows variations in anionic constituents F^-, Cl^-, SO_4^{-2}, and NO_3^- whose value ranges as 0-11.6 µeq/l, 1.43-88.95 µeq/l, 2.73-154.77 µeq/l and 0.69-213.73 µeq/l respectively. The lowest volume weighted average (VMA) concentration was observed for F^- ~ 2.28 µeq/l among anionic components while SO_4^{-2} shows maximum average concentration ~ 17.88 µeq/l. Mean concentration of anions F^-, Cl^-, SO_4^{-2}, and NO_3^- are 2.28, 11.85, 17.88 and 12.67 µeq/l respectively. Dominant anions are SO_4^{-2} and NO_3^- followed by Cl^-. In general, these different ions might or might not origin from similar sources.

In general it is known that SO_4^{2-} and NO_3^- are the secondary aerosols produced from anthropogenic sources. The ions of NO_3^- mainly originate from oxidation reaction from its precursors NO_x which is mainly due to the use of fossil fuels [*Seinfeld*, 1986]. SO_4^{2-} is also produced from the oxidation of gaseous

precursor SO_2. Cl^- essentially originate from ocean, apart from the anthropogenic sources (e.g. from industrial HCl).

Rainwater samples when examined at Nainital indicate that pH is neutral in nature with mean pH 5.62±0.34 (pH of neutral water being 5.6). It is observed that in most of the days, observed pH lies within the neutral pH range. The observed pH is usually above 5.0, except only one event when pH was less than 5.0. Further, events having pH greater than 6.0 are also less. pH value ranges from 4.95 to 6.6 during year 2012. The highest pH ~6.6 is observed in the month of June on 20-06-2012, while lowest pH ~4.95 is observed in September on 14-09-2012. It seems that the influence of the dust resulted in the high pH in June, as the site usually remains under the influence of dust during this month of June [*Hegde et al.,* 2007]. Frequency distribution (Figure 3.32) shows that 55% of samples have pH equal or greater than neutral pH of 5.6, while 45% cases have pH lesser than 5.6.

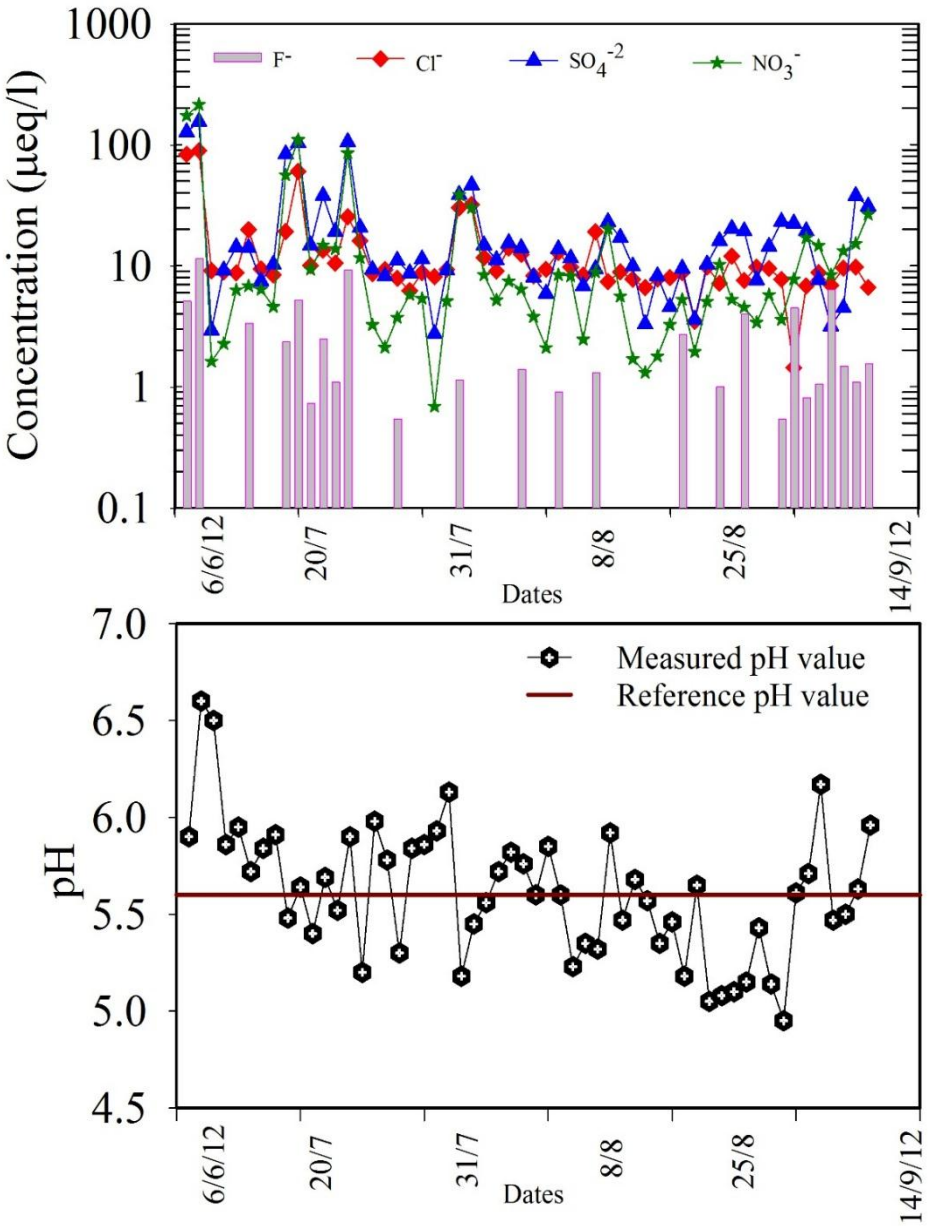

Figure 3.31: *Variations in anionic (F^-, Cl^-, SO_4^{-2}, and NO_3^-) concentrations in daily rainwater samples at Nainital and pH variations in rainwater for year 2012.*

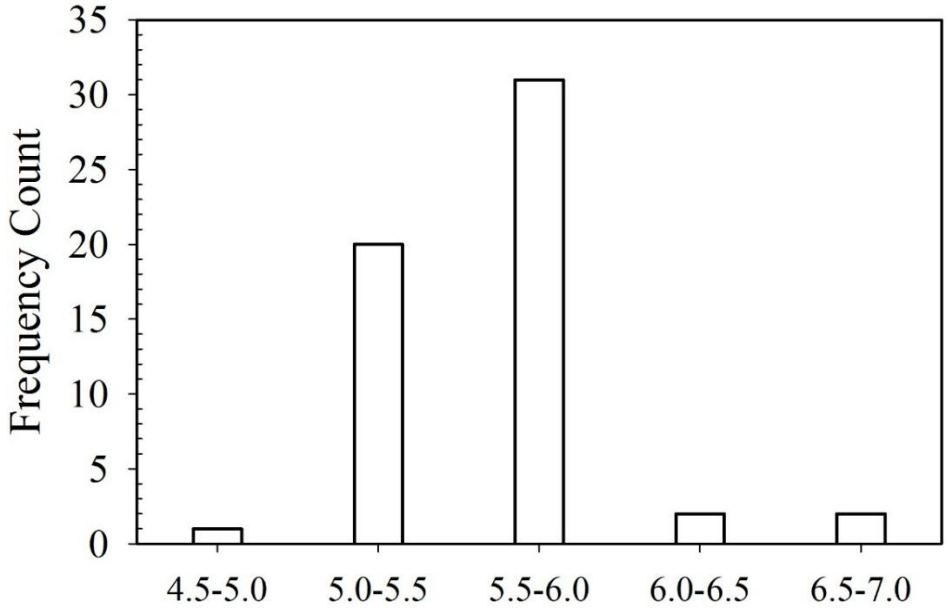

Figure 3.32: *Frequency distribution of rainwater pH at Nainital.*

3.12.2. Rainwater Chemistry Comparison With Other Sites

The observed pH at Nainital is compared with pH observed at North Western Himalayas site at Kothi, Kullu (32.31°N, 77.20°E, 2527 m amsl) in Himanchal Pradesh and pH values are somewhat similar at both sites [*Tiwari et al.,* 2012]. At a rural forest station near Bhubaneswar pH was reported as ~5.50 [*Das et al.*, 2010], while pH was 5.82 ± 0.45 at Varanasi, which varied from 5.18 to 7.08 [*Bisht et al.,* 2014]. At Comba, Madgaon, South Goa, in southern part of India, high pH (6.25 ± 0.28) was observed ranging from 5.36 to 6.91, due to high loading of particulate matter in the atmosphere [*Gobre et al.,* 2010]. High pH was also reported at a semiarid region at Gopalpura, Agra, between 6.1 and 7.4 [*Satsangi et al.,* 1998], at a semiarid location at Ahmedabad, pH ~6.7 pH [*Rastogi and Sarin,* 2005] and at western location, Sinhagad, Pune (5.73 - 7.21) [*Budhavant et al.,* 2009].

Common anions F^-, Cl^-, SO_4^{-2}, and NO_3^- shows mean concentration of 2 µeq/l, 28 µeq/l, 26 µeq/l and 17 µeq/l respectively at Kullu, while mean concentration of these anions are 2.28 µeq/l, 11.85 µeq/l, 17.88 µeq/l and 12.67 µeq/l respectively at Nainital. Comparison of rainwater samples at these two sites suggest that precipitation at Kullu is regularly influenced by aerosol and gaseous pollution, and might influence precipitation at Kullu on regular basis. This also suggest that sources of these anionic constituents might be regular or nearby. On the other hand, primary investigation at Nainital suggest that concentration of anions in rainwater shows low on an average, however episodic events leads to enhancement in these anions and significantly influence the day to day variability of precipitation chemistry at Nainital.

3.13. Summary and Conclusion

Long term aerosol optical depth (AOD) and black carbon (BC) observations from ground based observations at a high altitude site Nainital are examined for climatological synthesis and detail characterization. The aerosol measurements at the site represents a sort of background against which the urban impacts can be compared and provide a far-field picture quite away from potential sources. The seasonal variation of AOD and both BC indicate maximum in spring at the site. On the other hand minimum in AOD is observed in winter, while minimum BC is observed in summer-monsoon. The winter season shows quite a low aerosol loading over the site which indicate the presence of pristine environment over the site most of the time. The aerosol load at the site increases significantly in spring season. Climatological seasonal mean AOD (500 nm) is observed to be ~0.12, ~0.3, ~0.22, and ~0.15

in winter, spring, summer-monsoon and autumn respectively. The percentage enhancement in seasonal AOD with respect to winter reveals percentage enhancement of ~155%, ~85%, ~31% in spring, summer-monsoon and autumn respectively. AOD observations are also examined for spectral, diurnal, fine and coarse mode variations. Aerosol observations shows the presence of fine mode of aerosols over the site in winter (December-February) while aerosol are present in coarse mode in spring (especially in April to May) and early summer (June). The volume size distribution of aerosol shows sharp enhancement in coarse mode of aerosols ~300% in April to June. AOD observations are also compared with the ground based AERONET data which reveals quite good correlation (~0.96). The spatial variation of AOD obtained from satellite is also examined. Diurnal variation of BC at Nainital results in a single afternoon peak (1400 to 1800 hrs). Maximum amplitude is observed during winter (~1.50 μg m^{-3}), followed by autumn (~0.90 μg m^{-3}) and then spring (~0.72 μg m^{-3}). BC amplitude in summer-monsoon is lowest (~0.21 μg m^{-3}) with nearly flat pattern. BC is found to be maximum ~ 1.38 ± 0.75 μg m^{-3} in spring, which decreased to lowest value ~ 0.67 ± 0.51 μg m^{-3} in monsoon before increasing to ~ 0.96± 0.62 μg m^{-3} in autumn and ~ 1.05 ± 0.76 μg m^{-3} in winter season. The enhancement in background (during nighttime) BC and that transported due to valleys (during daytime) is also calculated. The enhancement in background BC is observed to be maximum in spring season. The role of air masses and source apportionment is also discussed. The ground based number concentration of aerosol is also examined, which shows sharp peak in the ultra coarse mode of aerosols in the month of June. The influence of dust episode is also observed in the aerosol number concentration at site and

shows quite high enhancement in coarse and ultra coarse mode of aerosols. The simultaneous measurement of surface, columnar and vertical aerosols characteristics are discussed in detail. The multiyear observations of aerosol has been examined for the first time for the long term trends. The observations are unique and it is first time reporting of long term trend analysis of AOD and BC over entire Himalayan range. The multiyear AOD and BC show slightly increasing trend. Further, the rainwater chemistry has also been examined at Nainital which reveals that pH values ranged from 4.95 to 6.6 with a mean of 5.61±0.34 during year 2012. Anionic constituents F^-, Cl^-, SO_4^{-2}, and NO_3^- ranges between 0.55-11.6 µeq/l, 1.43-88.95 µeq/l, 2.73-154.77 µeq/l and 0.69-213.73 µeq/l respectively in rainwater samples with mean concentration of anions F^-, Cl^-, SO_4^{-2}, and NO_3^- as 2.28, 11.85, 17.88 and 12.67 µeq/l respectively.

Chapter 4

Aerosol Characterization at a Semi-urban Site in the Central Himalayan Foothill Region

Studies based on space-borne observations and some of ground-based observations [*Jethva et al.,* 2005 and others] have revealed high pollution load over Indo-Gangetic Plain (IGP) region. Elevated pollution levels over the IGP not only affects the regional air quality including those of the pristine Himalayan locations [*Pant et al.,* 2006; *Lau et al.,* 2010; *Gautam et al.,* 2011], but also affects the adjacent oceanic regions [*Lelieveld et al.,* 2001; *Naja et al.,* 2004]. The IGP region encompasses a vast area stretching from the Indus river system in Pakistan to the delta of Ganges River in Bangladesh and is very

conducive for confinement of pollutants; both of local origin and those advected from the west [*Nair et al.,* 2007].

The columnar abundance of aerosols is relatively well studied over the IGP region using the Satellite data (MODIS, MISR etc.), ground based AERONET setup and few other ground based studies. However, the ground based surface measurements of BC are very limited, particularly with a complete seasonal cycle. The previous studies have proposed that the anthropogenic activities in the IGP region or emissions from the foothill of Himalayas are greatly influencing variability and levels of aerosols in the central Himalayas [*Pant et al.,* 2006; *Dumka et al.,* 2010; *Kumar et al.,* 2011]. However there is lack of ground based observations to confirm this.

Realizing this, the ground based observations of BC have been initiated for the first time at a semi-urban low altitude site Pantnagar (29.0^{o} N, 79.5^{o} E, 231 m amsl) in IGP, adjacent to central Himalayan foothills. The temporal variations in BC are characterized and the role of meteorology (both meso-scale and synoptic) in them are delineated. The BC and CO evolutions are also studied with the mixing layer depth. BC–CO association is further used to determine the sources of aerosols. The ground based BC observations are also used for source apportionment studies at Pantnagar. Further, ground based AOD data, and satellite retrieved aerosol index data is also utilized to qualitatively understand whether BC is a dominant component of the total and absorbing aerosol load over Pantnagar. The vertical profiles of aerosol extinction coefficient from CALIPSO are also examine for seasonal variation in vertical

distribution of aerosols over Pantnagar. In this study we have also evaluated the ability of WRF-Chem model in simulating the observed diurnal variation of BC at Pantnagar.

4.1. Observational Site and General Meteorology

Measurements of BC were initiated in the campus of Govind Ballabh Pant University of Agriculture and Technology, Pantnagar (29.0^{o} N, 79.5^{o} E, ~231m amsl; Figure 4.1) in May 2009. This university campus is spread in an area of about ~40.5 km^{2} (Figure 4.1b, image shown in inset) and located at a distance of about ~250 km due northeast of Delhi (Figure 4.1d). Elevated Himalayan Mountains of ~2000 m altitude are due north and east of the observation site at an aerial distance of ~20-30 km, while low altitude plains regions are due west and east of the site. Mountains of much higher altitudes range of ~4000–5000 m are around ~100 km from the observation site. The population density around Pantnagar is ~250–1000 per km^{2} but is much less (<250 persons per km^{2}) due north of the site (http://sedac.ciesin.columbia.edu/gpw). A small airport is located ~2.5 km west of the observation site, which is occasionally operated. A few small scale industries are located in nearby towns, Rudrapur (16 km, southwest of Pantnagar) and Haldwani (25 km, northeast of Pantnagar). A paper manufacturing unit is located at a distance of ~ 9 km to the north-east of the observation site. The other small scale industries of automobiles, food and agricultural products, etc. are about ~ 7 km towards south-west, but none of them involve any extensive combustion processes. Figure 4.1c shows spatial distribution of anthropogenic BC emissions in this

region. High BC emissions along the IGP region are also observed. Like BC emissions, AOD, retrieved from MODIS also shows elevated levels along the IGP (Figure 4.1d).

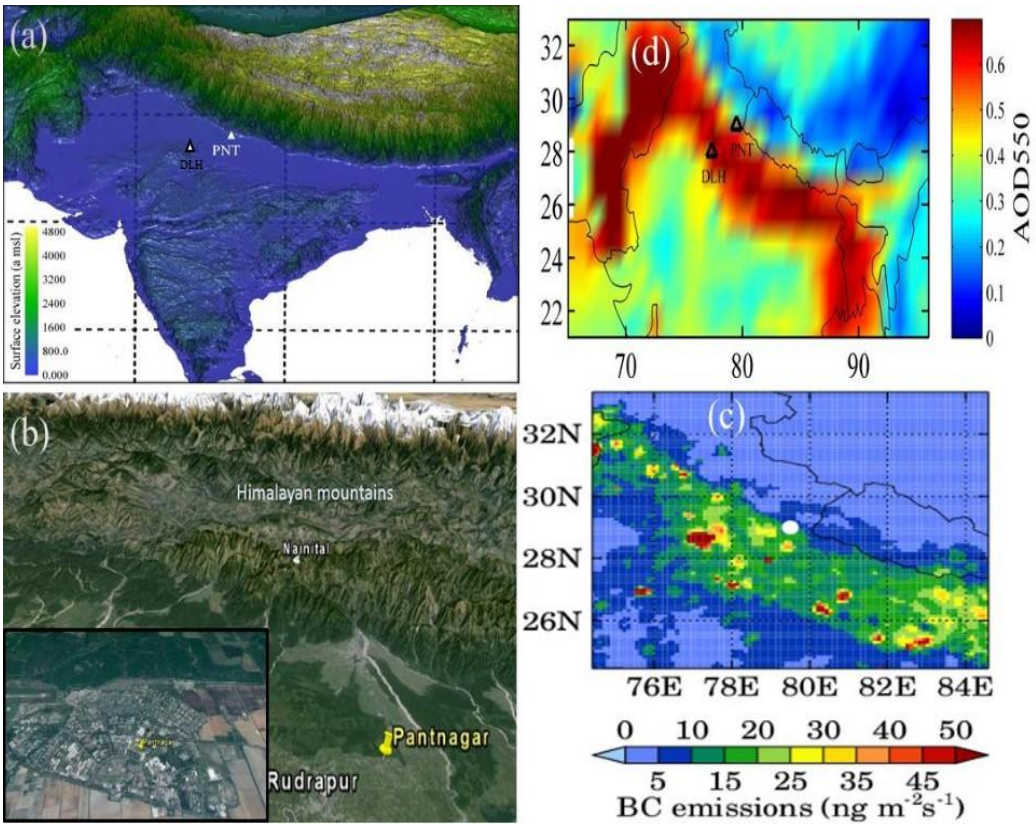

Figure 4.1: *(a) Geographical location of the observing site Pantnagar (29.0 ^{o}N; 79.5 ^{o}E; elevation ~231m amsl) shown by PNT. (b) Zoomed image of the observing site in IGP, along with the Himalayan mountain region. The zoom image of university campus spread in about ~40.5 km^{2} is also shown in Inset. (c) Anthropogenic BC emission used in WRF-Chem simulation. White filled circle marks the location of the observation site Pantnagar. (d) MODIS TERRA, AOD at 550 nm during observing period from year 2009 to 2012.*

Surface wind speed and wind direction data are obtained from an Automatic Weather Station setup by the Indian Meteorological Department (IMD).

Analysis of these wind datasets shows that the observational site is mostly under the influence of easterly and westerly winds (Figure 4.2). The surface winds in summer-monsoon emanates from west. In autumn, wind arises from relatively diverse direction as well. The wind speeds are generally low (< 1.5 m s^{-1}) in winter and high (> 3 m s^{-1}) in monsoon months. The in-situ measurement of solar radiation, relative humidity and rainfall were not available from ground based station. Therefore solar radiation and relative humidity are used from the Global Data Assimilation System (GDAS) and rainfall data are used from the Tropical Rainfall Measuring Mission (TRMM) as discussed in Chapter 2.

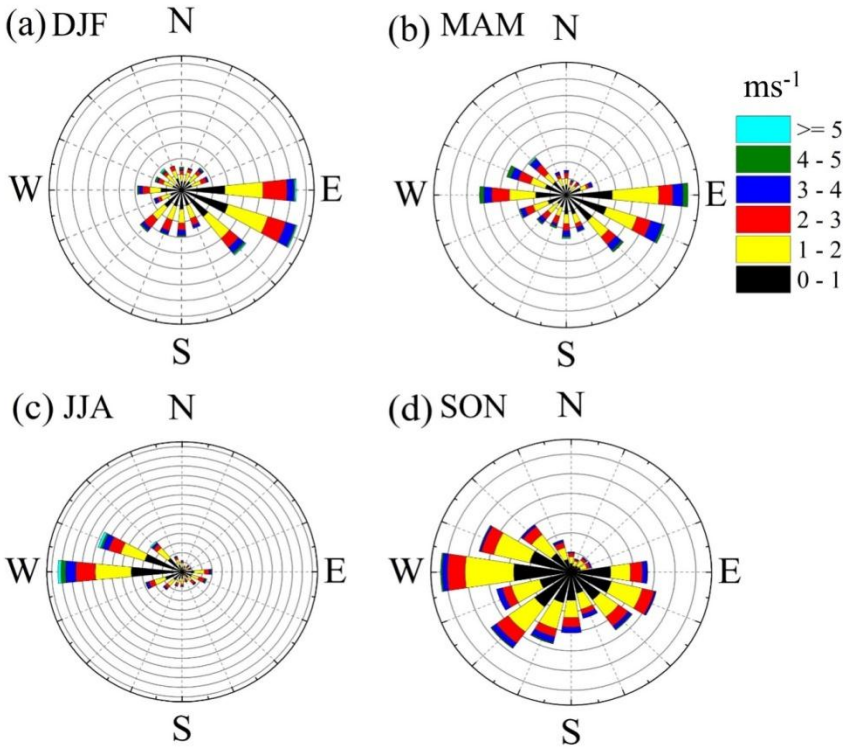

Figure 4.2: *Ground based surface wind speed and wind direction during different seasons (a) DJF (b) MAM (c) JJA and (d) SON at Pantnagar for the period of 2010-2012. The colored scale represents wind speed in m* s^{-1}.

Maximum temperature of 41-42 ^{o}C (hourly average) is observed in May-June and low (3^{o}C) in January (Figure 4.3). The solar radiation increases from January to June and decreases during July-September due to prevalent cloudy and rainy conditions. The relative humidity (RH) is lowest in April (19.2± 8.4 %) and highest in August (73.7 ± 9.1 %). The site starts experiencing intense rainfall from last week of June which increases in July-August month leading to the maximum rainfall in these two months (812 mm; 55 % of annual). The site receives the rainfall till mid of September, which ceases afterwards due to the withdrawal of southwest monsoon. The minimum rainfall was experienced in winter season ~85 mm (~5.8 % of annual) with November being the driest month of the year.

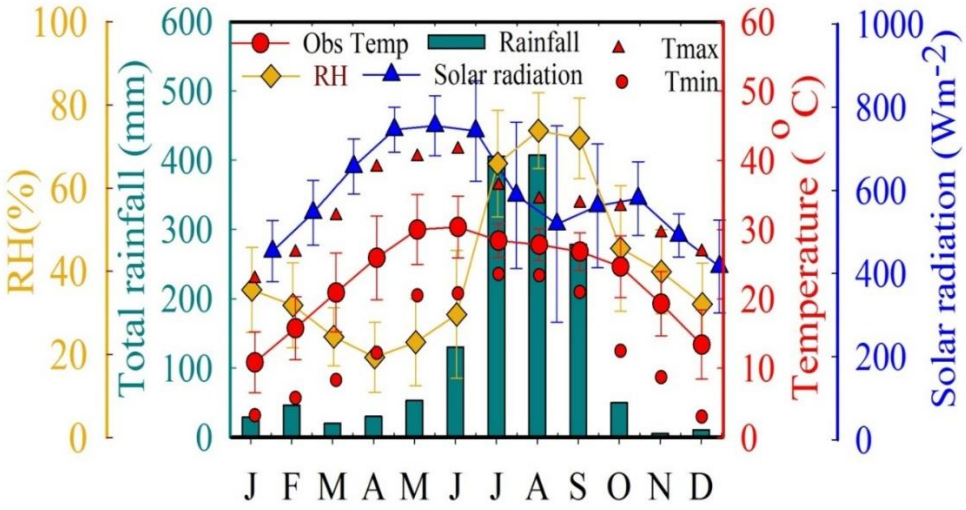

Figure 4.3: *Monthly average, maximum and minimum temperature (°C) from ground based observations. Daytime (12-14 hrs) average solar radiation (Wm^{-2}) and monthly average relative humidity (%) based on GDAS data. Monthly total rainfall (mm) from TRMM at Pantnagar during year 2009 to 2012. Error bars represents one sigma deviation from mean.*

4.2. Diurnal and Seasonal Variations in BC Mass Concentration

BC data from May 2009 to December 2012 are screened through three sigma filter and data points beyond three sigma levels in the nine point running mean are considered as outliers and hence removed. This led to the removal of about 2.5% data. The filtered data is then averaged over 15 minutes and used for further analysis. The detail regarding the data count is shown in Table 4.1.

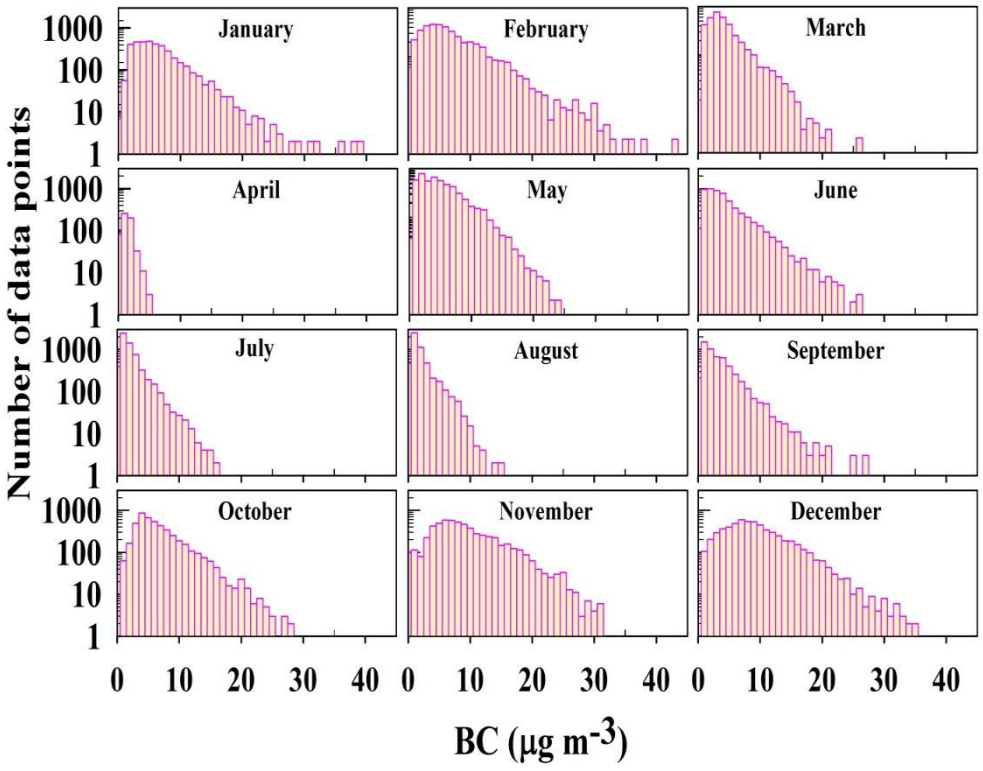

Figure 4.4: *Data distribution of BC mass concentration (15 minutes data) observed at Pantnagar during May 2009-December 2012. Each bin corresponds to a concentration of 1 μg m^{-3} of BC mass concentration.*

Frequency distribution of BC mass concentration (15 minutes averaged) at interval of 1 μg m^{-3} show positively skewed tendency in all the months with a sharp decrease in monsoon months (July-August) (Figure 4.4). BC mass concentrations up to the ceilings of 10 μg m^{-3}, 20 μg m^{-3} and 30 μg m^{-3} are found to constitute 84%, 98.7%, and 99.9% of the total data, respectively. A few events (less than 0.1% of the total data) of BC values greater than 30 μg m^{-3} are also observed especially during late evening hours of week days in winter.

Diurnal variations in monthly average BC, for the study period shown in Figure 4.5, depict two peaks; one in the morning (0700–0900 hrs; local time) and the other in the evening (1700–2100 hrs). The evening peak is much stronger than the morning peak in all the seasons, as indicated by a significantly higher amplitude (4.0-8.5 μg m^{-3}) of evening peak compared to the morning peak (1.4– 3.5 μg m^{-3}) (Table 4.2). BC starts increasing about an hour before sunrise, attains the morning peak within an hour or two and decreases afterwards, which result in lowest levels in the afternoon. BC again starts increasing around sunset time and attains evening peak after about an hour of sunset and then decreases later in night. It is interesting to note that the daytime BC levels are lower as compared to the night time BC levels. The morning peak in BC is mainly associated with fumigation effect arising due to entrainment of BC from the nocturnal residual layer [*Nair et al.,* 2007; *Beegum et al.,* 2009] and due to morning anthropogenic activities. As the day proceeds, surface heating leads to increase in the mixed layer height allowing BC to mix into a larger volume which in turn leads to dilution of surface BC.

Table 4.1: *Monthly average BC mass concentrations with standard deviation, maximum BC, minimum, number of BC data counts (15 min average) and average mixing layer depth (MLD) from 1200 to 1400hrs during the observation period from May 2009 to Dec 2012 at Pantnagar.*

Month	**BC** (μ**g m**$^{-3}$)	**Max**	**Count**	**MLD** **(m AGL)**
Jan	6.5±4.4	49.1	3843	1012±371
Feb	7.3±5.5	43.1	4325	1391±525
Mar	4.4±3.1	26.5	3762	2141±835
Apr	1.4±0.8	5.0	588	3057±981
May	5.4±3.8	24.0	5416	3041±850
Jun	4.3±3.6	26.3	5739	2811±1024
Jul	2.2±2.0	20.1	5920	1430±650
Aug	1.9±1.8	15.0	5224	989±436
Sep	3.3±3.0	27.5	5294	1029±287
Oct	6.7±3.9	40.5	4626	1048±263
Nov	9.2±5.2	36.3	5822	994±181
Dec	9.3±5.1	41.9	5887	832±193
Annual	**5.5±4.7**	**49.1**	**56446**[a]	**1644±302**

[a]represents total counts

After sunset, mixing reduces and soon after sunset as the land cools faster, this leads to formation of nocturnal layer and thus traps BC and other pollutants

After sunset, mixing reduces and soon after sunset as the land cools faster, this leads to formation of nocturnal layer and thus traps BC and other pollutants near the surface, as a result enhanced BC during nighttime. These diurnal variations are discerned from year to year, leading to specific pattern of morning, daytime and night time BC levels, due to boundary layer evolution.

Diurnal variability in BC is further quantified by calculating diurnal amplitude as the difference between maximum and minimum BC concentration within a day. The evening peak amplitude shows higher values from October (11.2 µg m^{-3}) to February (9.0 µg m^{-3}) and much lower amplitude is seen in July-August (about 3 µg m^{-3}), apart from in April, where only 9 days observations are available.

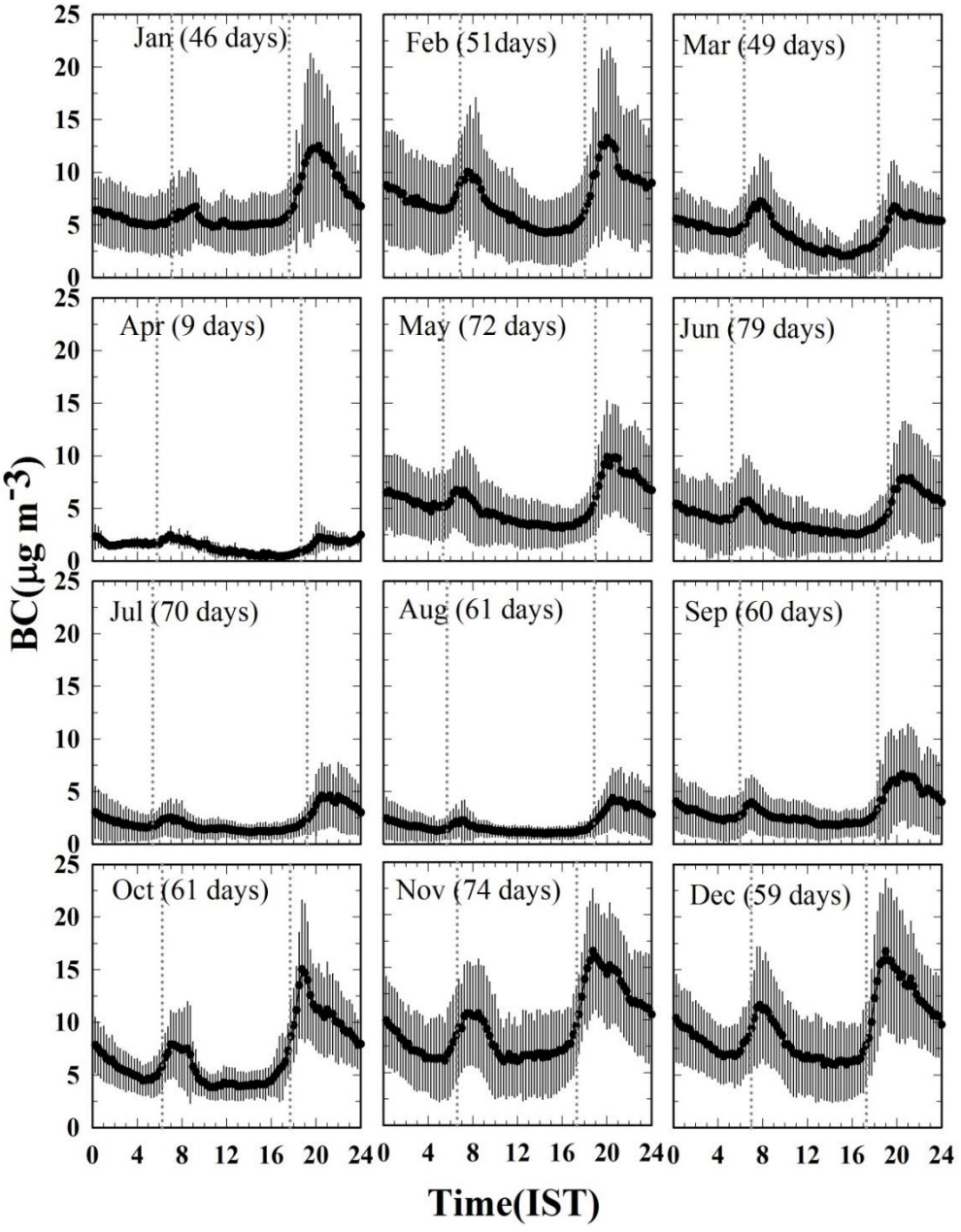

Figure 4.5: *Monthly average diurnal variations of BC mass concentration (μg m^{-3}) at Pantnagar during May 2009-Dec 2012. The sunrise and sunset time are shown by dotted lines. Total numbers of observations days are written within braces for each month. All the time mentioned are in Indian standard time (IST), which is 5.5 hrs ahead of GMT.*

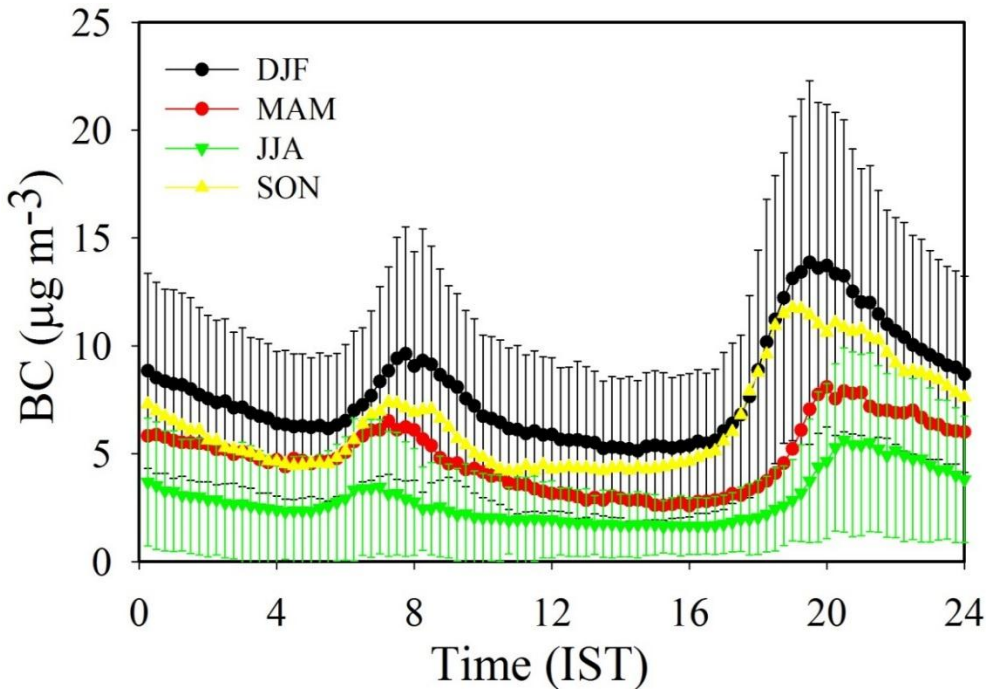

Figure 4.6: *Diurnal variation of BC mass concentration (µg m^{-3}) for different seasons, winter (DJF), spring (MAM), summer-monsoon (JJA) and autumn (SON) at Pantnagar.*

Seasonally, highest diurnal amplitude is seen in winter followed by autumn and minimum amplitude in summer-monsoon (Figure 4.6, Table 4.2). The amplitude of morning and evening peaks also show more-or-less similar seasonal variation. In addition, we also calculated the evolution rates of both peaks (morning and evening) for each season (Table 4.3). Evening time increase rates are observed to be about two times higher than the morning time increase rates, while their decrease rates are more-or-less similar. Similar to the amplitude, increase rates are maximum in winter and minimum in summer-monsoon period.

Seasonal variations in hourly and daily averages BC have been examined in Figure 4.7. BC is lowest in July-August, which increases after September and remains high until February. Hourly and daily average BC values as high as ~25 µg m^{-3} and ~15 µg m^{-3}, respectively, are observed at Pantnagar during late autumn and winter. Monthly average BC is maximum in December (9.3±5.1 µg m^{-3}) and minimum in August (1.9±1.8 µg m^{-3}) (Table 4.1). BC levels are also lower in April but as mentioned earlier, number of observations are lesser (9 days) in April. The seasonal mean BC is maximum in winter (7.9±5.2 µg m^{-3}) and minimum in summer-monsoon (2.8±2.8 µg m^{-3}) as shown in Figure 4.7. The seasonal variation in average BC has been found similar to the seasonal variation in amplitude of BC (Table 4.2).

Table 4.2: *Seasonal mean morning and evening BC amplitude, mixing layer depth (m AGL) and seasonal mean BC, along with the annual mean for year 2009-2012.*

	BC Amplitude		Mixed layer Depth	Mean BC
	Morning	Evening	(m AGL)	(µg m^{-3})
DJF	3.5	8.5	1078±285	7.9±5.2
MAM	2.4	5.5	2746±524	4.8±3.6
JJA	1.4	4.0	1743±950	2.8±2.8
SON	2.9	7.1	1023±27	6.5±4.9
Annual	3.3	6.4	1647±869	5.5±4.7

Table 4.3: *Rate of increase and decrease (µg m^{-3}/hr) of morning and evening BC mass concentration during different season at Pantnagar*

	Morning BC evolution rate		Evening BC evolution rate	
Season	Increase rate	Decrease rate	Increase rate	Decrease rate
DJF	1.5	1.3	3.1	1.5
MAM	1.1	1.0	2.1	0.6
JJA	0.7	0.5	1.1	0.5
SON	1.3	1.2	3.0	1

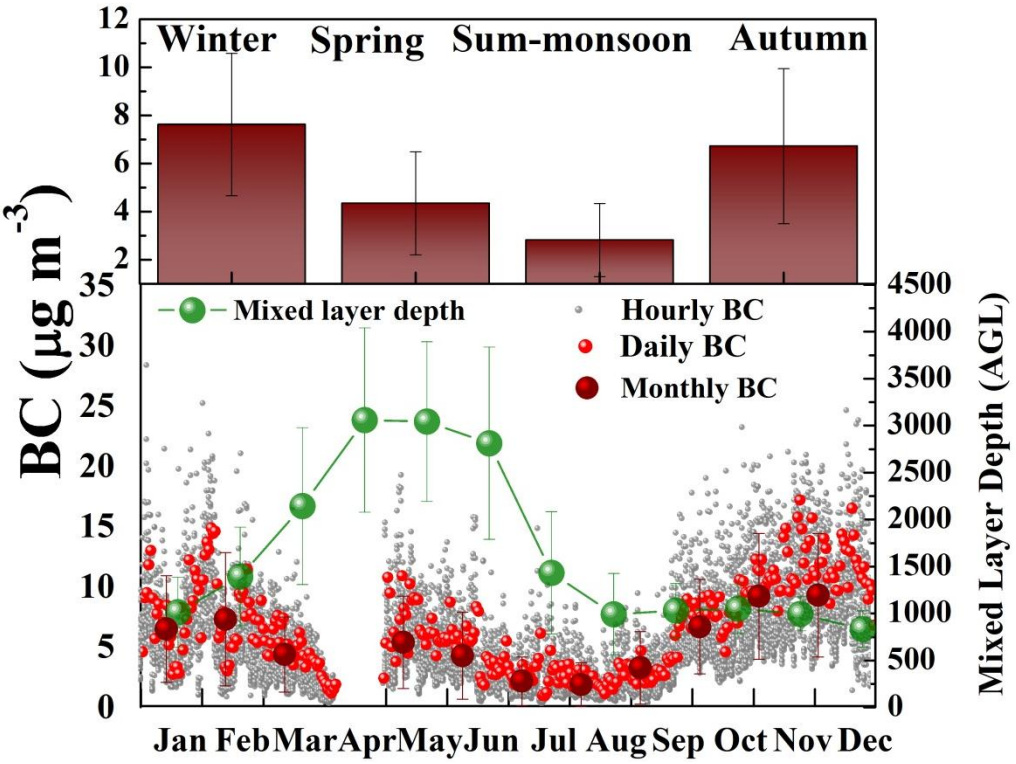

Figure 4.7: *Monthly variations in hourly and daily average BC mass concentrations from 15 min data from 2009 to 2012. Noontime (1200-1400 hrs) average monthly mixing layer depth estimated during 2009-2012 is also shown. BC mass concentrations during four seasons is shown in upper panel. Here error bars represents one sigma deviation from mean.*

4.3. Influence of Mixing Layer Depth on BC

In order to understand the influence of variations in planetary boundary layer height on diurnal and seasonal variations of BC, association between BC and mixed layer depth (MLD) have been examined. The MLD represents the volume available for dispersion of pollutants due to convection or mechanical turbulence and plays an important role in determining the concentration of pollutants at surface. As observations of planetary boundary layer height are not available at our site, we have used noon-time (1200-1400 hrs, IST) mixing layer depth (MLD) estimation from the HYSPLIT model around Pantnagar (1^{o}x1^{o}). The detail regarding MLD estimation from HYSPLIT is given in Chapter 2.

Seasonal variations in monthly average MLD during 2009-2012 is shown in Figure 4.7. Mixed layer depth is maximum (about 3000 m) during April-June. It decreases to about 1000 m during August-January with a minimum value of ~832±193 m in December (Table 4.1). Highest MLD in April-May results from higher solar radiation and surface temperature. The decrease in MLD during monsoon months is related to decrease in solar radiation due to cloudy conditions and rainfall. Higher BC level in winter (7.9±5.2 μg m^{-3}) and autumn (6.5±4.9 μg m^{-3}) coincide with lower height of MLD during these seasons (about 1050 m) (Table 4.2) indicating that BC emitted at the surface during these seasons is allowed to mix into a much smaller volume compared to spring and summer seasons.

A correlation analysis between daytime (1100-1700 hrs) BC and MLD is shown in Figure 4.8, an inverse correlation is observed between them, with highest anti-correlation (R^2=0.89) in winter followed by autumn (R^2=0.76), spring (R^2 = 0.61) and minimum in monsoon (July-August) (R^2=0.33). This suggest that variations in MLD have strong influences in wintertime BC variations, while MLD is not playing as an important role during the monsoon period when observations site is under the influence of the rainfall and receives air-masses from oceanic regions. We have further examined the Carbon Monoxide (CO) variations alongwith BC variations.

4.4. Black Carbon and Carbon Monoxide Evolution

We have examined the surface BC and Carbon monoxide (CO) variation with the mixing layer depth and their association with each other at Pantnagar. Their association with MLD provides information about their evolution, while BC-CO correlation provides useful information whether the site is influenced by fresh or aged emissions. A strong correlation means influence of fresh

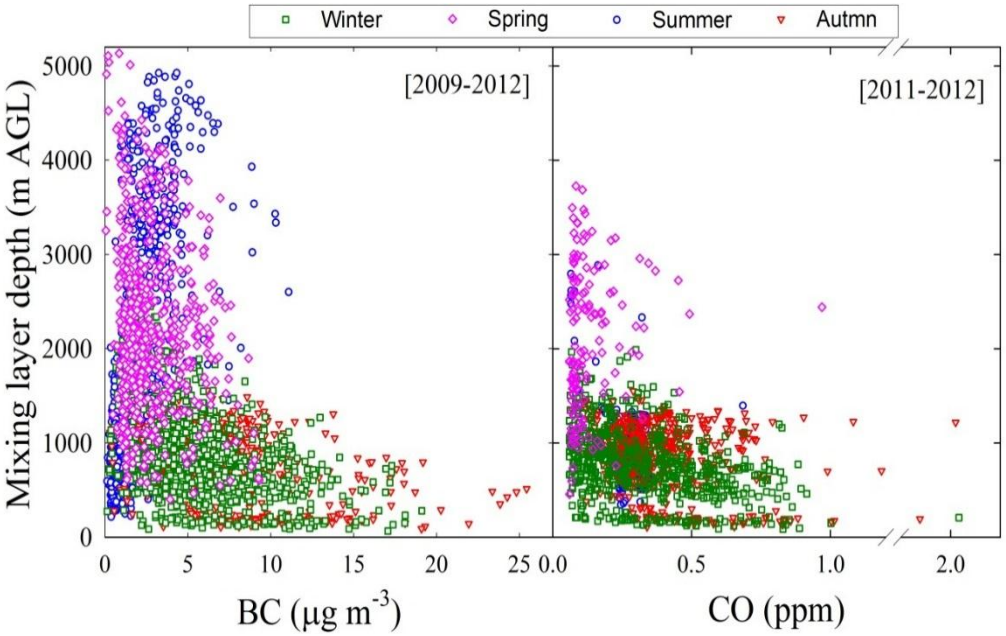

Figure 4.8: *Correlation of hourly BC mass concentration (µg m^{-3}) and Carbon Monoxide (CO) with mixed layer depth (m AGL) during day time (1100 hrs to 1700 hrs) for different seasons at Pantnagar from 2009-2012.*

emissions with same emission sources while a poor correlation means influence of aged emissions with different emission sources. The CO observations are made using an instrument based on non-dispersive infrared (4.6 µm) absorption technique, the detail description of which is described in *Sarangi et al.,* [2014]. Similar to BC, strong anti-correlation is seen between CO and MLD (Figure 4.8), suggesting similar evolution of both BC and CO along with MLD, which indicate that the surface BC and CO variations both are governed by similar boundary layer processes. It is noteworthy that the boundary layer evolution leads to minimum of ozone around sunrise time [*Ojha et al.,* 2012], while minimum BC does not occur around sunrise, but in the daytime. This is suggesting that role of the boundary layer dynamics needs

to be consider together with other physical/chemical processes as it has different impact on evolution of different species.

We have also used simultaneous observations of BC and CO at Pantnagar, as both are linked to each other by combustion process and depending on type and amount of combustion, their emission ratio changes in the combustion process [*Seinfeld and Pandis,* 1998]. Both BC and CO show a good positive correlation (Figure 4.9). In general, strong correlation among these two species suggests the common combustion sources and fresh emissions. BC and CO showed positive correlation during the winter (R^2 = 0.75) and late autumn seasons (R^2 = 0.72). During this period, the air masses were mostly circulating over this region and relatively shallower mixing layer depths were also observed. The positive correlation (R^2 = 0.62) is observed in spring, however during the summer-monsoon season the BC and CO are not well correlated (R^2 = 0.05). The airmasses arrives from different directions in summer-monsoon most of which are of marine origin. The marine airmasses leads to the scavenging of aerosols as well as gases during this season. This is allowing to mix different airmasses and leading to a poor correlation between BC and CO. Lifetime of CO is much higher than BC and the marine airmass could lead to the different level of the scavenging of BC than CO and hence poorer correlation in monsoon [*Baumgardner et al.,* 2002]. Air-masses relatively stagnate in colder temperatures during winter/autumn that is leading to show better correlation between BC and CO (Table 4.4).

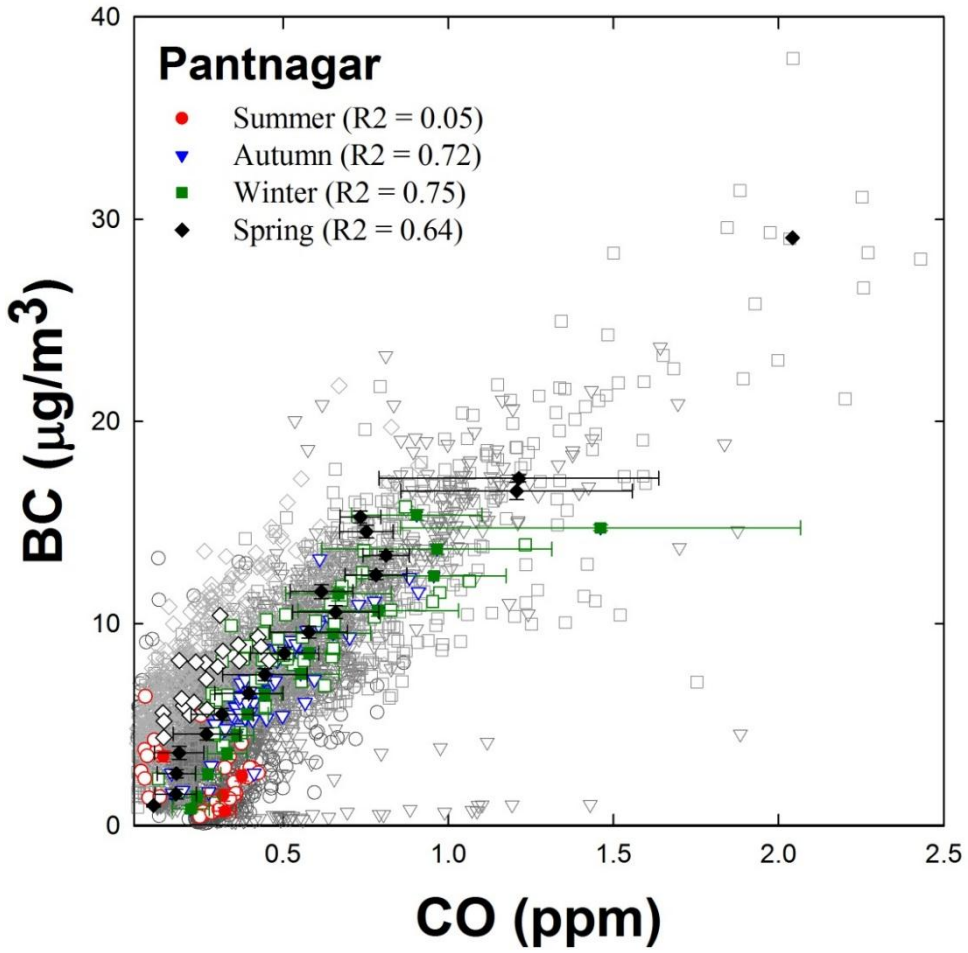

Figure 4.9: *Correlation between simultaneously observed hourly average (open grey symbols) surface CO and BC mass concentrations along with the daily average (color open symbols) binned averages (color filled symbols) for different seasons. CO observations are available during August 2011-December 2012.*

Table 4.4: *Data Statistics of Black Carbon (BC) versus Carbon Monoxide (CO) Regression Analysis.*

Season	Regression slope	Intercept	Correlation
Winter	11.4	2.8	0.75
Spring	13.5	4.5	0.62
Summer-Monsoon	4.3	0.7	0.05
Autumn	12.2	0.7	0.72

Thus based on BC and CO correlation it is inferred that airmasses of fresh origin might influence the air quality at Pantnagar significantly in winter, autumn and spring, while the aged airmasses with different sources might influence the site in summer-monsoon in the absence of scavenging. It is also inferred that the similar types of combustion sources are contributing both BC and CO mostly in winter and autumn at Pantnagar, while the sources of both BC and CO are different in summer-monsoon. Influence of simultaneous emissions from cooking/domestic use of fuel cannot be ruled out; however it is difficult to confirm it due to non-availability of suitable tracer's observations. The average slope (BC versus CO) value (10.4 μg $ppmv^{-1}$) over present IGP site is much higher than those over Mexico and Germany [*Baumgradner et al.*, 2002] indicating that BC emissions are dominating over this region. Simultaneous observations of CO and BC are not reported over other Indian sites to our knowledge, to make a comparison.

4.5. Association of BC with Large-Scale Wind Patterns

Seven-days back-air trajectories are calculated at 1000 m AGL for Pantnagar for each season during study period (2009-2012) (Figure 4.10) and then clustered. The Ward's Hierarchical method is used by combining the nearest trajectories according to angular distance, in order to

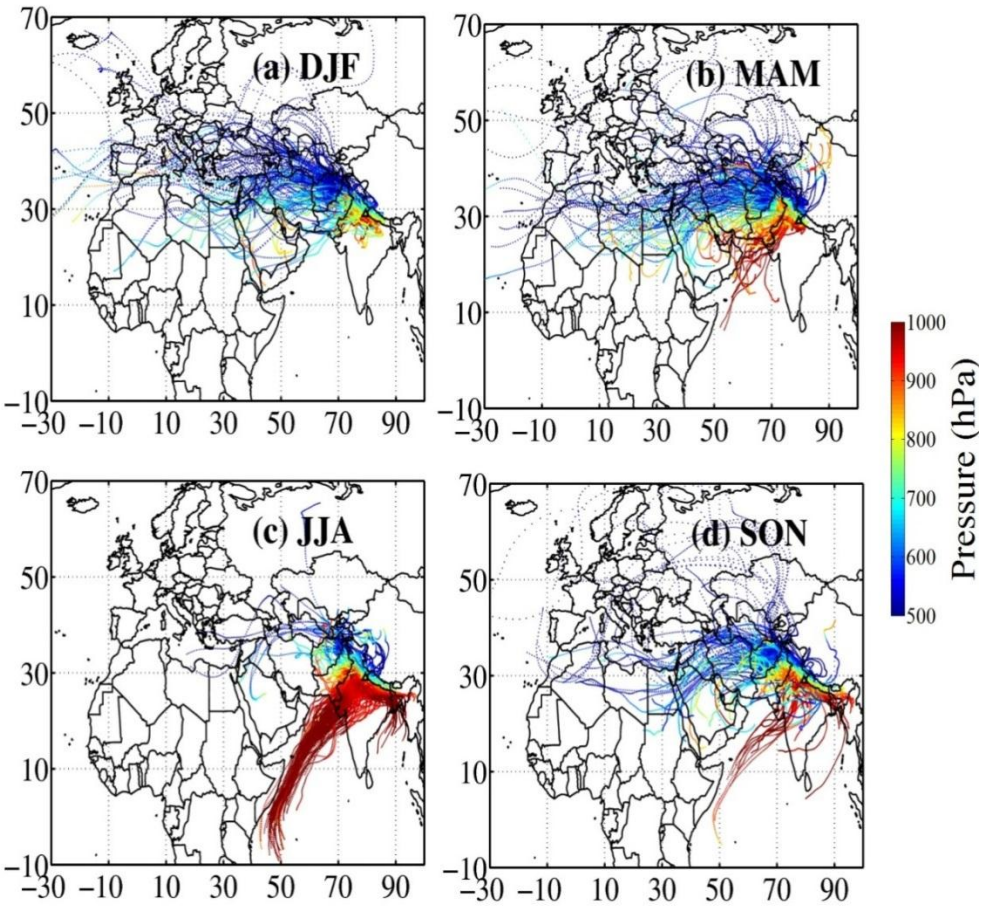

Figure 4.10: *Seven days back-air trajectories (1000 m AGL) at Pantnagar for different seasons (a) winter season (DJF) (b) spring (MAM) (c) summer-monsoon (JJA) and (d) autumn (SON) during study period from year 2009 to 2012. Atmospheric pressure (hPa) along the trajectories has been shown in order to represent altitude range attained by air masses before arriving at the observation site. The location of the observing site is shown by black upward triangle.*

determine the direction from which the air masses are reaching the site. The detail regarding the method is discussed in detail in Chapter 2. These back-air trajectories in four seasons are clustered in five different groups defined as follows. The trajectories originating from west, north-west, north-east, south-west and south-east are assigned to the groups W, NW, NE, SW and SE, respectively. The percentage contribution of these groups is shown in Table 4.5. During winter and spring, Pantnagar is influenced by the air masses originating from W and NW with a larger contribution from the NW group (~63%) in winter and from W group (55%) in spring. Additionally, air-masses are almost stagnated at lower altitudes in winter, while they are moving faster in spring. During summer-monsoon, marine airmasses (~63%, both SW and SE) from the oceanic regions of the Bay of Bengal (SE) and the Arabian Sea (SW) arrives at the site while the air mass from the continental origin from NW is less ~37% at Pantnagar. The air mass pattern changes again during autumn and is mostly of continental origin from W/NW, however airmass arriving from SE are quite less. This change in air mass is due to the withdrawal of the summer-monsoon from Indian region.

We further conducted the Concentration Weighted Trajectory (CWT) analysis [*Stohl*, 1996] the method of which is discussed in Chapter 2 and is used here to identify the possible sources contributing to the observed BC at Pantnagar. BC mass concentration weighted trajectories and percentage contribution of different clusters to the BC in four seasons are shown in Figure 4.11 and Table 4.5. This source apportionment study reveals that the BC contribution from

NW and W is maximum ~7-8 µg m^{-3} in both winter and autumn. It is estimated that the ~62% of air masses arrives via NW in winter contributing BC of ~8.54 µg m^{-3}.The air masses shifts from NW (45%) to W (55%) direction in spring and W sector contributes BC ~4.89 µg m^{-3}. Influences of SE (38%) and SW (24%) air masses are seen in summer-monsoon and BC levels drop to ~2.21-2.59 µg m^{-3} (Table 4.5). After the withdrawal of the southwest monsoon, contribution from NW direction again dominates in autumn and BC levels in this cluster are again high (~7.89 µg m^{-3}).

Table 4.5: *Trajectories cluster during different seasons and cluster mean value of BC (µg m^{-3}) with respect to different trajectories for corresponding seasons.*

Season	Direction	Trajectories (%)	Mean BC
DJF	W	37.5	7.15±3.15
	NW	62.5	8.54±3.66
MAM	W	55.0	4.89±2.65
	NW	45.0	5.14±2.88
JJA	NW	37.0	4.05±2.36
	SE	38.6	2.21±1.05
	SW	24.3	2.59±1.78
SON	SE	23.0	3.95±2.84
	W	22.1	7.11±4.31
	NW	54.5	7.89±3.18

The source apportionment study reveals higher level of BC along the IGP region (NW or W sector) in all the seasons (although in different amount). The air masses passes through the IGP region having high BC concentration before arriving to the site and thus BC levels at Pantnagar are expected to be

augmented and influenced mostly by air masses arriving via IGP, especially due north-west (NW) of the site. Lower levels in SE and SW regions are due to origin of these air masses from the oceanic regions. The marine air is poor in BC and also leads to dilution of continental emissions after it reaches mainland.

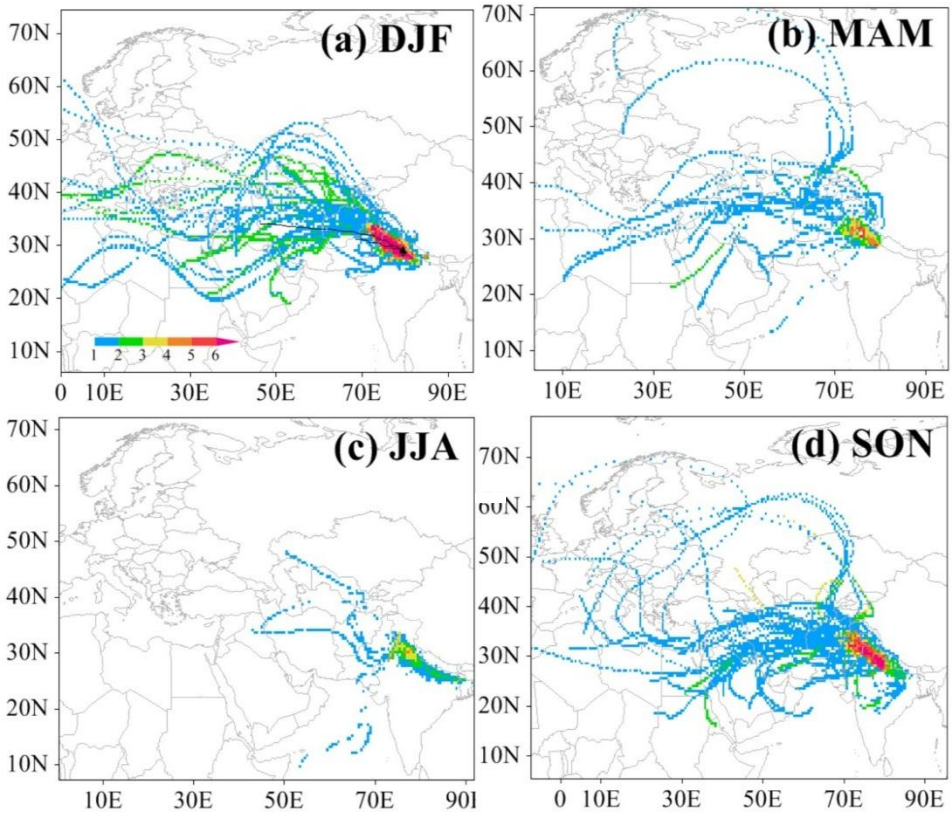

Figure 4.11: *Source apportionment using BC concentrated weighted trajectories during different seasons of 2009-2012. The color bar represents the BC mass concentration in µg* m^{-3}.

4.6. Weekly Variation in BC

The previous studies and present knowledge of weekly studies at several locations have revealed that the range and phase of the weekly cycles in aerosols and gases are

different at different places making the study of the weekly studies more important at individual places due to different habitat. This is also useful for studying the amount of anthropogenic emission during different days of a week. In this context, we assessed the impact of changes in anthropogenic activities around Pantnagar from weekdays (Monday to Friday) to weekend (Saturday and Sunday) on BC (Figure 4.12) which shows maximum for January month while less variation for other months. The diurnal variations during weekdays (Mon-Fri) and separate weekend days (separate variation for Saturday and Sunday) in the BC concentration at Pantnagar are examined in Figure 4.13 for January (winter) and November (autumn).

BC during weekends are lower than weekdays and are lowest on Saturday. The average evening peak BC is about ~15 µg m^{-3} in weekdays while it is only about ~8 µg m^{-3} on weekends in January. Lowest BC on Saturday at Pantnagar is likely due to the fact that market activities in a major business town, Haldwani, located about ~25 km due north of Pantnagar, are closed on Saturday. Consequently automobiles movement is significantly reduced on Saturday. Enhancement in BC levels is observed to be ~88 % during weekdays, when compared with weekends in January and it is statistically significant at $P \leq 0.001$ (students t-test). This difference is lesser (about 17%) in November but statistically significant (P=0.013). The difference is much lesser in spring and summer-monsoon.

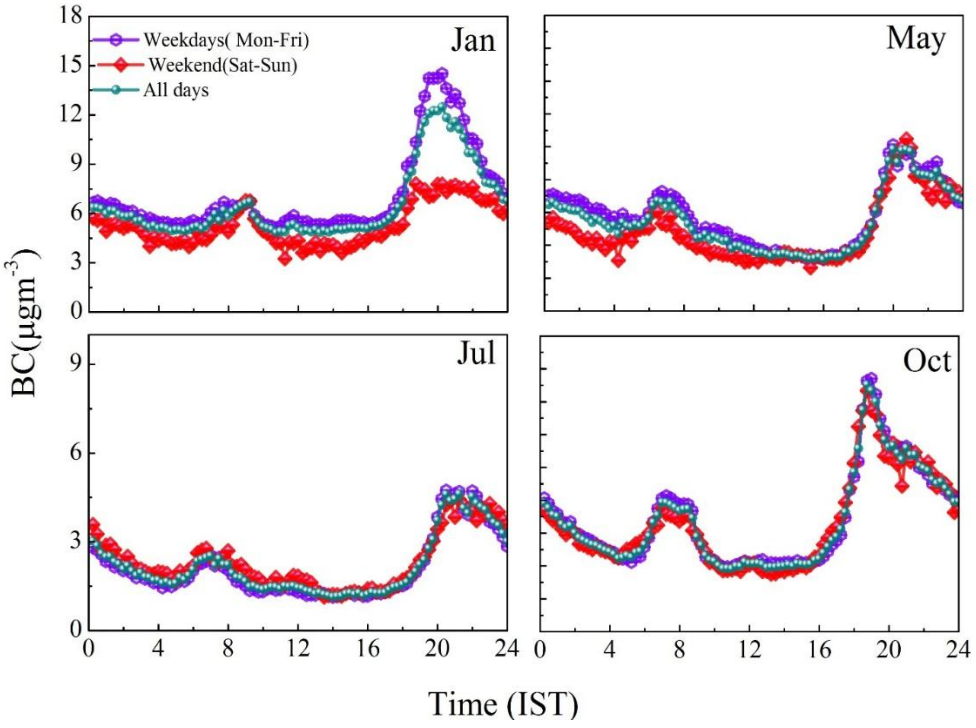

Figure 4.12: *Diurnal variation of weekly BC mass concentration at Pantnagar during different seasons for weekdays and weekend.*

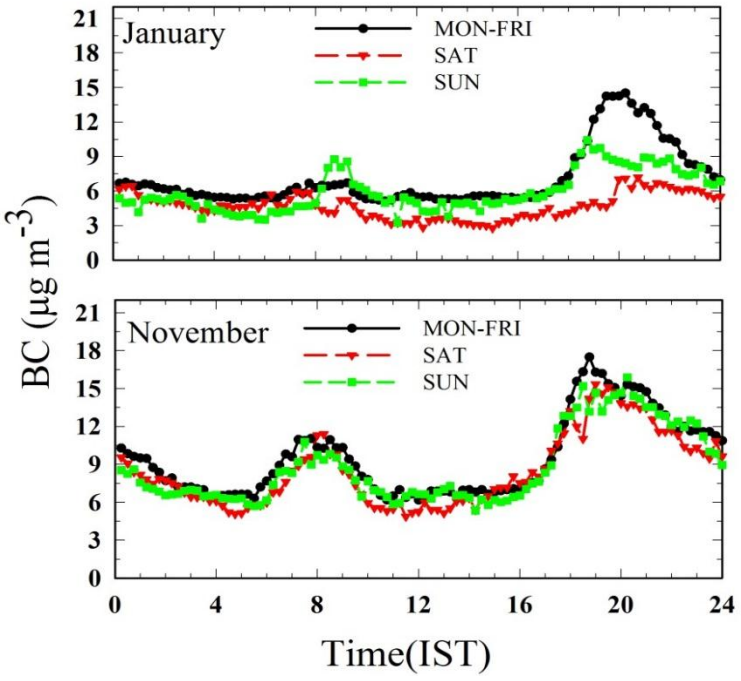

Figure 4.13: *Diurnal variations in BC mass concentration during weekdays and weekends (Saturday and Sunday) for January and November.*

Weekly cycle of aerosols are also studied at several locations in other studies. Weekly cycles at multiple locations in continental United States under IMPROVE network showed lower levels of elemental carbon on weekends [*Murphy et al.,* 2008]. The weekend low in PM10 was also observed over Mexico City where 10-40 % reduction was observed in weekends relative to weekdays [*Stephens et al.,* 2008]. A campaign mode study in Helsinki, Finland showed significantly lesser diurnal variation in weekend while enhanced variation in weekdays [*Järvi et al.,* 2008]. In contrast, aerosol loading was maximumduring the central weekdays and minimum in weekends at several locations of Europe [*Bäumer et al.,* 2008]. Over the Indian region, one of such weekly study by *Satheesh et al.,* [2011] at an urban city, Bangalore also reported reduction in BC, AOD and composite aerosol mass concentration during weekend by ~25%, ~15%, and

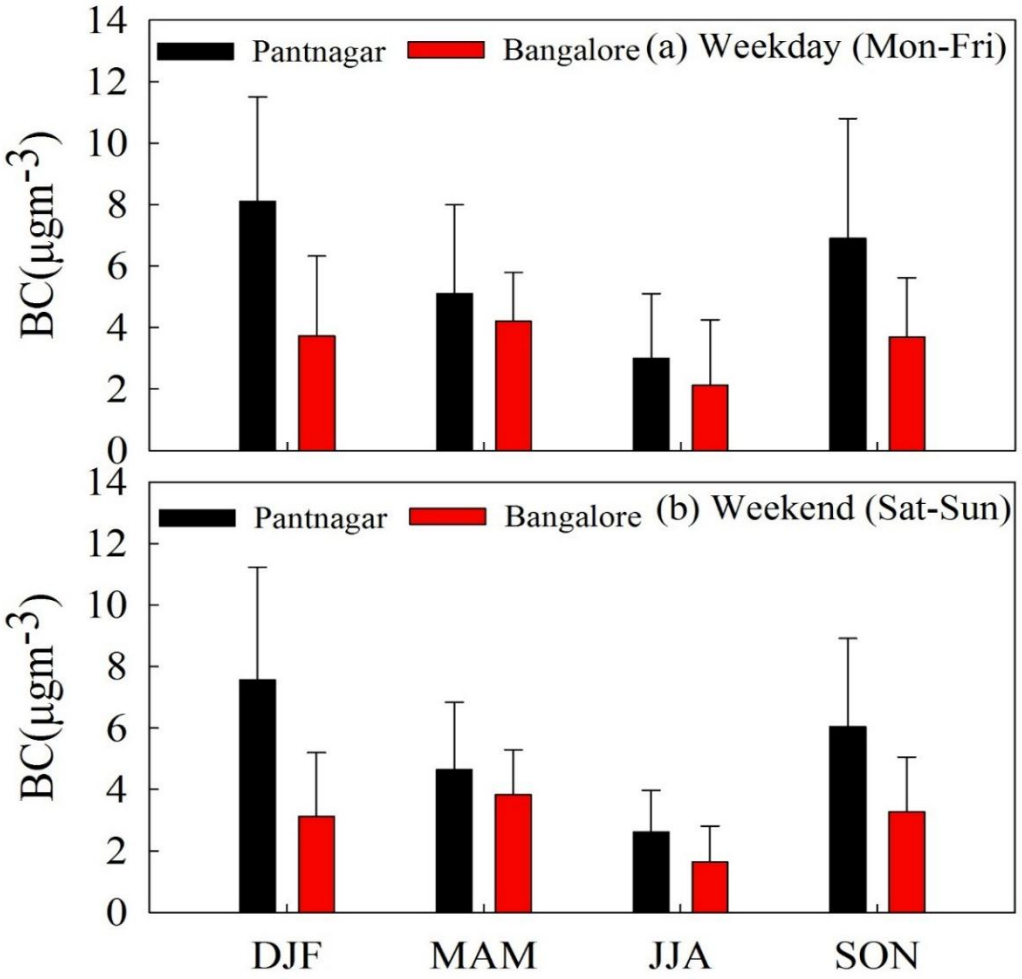

Figure 4.14: *Weekly BC mass concentration comparison during different seasons at Pantnagar and Bangalore.*

~24% respectively as compared with values in weekday indicating the columnar loading at this site was mainly governed by the local anthropogenic emissions. Weekly BC variation comparison at Pantnagar with that at Bangalore is shown in Figure 4.14.

Higher BC in weekdays might also be associated with traffic patterns and industrial activity during weekdays as compared to weekends with reduced industrial activity. The traffic during stable nocturnal boundary layer and in

stagnant air can also lead to higher BC which can alter these weekly variations. However these variations can be altered or completely masked by other factors like wind speed, wind direction, rainfall and long range transport. Nevertheless, it is shown in the previous section that wintertime higher BC levels are strongly associated with lower MLD.

4.7. Simulations of BC Using WRF-Chem

In this section, we have assess the ability of WRF-Chem model in simulating temporal, seasonal and diurnal variability of BC observed at Pantnagar. The detail description of the WRF-Chem and its set up is already discussed in Chapter 2. We could not conduct simulations for the entire year because of the limited computational resources. Alternatively, we chose to simulate three months namely January, May and July representing the winter, spring and summer/monsoon seasons.

The temporal variation of BC for each day for entire months has been compared (Figure 4.15) which shows high temporal variation in the observed ground based BC. The model, although is able to capture some of temporal variation, but the magnitude are highly underestimated by the model. It is quite interesting that the model simulated BC at 29N is quite low and also shows low episodic enhancements, while BC simulations at 28N are higher and also shows high episode

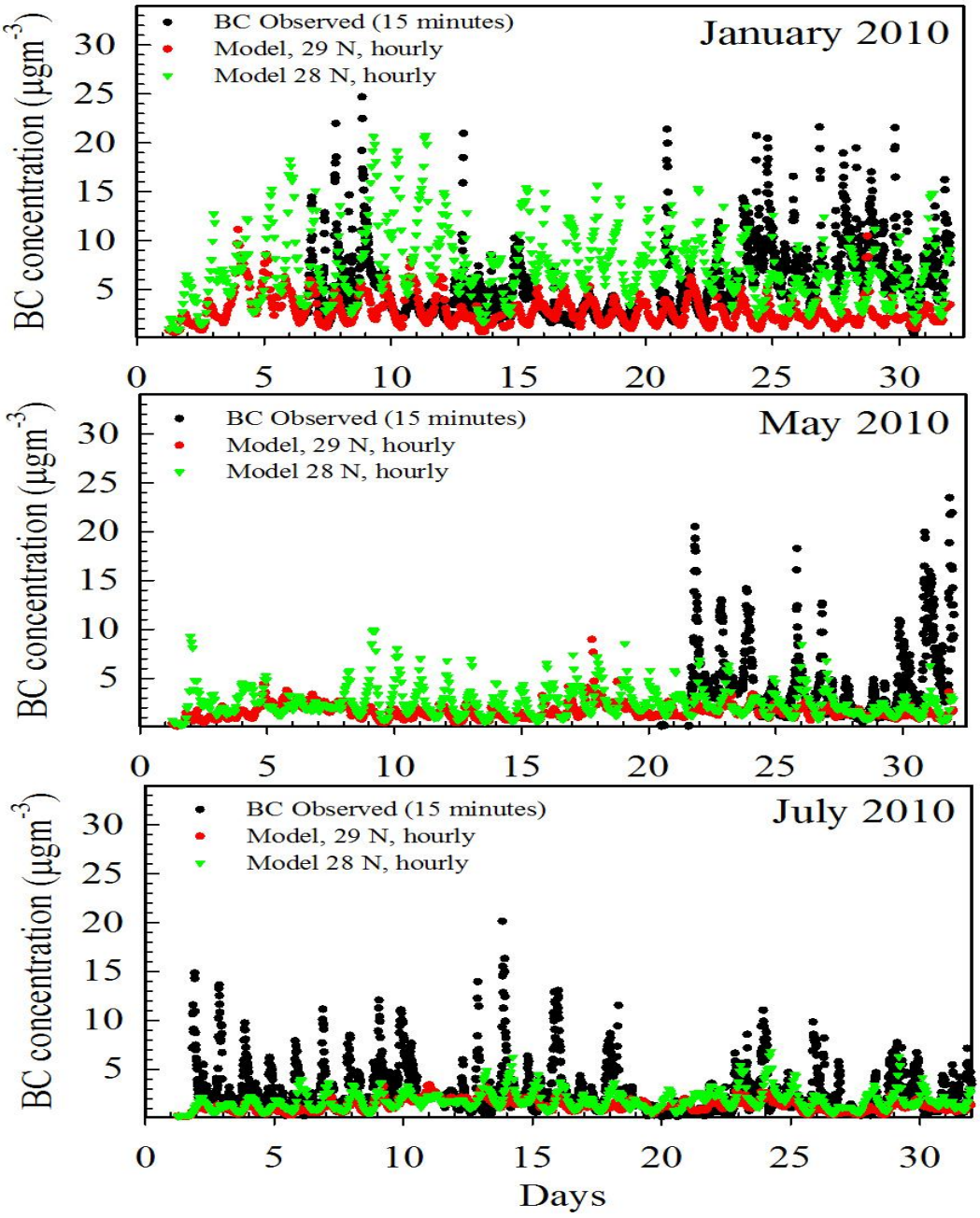

Figure 4.15: *The temporal variation of ground based BC mass concentration and model simulated BC mass concentration at Pantnagar for year 2010. The model simulations are available at 28N and 29N.*

enhancement in BC. Interestingly, sharp reduction in model simulated BC at both 28N and 29N is seen after the January month and both show significant low BC as compared to BC observed after January month. Although the

observed day to day episodic variations in BC are more related to the anthropogenic activities, we however has also examined if these episodic enhancement are associated with the mixing layer depths. The daily variation of MLD with observed and simulated BC is shown in Figure 4.16. BC variation with the PBL height reveals that the day to day variation of BC at Pantnagar are more related to local anthropogenic activities rather than the PBL heights.

Further the diurnal variations in BC are also simulated and are compared with the observed BC. The diurnal variations in observed and WRF-Chem simulated average BC mass concentrations during January, May and July are shown in Figure 4.17. The diurnal variations in deviation of BC from the observed and simulated mean BC for each hour is also shown in the right panel. Studies on diurnal pattern simulations of BC are sparse over Indian region. The model shows a mixed ability in simulating the observed diurnal variations in BC as it captures some features while misses some other. During all the months for which simulations were made, both the model and observations show higher values during nighttime and lower values during daytime indicating that model is able to qualitatively capture the variations in BC due to diurnal changes in the planetary boundary layer .

Average observed and modeled BC at Pantnagar during January, May and July are 6.6±2.2 and 2.4±1.2 μg m^{-3}, 5.5±1.8 and 1.6±0.7 μg m^{-3}, and 2.2±1.0 and 1.2±0.5 μg m^{-3}, respectively. Additional modeled BC levels at 28N are 6.1±3.1 μg m^{-3}, 2.5±1.6 μg m^{-3} and 1.8±1.0 μg m^{-3} during January, May and July,

respectively. These average levels at 28N are in better agreement with observations. Similar to the observations, the model also show a decrease in BC from January to

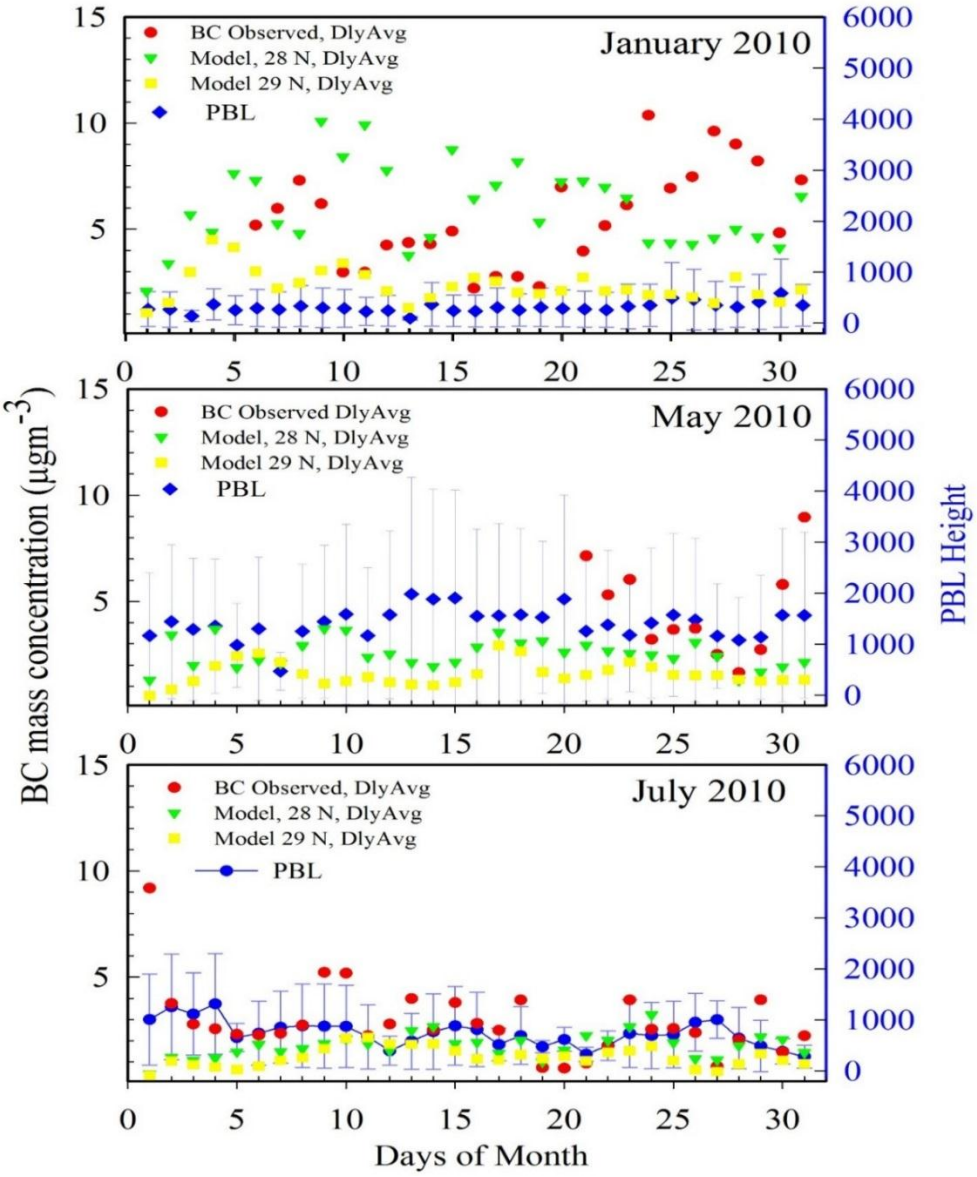

Figure 4.16: *The Daily average variation of ground based BC mass concentration and model simulated BC mass concentration along with the Planetary boundary layer height (PBL) at Pantnagar for year 2010. The model simulations are available at 28N and 29N.*

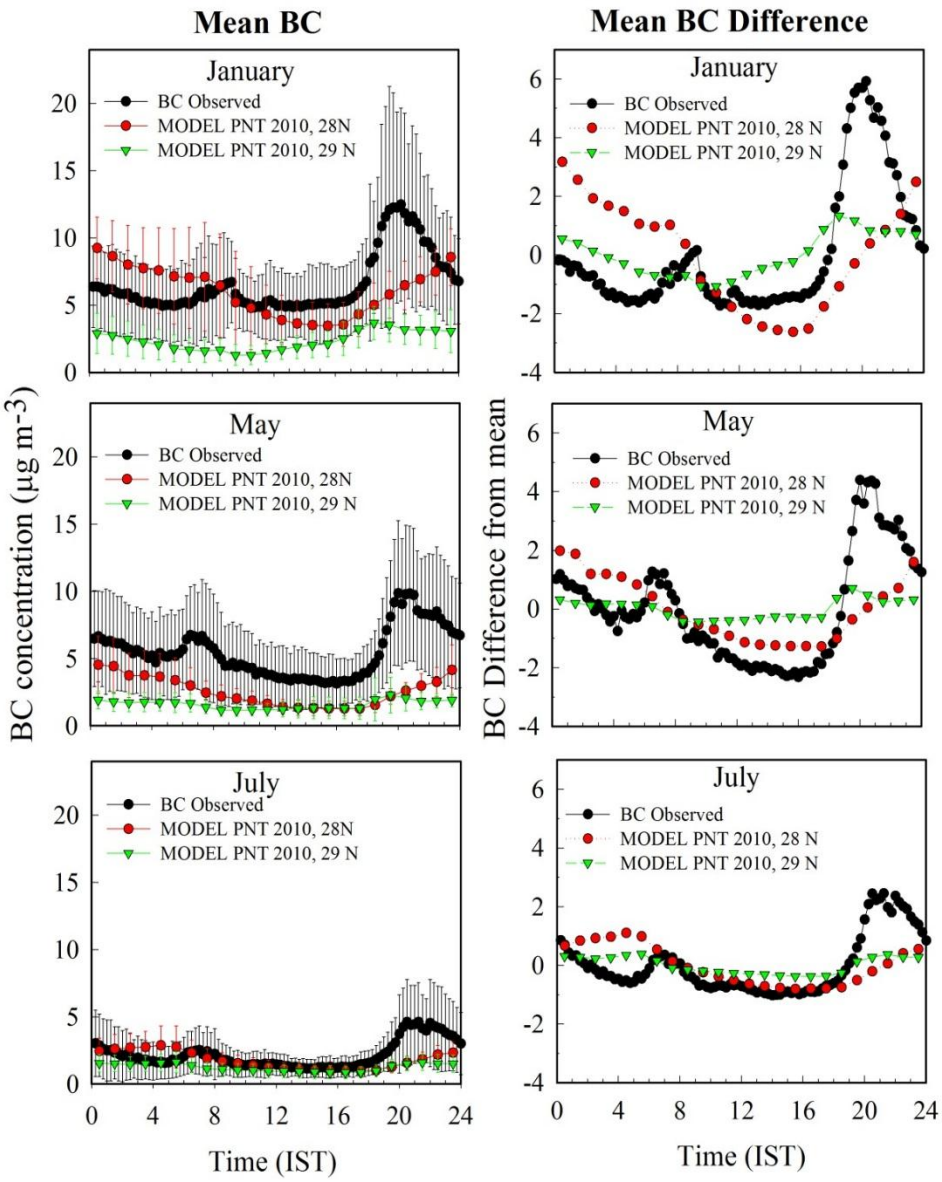

Figure 4.17: *Diurnal variations in observed and WRF-Chem simulated (year 2010) BC mass concentrations during January, May and July are shown in the left panel. Right panel shows the diurnal variation in deviation of observed and simulated BC from the respective mean BC mass concentrations.*

July indicating that model is able to qualitatively capture the seasonal variation in BC but fails to capture the magnitude of decrease. This also highlights the

role of meteorology in controlling seasonal diurnal variation of BC at Pantnagar because BC emissions provided as input to the model do not have a seasonal cycle.

In summary, the WRF-Chem model shows ability to capture features of the diurnal and seasonal variations of BC mass concentrations at Pantnagar but more work is required especially in improvement of diurnal and seasonal variability of BC emissions in and around Pantnagar. In addition, co-located observations of planetary boundary layer height are also essential for better evaluation of model performance.

4.8. Absorbing Aerosols and Aerosols Optical Depth (AOD)

In this section, the seasonal variations in AERONET retrieved AOD are examined over Pantnagar to qualitatively understand whether BC is a dominant component of the total and absorbing aerosol load over Pantnagar. The spatial variation of Ozone Monitoring Instrument (OMI) retrieved aerosol Index is also studied to understand large-scale distribution of absorbing aerosols over the Indian subcontinent. Generally, absorbing aerosols (desert dust, smoke, volcanic ash, etc.) decrease the spectral contrast yielding positive AI values, whereas non-absorbing aerosols and clouds increase it slightly resulting in small negative AI values [*Torres et al.,* 1998]. The spatial variation of AI reveals the presence of significant absorbing aerosols over the wide spread of IGP in spring season with high AI (AI > 1.5) (Figure 4.18). In the monsoon months of July-August, AI is lowest due to rainfall leading to scavenging of aerosols over most of Indian regions, except over western border.

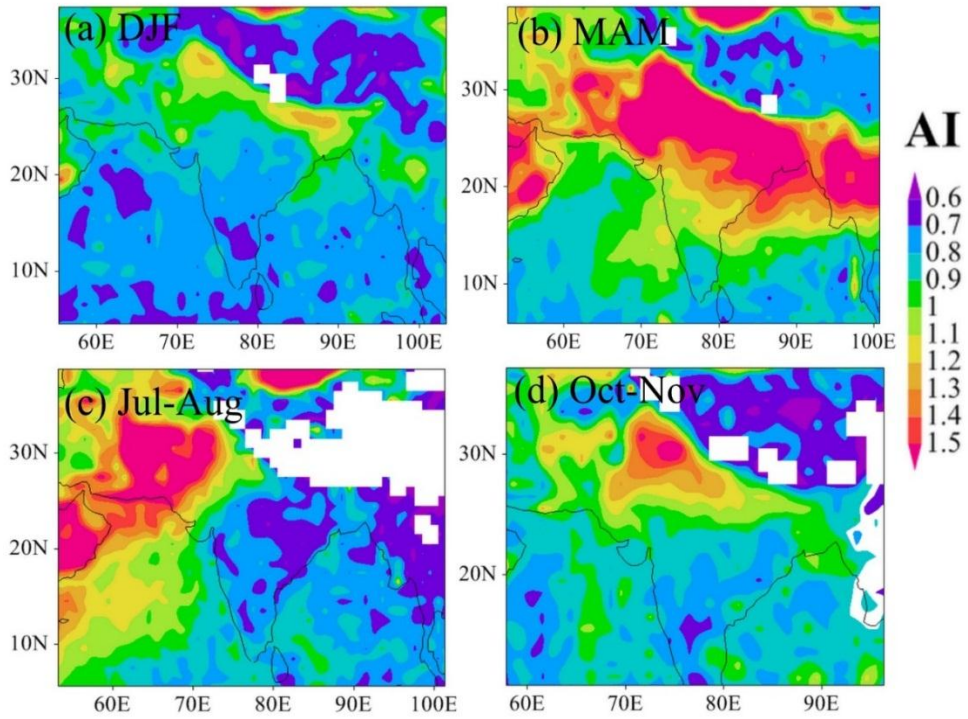

Figure 4.18: *Spatial variation of OMI aerosol index (AI) during (a) winter (DJF), (b) spring (MAM), (c) monsoon (July-August), and (d) autumn (October-November).*

Monthly average AERONET AOD (500 nm) at Pantnagar for the year 2008-2009. Monthly average AOD is maximum (>0.6) during late spring (Figure 4.19). The data statistics reveals that about 50% of data have AOD value more than 0.5 and about 90% data have AOD up to 1.0. This implies that the columnar abundance of aerosols is quite significant throughout the year. The annual mean AOD (500 nm) is~ 0.56±0.32 at Pantnagar. AOD in winters (December–February) is also higher (AOD > 0.4), indicating the significantly aerosol loading, suggesting urban like characteristic of the site. However, different seasonal cycle of AOD, when compared to BC, observed at

Pantnagar indicates that BC is likely not the dominant component of aerosol loading at Pantnagar by mass.

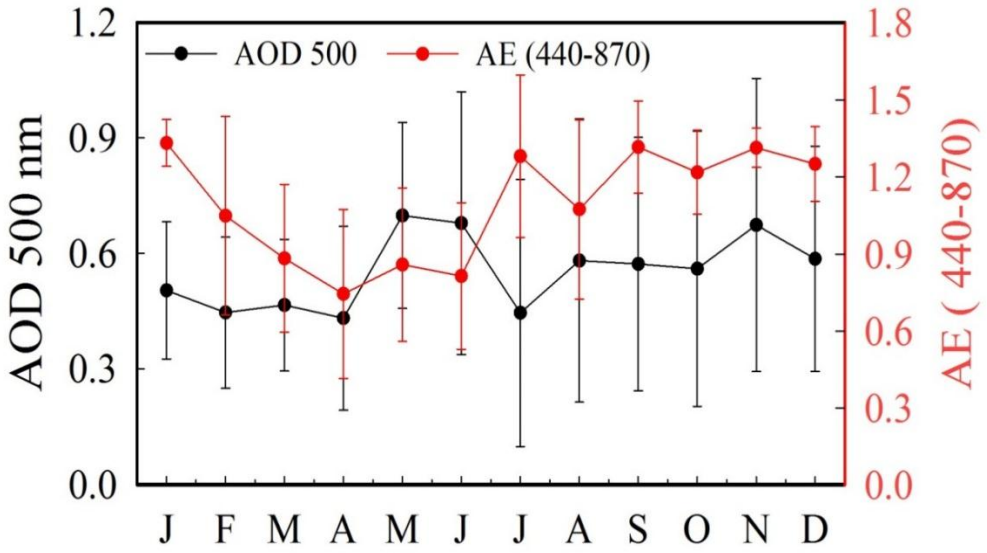

Figure 4.19: *Seasonal variation of AOD (500 nm) and AE (440-870 nm) at Pantnagar from ground based AERONET (2008-2009).*

AOD data is also used to understand whether aerosol loading over Pantnagar is dominated by fine mode or coarse mode particles. This is done by calculating angstrom exponent (AE), which is characterized by the logarithms of aerosol optical depth and wavelength. Here, AE is calculated for wavelength range from 440 to 870 nm, utilizing a linear fit of τ versus λ on a logarithmic scale. The seasonal variation in AE (440-870 nm) shows a clear and distinct change in aerosol size. Lower values of AE during March-June indicates presence of coarse mode aerosols at Pantnagar while higher values during rest of the year indicates the presence of fine mode aerosols. The presence of coarse mode aerosols (during March-June) is expected because this region is influenced by dust storms during this period [*Hegde et al.,* 2007;

Kumar et al., 2014]. The dust aerosols transported over this region adds to the aerosols emitted by industrial, transportation, power generation sectors and crop residue burning [*Venkataraman et al.,* 2006; *Satheesh et al.,* 2008; *Kumar et al.,* 2011; *Moorthy et al.,* 2013a], which in turn leads to highest AOD during spring/early summer in the Indo-Gangetic Plain.

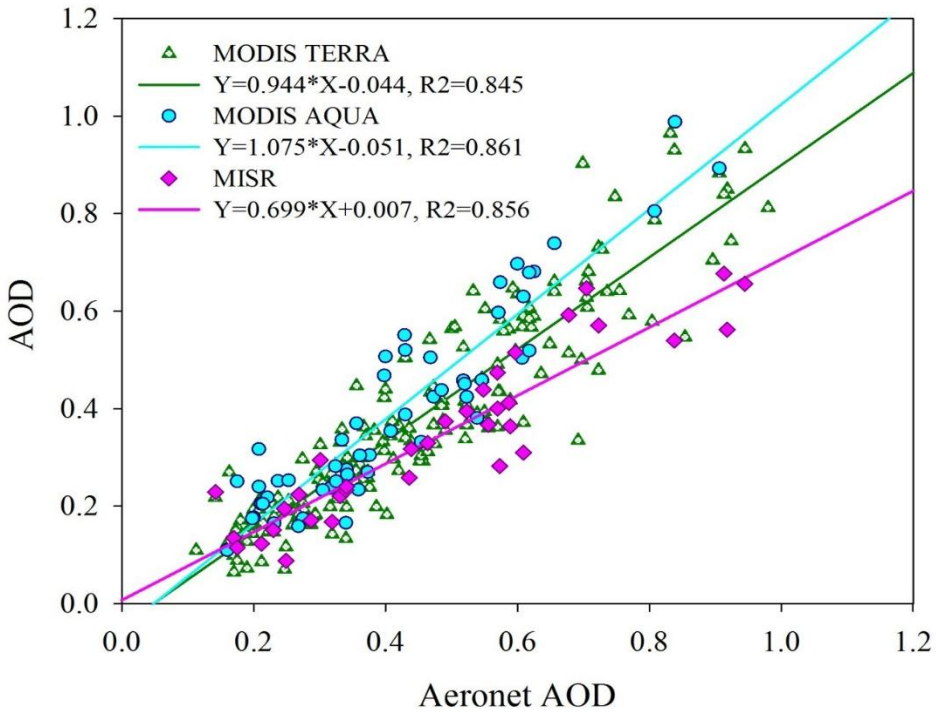

Figure 4.20: *Comparison of Satellite AOD from MISR, MODIS Terra and MODIS Aqua with the ground based available AOD data from AERONET at Pantnagar.*

The observed AOD is also compared with satellite data (Figure 4.20) from MODIS Terra, MODIS Aqua and MISR Level 2 data. The AOD data retrieval from MODIS (Terra and Aqua) and MISR is already discussed in Chapter 2 and is not discussed here. The correlation has been observed to be satisfactory.

The correlation was found to be maximum for MODIS Aqua ~0.86. However, the amount of satellite data is limited depending upon the satellite overpass and is therefore not continuous. The importance of the ground based AOD data cannot be ruled out as it provides continuous data as compared to the satellite data due to satellite overpass constraint.

4.9. Aerosol Vertical Profile From CALIPSO

In the previous section, it was found that aerosol loading at Pantnagar is dominated by coarse mode aerosols during March-June and fine mode aerosols during rest of the year. In this section, CALIPSO retrieved aerosol extinction coefficients is used to understand how aerosols are distributed vertically over Pantnagar. The detail description regarding the satellite detail and data retrieval has already been discussed in Chapter 2 and is not discussed here. CALIPSO vertical profiles of seasonally averaged aerosols extinction coefficient at 532 nm during four seasons (2010-2011) is shown in the Figure 4.21. During winter, aerosol extinction coefficient is highest near the surface (more than 2 km^{-1}) and decreases sharply to less than 0.25 km^{-1} at about 1.5 km indicating that aerosols are confined mostly below 2 km. During spring and summer, aerosol extinction coefficient shows a very small vertical gradient indicating mixing of aerosols between surface and 3 km. During autumn, aerosol extinction coefficient shows a vertical distribution similar to winter but the values at the surface do not reach as high as they do in winter and vertical gradient is also smaller. These features deduced from CALIPSO observations at Pantnagar are consistent with few other studies over different locations in India, which also revealed confinement of aerosols near the

surface in winter and existence of elevated aerosols layer has been found in other few studies in spring (March-May).

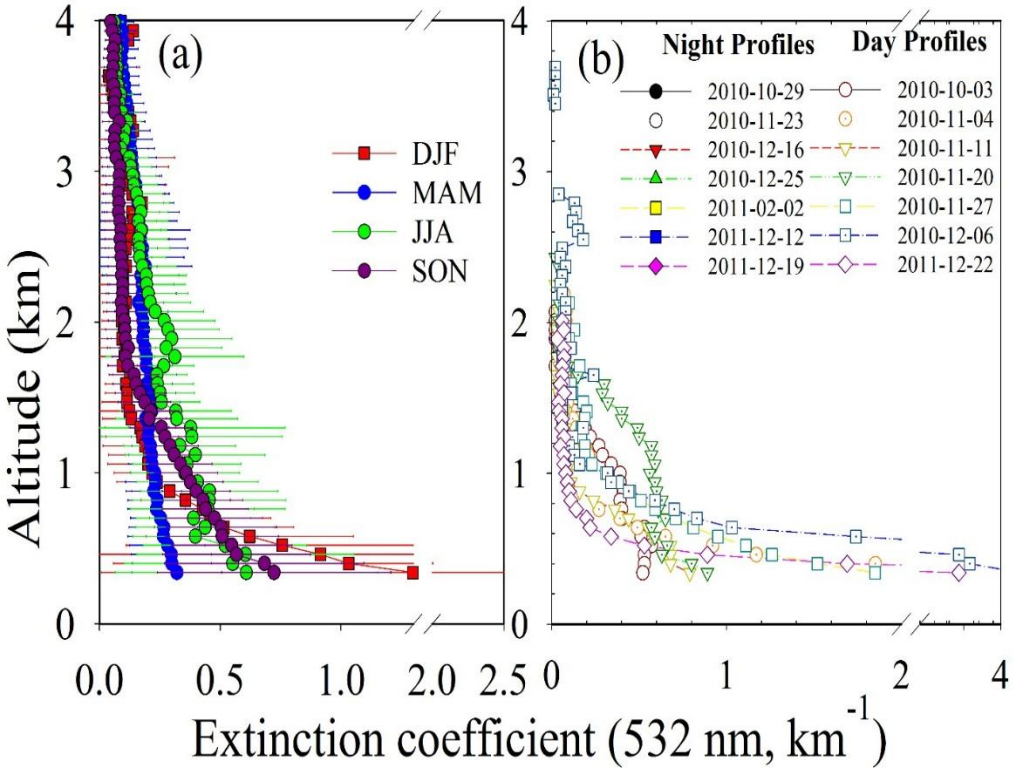

Figure 4.21: *Aerosol extinction profiles at 532 nm from CALIPSO (a) Seasonal variation of extinction coefficient (532 nm) during 2010-2011. (b) Extinction coefficient variation (532 nm) corresponding to high BC days. The profiles are separately shown as day and night profiles.*

Here, days of high BC are also identified and corresponding CALIPSO vertical extinction profiles are examined. BC mass concentrations greater than 20 µg m^{-3} (hourly average) are identified during 70 days (39 days in 2010 and 31 days in 2011) in winter and autumn. Cloud free and quality controlled CALIPSO extinction profiles (532 nm) are examined at 2x2 degree around Pantnagar, which results to 5 to 8 profiles per month leading to total of 166

profiles (during 2010-2011) out of which 83 profiles corresponds to winter and autumn. Total number of 14 profiles are found (7 daytime and 7 nighttime) when both surface BC and CALIPSO measurements are available. Similar exercise leads to total 8 profiles, if CALIPSO data is extracted at 1x1 degree region around Pantnagar.

The nighttime profiles shows somewhat higher extinction coefficient near ground and it decreases sharply above ~ 1 km, when compared with the daytime profiles. It is interesting to note that surface BC constitute a minor fraction of columnar AOD, however surface BC may significantly influence aerosols characteristics in winter and autumn when near surface aerosols (with BC and other aerosols) are mostly confined near surface usually below ~ 1 km. However during day time, BC along with other aerosols might have uplifted and mixed, which is clear from daytime surface levels BC, its association with daytime MLD and from daytime profile of extinction coefficient. The surface BC, as well as aerosol extinction profile both reveals high aerosols in nighttime in winter and autumn.

4.10. Summary and Conclusion

Long-term (2009-2012) data from ground-based measurements of aerosol black carbon (BC) from a semi-urban site, Pantnagar (29.0° N, 79.5° E, 231 m amsl), in the Indo-Gangetic Plain (IGP) near the Himalayan foothills are analyzed to study the regional characterization. Large variations are seen in BC at both diurnal and seasonal scales, associated with the mesoscale and synoptic meteorological processes, and local/regional anthropogenic activities. BC diurnal variations show two peaks one at

morning (0700–0900 hrs; local time) and another at evening (1700–2100 hrs) arising from the combined effects of the atmospheric boundary layer (ABL) dynamics and local emissions. The diurnal amplitudes as well as the rates of diurnal evolution are the highest in winter season, followed by autumn, and the lowest in summer-monsoon. BC levels, amplitude and variations in winter, autumn and spring are strongly governed by boundary layer evolution. BC concentration observed in winter, spring, summer-monsoon and autumn are ~7.9±5.2 μg m^{-3}, 4.8±3.6 μg m^{-3}, 2.8±2.8 μg m^{-3}, and 6.5±4.9 μg m^{-3} respectively with the annual mean BC ~5.5±4.7 μg m^{-3}. The association of BC when examined with the daytime MLD reveals nearly inverse relation in all seasons; being strongest in winter (R^2=0.89) and weakest (R^2=0.33) in monsoon (July-August). The low MLD in winter and autumn leads to high BC, while high MLD in spring leads to low BC. The lowest BC in summer-monsoon is mainly controlled by the rainfall and the effect of MLD is less in controlling BC in this season. Similar to BC, CO also shows anti-correlation with MLD. BC-CO correlation is further used for identifying the sources. The BC-CO association indicate the influence of fresh emissions and common combustion sources mainly in winter and autumn, while in summer-monsoon the site is influenced by aged airmass and emissions from different combustion sources. Unlike BC, co-located aerosol optical depths (AOD) and aerosol absorption are highest in spring over IGP, probably due to the presence of higher abundances of aerosols (including dust) above the ABL (in the free troposphere). AOD (500 nm) showed annual peak (>0.6) in May-June, dominated by coarse mode, while fine mode aerosols dominated in late autumn and early winter. The presence of absorbing aerosols over IGP is also seen in aerosol index data from OMI. The presence of coarse mode aerosols during spring is also observed possibly due to influence of dust.

Further, WRF-Chem model is used to simulate BC temporal, diurnal and seasonal variations and then compared with observed BC. The model although captures the temporal variations but the magnitude is highly underestimated by model. The temporal variations in BC are also examined in association with the mixing layer depth which reveals that the temporal variation in BC at Pantnagar are more related to the anthropogenic activities rather than the daily variation of mixing layer depth. The observed magnitude of BC concentration when compared with simulations, reveals that the average observed and modeled BC at Pantnagar during January, May and July are 6.6±2.2 and 2.4±1.2 μg m^{-3}, 5.5±1.8 and 1.6±0.7 μg m^{-3}, and 2.2±1.0 and 1.2±0.5 μg m^{-3}, respectively. The model captures most of the important features of the diurnal and seasonal variations but significantly underestimated the observed BC levels, suggesting improvements in diurnal and seasonal varying BC emissions apart from the boundary layer processes. The WRF-Chem simulations capture important features of the BC diurnal variations but significantly underestimate the levels. More works in improving an emission inventory with finer temporal and spatial resolution in IGP region is strongly suggested.

The vertical profiles of aerosols are further examined with the help of CALISO data. CALIPSO retrieved aerosol extinction confirms that aerosols are confined near ground and they are maximum in winter, similar to surface BC observation. While, aerosol extinction shows least vertical gradient in spring and its levels are maximum at higher heights. The extinction is maximum in spring/summer at altitudes > 2 km. Thus, the simultaneous characterization of surface, columnar and vertical distribution of aerosols are made in this present study

Chapter 5

Comparison of Aerosol Characteristics over Different Regions and Role of Different Processes

The increase of aerosol loading including black carbon (BC) has attracted the significant global scientific interest in context to climate change especially over the Himalayas in the recent years. Some of the studies have reported increase of aerosol loading over Himalayan regions in pre-monsoon season

[*Pant et al.,* 2006; *Gautum et al.,* 2009; *Lau et al.,* 2010 and others]. A clear evidence of increased warming, accompanied by earlier snow melt and high mountain glaciers retreat has been clearly reported over Himalayas and Tibetan Plateau (TP) regions [*Ramanathan et al.,* 2007; *Menon et al.,* 2010]. BC aerosols, although constitutes only a few percent of the aerosol mass, even though can have a significant positive forcing. Interestingly, several investigations using ground and satellite datasets has also reported that the Indo-Gangetic Plain (IGP) region is the most polluted region with high aerosol loading [*Jethva et al.,* 2005*; Habib et al.,* 2006*; Nair et al.,* 2007; *Pandithurai et al.,* 2008; *Gautam et al.,* 2010] persistent throughout the year. The aerosol load from low altitude IGP locations can be directly uplifted to higher altitudes due to turbulent mixing and high boundary layer in April-June months.

The ground based measurements of aerosols are sparse, despite their crucial importance as far as Himalayan region is concerned. Aerosol temporal and spatial variations are also found to be different over the Himalayan locations and over the IGP region. Aerosols are characterized by short lifetime, due to which their properties vary with time and location. The ground based aerosol measurements of aerosols at a high altitude rural location in the central Himalayas at Nainital (29.4° N, 79.5° E, 1958 m amsl) are discussed in detail in Chapter 3. The first time aerosol observation from a semi-urban low altitude site, Pantnagar (29.0° N, 79.5° E, 231 m amsl), in the Indo-Gangetic Plain (IGP) near the Himalayan foothills were also studied and is discussed in detail in Chapter 4. Seasonal variation of aerosol optical depth and BC are different

at these two locations revealing significant difference in the observed levels. Additionally, the temporal and diurnal variation varies quite significantly at these sites. It is therefore, crucial to examine the detail quantitative information about the differences in aerosol characteristics at both the sites and the processes governing the observed concentrations. The quantitative characterization of aerosols at these two locations is also important for model evaluation studies of aerosols as well.

5.1. Comparison of BC at High Altitude and Semi urban Site

5.1.1. Diurnal Variation of BC at Nainital and Pantnagar

Ground based surface concentration of absorbing aerosol BC, observed at Nainital has been discussed in detail in Chapter 3 and the detail characterization of BC at Pantnagar has been discussed in Chapter 4. Figure 5.1 shows a comparison between diurnal variations at Nainital and Pantnagar during four seasons. At a low altitude site Pantnagar, the two peaks in observed concentrations are due to fumigation effect of boundary layer along with the morning and evening anthropogenic activities. While BC variation shows noontime higher levels at Nainital.

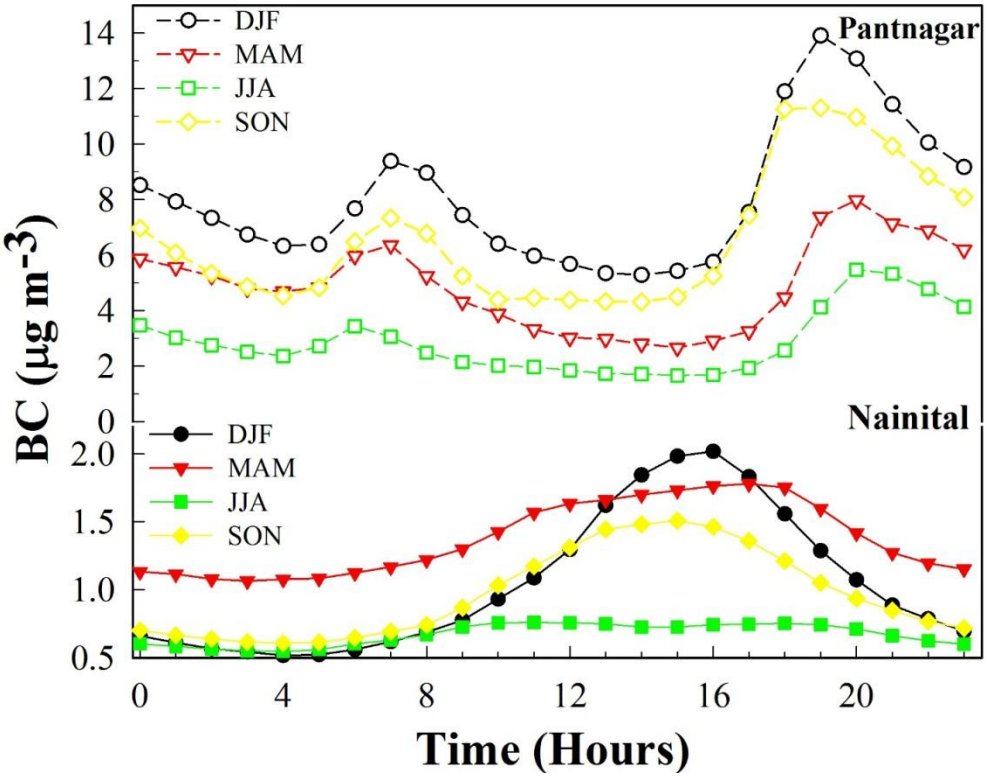

Figure 5.1: *Average diurnal variation of BC during four seasons at Nainital (upper panel) and at Pantnagar (lower panel). The time shown here is local time in Indian standard time (IST).*

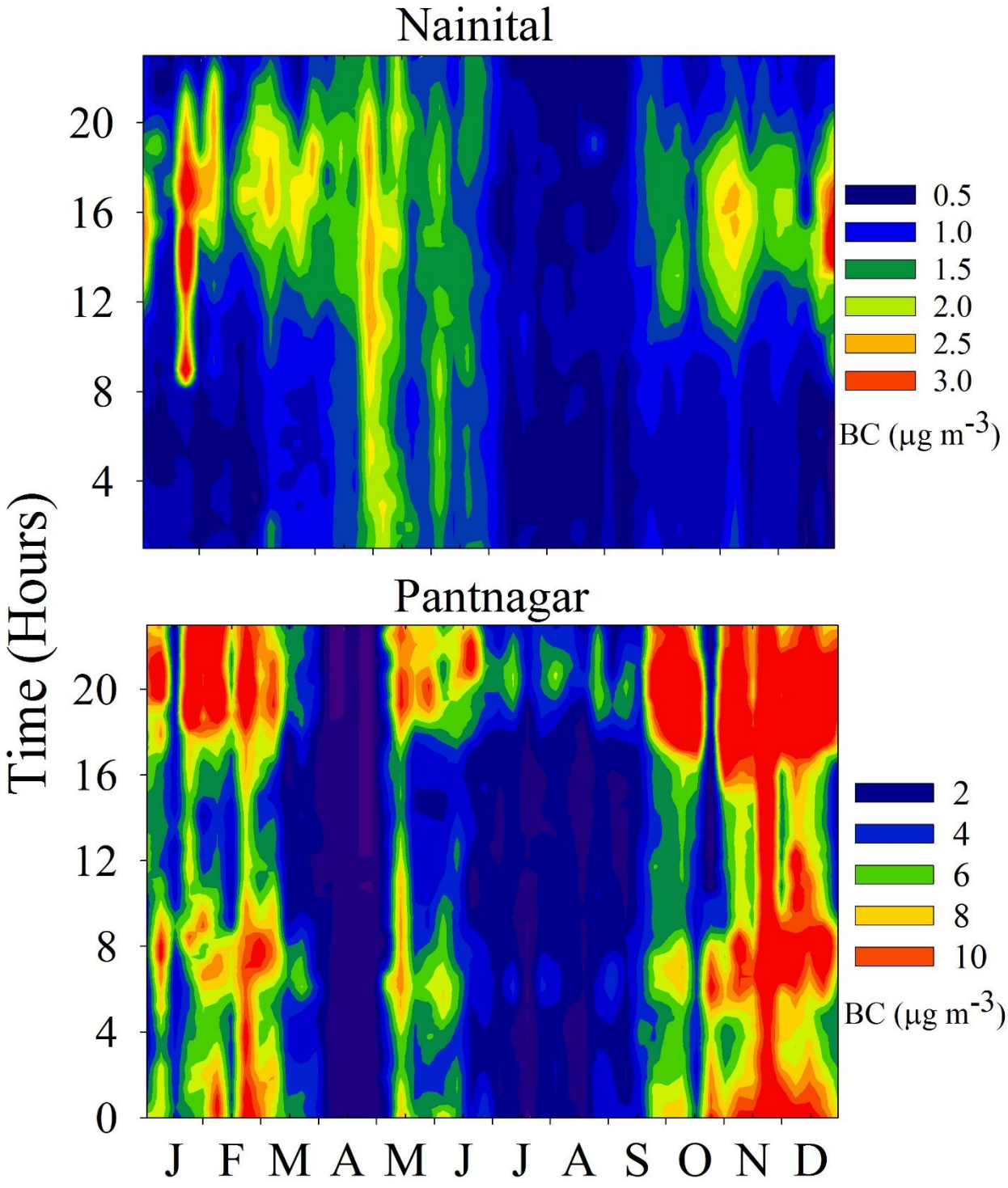

Figure 5.2: *Average diurnal and seasonal variations in BC mass concentration at high altitude site, Nainital at low altitude site, Pantnagar in IGP.*

The morning and evening peak in BC is observed even in July-August month at Pantnagar while flat pattern in BC is observed at Nainital during these months. BC amplitudes at both the sites show maximum in winter. Similarly, both Nainital and Pantnagar show minimum amplitude in BC during summer-monsoon. Quite high BC levels, particularly in winter, are explicit at Pantnagar when compared with those at Nainital (Figure 5.2). Generally it is seen that magnitude of BC amplitude at Pantnagar are larger as compared to that at Nainital.

It is to be noted that BC levels at Pantnagar gradually decreases after sunrise and leading to minimum BC in daytime and at the same time BC levels at Nainital gradually increases after sunrise resulting to maximum BC peak in the afternoon. This indicates the reduction in the surface level pollution during daytime at adjacent low altitude locations and valley regions while gradual buildup of aerosol load in high altitude mountain locations. The aerosols and other pollutants gradually starts dilution or uplifting from the low altitudes regions to high altitudes as the boundary layer evolves during daytime. Aerosols can also be uplifted to higher altitudes and then to free troposphere especially in spring. Aerosols when uplifted to free troposphere can reside there for long time and can also undergo free tropospheric transport to other clean and far away locations. Additionally, aerosols from IGP region can also arrive along the valleys to clean mountainous regions of Himalayas along the mountain slopes.

5.1.2. Comparison of BC Seasonal and Annual Variations

Seasonal variation in BC at both the sites is examined for daily, monthly and seasonal mean. The seasonal variations in BC from hourly as well as monthly average data at Nainital and Pantnagar are shown in Figure 5.3. Seasonal variation of BC reveals maximum monthly mean in May ~1.5 µg m^{-3} month at Nainital, while maximum BC at Pantnagar is observed in November-December months with mean BC ~9.2 µg m^{-3} and ~9.3 µg m^{-3} respectively. In order to examine the differences in the seasonal variation of BC at both of the sites, BC difference from annual mean is further calculated at both of the sites by utilizing annual BC mean. The seasonal variation in BC difference (BC difference from annual mean) shows some seasonal difference in BC at both the sites (Figure 5.4).

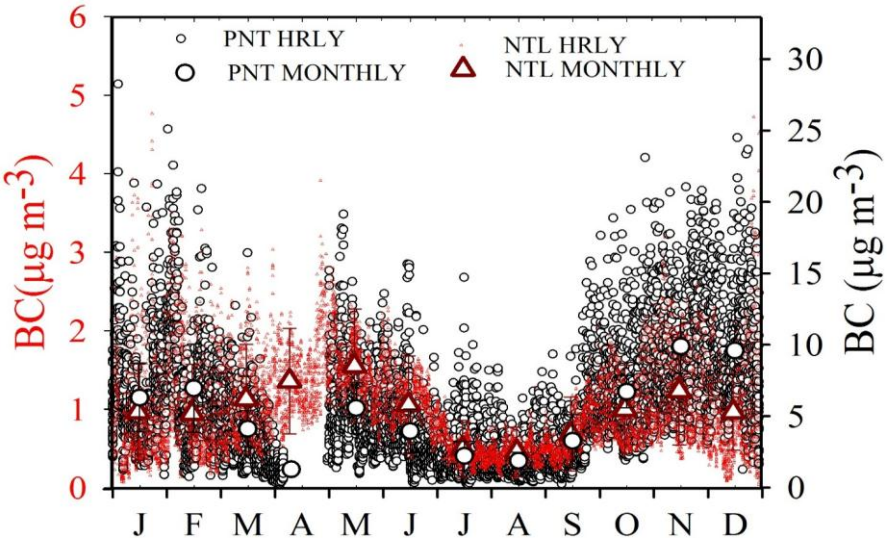

Figure 5.3: *Seasonal variation of hourly and monthly average BC mass concentration at Nainital (2005-2012) and at Pantnagar (2009-2012) shown by NTL and PNT respectively. BC mass concentration at both the sites is shown in different axis with different scale.*

The BC difference shows maximum positive deviation in April-May at Nainital while maximum positive deviation is observed in November-February at Pantnagar. The negative deviation is observed in July-August month at both the sites. Large seasonal variability in BC is clearly seen at Pantnagar while change in BC is almost constant around (Figure 5.4 inset).

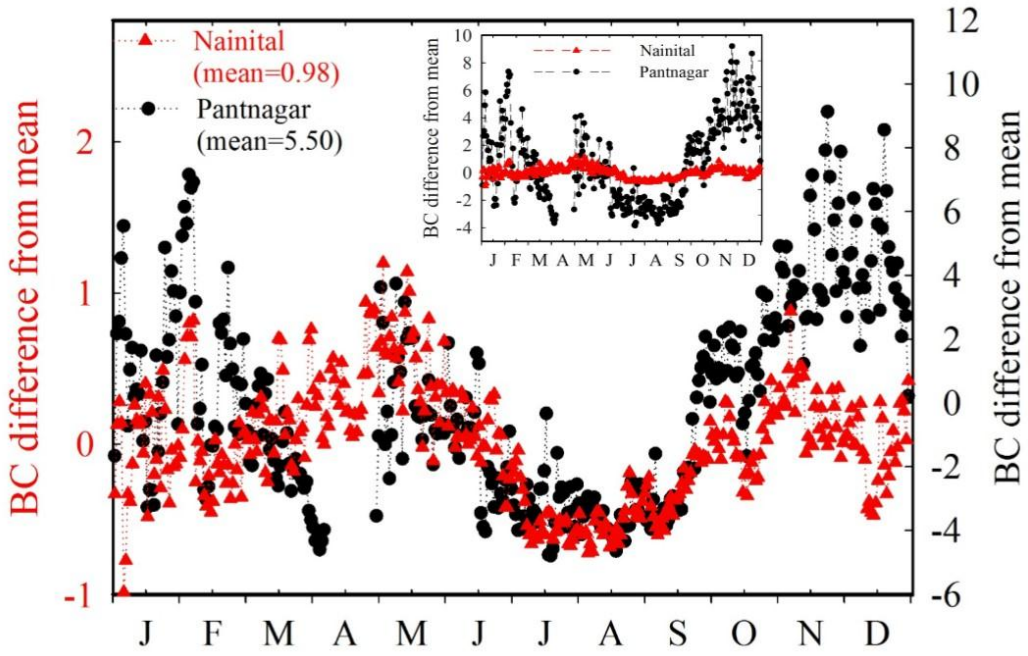

Figure 5.4:*.Seasonal variation of BC mass concentration difference from annual mean at Nainital (2005-2012) and at Pantnagar (2009-2012). BC mass concentration at both the sites is shown in different axis with different scale. However, the image in inset shows the level at both the sites with same scale.*

The seasonal mean BC is maximum in spring at Nainital, it is maximum in winter at Pantnagar (Figure 5.5). The percentage enhancement in the seasonal mean BC at Pantnagar as compared to Nainital is found to be ~ 652%, ~248%,

~318%, and ~577% in winter, spring, summer-monsoon and autumn respectively. The annual mean BC (5.50 µg m^{-3}) is about six times higher at Pantnagar, when compared with those at Nainital (0.98 µg m^{-3}).

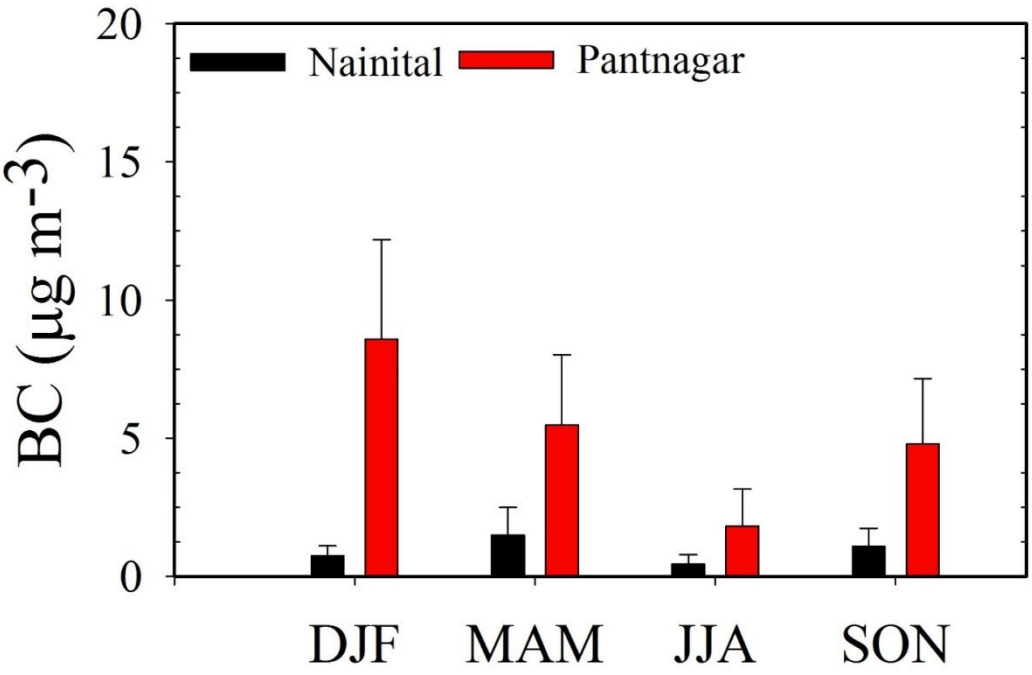

Figure 5.5: *Seasonal mean BC variation at Nainital and Pantnagar during the observation period.*

5.2. BC Comparison with other High Altitude and Urban Sites

BC measurements observed at Nainital are compared with those available from recent literature. Over the Indian region, BC variation at Nainital are somewhat similar to those reported by *Hyvärinen et al.,* [2009] at Mukteshwar (29.43°N, 79.61°E, 2180 m amsl). However, increase in BC from winter to spring is greater at Nainital than those at Mukteshwar. This could be due to the

lesser influence of biomass and anthropogenic activities at Mukteshwar as compared to Nainital.

BC diurnal and seasonal variations are also compared with the data available at other locations from available literature till present. Seasonal variations at Hanle (32.78°N, 78.96°E, 4520 m amsl) are similar to that at Nainital but the diurnal variation is not very clear at Hanle [*Babu et al.,* 2011]. BC mass concentration is also compared with those at Mohal (31.9°N, 77.12°E, 1154 m amsl) in the Kullu valley of Himachal Pradesh [*Kuniyal* [2010] and found to be higher (4.6 μg m^{-3}). BC mass concentration at another high altitude site in the western India (Sinhagad (18° 21N, 73° 45E, 1450 m amsl) are found be higher than those at Nainital [*Safai et al.,* 2014]. Additionally, the seasonal variation of BC over the Sinhagad shows winter time high BC while at Nainital BC is maximum in spring. The diurnal variations at both these sites are similar. BC at Nainital is also compared with BC reported by *Bhugwant et al.,* [2001] at remote location at Sainte-Rose, a tropical marine site of La Réunion Island (21.5°S, 55°E) in Indian Ocean during 1998–1999. BC concentration is quite low at this island site than that at Nainital. In-contrast, BC also shows two peak one at morning hours and another at evening hours at La Réunion. Seasonal variations in BC mass concentration at NCO-P, Nepal (27.95 N, 86.82 E, 5079m amsl) [*Marinoni et al.,* 2010] are similar to that at Nainital, though the BC levels at NCO-P are quite low.

The seasonal BC variations at Pantnagar are similar to that at Pune [*Safai et al.,* 2007] but diurnal variations in BC at both the sites are entirely different. It

is seen that all the low altitude locations are characterized by two peaks, however the magnitude of the morning and evening amplitudes are different at other sites and are characterized by the regular local anthropogenic activities. As expected, BC levels are higher at Delhi [*Tiwari et al.,* [2013] and Ahmedabad [*Ramachandran and Kedia,* [2010], when compared with that observed at Pantnagar. Another site in the northern India, Dehradun show somewhat lower levels than those observed at Pantnagar [*Kant et al.,* 2012]. BC at Dibrugarh reported by *Pathak et al.,* [2010] is also compared with that of Pantnagar. It is found that BC is also quite high as compared to Pantnagar.

BC values reported at a suburban location in southeast India at Anantapur (14.62°N, 77.65°E, 331 m amsl) reported by *Reddy et al.,* [2012] are however lower than what observed at Pantnagar with annual mean ~ 3.03 ± 0.27 μg m^{-3}

.

5.3. Daytime and Nighttime Variation of BC at Nainital and Pantnagar

BC mass concentration at both the sites Nainital and Pantnagar is examined for daytime (1400 hrs to 1700 hrs) and nighttime (0000 hrs to 0300 hrs) variation (Figure 5.6). The daytime variation of BC at Nainital is similar to what observed at any low altitude location with high BC in December-February month which reduces afterwards in April –May month. On the other hand BC in nighttime shows different variation than what observed for daytime. BC during nighttime at Nainital shows low in December-February and maximum in April-May months typical to what observed at high altitude

locations, suggesting that the nighttime BC is representative of the background concentration of BC at Nainital.

The percentage enhancement (night-to-day) in BC is also calculated, which shows maximum from November to February. The percentage difference is usually more than ~200% during December-February (Figure 5.6). The percentage difference of day-night BC reduces in April-May. The minimum percentage is found in the month of May ~20%. Percentage BC enhancement observed in May and July is nearly similar.

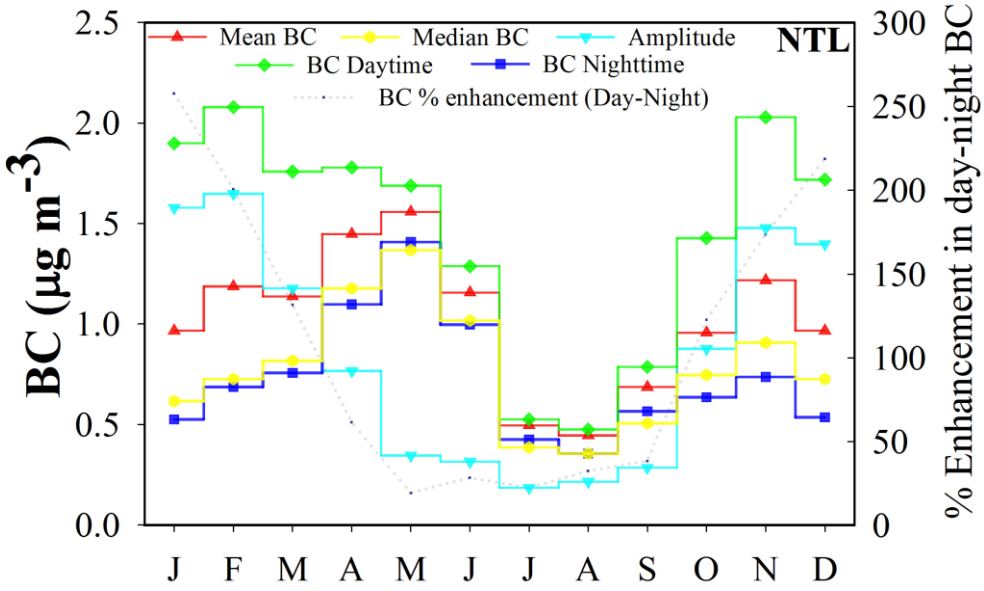

Figure 5.6: *The variation in mean BC, median BC, BC during daytime (1400 hrs to 1700 hrs), BC during nighttime (0000 hrs to 0300 hrs) and BC amplitude at Nainital. The percentage enhancement in the day and nighttime BC is also shown (right scale).*

5.4. Effect of Scavenging

Seasonal variation in the monthly BC levels at both the site Nainital and Pantnagar are studied and discussed in the above sections. Reduction in the BC levels from June to August is observed at both the site, although in different magnitude because of rainfall scavenging caused due to arrival of southwest monsoon. In this section BC levels are examined at both of the locations during June to August along with the rainfall data to study the influence of scavenging on BC concentration. The data is not available for September at Nainital. The variation in the daily average BC, difference from mean and rainfall at both the sites is shown in Figure 5.7.

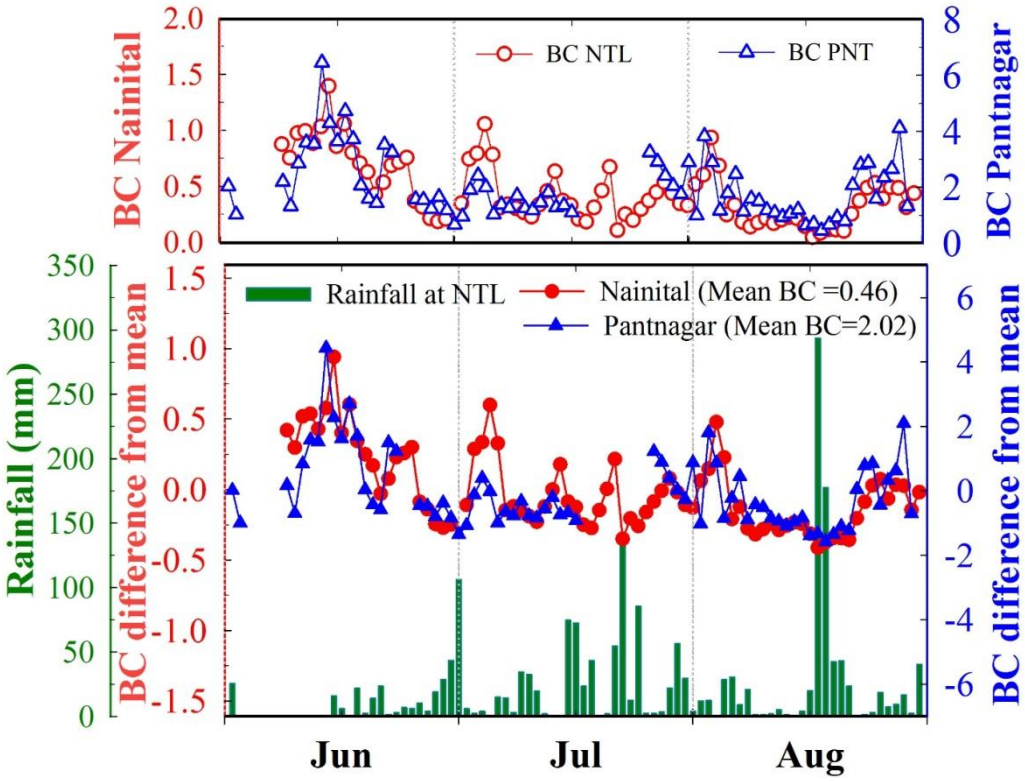

Figure 5.7: *BC variation at Nainital and Pantnagar during June, July and August 2011. BC level at both the sites are shown in the upper panel with*

different scale. BC difference from mean at both the sites is shown in the lower scale. Daily rainfall during the period is also shown.

The day to day variations in BC are observed to be nearly similar at both the sites. Reduction in BC level could be noticed during the days of the high rainfall, while build-up of BC is also seen in the absence of the rainfall (Figure 5.7). The similar type of the variation (though with different magnitude) in daily mean at both the sites indicate that the BC concentration at both the sites might be governed by same physical process leading to similar type of variations in most of the cases.

5.5. Aerosol Optical Depth Variation

Aerosol columnar loading at Nainital and Pantnagar is compared utilizing ground based AOD observations, using MICROTOP Sunphotometer (Solar light Co.) and AERONET. It has already been shown that data from both these instrument are in good agreement (Chapter 3). Nevertheless, the mean AOD obtained from AERONET and MICROTOP at Nainital show consistency (Figure 5.8). Seasonal variation of AOD at both the sites significantly differs from October to February, though maximum AOD is seen at both the sites in May–June month (Figure 5.8).

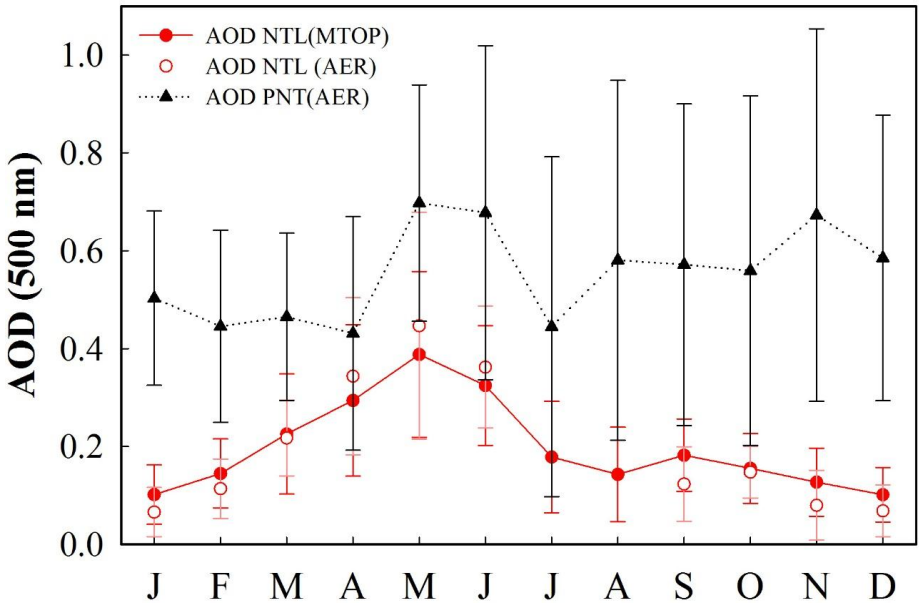

Figure 5.8: *Monthly mean AOD (500 nm) variation at Nainital and Pantnagar. The monthly mean AOD (500 nm) at Nainital is utilized from ground based MICROTOP data shown by AOD NTL (MTOP) as well as from ground based AERONET data AOD NTL (AER) while AOD at Pantnagar is taken from ground based AERONET data shown by AOD PNT (AER).*

AOD (500 nm) in the month of December-January is lowest (AOD ~0.10) at Nainital and represent nearly clean environment, while significant aerosol loading is observed at Pantnagar during this period. AOD does not show minimum in July-August month unlike, the surface concentration of BC. It is observed that seasonal variation in AOD is rather more distinct at Nainital than at Pantnagar. AOD at both the site shows significant enhancement in spring, indicating the possibility of aerosol direct influence/transport from low altitude IGP locations to the high altitude.

5.6. Aerosol Optical Depth Comparison with Other Sites

AOD observed at Nainital is compared with other locations in India. AOD values from the ground based stations are used for comparison and the satellite measured optical depths are not used in the present study for comparison. AOD at Nainital is compared with the seasonal mean AOD reported at other Himalayan location at Kullu [*Guleria et al.,* 2012]. AOD values at Nainital during all seasons are lower than what observed at Kullu. AOD values are also compared with AOD values at Dehradun (30.34°N, 78.4°E, 690 m amsl). AOD values are seen to be ~ 255% higher at Dehradun during winter [*Kant et al.,* 2010]. The high values of AOD in winter at Dehradun indicate the presence of significant aerosol loading, unlike over the Nainital.

Aerosol optical depth observed at Nainital is also compared with the other location in India from the available literature. The observed AOD in winter and spring over the oceanic regions of the Arabian Sea [*Satheesh et al.,* 2006a], Port Blair [*Beegum et al.,* 2012], and Minicoy [*Satheesh et al.,* 2002] are found to be higher than those at Nainital. It is interesting that high altitude locations show low AOD in winter while semi urban and urban locations shows significant aerosol load even in winter.

5.7. Size Distribution of Aerosol

The size distribution of aerosol is studied at Nainital and Pantnagar. The inversion algorithm is used for retrieving aerosol volume size distributions in the size range from 0.05 to 15 μm using 22 radius size bins from spectral sun and sky radiance data. Retrieval errors in dV(r)/dlnr typically do not exceed 15–35% (depending on the aerosol type) for each particle radius bin within the 0.1–7 μm range [*Dubovik et al.,* 2000]. Aerosol size distribution is characterized by two distinct modes: fine particles with particle size < 0.6 μm and coarse with particle size > 0.6 μm [*Dubovik et al.,* 2002]. The size distribution for each month is shown in Figure 5.9, which reveals the two modes in aerosol size distribution.

The size distribution of aerosol at Nainital shows quite low while the size distribution of aerosols at Pantnagar shows quite high peak as compared to Nainital. The two modes of aerosols fine and coarse mode show different peaks at both the sites. The fine mode have larger peak in December-January month at both the sites. The fine mode peak shows slight shift towards the lower size range in fine mode from March to June month at Pantnagar. The coarse mode of aerosols shows nearly flat pattern from November to February month at Nainital where most of the aerosols are present in the fine mode, while at Pantnagar aerosols are present both in fine mode as also in coarse mode. The coarse mode of aerosols shows minimum in January month at Pantnagar, while from October to February, coarse mode of aerosols is also higher except January. The fine mode peak shows maximum up to 0.04 μm3 /

μm2, in the size range centered around 0.11–0.15 μm, while at Pantnagar the fine mode shows maximum up to 0.08 μm3 / μm2. The coarse mode however shows maximum of ~ 0.16 μm3 / μm2 in the size range from 2.24-3.89 μm radius at Nainital while at Pantnagar maximum is observed as ~0.22 μm3 / μm2 in the 2.94-3.86 μm radius. The examination of the aerosols distribution from March to June reveals significant enhancement in the coarse mode of aerosols at both the sites.

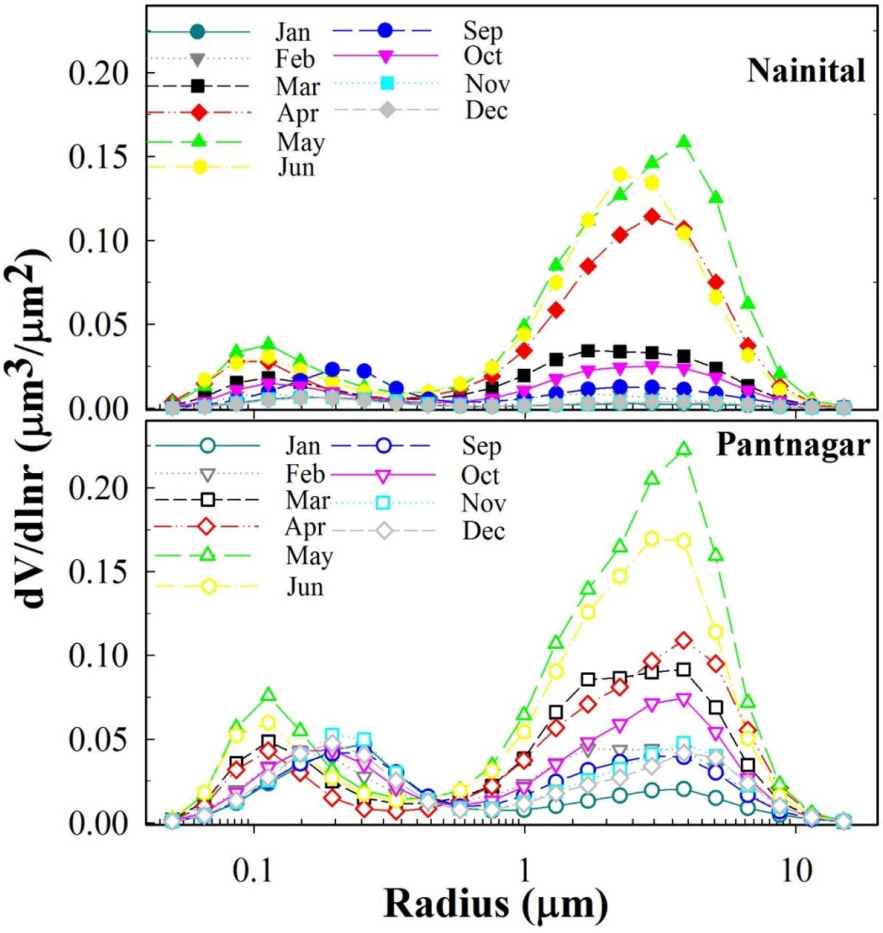

Figure 5.9: *Monthly mean aerosol size distribution from AERONET data at Nainital and Pantnagar.*

5.8. Single Scattering Albedo (SSA) Variation

Spectral variation in Single Scattering Albedo (SSA) during different seasons is also examined. SSA is defined as the ratio of scattering to extinction (extinction is the sum of absorption and scattering) and is a key variable in assessing the climatic effects of aerosols [*Dubovik et al.,* 2002]. The detail description regarding SSA retrieval from AERONET is well documented [*Dubovik et al.,* 1998, 2000]. Theoretically, SSA values can vary between 0 (totally absorbing aerosol) and 1 (totally scattering aerosol). In actual, SSA values in the visible and UV wavelengths region ranges from 0.5 to 1.0. Single scattering albedos are expected to have an uncertainty of 0.03–0.05 depending on aerosol type and loading [*Dubovik et al.,* 2000]. SSA is one of the most relevant optical properties of aerosols, since aerosol direct radiative effect is very sensitive to it. Optical properties of aerosol particles suspended in the atmosphere in general show a great spatial and temporal variability and are determined by their chemical composition, size, shape, mixing state and concentration [*Kokhanovsky*, 2008]. Sulfate and nitrate aerosols from anthropogenic sources, are considered the primary particles responsible for net cooling, while black carbon, produced by incomplete combustion of carbonaceous fuels is effective absorbers of solar radiation and have opposite effect and warm the atmosphere. The absorption of solar radiation by aerosols causes heating of the lower troposphere and may lead to altered vertical stability, with implications for the hydrological cycle [*Ramanathan et al.,* 2001]. It is reported that in general single-scattering albedo greater than 0.85

generally cools the planet, while those with less than 0.85 warm the planet [*Hansen et al.*,1981].

SSA variation during different season at Pantnagar is shown in Figure 5.10. SSA is found to increase with wavelength in the presence of dust and shows a reverse trend in dust-free conditions. SSA variation shows similar variation in winter and autumn which shows decrease in SSA with wavelength i.e. high SSA at shorter wavelength and low SSA at higher wavelength. The lower SSA at longer wavelength indicate dominance of absorbing aerosol over the site. SSA variation during spring and June month however, show different variation with increase in SSA with wavelength i.e. low SSA at shorter wavelength and high SSA at higher wavelength. The increase in SSA with wavelength during spring and the month of June indicate the dominance of the coarse mode (mostly dust) of aerosols. The SSA data of July and August month was not available. During premonsoon months (April–June) the anthropogenic aerosols along with BC gets mixed with the mineral dust aerosols from deserts due to the dominance of dust emissions.

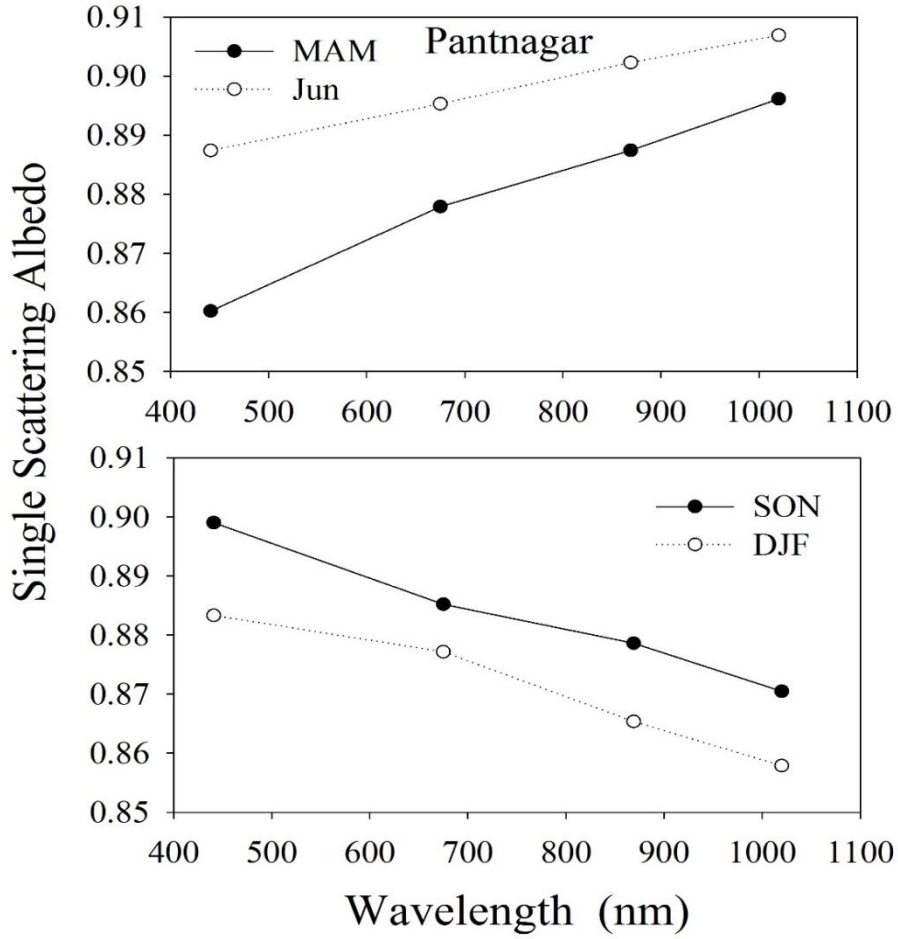

Figure 5.10*: Spectral variation of single scattering albedo (SSA) during different seasons at Pantnagar.*

The SSA varies from ~0.76 to 0.96 (at 441 nm wavelength) at Pantnagar with the average value of ~ 0.88. SSA could not be obtained for Nainital due to few data points. SSA variations at Nainital in a previous study by *Pant et al.,* [2006] were reported to vary from 0.94 to 0.87 during the month of December 2004 with mean SSA 0.9 ± 0.03 at Nainital.

SSA variation (500 nm) at Pune was found to be about 0.81 during dry season of 2001–2002 [*Pandithurai et al.,* 2004], at Kanpur SSA was reported to be 0.76 during December 2004 [*Tripathi et al.,* 2005], at Chennai it was 0.77 during February– March 2001 [*Ramachandran,* 2005], at Hissar it was 0.88 during December 2004 [*Ramachandran et al,* 2006] and at Bangalore it was ~0.78 [*Babu et al.,* 2002]. On the basis of the observations over the tropical Indian Ocean during pre-INDOEX campaign in 1998, SSA value of ~0.9 has been reported by *Satheesh et al.,* [1999]. It is shown that SSA values are affected by particle morphology (shape and size), and composition [*Parungo,* 1997; *Dubovik et al.,* 2006]. The effect of dust particle shape and composition on SSA over the Great Indian Desert has been studied by *Mishra et al.,* [2008] and has also reported increase in the SSA as the hematite content in the dust increases, so aerosol chemical composition also need to be investigated.

5.9. Aerosol Vertical Variation and Associated Processes

Figure 5.11 shows few aerosol vertical profiles from CALIPSO corresponding to different seasons. The satellite track in each profile is also shown. Few representative profiles are selected to show aerosol vertical distribution in May-June representing aerosol vertical distribution in spring and early summer-monsoon when the influence of dust and anthropogenic pollution is more leading to more columnar abundance of aerosols and another in December to represent winter season. We have also showed the aerosol vertical profile in February to show how aerosol builds up as soon as the winter approaches towards ending. It is observed that aerosols are extended up

to higher altitude reaching nearly upto ~5 km in May–June. The aerosols loading in December representing winter (shown in Figure 5.11) shows low extinction near the ground mostly below ~1.5 km and most of the high altitude locations are free of aerosol loading. It is also examined that the presence of dust can be noted nearly throughout the year over the low altitude regions and foothills of Himalayas.

Further the seasonal variation of aerosol vertical extinction profile is also examined. The aerosol total backscattering data is used for studying the seasonal variation of backscattering coefficient. The seasonal variation of the backscattering coefficient is studied using a 2 by 2 degree data centered at Pantnagar. The seasonal variation of aerosols shows most of the aerosols are located below 1-1.5 km from October-February, while in April-May month the backscattering is seen to be high ~3 km and above (Figure 5.12). The seasonal variation of the aerosol vertical profile indicate that the aerosol are mostly confined near surface at low altitudes from October-February and most of the columnar loading of aerosols is contributed from the aerosols near surface below ~1-1.5 km, while in April-June vertical extension of the aerosols to higher heights is clearly evident indicating buildup of aerosols to higher heights consequently aerosol are not confined to the low altitudes near ground. The elevated layers of aerosols also exist during this period which results in the aerosols layers high above the grounds at higher heights. Interestingly, the surface concentration also shows enhanced concentration from October to February similar to what observed for the columnar loading. The vertical

distribution of aerosols thus explores the reason of low surface concentration/loading at low altitude region while enhanced concentration/loading at high altitude regions.

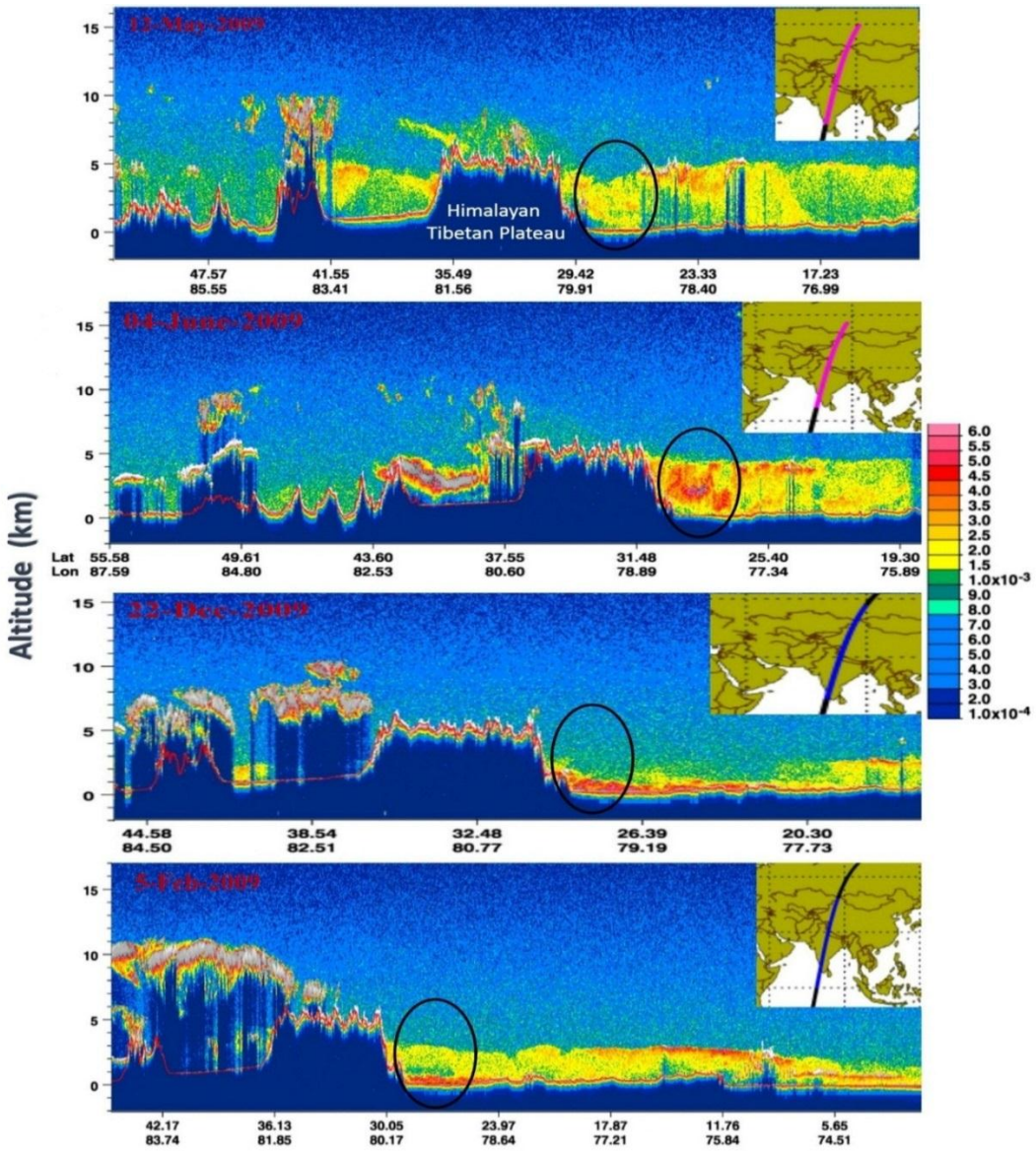

Figure 5.11: *CALIPSO, 532 nm total attenuated backscattered profiles (km^{-1} sr^{-1}) mainly from the Central India to the Himalayas. The insert image shows the transect from the South India to the Himalayan Tibetan Plateau region (HTP). The color scale corresponds to the attenuated backscattered mainly due to aerosols. The backscattered due to clouds is not shown is scale and*

corresponds to the grey color in the image. The profiles are for 12 May 2009, 4 June 2009, 22 Dec 2009 and 5 Feb 2009.

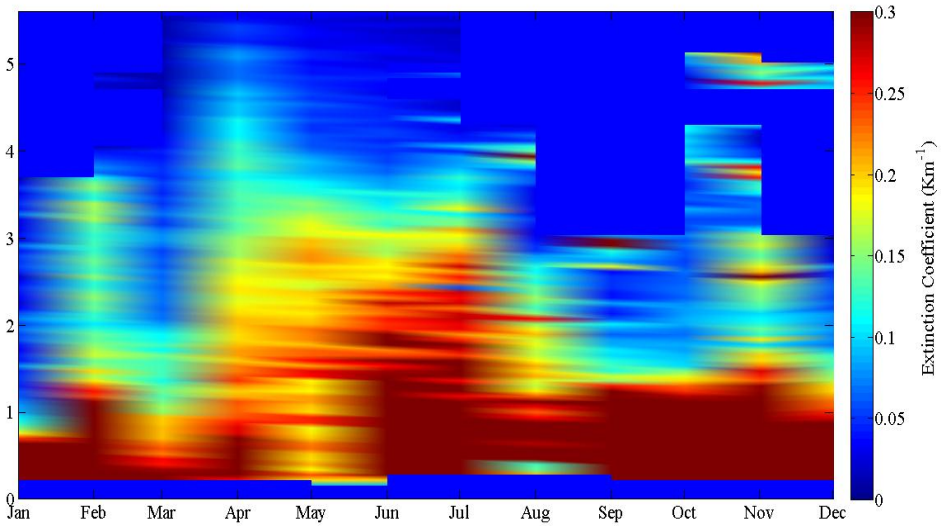

***Figure 5.12**: Seasonal variation of aerosol extinction coefficient at 532 nm from CALIPSO*

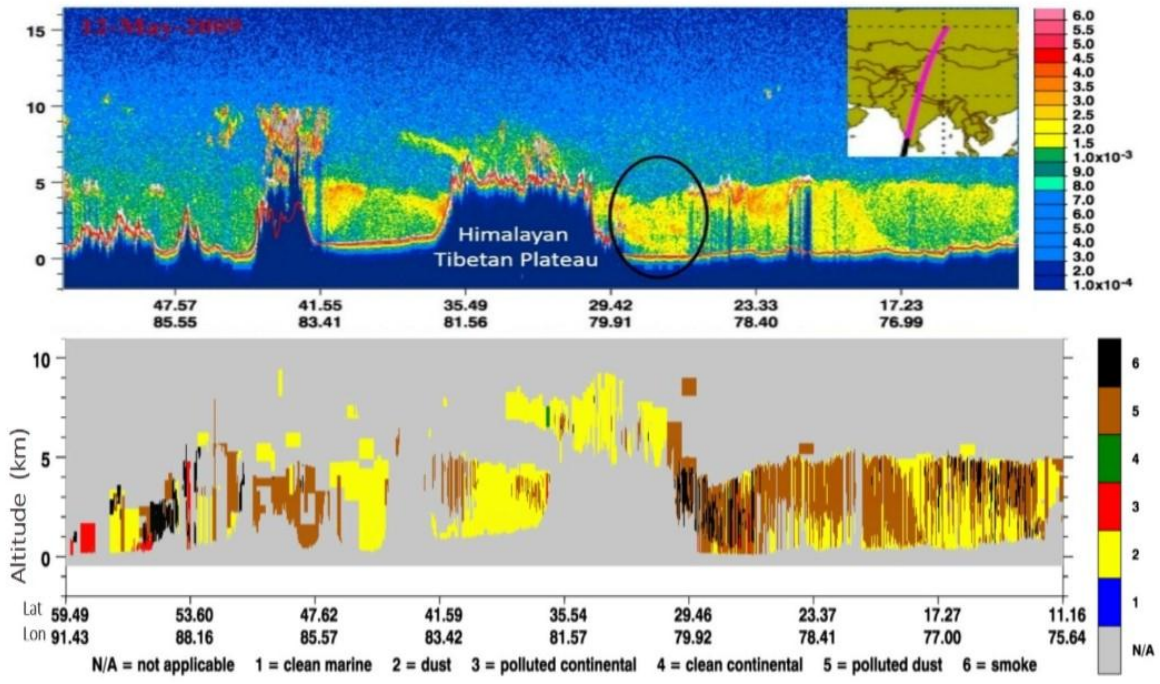

Figure 5.13: *The aerosol vertical profile observed on 12 May 2009. The aerosol types are identified in the vertical profile. The color scale on the right represents the aerosols type blue –clean marine, 2-dust, 3-polluted continental, 4- clean continental, 5-polluted dust and 6-smoke.*

As a case study, aerosol vertical profile on 12 May 2009 (nighttime) is examined which reveals the presence of aerosol loading on both of the side of the Himalayas. The track of the satellite overpass is shown in Figure 5.13 (top panel). Aerosols build up is seen along the slope of the Himalayas and also along the Himalayan Tibetan Plateau (HTP). The presence of dust is also noticed above the HTP. Interestingly the other side (towards north) of the Himalayas beyond HTP also indicates the significant amount of the dust. In order to investigate the buildup of the aerosols over this region we have investigated the meridional wind at 500 hPa. The spatial variation of winds reveals north to south flow which is high over the northern and western Indian region (Figure 5.14).

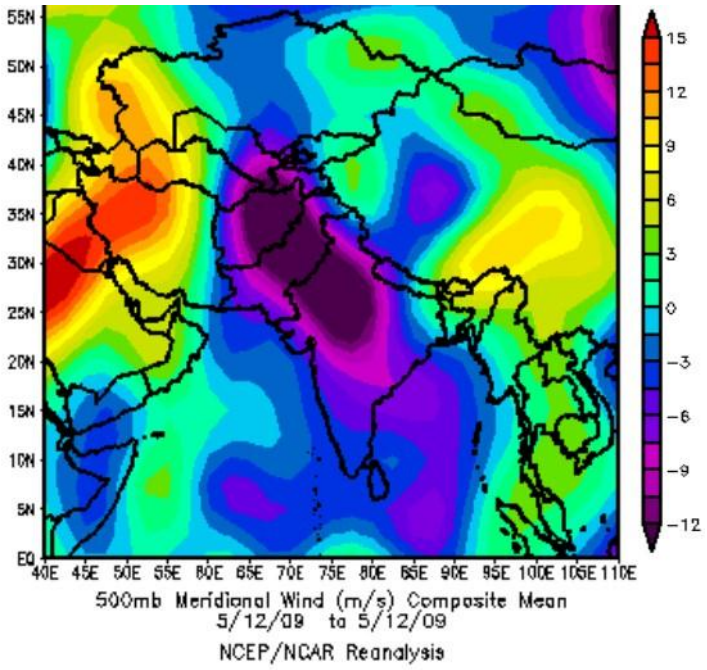

Figure 5.14: *Meridionial wind (m/s) on 12 May 2009 obtained from the NCEP/NCAR data at 500 mb.*

The high level flow of the winds clearly indicates the north to south flow. The direct transport of pollution load is indicated from the northern side of HTP towards south that suggests that the aerosols are not transported from IGP region. However, the aerosol along the south slope from IGP region can reach to Himalayas along the slope not free tropospheric transport. In addition the slopes from both the side (north and south) of the HTP regions might build up the aerosols along valleys.

5.10. Role of Different Processes

The influence of the northern Indian biomass burning was examined over the central Himalayas [*Kumar et al.,* 2011]. Ground based BC observations were used for three years (2007–2009) during spring along with the MODIS fire data

for classifying the days of high and low fire events and the impact of fire was accessed to quantify the enhancement in BC and AOD. The enhancement in the BC and AOD (0.5 mm) due to biomass burning were estimated to be ~1.8 μg m^{-3} (~145%) and 0.3 (~150%) respectively. BC was found to be ~1.24 ± 0.9 μg m^{-3} during the low fire activity period and was increased to 3.04 ± 1.12 μg m^{-3} during the high fire activity period. AOD also showed similar enhancement and was 0.2 ± 0.1 during the low fire activity period and increased to 0.5 ± 0.2 during the high fire activity periods. A large enhancements (53–100%) was also reported in the satellite derived parameters over a 2° × 2° region around Nainital over these fire impacted periods. It was found that the northern Indian biomass burning induced cooling at the surface (−27 W m^{-2}) and top of the atmosphere (−8 Wm^{-2}) in the lesser polluted high altitude regions of the central Himalayas. This cooling leads to an additional atmospheric warming of 19 W m^{-2} and increased the lower atmospheric heating rate by 0.8 K day^{-1} .

AOD observations during November 2008, along with the other data were used to study the effect of Dalaffilla volcanic eruption (Volcano number 0201-07) (http://www.volcano.si.edu/) on 4 November 2008 [*Malik et al*., 2012]. Higher AOD was observed on 6 November compared to other days. Enhancement in AOD was observed at several places including the present observation site (Nainital). Besides many other factors contributing to a large day-to-day variability, the possibility of the volcanic SO2 transforming into

sulphate aerosols during transect was proposed as one of the reason for high AOD.

The long-period modulations in aerosol optical depth were reported at Nainital emphasizing importance of wave-induced aerosol dynamics and the corresponding radiative effects [*Phanikumar et al.,* 2014]. Fourier analysis was performed in order to find the period of oscillation. It was found that AOD showed dominant 25–45 day oscillations in MODerate-resolution Imaging Spectro radiometer data. This dominant oscillation in AOD was effective in modulating accumulation mode of aerosols. The westward propagation at a different longitude and northward propagation at a different latitude was reported, confirming the association of these modulations with Rossby waves. It was found that the Rossby wave induce an additional warming of 4.16±0.98W m^{-2}.

The influence of aerosols diurnal variation in affecting the direct aerosol radiative forcing was studied over central Himalayan region utilizing data available at ARIES, Nainital [*Reddy et al.,* 2015]. The diurnal cycle of AOD at different wavelengths, AE, and BC were studied and were utilized for the derivation of optical properties of aerosols in the regionally polluted aerosol layer. Aerosol extinction profiles from LIDAR were also studied. It was found that the atmospheric radiative forcing due to diurnal variation of aerosols shows enhancement of 10% and 16% during winter and post monsoon. This enhancement was seen in the diurnal variation of aerosols rather than the

average aerosols. The importance of the diurnal variation of aerosol in estimating the radiative forcing of aerosols was reported.

5.11. Summary and Conclusions

In this present chapter, the ground based aerosol measurements at two different environments, a high altitude site in the central Himalayas and a semi-urban site, are compared. Both of these sites are characterized by different geographical, topography, meteorological and environmental conditions.

BC variations when examined reveals different diurnal pattern at both of the sites. BC results in the single afternoon peak at Nainital, while two peaks; one less pronounced peak in morning and another more pronounced peak is observed in evening at Pantnagar. The diurnal amplitude in BC is pronounced from October-February at both the sites. BC at Nainital shows minimum just before sunrise while at Pantnagar minimum value is observed in the daytime. The seasonal variation in the diurnal variation of BC shows low nighttime value of BC at Nainital while the nighttime BC is significantly high at Pantnagar. The background concentration of BC shows significant enhancement in spring at Nainital while in other seasons background BC is low and nearly similar which indicate that the seasonally changing anthropogenic activities has less influence on the background BC at Nainital except spring. On the other hand the influence of the seasonally changing anthropogenic activities is much evident at Pantnagar and shows clear seasonal changes. The daytime maximum in BC at Nainital corresponds to the

daytime minimum observed at Pantnagar. The seasonal variation in BC at both of the sites is also entirely different.

The effect of rainfall scavenging is also observed in BC. Low BC is observed on the days of high rainfall while high BC is observed on the low rainfall days. Simultaneous daily evolution of BC from June to August month at both the sites also reveals the similar evolution of BC at both the sites most of the time although with different magnitude. BC diurnal and seasonal variations at Nainital and Pantnagar are also compared with the some of the other locations and the differences in the diurnal as well as the seasonal variations are explained in detail. BC is found to vary according to the seasonal changes in the anthropogenic activities and airmasses. The diurnal variations in BC are characterized by the boundary layer. The morning and evening peak in BC is characterized by the location of the site and local anthropogenic activities.

The columnar loading of aerosols is also studied and compared at both of the location. AOD at both the sites shows high in spring at both the sites, while significant difference in AOD is observed in winter. Columnar loading is minimum and quite low in winter representing nearly clean and nearly free troposphere at Nainital while AOD in winter at Pantnagar is significantly higher, typical to what observed at urban, semi-urban location in IGP. AOD at both the site shows significant enhancement in spring, indicating the possibility of aerosol direct influence/transport from low altitude IGP locations

to high altitude. Quite interestingly, AOD variation at both the sites in winter indicate less possibility of direct influence of IGP pollution load to high altitude clean sites, however the aerosols might influence nearby locations via transport through valleys. The physical and optical properties of aerosols in winter might be different at both the sites, while in spring the physical and optical properties of aerosols might be similar. The high amount of absorbing aerosol BC along with AOD in winter season at Pantnagar indicate that the site might be under the influence of the atmospheric brown clouds (ABC) as other IGP sites and needs further detail investigation. Further the differences in size distribution and SSA variations were also examined and reported at both of the sites.

The vertical distribution of aerosols has also been also studied along with the surface concentration and columnar loading of aerosols, as surface BC shows different seasonal variation at both of the locations, columnar AOD however, shows similar maximum in spring but shows different variation in winter. Since the ground based observations of the vertical structure of the aerosols are not available so we have utilized the CALIPSO data for studying the aerosol vertical structure. The presence of dust can be noted nearly throughout the year over the low altitude regions and foothills of Himalayas. The seasonal variation of aerosol vertical extinction profile indicate most of the aerosols are located below ~1-1.5 km from October-February, while in April-May month the aerosols are found at higher heights ~3 km and above. The elevated layers of aerosols also exists during spring which results in the aerosols layers high

above the grounds at higher heights. The vertical distribution of aerosols explores the reason of low surface concentration/loading at low altitude region while enhanced concentration/loading at high altitude regions. The vertical distribution also explains the reason of observed high aerosol loading i.e. AOD at both the low altitude regions and high altitude regions. The lower altitudes shows less aerosols loading and less surface concentration, while the aerosol loading at higher heights shows significant aerosol loading. The increased anthropogenic sources especially biomass activity of northern India might build up a significant aerosol loading which might get dispersed, uplifted or distributed to higher heights due to high convection. Additionally, aerosols can also be transported from other location along with the free tropospheric enhancement in this season. Interestingly, aerosols from the IGP region might be directly transported to the high altitudes especially to the adjacent Himalayas in spring, while in winter most of the aerosols can be contributed via valley regions rather than direct vertical updraft in most of the cases. The role of boundary layer and updraft/downdraft is also discussed.

Ground based BC observations were used extensively for three years (2007–2009) during spring along with the MODIS fire data for assessing the impact of fire at Nainital. BC radiative forcing estimation was studied in [*Srivastava et al.*, 2011] from July 2006 to May 2007 at Nainital. In other study the effect of Volcaonic emission was studied. Additionally, the long-period modulations in AOD and importance of wave-induced aerosol dynamics and the corresponding radiative effects were studied and reported at Nainital. The effect of diurnal

variation of aerosols in affecting the direct aerosol radiative forcing was reported at Nainital utilizing diurnal cycle of AOD, AE and BC.

Chapter 6

Summary and Future Scope

The characteristics of atmospheric aerosols vary strongly from one region to another due to spatial and temporal variations in the emission sources, transport, atmospheric transformation and removal of aerosol particles. Thus, in order to understand the effect of aerosols on our Geosphere–Biosphere system, their detailed characterization is very important at multiple locations because of the regional nature of their properties and the short lifetime [*Moorthy et al.,* 1999; *Satheesh et al.,* 2002]. In light of the key role played by aerosols in climate change, air quality, radiation budget and myriad of other direct and indirect effects, the present thesis work examines the climatological variations of aerosols at a high altitude site and at a foothill site of the central Himalayas.

The long terms trends in the ground based aerosol BC and AOD are estimated for the first time over a high altitude site (Nainital) in the central Himalayas.

The episodic enhancements in aerosols at Nainital are studied using simultaneous observations of the columnar and surface characteristics of aerosols. The observations of BC at the site are also utilized to identify the possible source regions. Further, the ground based observations are initiated at a low altitude semi-urban site, Pantnagar in Indo-Gangetic Plain (IGP) region adjacent to the central Himalayan foothills and are examined in detail. The observations over Nainital are representative of the cleaner high altitude environment in the Himalayan region while the measurements at Pantnagar are representative of the semi-urban environment in the IGP. The aerosol characteristics over these different environments have been studied and the associated processes are discussed. This chapter presents a summary of the results followed by key conclusions and future scopes. The inferences drawn from the present work are discussed under the following three main categories.

6.1. Aerosol Climatology over a High Altitude Site in the Central Himalayas

The aerosols characterization over the remote clean sites especially, Himalayas are of special importance as the aerosols measurements at these sites are crucial to assess the impact of aerosols far away from the major anthropogenic sources. However, such studies over the Himalayan region are relatively sparse. In view of this, aerosol characterization studies were initiated at a high altitude site Nainital in the central Himalayas and aerosol climatology, including long term trends are discussed (Chapter-3).

Long term (2005-2012) aerosol optical depth (AOD) observations and BC mass concentrations at Nainital are examined for daily, seasonal and annual variations. The ground based observations of AOD and BC are also utilized for climatological synthesis. AOD observations at Nainital show large variability in aerosol loading at all the scales from daily to seasonal and annual. AOD increases each year after March and reaches maximum in May-June and then decreases. The lowest AOD values are observed in December-January. The magnitude of maximum AOD in April-June show large inter-annual variability that depends upon the pollution received by the site which in turn mainly depends upon the intensity of the biomass burning and dust storm events occurring in northern India, which are known to peak during spring in northern India. Monthly mean (climatological) AOD at 500 nm, outside the period of March-June generally remains below 0.2. AOD in December-January reduces to values less than 0.1. The maximum (0.38±0.17) AOD (500 nm) is found for the month of May at Nainital. Seasonal mean AOD at 500 nm is observed to be ~0.127, ~0.3, ~0.226, and ~0.15 in winter, spring, summer-monsoon and autumn, respectively at Nainital. The percentage enhancements in seasonal AOD compared to the winter season are 155%, 85% and 31% in spring, summer-monsoon and autumn respectively.

The performances of MICROTOPS and AERONET are also examined from time to time and both shows good agreement (R^2=0.96) at Nainital for AOD measurements. Both the Angstrom exponent and fine mode AOD show the presence of fine mode aerosols during December-February while the coarse mode aerosols dominate the aerosol load during April-June. The enhancement

in the volume size distribution of coarse mode with respect to the fine mode of aerosol is found to be ~300% and ~367 % in May and June respectively. The volume size distribution of aerosols clearly shows a peak in the coarse mode of aerosol in its bimodal distribution, while a negligible coarse mode is noticed in December-February month. The fine mode aerosols also peak in April-May although the total aerosol load is dominated by the coarse mode.

In addition to the columnar measurements of AOD, long term surface concentrations of BC are also examined. The long term trend in BC are examined for the first time in the central Himalayas. The diurnal variations, diurnal amplitudes, the evolution of BC peak, day and nighttime variation, seasonal, and annual variations are discussed in detail. BC shows single afternoon peak with lower values during nighttime during all the seasons except during spring when nighttime levels are also higher. BC shows highest values in May with a mean value of 1.56±0.91 μg m^{-3}. Maximum diurnal amplitude of BC is observed during winter (~1.50 μg m^{-3}), followed by autumn (~0.90 μg m^{-3}) and spring (~0.72 μg m^{-3}). BC amplitude in summer-monsoon is the lowest (~0.21 μg m^{-3}) with nearly flat pattern. The seasonal mean BC is estimated to be 1.05±0.76 μg m^{-3}, 1.38±0.75 μg m^{-3}, 0.67±0.51 μg m^{-3}, and 0.96±0.62 μg m^{-3} during winter, spring, summer-monsoon and autumn respectively. The seasonal variation in daytime and nighttime BC is also examined, both of which shows different seasonal variations. The daytime BC shows maximum concentration in winter, while the nighttime BC is highest in spring. This suggests an increase in the background concentration of BC during spring which could be related to significant anthropogenic

activities. Backward air mass trajectories have been calculated at Nainital to identify possible sources contributing to BC load at Nainital. The trajectory based analysis reveals the influence of westerly air masses that pass over the Indo Gangetic Plain, a region of very strong BC emissions, before arriving at the site.

The seasonal variation in aerosols number concentration of fine mode (0.3-1.0 μm) shows high concentration in January which reduces during March-June and again increases after the monsoon withdraws. In contrast, the number concentration in coarse mode (1-10 μm) shows highest values during May-July while ultra-coarse (10-20 μm) mode shows sharp peak in June. The diurnal variations in the fine, coarse and ultra-coarse mode of aerosols are also described and used to assess the contribution during dust episode. The sharp enhancement in the coarse mode and ultra-coarse mode of aerosols is observed during the dust episode.

Long term trends in AOD and BC are also examined. The linear trend in AOD shows slightly increasing tendency suggesting increase in the aerosol loading over the central Himalayan region. The trend in BC is also estimated for the first time at Nainital. BC is found to increase at a rate of ~21 ng m^{-3} per year. BC trends over Indian location, especially over the Himalayas are very scanty due to the lack of long term ground based observations. The important inference of our present study indicate that although the low altitude region might show decrease in BC over the years as in the case of Trivandrum but the BC over the high altitude regions of the Himalayas are showing positive trend.

6.2. Aerosol Characterization at a Semi-urban Site in the Central Himalayan Foothill Region

This study uses data from ground-based measurements of aerosol black carbon (BC) from a semi-urban site, Pantnagar (29.0°N, 79.5°E, 231 m amsl), located in the Indo-Gangetic Plain (IGP) near the Himalayan foothills to characterize aerosols in a semi-urban environment. Large variations are seen in BC at both diurnal and seasonal scales which are associated with the mesoscale and synoptic meteorological processes, and local/regional anthropogenic activities. BC diurnal variations show two peaks, one in the morning and another in the evening; arising from the combined effects of the atmospheric boundary layer dynamics and local emissions. Evening peaks in BC are more pronounced, throughout the year with maximum amplitude in winter (8.5 μg m^{-3}), followed by autumn (7.1 μg m^{-3}) and spring (5.5 μg m^{-3}) with minimum amplitude in summer-monsoon (4 μg m^{-3}). Similar to the diurnal amplitude, average BC levels also follow similar seasonal variation with maximum value in winter (7.9±5.2 μg m^{-3}), followed by autumn (6.5±4.9 μg m^{-3}) and spring (4.8±3.6 μg m^{-3}) and minimum in summer-monsoon (2.8±2.8 μg m^{-3}).

BC evolution rates (increase and decrease rates) during morning and evening peaks also follow similar seasonal behavior. The diurnal amplitudes as well as the rate of diurnal evolution rates are the highest in winter season, followed by autumn, while they are the lowest in summer-monsoon. BC levels, amplitude and variations in winter followed by autumn are strongly governed by the boundary layer evolution. Weekly variations in BC are also examined which

shows maximum variation in weekday and weekend in winter. The observed weekly variations are examined and discussed with other locations.

BC variations are further examined along with the mixing layer depth (MLD) variations during the daytime. It is examined that BC exhibits nearly an inverse relation with mixing layer depth in all seasons; being strongest in winter (R^2=0.89) and weakest (R^2=0.33) in monsoon (July-August). The low MLD in winter and autumn leads to high BC due to confinement, while high MLD in spring leads to low surface BC. Higher MLD in spring, could induce uplifting of significant amount of BC to the high altitude locations. The lowest BC in summer-monsoon is a combination of the loss due to rainfall and higher MLD. Similar to BC, CO also shows anti-correlation with MLD.

BC-CO relation is also examined to study the common sources of both BC and CO. The BC-CO correlation indicates the influence of fresh emissions and common combustion sources mainly in winter and autumn, while in summer-monsoon the site is influences by aged airmasses with emissions from different combustion sources. Influence of simultaneous emissions from cooking/domestic use of fuel cannot be ruled out; however it is difficult to confirm it due to non-availability of suitable tracer's observations. The average slope (BC-CO) value (10.4 µg $ppmv^{-1}$) over present IGP site is much higher than those over Mexico and Germany indicating that BC emissions are dominating over this region.

Ground based BC are also utilized for source apportionment studies which reveals that the BC contribution from NW and W is maximum (~7-8 μg m^{-3}) in both winter and autumn. It is estimated that the ~62% of air masses arrives via NW in winter contributing BC of ~8.54 μg m^{-3}. The air masses shifts from NW (45%) to W (55%) direction in spring and W sector contributes ~4.89 μg m^{-3} to BC. Influences of SE (38%) and SW (24%) air masses are seen in summer-monsoon and BC levels drop to ~2.21-2.59 μg m^{-3}. After the withdrawal of the southwest monsoon, contribution from NW direction again dominates in autumn and BC levels in this cluster are again high (~7.89 μg m^{-3}).

Co-located aerosol optical depths (AOD) along with aerosols extinction retrieved from CALIPSO data reveal that, unlike BC, columnar AOD and aerosol absorption are highest in spring over the IGP, probably due to the presence of higher abundances of aerosols (including dust) above the ABL. AOD (500 nm) showed annual peak (>0.6) in May-June, dominated by coarse mode, while fine mode aerosols dominate in late autumn and early winter. The calculated values of Angstrom exponent also support the presence of coarse mode aerosols during spring, when dust storms significantly affect this region. Vertical aerosols extinction profiles from CALIPSO show highest values close to the surface during winter/autumn, similar to the feature seen in surface BC concentration, whereas at altitudes > 2 km, the extinction is highest in spring/summer. Aerosol extinction shows least vertical gradient in spring and its levels are maximum at higher heights. The spatial variation of aerosol index

data from OMI also reveals presence of significant absorbing aerosols over the IGP, especially in spring.

The ground based BC observations are also used to evaluate the performance of Weather Research and Forecasting Model coupled with Chemistry (WRF-Chem) in simulating seasonal and diurnal variations of BC at Pantnagar. The model although captures temporal variations but the levels of temporal variations are significantly underestimated by model. The high temporal variation in observed BC is mainly due to the anthropogenic activities and is less associated with the day to day variability of mixing layer depth. The WRF-Chem simulations capture important features of the diurnal and seasonal variations of BC in January, May and July but significantly underestimate the observed BC levels. Average observed and modeled BC at Pantnagar during January, May and July are 6.6±2.2 μg m^{-3} and 2.4±1.2 μg m^{-3}, 5.5±1.8 μg m^{-3} and 1.6±0.7 μg m^{-3}, and 2.2±1.0 μg m^{-3} and 1.2±0.5 μg m^{-3}, respectively. Further work in improving the current BC emission estimates at a finer temporal (diurnal to seasonal) and spatial resolution in the IGP region is strongly suggested. In addition, co-located observations of planetary boundary layer height are also essential for better evaluation of model performance.

6.3. Comparison of Aerosol Characteristics over Different Regions and Role of Different Processes

In this section, the surface and columnar characteristics of aerosols at Nainital and Pantnagar are compared, and the role of associated processes are investigated and discussed in the context to other locations.

Ground based observations of BC and AOD at both the sites Nainital and Pantnagar are compared for diurnal, seasonal and annual variations for the first time to examine the associated processes governing the observed variations. Aerosol loadings as well as BC at Pantnagar are quite high throughout the year as compared to those observed at Nainital. The seasonal variation of BC shows maximum in spring at Nainital while maximum is observed in winter at Pantnagar. Seasonal mean values of BC at Nainital are 1.05±0.76 μg m^{-3}, 1.38±0.75 μg m^{-3}, 0.67±0.51 μg m^{-3}, and 0.96±0.62 μg m^{-3} in winter, spring, summer-monsoon and autumn, respectively, while the corresponding values at Pantnagar are 7.9±5.2 μg m^{-3}, 4.8±3.6 μg m^{-3}, 2.8±2.8 μg m^{-3}, and 6.5±4.9 μg m^{-3}, respectively. The percentage enhancement in the seasonal mean BC at Pantnagar as compared to Nainital is found to be ~ 652%, ~248%, ~318%, and ~577% in winter, spring, summer-monsoon and autumn respectively. The annual mean BC at Pantnagar is found to be higher by about six times than those at Nainital.

BC diurnal variations at both the sites are different. BC shows two peaks (morning and evening) at Pantnagar while noontime peak is observed at Nainital. Additionally, the daytime minimum is observed at Pantnagar, while minimum BC is in the morning (before sunrise) at Nainital. The percentage difference of BC amplitudes at Pantnagar with respect to Nainital are estimated to be ~133%, ~235%, ~558%, ~222% in morning and ~466%, ~668%, ~1779%, and ~688% in evening for winter, spring, summer-monsoon and autumn, respectively. It is very interesting to note that after sunrise BC levels at Pantnagar gradually decreases leading to minimum BC in daytime and at the same time BC levels at Nainital gradually increases after sunrise resulting to maximum BC peak in the afternoon. This important feature indicates the reduction in the surface level pollution during daytime at adjacent low altitude locations and valley regions while gradual buildup of aerosols in the high altitude

mountain locations. The aerosols and other pollutants are uplifted from the low altitudes regions to high altitudes as the boundary layer evolves during daytime. Simultaneous variation of BC at both the sites is also studied and the effect of rainfall scavenging is also examined which reveals low BC on high rainfall days.

Further, AOD at both the sites is also examined which shows high in spring at both the sites, while significant difference in AOD is observed in winter. Columnar loading is minimum and quite low in winter representing nearly clean and nearly free troposphere at Nainital while AOD in winter at Pantnagar is significantly higher, typical to what observed at urban, semi-urban location in IGP. AOD at both the site shows significant enhancement in spring, indicating the possibility of aerosol direct influence/transport from the low altitude IGP region to high altitude. The observed surface concentration and columnar loading at both the sites is examined and explained in context to the vertical distribution of aerosols. The aerosol vertical profiles show low extinction near ground which results in high BC near surface and high AOD at low altitude, while it results in the low AOD at high altitude site. On the other hand, relatively low extinction near ground in spring is the possibly reason of BC getting transported to higher altitudes. As AOD is the total columnar characteristics thus is high at both the sites in spring. The size distribution of aerosols and SSA variations at Nainital and Pantnagar is also discussed and is also compared with the other locations.

BC variations at Nainital are compared with the other high altitude sites. BC values at Nainital are somewhat similar to those reported at Mukteshwar [*Hyvärinen et al.,* 2009]. BC levels are lower during March-May at Mukteshwar than those observed at Nainital. This could be due to lesser influences of biomass and anthropogenic activities at Mukteshwar. Another

high altitude site in the western India (Sinhagad) shows higher BC (2.2 µg m^{-3}) levels than those at Nainital (0.98 µg m^{-3}) [*Safai et al.,* 2014]. The seasonal variation of BC at Sinhagad shows winter time higher BC while at Nainital BC is maximum in spring. BC variations at La Réunion Island are different than those observed at Nainital, but their levels are comparable [*Bhugwant et al.,* 2000]. BC is also compared with another high altitude site in Nepal (NCO-P), which shows similar seasonal variation in BC as at Nainital, though the BC levels at NCO-P are lower **[***Marinoni et al.,* 2010]. BC levels at Nainital are also compared with those at Hanle and Kullu.

BC levels at Pantnagar are compared with other semi-urban and urban locations. The variations are different at nearly all the sites over the Indian region and are characterized by the regular local anthropogenic activities nearby the site and depend on the location of the site. The seasonal BC variations at Pantnagar are somewhat similar to those at Pune [*Safai et al.,* 2007] but diurnal variations of BC are different. BC variations at Delhi [*Tiwari et al.,* 2013], Ahmedabad [*Ramachandran and Kedia,* 2010] and Dibrugarh [*Pathak et al.,* 2010] are much stronger as compared to Pantnagar. BC level at a nearby urban site (Dehradun) is quite low as compared to that at Pantnagar [*Kant et al.,* 2012]. BC level reported at Anantapur [*Reddy et al.,* 2012] is also lower than that observed at Pantnagar. Few other coastal sites also show lesser BC level than that observed at Pantnagar. Generally, the magnitude and evolution of BC is influenced by the local anthropogenic activities and site location e.g. maximum anthropogenic activities are reported in spring season over the northern India.

AOD at Nainital is compared with seasonal mean AOD reported at Northwestern Himalayan site in Kullu [*Guleria et al.,* 2012] and found be to be lower, especially winter time AOD is quite small at Nainital as compared to Kullu. AOD observed at Nainital is also lower or comparable to those observed at many marine sites. The observed AOD when compared to AOD reported for oceanic regions of Arabian Sea [*Satheesh et al.,* 2006a], Port Blair [*Beegum et al.,* 2012], and Minicoy [*Satheesh et al.,* 2002] reveals that AOD at these oceanic regions in winter is higher than those observed at Nainital. Mean AOD reported for winter at Arabian Sea, Port Blair, and Minicoy were 0.29, 0.31, 0.32 respectively, the percentage difference of these AOD with respect to Nainital are found to be 142%, 158%, 167% respectively. The spring values at these locations are also higher as compared to Nainital. As expected, the observed AOD at Nainital is quite lower than those observed at other semi-urban and urban locations. AOD loading at Pantnagar is typical to any semi-urban, urban location in the IGP with significant winter time loading. The magnitude of AOD at both Kanpur and Delhi is observed to be high as compared to what observed at Pantnagar.

6.4. Future Scope

This thesis provides climatological characterization of aerosols (AOD and BC) at a high altitude site Nainital in the central Himalayas. The long term trends especially in BC are calculated for the first time over the central Himalaya. This work also initiated aerosol measurements at a semi -urban low altitude site Pantnagar in the Indo-Gangetic Plain. The analysis of simultaneous

observations from these two sites provided important information about the variability of aerosols in this region and different processes governing the distribution of aerosols at both these sites. It is shown that the aerosol characteristics are quite different at these sites, which indicate the difference in aerosol optical and physical properties at these sites and suggest for the detail study. The study also indicates the necessity of observations of various other aerosol parameters in this region. The present research needs to be supplemented by the further research to improve our understanding of aerosol characteristics over this region. A list of possible future research activities that can be undertaken as a continuation of the current efforts are listed below.

- The measurements of the aerosol BC and AOD should continue at both the sites. These observations will provide crucial information about the long term change in both the surface as well as columnar abundance of aerosols.
- The existing measurements at Pantnagar are not sufficient for the detailed aerosol characterization and should be supplemented by the measurement of aerosol number or mass concentration. The ground based aerosol number concentration will also provide imperative information about the episodic enhancement of fine or coarse mode aerosol concentration and thus will be useful to better understand elevated aerosol loading episodes in this region.
- The current observations of BC aerosols are not sufficient to constrain parameterization of different processes (e.g. aging, activation and scavenging efficiency) controlling the distribution of BC aerosols. Additional measurements capable of providing information about the refractory BC mass, mixing state and vertical distribution of BC aerosols should be initiated to improve the parameterization of different physical processes affecting BC aerosols in the model.

- The chemical composition measurements of aerosols are missing at both Nainital and Pantnagar. Such measurements are highly essential for accurately estimating the aerosol radiative forcing and must be started as soon as possible.
- There is almost no knowledge about the Secondary Organic Aerosol (SOA) and new particle formation mechanism in this part of the world. The measurements of different volatile organic compounds and their intermediate reaction products known as semi-volatile organic compounds must be initiated to examine possible pathways of new particle formation in this region.
- In addition to different aerosol measurements mentioned above, there is an urgent need to better understand the circulation patterns in this region. Specifically, we need to understand the evolution of planetary boundary layer evolution and mountain valley circulation affecting these sites. Therefore, advanced meteorological measurements should be started.
- The measurements presented in this work partially should be used to assess the performance of different global and regional models and validate retrievals of aerosol optical properties from different satellites. In this direction, we made an attempt of evaluating BC at Pantnagar and it turned out that future research should focus on the development of high resolution emission inventory for this region.

Bibliography

Ackerman, A.S., O.B. Toon, D.E. Stevens, A.J. Heymsfield, V. Ramanathan, and E.J. Welton (2000), Reduction of tropical cloudiness by soot, *Science*, 288, 1042-1047.

Adhikary, B., G. R. Carmichael, Y. Tang, L. R. Leung, Y. Qian, J. J. Schauer, E. A. Stone, V. Ramanathan, and M. V. Ramana (2007), Characterization of the seasonal cycle of south Asian aerosols: A regional-scale modeling analysis, *J. Geophys. Res.*, 112, D22S22, doi:10.1029/2006JD008143.

Agnihotri, R., T. K. Mandal, S. G. Karapurkar, M. Naja, R. Gadi, Y. N., Ahammmed, A. Kumar, T. Saud, and M. Saxena (2011), Stable carbon and nitrogen isotopic composition of bulk aerosols over India and northern Indian Ocean, *Atmos. Environ.*, 45, 2828-2835. doi: 10.1016/j.atmosenv.2011.03.003.

Alfaro, S. C., A. Gaudichet, L. Gomes, and M. Maillé (1997), Modeling the size distribution of a soil aerosol produced by sandblasting, J. Geophys. Res., 102(D10), 11239–11249, doi:10.1029/97JD00403.

Al-Momani, I, F., O. Y. Ataman, M. A. Anwari, S. Tuncel, C. Kosc, and G. Tuncel (1995), Chemical composition of precipitation near an industrial area at Izmier, Turkey, *Atmos. Environ.*, 20:965–969.

Andreae, M. O., C. D. Jones, and P. M. Cox, (2005), Strong present-day aerosol cooling implies a hot future, *Nature*, 435, 1187–1190.

Andreae, M.O., H. Berresheim, T.W. Andreae, M.A. Kritz, T.S. Bastes, and J.T. Merrill (1988), Vertical distribution of dimethylsulfide, sulfur dioxide, aerosol ions, and radon over the Northeast Pacific Ocean, *J. Atmos. Chem*., 6, 249-273.

Arimoto, R. (2001), Eolian dust and climate: relationships to sources, tropospheric chemistry, transport and deposition, *Earth-Science Reviews*, 54 (1–3), pp. 29–42

Arnott, W. P., K. Hamasha, H. Moosmüller, P. J. Sheridan, and J. A. Ogren (2005), Towards Aerosol Light-Absorption Measurements with a 7-Wavelength Aethalometer: Evaluation with a Photoacoustic Instrument and 3-Wavelength Nephelometer, *Aerosol Science and Technology* 39 (1): 17–29. doi:10.1080/027868290901972.

Ashbaugh, L. L. (1983) A statistical trajectory technique for determining air pollution source regions *J. Air Pollut. Control.*, Ass., 33, pp. 1096–1098

Ashbaugh, L. L., W.C. Malm, W.Z. Sadeh (1985), A residence time probability analysis of sulfur concentrations at Grand Canyon National Park, *Atmospheric Environment*, 19, pp. 1263–1270

Babu S. S, S. K. Satheesh, K. Krishna Moorthy, C. B. S. Dutt, Vijayakumar S Nair, Denny P Alappattu and P K Kunhikrishnan (2008), Aircraft Measurements of Aerosol Black carbon from a coastal location in the north-east part of peninsular India during ICARB, *J. Earth. Sys. Sci.*, 117, 263-272.

Babu, S. S., and K. K. Moorthy (2001), Anthropogenic impact on aerosol black carbon mass concentration at a tropical coastal station: A case study, *Curr. Sci.*, 81, 1208–1214.

Babu, S. S., et al. (2011), High altitude (~4520 m amsl) measurements of black carbon aerosols over western trans-Himalayas: Seasonal heterogeneity and source apportionment, *J. Geophys. Res.*, 116, D24201, doi:10.1029/2011JD016722.

Babu, S. S., K. K. Moorthy, and S. K. Satheesh (2004), Aerosol black carbon over Arabian Sea during intermonsoon and summer monsoon seasons, *Geophys. Res. Lett.*, 31, L06104, doi:10.1029/2003GL018716.

Babu, S.S, and K. K. Moorthy (2002), Aerosol black carbon over a tropical coastal station in India (2002), *Geophys. Res Lett*., 29 (23): art. no. 2098.

Babu, S.S, S. K. Satheesh S.K, and K. K. Moorthy (2002), Aerosol radiative forcing due to enhanced black carbon at an urban site in India, *Geophys. Res Lett*., 29 (18): art. no. 1880.

Baltensperger, U., H. W. Gaggeler, D. T. Jost, M. Lugauer, M. Schwikowski, E. Weingartner, and P. Seibert (1997), Aerosol climatology at the high-alpine site Jungfraujoch, Switzerland, *J. Geophys. Res.*, 102, 19707–19715.

Bauer, S. E., S. Menon, D. Koch, T. C. Bond, and K. Tsigaridis, (2010), A global modeling study on carbonaceous aerosol microphysical characteristics and radiative effects, *Atmos. Chem. Phys.*, 10, 7439-7456, doi:10.5194/acp-10-7439-2010.

Bäumer, D., R. Rinke, and B. Vogel (2008), Weekly periodicities of aerosol optical thickness over Central Europe - evidence of an anthropogenic direct aerosol effect, *Atmos. Chem.*, Phys., 8, 83–90. doi:10.5194/acp-8-83-2008.

Baumgardner, et al., (2002), Diagnosing black carbon trends in large urban areas using carbon monoxide measurements. J. Geophys. Res.-Atmos 107 (D21), 8342. Doi:10.1029/2001JD000626.

Beegum, S. N., K. K. Moorthy, M. M. Gogoi, S. S. Babu, and S. K. Pandey (2012), Multi-year investigations of aerosols from an island station, Port Blair, in the Bay of Bengal: Climatology and source impacts, *Ann. Geophys.*, 30, 1113–1127.

Beegum,S. N., K. Krishna Moorthy, S. Suresh Babu, S.K. Satheesh, V. Vinoj, K.V.S. Badarinath, P.D. Safai, P.C.S. Devara, Sacchidanand Singh, Vinod, U.C. Dumka, P. Pant (2009), Spatial distribution of aerosol black carbon over India during pre-monsoon season, *Atmospheric Environment*, 43, 1071-1078, doi:10.1016/j.atmosenv.2008.11.042.

Beljaars, A. C. M. (1994), The parameterization of surface fluxes in large scale models under free convection. Q. J. Roy, *Meteor. Soc.*, 121, 255–270.

Bhugwant, C., M. Bessafi, E. Rivière, J. Leveau (2001), Diurnal and seasonal variation of carbonaceous aerosols at a remote MBL site of La Réunion island, *Atmospheric Research*, Volume 57, Issue 2, March 2001, Pages 105-121, ISSN 0169-8095, doi:10.1016/S0169-8095(01)00066-7.

Bisht, D. S., S. Tiwari, A. K. Srivastava, J. V. Singh, B. P. Singh, and M. K. Srivastava (2014), High concentration of acidic species in rainwater at Varanasi in the Indo-Gangetic Plains, India, *Natural Hazards*, doi: 10.1007/s11069-014-1473-0.

Blanchard, D.C. (1985), The oceanic production of atmospheric sea salt, *J. Geophys. Res.*, 90, 961-963.

Blanchard, D.C., and A. H. Wookcock (1980), The production, concentration and vertical distribution of the sea salt aerosols, *Annals of the New York Academy of Sciences*, 338, 330-347, 1980.

Blanchard, D.C., and A.H. Woodcock (1957), Bubble formation and modification in the sea and its meteorological significance, *Tellus*, 9, 145-158.

Bluth, G. J. S., S. D. Dorinson, S. C. Schnetzler, A. J. Krueger, and L. S. Walter (1992), Global tracking of the SO2 clouds from the June 1991 Mount Pinatubo eruptions, *Geophys. Res. Lett*., 19, 151-154.

Bodhaine, B. A. (1995), Aerosol absorption measurements at Barrow, Mauna Loa and the south pole, *J. Geophys. Res.* 100(D5), 8967–8975. doi:10.1029/95JD00513.

Bonasoni, P., et al. (2008), The ABC-Pyramid Atmospheric Research Observatory in Himalayas for aerosol, ozone and halocarbon measurements, *Sci. Total Environ.*, 391, 241–251.

Bonasoni, P., et al. (2010), Atmospheric Brown Clouds in the Himalayas: First two years of continuous observations at the Nepal-Climate Observatory at Pyramid (5079 m), Atmos. Chem. Phys. Discuss., **10**,4823–4885.

Bond, T. C., et al. (2013), Bounding the role of black carbon in the climate system: A scientific assessment, *J. Geophys. Res.*, 118, 5380–5552. doi: 10.1002/jgrd.50171.

Brasseur, G., and Matthew H. Hitchman, (1992), Stratospheric Response to Trace Gas Perturbations: Changes in Ozone and Temperature Distributions, *Science*, 1239-1242. DOI:10.1126/science.257.5074.1239

Budhavant, K. B., P. S. P. Rao, P. D. Safai, and K. Ali (2009), Chemistry of monsoon and post-monsoon rains at a high altitude location, Sinhagad, India, *Aerosol Air Qual. Res.* 9, 65–79.

Cachier, H (1998), Carbonaceous combustion aerosols, *Atmospheric particles*, edited by R. M. Harrson and R. E. van Grieken, IUPAC series on analytical and physical chemistry of environmental systems, volume 5, John Wiley and Sons.

Carlson, T.N., and J.M. Prospero (1972), The large-scale movement of Saharan air outbreaks over the North equatorial Atlantic, *J. Appl. Meteorol*., 11, 283-297.

Carrico, C. M., M. H. Bergin, A. B. Shrestha, J. E. Dibb, L. Gomes, and J. M. Harris (2003), The importance of carbon and mineral dust to seasonal aerosol properties in the Nepal Himalaya, *Atmos. Environ.,* 37, 2811–2824.

Charlson, R.J., J. Langner, H. Rodhe, C. B. Leovy and S. G. Warren (1991), Perturbation of the northern hemisphere radiative balance by backscattering from anthropogenic sulfate aerosols, *Tellus*, 43AB,152-163.

Charlson, R.J., S.E. Schwartz, J.M. Hales, R.D. Cess, J.A. Coakley, J. E. Hansen, and D.J. Hofmann (1992), Climate forcing by anthropogenic aerosols, *Science*, 255, 423-430.

Chate, D. M., P. C. S. Devara, (2009), Acidity of raindrop by uptake of gases and aerosol pollutants, Atmos. Environ. 43, 1571–1577.

Chen, F., and J. Dudhia (2001), Coupling an advanced land-surface/hydrology model with the Penn State/NCAR MM5 modeling system Part I: model description and implementation, *Monthly Weather Review.*, 129, 569e585.

Cheng, T.T., Z.W. Han, R.J. Zhang, H.H. Du, X.A. Jia, J.J. Wang, J.Y. Yao (2010), Black carbon in a continental semi–arid area of Northeast China and its possible sources of fire emission, *Journal of Geophysical Research–Atmospheres*, 115, art. no. D23204.

Chin, M., et al. (2002), Tropospheric aerosol optical thickness from the GOCART model and comparisons with satellite and sunphotometer measurements, *J. Atmos. Sci.*, 59, 461–483.

Mallik, C., Shyam Lal, Manish Naja, Duli Chand, S. Venkataramani, Hema Joshi and P. Pant (2013), Enhanced SO2 concentrations observed over northern India: role of long-range transport, International Journal of Remote Sensing, 34:8, 2749-2762.

Chinnam, N., S. Dey, S. N. Tripathi, and M. Sharma (2006), Dust events in Kanpur, northern India: Chemical evidence for source and implications to radiative forcing, *Geophys. Res. Lett*, 33, L08803, doi: 10.1029/2005GL025278.

Chow, J. C., (1995), Measurement methods to determine compliance with ambient air quality standards for suspended particles, *J. Air Waste Manag. Assoc.*, 45, 320-382.

Chu, D.A., Y.J. Kaufman, C. Ichoku, L.A. Remer, D. Tanré, B.N. Holben (2002), Validation of MODIS aerosol optical depth retrieval over land, *Geophys. Res. Lett.*, 29 (12), 8007.

Chung, C. E., V. Ramanathan, and J. Kiehl (2002), Effects of the south Asian absorbing aerosol haze on the northeast monsoon and surface-air heat exchange. *J. Clim*, 15, 2462–2476.

Corrigan, C.E., V. Ramanathan, J.J. Schauer (2006), Impact of monsoon transitions on the physical and optical properties of aerosols, *J. Geophys. Res.*, 111, D18208, doi:10.1029/2005JD006370.

Das, N., R. Das, G. R. Chaudhury, and S. N. Das (2010), Chemical composition of precipitation at background level, *Atmos. Res.* 95, 108–113.

Deng, X., et al. (2012), Analysis of aerosol characteristics and their relationships with meteorological parameters over Anhui province in China, *Atmospheric Research*, Volumes 109–110, Pages 52-63, ISSN 0169-8095, doi:10.1016/j.atmosres.2012.02.011.

Dey, S., S. N. Tripathi, and R. P. Singh (2004), Influence of dust storms on the aerosol optical properties over the Indo-Gangetic basin, *J. Geophys. Res.*, **109**, **D20211**, doi: 10.1029/2004JD004924.

Diner, D., et al. (1989), MISR: A Multiangle Imaging Spectroradiometer for geophysical and climatological research from Eos, IEEE Trans. *Geosci. Remote Sens.*, 27(2), 200– 214.

Diner, D., et al. (1998), Multiangle Imaging Spectroradiometer (MISR) Instrument Description and experiment overview, IEEE Trans. *Geosci. Remote Sens.*, 36(4), 1072– 1087.

Draxler R. R and G.D Hess (1998), An overview of the HYSPLIT_4 modelling system for trajectories, dispersion and deposition, *Australian Meteorological Magazine*, 47, pp. 295–308.

Draxler, R. R. and G. D. Rolph (2003), Real-time Environmental Applications and Display System (READY). Website http://www.arl.noaa.gov/ready/hysplit4.html, NOAA Air Resources Laboratory. Silver Spring, MD.

Dubovik, O., A. Sinyuk, T. Lapyonok, B. N. Holben, et al. (2006), Application of spheroid models to account for aerosol particle nonsphericity in remote sensing of desert dust, *J. Geophys. Res.*, 111, D11208, doi:10.1029/2005JD006619.

Dubovik, O., T. Yokota, and Y. Sasano (1998), Improved technique for data inversion and its application to the retrieval algorithm for ADEOS/ ILAS, *Adv. Space. Res.*, 21,397-403.

Dubovik, O., A. Smirnov, B. N. Holben, M. D. King, Y. J. Kaufman, T. F. Eck, and I. Slutsker (2000),Accuracy assessments of aerosol optical

properties retrieved from Aerosol Robotic Network (AERONET) Sun and sky radiance measurements, J. Geophys. Res., 105(D8), 9791–9806, doi:10.1029/2000JD900040.

Dubovik, O., B. Holben, T. F. Eck, A. Smirnov, Y. J. Kaufman, M. D. King, D. Tanre, and I. Slutsker (2002), Variability of absorption and optical properties of key aerosol types observed in worldwide locations, J. Atmos. Sci., **59**, 590–608.

Dumka, U. C., Deepika Bhattu, S.N. Tripathi, D.G. Kaskaoutis, B. L. Madhavan (2015), Seasonal inhomogeneity in cloud precursors over Gangetic Himalayan region during GVAX campaign, *Atmospheric Research*, 155, 158-175, ISSN 0169-8095, doi:10.1016/j.atmosres.2014.11.022.

Dumka, U. C., et al. (2013), Temporal variability and radiative impact of black carbon aerosol over tropical urban station Hyderabad, *Journal of Atmospheric and Solar-Terrestrial Physics*, 105–106, 81-90. doi:10.1016/j.jastp.2013.08.003.

Dumka, U. C., K. K. Moorthy, R. Kumar, P. Hegde, R. Sagar, P. Pant,N. Singh, and S. S. Babu (2010), Characteristics of aerosol black carbon mass concentration over a high altitude location in the Central Himalayas from multi-year measurements,Atmos. Res., **96**, 510–521, doi:10.1016/j.atmosres.2009.12.010.

Dumka, U. C., R. Sagar, and P. Pant (2009), Retrieval of columnar aerosol size distributions from spectral attenuation measurements over Central Himalayas, *Aerosol Air Qual. Res.*, **9**, 344–351.

Dumka, U.C. et al. (2006), Surface changes in solar irradiance due to aerosols over central Himalayas, J. Geophys. Res., 33 (20): Art. No. L20809, doi:10.1029/2006GL027814.

Dumka, U.C., D.G. Kaskaoutis (2014), In-situ measurements of aerosol properties and estimates of radiative forcing efficiency over Gangetic-Himalayan region during the GVAX field campaign, *Atmospheric*

Environment, 94, 96-105, ISSN 1352-2310, doi:10.1016/j.atmosenv.2014.05.021.

Eck, T. F., B. N. Holben, J. S. Reid, O. Dubovik, S. Kinne, A. Smirnov, N. T. O'Neill, I. Slutsker (1999), The wavelength dependence of the optical depth of biomass burning, urban and desert dust aerosols, J. Geophys. Res., **104**, 31333–31350.

Exton H.J., J. Latham, P.M. Park, S.J. Perry, M.H. Smith and R.R. Allan (1985), The production and dispersal of marine aerosol, *Q. J. Roy. Meteorol. Soc*., 111, 817-837.

Favez, O., S. C. Alfaro, J. Sciare, H. Cachier, and M. M. Abdelwahab (2009), Ambient measurements of light-absorption by agricultural waste burning organic aerosols, *Aerosol Sci.,* 40, 613–620.

Feingold, G., W. R. Cotton, S. M. Kreidenweis, and J. T. Davis (1999), Impact of giant cloud condensation nuclei on drizzle formation in marine stratocumulus: Implications for cloud radiative properties, *J. Atmos. Sci***.,** 56**,** 4100- 4117**.**

Finlayson-Pitts, B. J., and J. N. Pitts Jr. (1986), Atmospheric Chemistry: Fundamentals and Experimental Techniques, John Wiley, ISBN 0-471-88227-5.

Finlayson-Pitts and James N. Pitts Jr. (2000), Particles in the Troposphere, Chemistry of the Upper and Lower Atmosphere, *ISBN 978-0-12-257060-5*, doi: 10.1016/B978- 012257060-5/50011-3.

Fitzgerald, J.W. (1991), Marine aerosols: A review, *Atmos. Environ*., 25A, 533-545.

Flanner, M. G., C. S. Zender, P. G. Hess, N. M. Mahowald, T. H. Painter, V. Ramanathan, and P. J. Rasch (2009), Springtime warming and reduced snow cover from carbonaceous particles, Atmos. Chem. Phys., **9**(7), 2481–2497, doi:10.5194/acp-9-2481-2009.

Flossmann, A.I., W.D. Hall, and H.R. Pruppacher (1985), A theoretical study of the wet removal of atmospheric pollutants, I, The redistribution of aerosol particles captured through nucleation and impaction scavenging by growing cloud drops, *J. Atmos. Sci*., 42, 583-606.

Freitas, S. R., et al. (2007), Including the sub-grid scale plume rise of vegetation fires in low resolution atmospheric transport models, *Atmos. Chem. Phys*., 7, 3385–3398. doi:10.5194/acp-7-3385-2007.

Garc´ıa, M. A., et al. (2007), Characterisation of the mixing height temporal evolution by means of a laser dial system in an urban area – intercomparison results with a model application, *Ann. Geophys*., 25, 2119–2124.

Gautam R., Z. Liu, R. P. Singh, and N. C. Hsu, (2009), Two contrasting dust-dominant periods over India observed from MODIS and CALIPSO data, *Geophys. Res. Lett*., 36, L06813, doi:10.1029/2008GL036967.

Gautam, R., et al. (2011), Accumulation of aerosols over the Indo-Gangetic plains and southern slopes of the Himalayas: distribution, properties and radiative effects during the 2009 pre-monsoon season, *Atmos. Chem. Phys.*, 11, 12841-12863. doi:10.5194/acp-11-12841-2011.

Gautam, R., N. C. Hsu, and K.-M. Lau (2010), Premonsoon aerosol characterization and radiative effects over the Indo-Gangetic Plains: Implications for regional climate warming, J. Geophys. Res.,115, D17208, doi:10.1029/2010JD013819.

Gelencsér, A., B. May, D. Simpson, A. Sánchez-Ochoa, A. Kasper-Giebl, H. Puxbaum, A. Caseiro, C. A. Pio, and M. Legrand (2007), Source apportionment of PM2.5 organic aerosol over Europe: Primary/secondary, natural/anthropogenic, and fossil/biogenic origin, J. Geophys. Res., **112**, D23S04, doi:10.1029/2006JD008094.

Gobre, T., P. R. Salve, R. J. Krupadam, A. Bansiwal, S. Shastry, and S. R. Wate (2010), Chemical composition of precipitation in the coastal environment of India, *Bull. Environ. Contam. Toxicol.,* 85:48–53.

Gogoi, M. M., et al. (2013), Absorption characteristics of aerosols over the northwestern region of India: Distinct seasonal signatures of biomass burning aerosols and mineral dust, *Atmos. Environ.*, 73, 92-102. doi: 10.1016/j.atmosenv.2013.03.009.

Gogoi, M. M., S. S. Babu, V. Jayachandran, K. K. Moorthy, S. K. Satheesh, M. Naja, and V. R. Kotamarthi (2015), Optical properties and CCN activity of aerosols in a high-altitude Himalayan environment: Results from RAWEX-GVAX. J. Geophys. Res. Atmos., 120, 2453–2469. doi:10.1002/2014JD022966.

Goncalves, F. L. T., M.F. Andrade, M.C. Forti, R. Astolfo, M.A. Ramos, O. Massambani, A.J. Melfi (2003), Preliminary estimation of the rainfall chemical composition evaluated through the scavenging modeling for north-eastern Amazonian region (Amapa State Brazil), *Environ. Pollut.*, 121, p. 63.

Gonçalves, F.L.T., A.M Ramos, S Freitas, M.A Silva Dias, O Massambani (2002), In-cloud and below-cloud numerical simulation of scavenging processes at Serra Do Mar region, SE Brazil, *Atmospheric Environment*, Volume 36, Issue 33, , Pages 5245-5255, ISSN 1352-2310, doi: 10.1016/S1352-2310(02)00461-2.

Gong, S.L., X.Y. Zhang, T.L. Zhao, I.G. McKendry, D.A. Jaffe, N.M. Lu (2003), Characterization of soil dust aerosol in China and its transport and distribution during 2001 ACE-Asia. 2: Model simulation and validation, *Journal of Geophysical Research*, 108 (D9), doi:10.1029/2002JD002633.

Gordon, G. E. (1980), Receptor Models, Environ. *Sci. Technol.*, 14, 792.

Grell, G. A., et al. (2005), Fully coupled “online” chemistry within the WRF model, *Atmos. Environ.*, 39, 6957–6975.

Grell, G. A., and D. Dévényi (2002), A generalized approach to parameterizing convection combining ensemble and data assimilation

techniques, Geophys. Res. Lett., 29(14), 1693, doi:10.1029/2002GL015311.

Guleria, R. P., J. C. Kuniyal, N. L. Sharma, P. P. Dhyani (2012), Seasonal variability in aerosol optical and physical characteristics estimated using the application of the Ångström formula over Mohal in the northwestern Himalaya, India, *Journal of Earth System Science*, 2012, 121, pp 697-710

Habib, G., C. Venkataraman, I. Chiapello, S. Ramachandran, O. Boucher, and M. S. Reddy (2006), Seasonal and interannual variability in absorbing aerosols over India derived from TOMS: Relationship to regional meteorology and emissions, *Atmos. Environ.*, 40, 1909–1921.

Hadley, O. L., V. Ramanathan, G. R. Carmichael, Y. Tang, C. E. Corrigan, G. C. Roberts, and G. S. Mauger (2004), Trans-Pacific transport of black carbon and fine aerosol (D Hansen, J., and Nazarenko, L.: Soot climate forcing via snow and ice albedos, *Proc. Natl. Acad. Sci.* USA, 101, 423–428.

Hansen, A. D., A. H. Rosen, and T. Novakov (1984), The Aethalometer-An instrument for the real-time measurement of optical absorption by aerosol particles, *Sci. Total Environ.*, 36, 191–196. doi:10.1016/0048-9697(84)90265-1.

Hansen, A.D. A. (1996), Magee Scientific Aethalometer User's Guide, 56 pp., Magee Sci. Company, Berkeley, Calif.

Hansen, J. E., M. Sato, R. Reudy, A. Lacis, and V. Oinas (2000), Global warming in the 21st century : an alternative scenario, *Proc. Nat. Acad. Sci*, 97, 9875-9880.

Hansen, J., A. Lacis, R. Ruedy, and M. Sato (1992), Potential climate impact of Mount Pinatubo eruption, *Geophys. Res. Lett.*, 19, 215-218.

Hansen, J., and L. Nazarenko (2004), Soot climate forcing via snow and ice albedos, P. Natl. Acad. Sci. USA, **101**(2),423–428, doi:10.1073/pnas.2237157100.

Hansen, J., D. Johnson, A. Lacis, S. Lebedeff, P. Lee, D. Rind, and G. Russell (1981), Climate impact of increasing atmospheric carbon dioxide, *Science*, 213, 957-966.

Hansen, J.E., M. Sato, A. Lacis, R. Ruedy, I. Tegen, and E. Matthews (1998), Climate forcings in the industrial era, *Proc. Natl. Acad. Sci*., 12753-12758.

Hansen, J.E., M. Sato, and R. Ruedy (1997), Radiative forcing and climate response, *J. Geophys. Res*., 102, 6831-6864.

Haywood, J.M., and K. P. Shine (1997), Multi-spectral calculations of the direct radiative forcing of tropospheric sulphate and soot aerosols using a column model, *Q. J. R. Meteol. Soc*., 123, 1907-1930.

Haywood, J.M., and V. Ramaswamy (1998), Global sensitivity studies of the direct radiative forcing due to anthropogenic sulfate and black carbon aerosols, *J. Geophys. Re*s., *10*3, 6043-6058.

Hegde, P., P. Pant, M. Naja, U. C. Dumka, and R. Sagar (2007), South Asian dust episode in June 2006: Aerosol observations in the Central Himalayas, *Geophys, Res. Lett*, 34, L23802, doi: 10.1029/2007GL030692.

Hegg, D. A. (1990), Heterogeneous production of cloud condensation nuclei in the marine atmosphere, *Geophys. Res. Lett*., 17, 2165- 2168.

Hegg, D.A., J. Livingston, P.V. Hobbs, T. Novakov, and P. Russell (1997), Chemical apportionment of aerosol column optical depth off the Mid-Atlantic coast of the United States, *J. Geophys. Res*., 102, 25293-25303.

Heintzenberg, J.R., R. J. Charlson, A.D.Clarke, C.Liousse, V.Ramaswamy, K.P.Shine, and M.Wendisch (1997), Measurement and modelling of aerosol singlre scattering albedo: Progress, problems and prospects, *Contrib. Atmos. Phys*., 70, 249-264.

Hinds, W. (1999), Aerosol technology: Properties, behavior, and measurement of airborne particles, Wiley: New York.

Hitzenberger, R., A. Petzold, H. Bauer, P. Ctyroky, P. Pouresmaeil, L. Laskus, H. Puxbaum (2006), Intercomparison of thermal and optical measurement methods for elemental carbon and black carbon at an urban location, *Environ. Sci. Technol.,* 6377–6383.

Hoffmann, D. J., et al. (1987), Perturbations to the global atmosphere associated with the El Chichon volcanic eruption of 1982, *Reviews of Geophysics*, 25, pp. 743–759

Hoffmann, D.J., and J. M. Rosen (1983), Stratospheric sulphuric acid fraction and mass estimate for the 1982 eruption of El Chichon, *Geophys. Res. Lett*., 10, 313-316.

Holben, B. N., et al. (1998), AERONET—A federated instrument network and data archive for aerosol characterization, *Remote Sens. Environ.*, 66, 1–16.

Holben, B. N., et al. (2001), An emerging ground-based aerosol climatology: Aerosol optical depth from AERONET, *J. Geophys. Res.,* 106(D11). 12067–12097. doi:10.1029/2001JD900014.

Hong, S.-Y., J. Dudhia, S. H. Chen (2004), A revised approach to ice microphysical processes for the bulk parameterization of clouds and precipitation, *Monthly Weather Review.*, 132, 103, 120.

Hoppel, W. A., G. M. Frick, and R. E. Larson (1986), Effect of non-precipitating clouds on the aerosol size distribution, *Geophys. Res. Lett*., 13, 125- 128.

Hoppel, W.A., J.W. Fitzgerald, G.M. Frick, and R.E. Larson (1990), Aerosol size distribution and optical properties found in the marine boundary layer over the Atlantic ocean, *J. Geophys. Res*., 95, 3659-3686.

Horvath, H. (1993), Atmospheric light absorption – a review, *Atmos. Env*., 27A, 293- 317.

Hyvärinen, A.-P., H. Lihavainen, M. Komppula, V. P. Sharma, V.-M. Kerminen, T. S. Panwar, and Y. Viisanen (2009), Continuous

measurements of optical properties of atmospheric aerosols in Mukteshwar, northern India, J. Geophys. Res., 114, D08207, doi:10.1029/2008JD011489.

Ichoku, et al. (2002), Analysis of the performance characteristics of the five-channel Microtops II Sun photometer for measuring aerosol optical thickness and precipitable water vapour, *Geophys. Res.* 107, No D13, 10.1029/2001JD001302.

Intergovernmental Panel on Climate Change (2013), Climate Change 2013: The Physical Science Basis. Contribution of Working Group I to the Fifth Assessment Report of the Intergovernmental Panel on Climate Change, edited by T. F. Stocker, pp. 1535, Cambridge Univ. Press, Cambridge, U. K., and New York.

Intergovernmental Panel on Climate Change, Climate Change 1995: The Science of Climate Change, The Contribution of Working Group I to the Second Assessment Report of the IPCC, edited by J. T. Houghton et al., 572 pp., Cambridge Univ. Press, New York, 1996.

IPCC, 2007. Summary for Policymakers. In: Solomon, S., Qin, D., Manning, M., Chen, Z., Marquis, M., Averyt, K.B., Tignor, M., Miller, H.L. (Eds.), Climate Change 2007: The Physical Science Basis. Contribution of Working Group I to the Fourth Assessment Report of the Intergovernmental Panel on Climate Change. Cambridge University Press, Cambridge, United Kingdom\New York, NY, USA.

Jacobson, M. Z. (2001), Strong radiative heating due to the mixing state of black carbon in atmospheric aerosols, *Nature*, 409, 695–697.

Jaenicke, R. (1984), Physical aspects of atmospheric aerosol, in *Aerosols and their climatic effects*, (Ed. H.E. Gerbard and A. Deepak), A. Deepak Publishing, Hampton, Virginia, pp.7-34.

Jain S. K. (2008), Impact of retreat of Gangotri glacier on the flow of Ganga River *Curr. Sci.* 95 1012–4.

Janssens-Maenhout, G., et al. (2012), EDGAR-HTAP: a Harmonized Gridded Air Pollution Emission Dataset Based on National Inventories,

European Commission Publications Office, Ispra, Italy, EUR report No EUR 25229, 40.

Järvi, L., et al. (2008), Temporal variations in black carbon concentrations with different time scales in Helsinki during 1996-2005, *Atmos. Chem. Phys.*, 8, 1017–1027. doi:10.5194/acp-8-1017-2008.

Jayaraman, A., S. Ramachandran, Y.B. Acharya, and B.H. Subbaraya (1995), Pinatubo volcanic aerosol layer decay observed at Ahmedabad (23°N), India using Nd YAG backscatter Lidar, *J. Geophys. Res*., **100**, 23209-23214.

Jethva, H., S. K. Satheesh, and J. Srinivasan (2005), Seasonal variability of aerosols over the Indo-Gangetic basin, *J. Geophys. Res.*, 110, D21204. doi:10.1029/2005JD005938.

Joshi, H., M. Naja, K.P. Singh, R. Kumar, P. Bhardwaj, S. S. Babu, S.K. Satheesh, K. K. Moorthy, H.C. Chandola, Investigations of aerosol black carbon from a semi-urban site in the Indo-Gangetic Plain region, *Atmospheric Environment*, 2015, doi:10.1016/j.atmosenv.2015.04.007.

Junge, C. E. (1963), Air Chemistry and Radioactivity, *Academic Press, New York*.

Kant, Y., A.K. Mishra, V.K. Dadhwal, (2010), Characteristic of spectral properties of aerosols over Dehradun environment, Scientific progress report, ISRO Geosphere Biosphere Program (IGBP), Vikram Sarabhai Space Centre, *Indian Space Research Organization*, Thiruvananthapuram, 89-92.

Kant, Y., et al. (2012), Diurnal and seasonal aerosol optical depth and black carbon in the shiwalik hills of the north western Himalayas: a case study of the doon valley, India, *International Journal of Geology, Earth and Environmental Sciences*, 01/2012; 2(2):173-192.

Kaufman, Y. J. and R. S. Fraser (1983), Light extinction by aerosols during summer air pollution, *J. Clim. Appl. Metero,* **22,** 1694-1706.

Kaufman, Y. J., and R. S. Fraser (1997), The effect of smoke particles on clouds and climate forcing, Science, **277**, 1636–1639.

Kaufman, Y. J., D. Herring, K. Ranson, and G. Collatz (1998), Earth Observing System AM 1 Mission to Earth, IEEE Trans. *Geosci. Remote Sens.*, 36(4), 1045– 1055.

Kaufman, Y. J., D. Tanre, L. A. Remer, E. F. Vermote, A. Chu, and B. N. Holben (1997), Operational remote sensing of tropospheric aerosol over land from EOS moderate resolution imaging spectroradiometer, *J. Geophys.*, Res. 102, 17051 – 17-067.

Koch, D., and J. Hansen (2005), Distant origins of Arctic black carbon: A Goddard Institute for Space Studies ModelE experiment, J. Geophys. Res., 110, D04204, doi:10.1029/2004JD005296.

Kokhanovsky. A.A., (2008), Aerosol Optics — Light Absorption and Scattering by Particles in the Atmosphere, Springer Praxis Books, Springer Berlin Heidelberg.

Komppula, M., H. Lihavainen, A.-P. Hyvarinen, V.-M. Kerminen, T. S. Panwar, V. P. Sharma, and Y. Viisanen (2009), Physical properties of aerosol particles at a Himalayan background site in India, *J. Geophys. Res.*, 114, D12202, doi:10.1029/2008JD011007.

Kotamarthi, V. R. (2011), Ganges Valley Aerosol Experiment Science and Operations Plan, available at: http://www.arm.gov/sites/amf/pgh/ (last access: May 2012).

Kulshrestha, U. C., A. K. Sarkar, S. S. Srivastava, and D. C. Parashar, (1996), Investigation into atmospheric deposition through precipitation studies at New Delhi [India], *Atmos. Environ.,* 30, 4149–4154.

Kumar, R., M. C. Barth, G. G. Pfister, M. Naja, and G. P. Brasseur (2014), WRF-Chem simulations of a typical premonsoon dust storm in northern India: Influences on aerosol optical properties and radiation budget, *Atmos. Chem. Phys.*, 14, 2431–2446.

Kumar, R., M. Naja, S. K. Satheesh, N. Ojha, H. Joshi, T. Sarangi, P. Pant, U. C. Dumka, P. Hegde, and S. Venkataramani, (2011), Influences of the springtime northern Indian biomass burning over the central

Himalayas, *J. Geophys. Res.*, 116, D19302. doi:10.1029/2010JD015509.

Kumar, R., M. Naja, G. G. Pfister, M. C. Barth, and G. P. Brasseur (2012), Simulations over South Asia using the Weather Research and Forecasting model with Chemistry (WRF-Chem): set-up and meteorological evaluation, *Geosci. Model Dev.*, 5, 321-343. doi:10.5194/gmd-5-321-2012.

Kuniyal J. C. and S. C. R. Vishvakarma (2006), Changing behaviour of ambient air quality and surface ozone in hill spots: a case study of Kullu-Manali Tourist Complex (KMTC), Northwestern Himalaya; DST final technical report submitted to the Department of Science & Technology, Govt. of India, November 2006, pp 1–36.

Kuniyal, J. C. (2010), Aerosols climatology over the northwestern Himalayan region. pp. 93-99. In: Proc. ARFI & ICARB Scientific Progress Report. ISRO Geosphere Biosphere Programme (IGBP), *Space Physics Laboratory*, VSSC, Thiruvanthapuram.

Kurokawa, J., T. Ohara, T. Morikawa, S. Hanayama, G. Janssens-Maenhout, T. Fukui, K. Kawashima, and H. Akimoto (2013), Emissions of air pollutants and greenhouse gases over Asian regions during 2000–2008: Regional Emission inventory in ASia (REAS) version 2, *Atmos. Chem. Phys.*, 13, 11019-11058, doi:10.5194/acp-13-11019-2013.

Lawrence, M. G., and J. Lelieveld (2010), Atmospheric pollutant outflow from southern Asia: A review, *Atmos. Chem. Phys.*, 10,11,017–11,096, doi:10.5194/acp-10-11017-2010.

Lau, K. M., et al. (2010), Enhanced surface warming and accelerated snow melt in the Himalayas and Tibetan Plateau induced by absorbing

aerosols, *Env. Res. Lett.*, 5, 025204. doi:10.1088/1748-9326/5/2/025204.

Lau, K. M., M. K. Kim and K. M. Kim (2006), Asian monsoon anomalies induced by aerosol direct forcing: the role of the Tibetan Plateau *Clim. Dyn.* 26 855–64

Lau, K.-M., and K.-M. Kim (2006), Observational relationships between aerosol and Asian monsoon rainfall, and circulation, Geophys. Res. Lett., 33, L21810, doi:10.1029/2006GL027546.

Lau, K.-M.et al. (2008), The joint aerosol-monsoon experiment: a new challenge in monsoon climate research, *Bulletin of the American Meteorological Society.*, 89 (3), 369–383. doi: 10.1175/BAMS-89-3-369.

Lelieveld et al. (2001), The Indian Ocean Experiment: Widespread Air Pollution from South and Southeast Asia, *Science*, 291 (5506), 1031-1036. doi: 10.1126/science.1057103.

Léon, J.-F., P. Chazette, J. Pelon, F. Dulac, and H. Randriamiarisoa (2002), Aerosol direct radiative impact over the INDOEX area based on passive and active remote sensing, J. Geophys. Res., 107(D19), doi:10.1029/2000JD000116.

Levy, R.C., L.A. Remer, S. Mattoo, E.F. Vermote, Y.J. Kaufman (2007), Secondgeneration operational algorithm: retrieval of aerosol properties over land From inversion ofModerate Resolution Imaging Spectroradiometer spectral reflectance, *J. Geophy. Res.* 112 (D13211). doi:10.1029/2006JD007811.

Li, F., and V. Ramanathan (2002), Winter to summer variation of aerosol optical depth over the tropical Indian Ocean, *J. Geophys. Res*., 107, 10.1029/2001JD000949.

Liu, X., and B. Chen (2000), Climatic warming in the Tibetan Plateau during recent decades, *Int. J. Climatol.*, 20, 1729– 1742.

Lovett, R.F. (1978), Quantitative measurement of airborne sea salt in the North Atlantic, *Tellus*, 30, 358-364.

Lu, Z., D. G. Streets, Q. Zhang, and S. Wang (2012), A novel back-trajectory analysis of the origin of black carbon transported to the Himalayas and Tibetan Plateau during 1996–2010, Geophys. Res. Lett., 39, L01809, doi:10.1029/2011GL049903.

Mallik, C., S. Lal, M. Naja, D. Chand, S. Venkataramani, Hema Joshi and P. Pant (2013), Enhanced SO2 concentrations observed over northern India: role of long-range transport, International Journal of Remote Sensing, 34:8, 2749-2762.

Manoharan, V. S., R. Kotamarthi, Y. Feng, M.P. Cadeddu (2014), Increased absorption by giant aerosol particles over the Gangetic–Himalayan region, *Atmos. Chem. Phys.*, 14, pp. 1–7 http://dx.doi.org/10.5194/acp-14-1-2014.

Marcq, S., P. Laj, J. C. Roger, P. Villani, K. Sellegri, P. Bonasoni, A. Marinoni, P. Cristofanelli, G. P. Verza, and M. Bergin (2010), Aerosol optical properties and radiative forcing in the high Himalaya based on measurements at the Nepal Climate Observatory-Pyramid site (5079 m a.s.l.), *Atmos. Chem. Phys.*, 10, 5859-5872, doi:10.5194/acp-10-5859-2010.

Maring, H., D. L. Savoie, M. A. Izaguirre, L. Custals, and J. S. Reid (2003), Mineral dust aerosol size distribution change during atmospheric transport, J. Geophys. Res., 108, 8592, doi:10.1029/2002JD002536, D19.

Marinoni, A., P. Cristofanelli, F. Calzolari, F. Roccato, U. Bonafe, and P. Bonasoni (2008), Continuous measurements of aerosol physical parameters at the Mt. Cimone GAW Station (2165 m asl, Italy) *Sci. Tot. Environ.*, 391, 241–251.

Marinoni, A., P. Cristofanelli, P. Laj, R. Duchi, F. Calzolari, S. Decesari, K., Sellegri, E. Vuillermoz, G. P. Verza, P. Villani, and P. Bonasoni (2010), Aerosol mass and black carbon concentrations, a two

year record at NCO-P (5079 m, Southern Himalayas), *Atmos. Chem. Phys.,* 10, 8551-8562, doi:10.5194/acp-10-8551-2010.

McCartney, E.J. (1976), Optics of the atmosphere, John Wiley, New York.

McClatchey, R.A., R.W. Fenn, J.E.A. Selby, F.E. Volz, and S. Garing (1972), Optical properties of the atmosphere, AFCRL Report, 72-997, Air Force Cambridge Research Laboratories, Bedford, MA.

Meloni, D., A. di Sarra, G. Pace, and F. Monteleone (2006), Aerosol optical properties at Lampedusa (Central Mediterranean). 2. Determination of single scattering albedo at two wavelengths for different aerosol types, *Atmos. Chem. Phys.,* 6, 715-727, doi:10.5194/acp-6-715-2006.

Menon, S., J. Hansen, L. Nazarenko, and Y. Luo (2002), Climate effects of black carbon aerosols in China and India. *Science*, 297, 2250–2253.

Menon, S., D. Koch, G. Beig, S. Sahu, J. Fasullo, and D. Orlikowski (2010), Black carbon aerosols and the third polar ice cap, *Atmos. Chem. Phys.,* 10, 4559-4571, doi:10.5194/acp-10-4559-2010.

Merrill, J.T., R. Bleck, and L. Avila (1985), Modeling atmospheric transport to the Marshall Islands, *J. Geophys. Res*., 90, 12927-12936.

Middleton, N. J. (1986), A geography of dust storms in southwest Asia, *Int. J. Clim.,* 6, 183–196.

Mielonen, T., A. Arola, M. Komppula, J. Kukkonen, J. Koskinen, G. de Leeuw, and K. Lehtinen (2009), Comparison of CALIOP level 2 aerosol subtypes to aerosol types derived from AERONET inversion data, *Geophys. Res. Lett.*, 36, L18804, doi:10.1029/2009GL039609.

Mikhailov, E. F., S. S. Vlasenko, I. A. Podgorny, V. Ramanathan, and C. E. Corrigan (2006), Optical properties of soot-water drop agglomerates: An experimental study, J. Geophys. Res., 111, D07209, doi:10.1029/2005JD006389.

Minnis, P., E. F. Harrison, L. L. Stowe, G. G. Gibson, F. M. Denn, D. R. Doelling, and W. L. Smith Jr. (1993), Radiative Climate Forcing by the

Mount Pinatubo Eruption, *Science*, 259 (5100), 1411-1415. DOI:10.1126/science.259.5100.1411.

Mishra, S. K., S. Day, and S. N. Tripathi, (2008), Implications of particle composition and shape to dust radiative effect: A case study from the Great Indian Desert, *Geophys. Res. Lett.*, 35, L23814, doi:10.1029/2008GL036058.

Monahan, E. C. (1986), The ocean as a source for atmospheric particles, The role of air-sea exchange in Geochemical Cycling, (Eds: P. Buat-Menard), D. Reidel, Hingham, Mass, 129-163.

Monahan, E.C. (1968), Sea spray as a function of low elevation wind speed, *J. Geophys. Res*., 73, 1127-1137.

Monahan, E.C., C.W. Fairall, K.L. Davidson, and P. Jones Boyle (1983), Observed inter-relations between 10 m winds, ocean white caps and marine aerosols, *Q. J. R. Meteorol. Soc*., 109, 379-392.

Moody, J. L., and P. J. Samson (1989), The influence of atmospheric transport on precipitation chemistry at two sites in the midwestern United States, *Atmospheric Environment*, 23, pp. 2117–2132

Moorthy et al. (1999), Aerosol Climatology over India. 1 - ISRO GBP MWR network and database, *ISRO/GBP, SR-03- 99*.

Moorthy, K. K. (2001), Aerosol optical depths over peninsular India and adjoining oceans during the INDOEX campaigns: spatial, temporal, and spectral characteristics, *J. Geophys. Res.*, 106, D22, 28539-28554. doi:10.1029/2001JD900169.

Moorthy, K. K., and S. K. Satheesh (2011), Black carbon aerosols over India, *UNEP's Black Carbon e-Bulletin*, **3**, 1–3.

Moorthy, K. K., S. S. Babu, and S. K. Satheesh (2007), Temporal heterogeneity in aerosol characteristics and the resulting radiative impact at a tropical coastal station. Part 1: Microphysical and optical properties, *Ann. Geophys.*, 25, 2293–2308. doi:10.5194/angeo-25-2293-2007.

Moorthy, K. K., S. S. Babu, S. V. Sunilkumar, P. K. Gupta, and B. S. Gera (2004), Altitude profiles of aerosol BC, derived from aircraft

measurements over an inland urban location in India, Geophys, *Res. Lett.*, 31, L22103, doi:10.1029/2004GL021336.

Moorthy, K. K., S.K. Satheesh, SS Babu and CBS Dutt (2008), Integrated Campaign for Aerosols, gases and Radiation Budget (ICARB): An Overview, *J. Earth. Sys. Sci.*, 117, 243-262.

Moorthy, K. K., et al. (2013a). Buildup of aerosols over the Indian Region. Geophys. Res. Lett. 40, 1011–1014. doi:10.1002/grl.50165.

Moorthy, K. K., et al. (2013b), Performance evaluation of chemistry transport models over India, *Atmos. Environ.*, 71, 210-225. doi: 10.1016/j.atmosenv.2013.01.056.

Moorthy, K.K., A. Saha, and K. Niranjan (2001), Spatial variation of aerosol spectral optical depth and columnar water vapour content over the Arabian Sea and Indian Ocean during the IFP of INDOEX, *Curr. Sci*., 80, 145-150.

Moorthy, K. K., and S.K. Satheesh (2000), Characteristics of aerosols over a remote island Minicoy in Arabian Sea: Optical properties and retrieved size characteristics, *Q. J. Roy. Meteorol. Soc*., 126, 81-109.

Moorthy, K.K., K. Niranjan, B. Narasimhamurthy, V.V. Agashe, and B.V.K. Murthy (1999), Aerosol Climatology over India, 1. ISRO GBP MWR Network and Database, Scientific Report, ISRO GBP, SR 03 99, Indian Space Research Organisation, India.

Moorthy, K. K., P.R. Nair, B.V.K. Murthy, and S.K. Satheesh (1996), Time evolution of the optical effects and aerosol characteristics of Mt. Pinatubo origin from ground based observations, *J. Atmos. Terr. Phys*., 58, 1101-1116.

Moorthy, K. K., S. K. Satheesh, and B. V. K. Murthy (1997), Investigations of marine aerosols over the tropical Indian Ocean, *J. Geophys. Res*., 102,18827-18842.

Moorthy, K. K., et al. (2004), Altitude profiles of aerosol BC, derived from aircraft measurements over an inland urban location in India, *Geophys. Res. Lett.*, 31, L22103.

Morys, M., F. M. Mims III, S.Hagerup, S. E. Anderson, A. Backer, J. Kia and T. Walkup (2001), Design, calibration and performance of Microtops II hand-held ozone monitor and sun photometer, *J. Geophys. Res.* 106, 14,573-14,582.

Müller, T., et al. (2011), Characterization and intercomparison of aerosol absorption photometers: result of two intercomparison workshops, *Atmos. Meas. Tech.* 4, 245-268. doi:10.5194/amt-4-245-2011.

Murphy, D. M., D. S. Thomson and T. M. J. Mahoney (1998), In situ measurement of organics, meteoritic material, mercury, and other elements in aerosols at 5 to 19 kilometers, *Science*, 282, 1664-1669.

Murphy, D. M., et al. (2008), Weekly patterns of aerosol in the United States, *Atmos. Chem. Phys. Discuss.*, 8, 521-548. doi:10.5194/acpd-8-521-2008.

Myhre, G., F. Stordal, K. Restad, and I. Isaksen (1998), Estimates of the direct radiative forcing due to sulfate and soot aerosols, *Tellus, Ser. B, 50*, 463–477.

Naiagu J. R. (1979), Global inventory of natural and anthropogenic emissions of trace metals to the atmosphere, *nature*, 279, 409.

Nair, V. S., et al. (2012), Simulation of South Asian aerosols for regional climate studies, *J. Geophys. Res.*, 117, D04209. doi:10.1029/2011JD016711.

Nair, V. S., et al. (2007), Wintertime aerosol characteristics over the Indo-Gangetic Plain (IGP): Impacts of local boundary layer processes and long-range transport, *J. Geophys. Res.*, 112, D13205. doi:10.1029/2006JD008099.

Nair, V. S., et al., (2007), Wintertime aerosol characteristics over the Indo-Gangetic Plain (IGP): Impacts of local boundary layer processes and long-range transport, *J. Geophys. Res.*, 112, D13205. doi:10.1029/2006JD008099.

Naja, M., D. Chand, L. Sahu, S. Lal (2004), Trace gases over marine region around India, *Indian Journal of Marine Sciences*, 33, 95-106.

Novakov, T., D.A. Hegg, and P.V. Hobbs (1997), Airborne measurements of carbonaceous aerosols off the East coast of the United States, *J. Geophys. Res*., 102, 30023-30030.

O'Dowd, C.D., J. A. Lowe, M. H. Smith, and A. D. Kaye (1999), The relative importance of Nss-sulphate and sea salt aerosol to the marine CCN population: an improved multi-component aerosol cloud droplet parameterization, *Quart. J. Roy .Meteorol. Soc*., 125, 1295-1313.

O'Dowd, C.D., M.H. Smith, I.E. Consterdine, J.A. Lowe (1997), Marine aerosol, sea-salt, and the marine sulphur cycle: A short review, *Atmos. Environ*., 31, 73-80.

O'Neill, N. T., T. F. Eck, A. Smirnov, B. N. Holben, and S. Thulasiraman (2003), Spectral discrimination of coarse and fine mode optical depth, J. Geophys. Res., 108(D17), 4559, doi:10.1029/2002JD002975.

Ogren, J.A., and R. J. Charlson (1984), Wet deposition of elemental carbon and sulfate in Swden, *Tellus*, 36B, 262-271.

Ojha, N., M. Naja, K. P. Singh, T. Sarangi, R. Kumar, S. Lal, M. G. Lawrence, T. M. Butler, and H. C. Chandola (2012), Variabilities in ozone at a semi-urban site in the Indo-Gangetic Plain region: Association with the meteorology and regional processes, *J. Geophys. Res.*, 117, D20301. doi:10.1029/2012JD017716.

Omar, A. H., et al. (2009), The CALIPSO automated aerosol classification and lidar ratio selection algorithm, *J. Atmos. Oceanic Technol.*, 26, 1994–2014.

Pandithurai, G., R.T. Pinker, T. Takamura, P.C.S. Devara, (2004), Aerosol radiative forcing over a tropical urban site in India, *Geophys. Res. Lett.* 31 (12), L12107.

Pandithurai, G., S. Dipu, K. K. Dani, S. Tiwari, D. S. Bisht, P. C. S. Devara, and R. T. Pinker (2008), Aerosol radiative forcing during dust events over New Delhi, India, *J. Geophys. Res.*, 113, D13209, doi:10.1029/2008JD009804.

Pant, P., P. Hegde, U. C. Dumka, R. Sagar, S. K. Satheesh, K. K. Moorthy, A. Saha, and M. K. Srivastava (2006), Aerosol characteristics at a high-altitude location in central Himalayas: Optical properties and radiative forcing, *J. Geophys. Res.*, 111, D17206, doi:10.1029/2005JD006768.

Parungo, F. (1997), Asian dust storms and their effect on radiation and climate: Part 4, *NOAA Science Technology Report*, 3134.

Pathak, B., et al. (2010), Aerosol temporal characteristics and its impact on shortwave radiative forcing at a location in the northeast of India, *J. Geophys. Res.*, 115, D19204. doi:10.1029/2009JD013462.

Peng Yan, et al. (2009), Hygroscopic growth of aerosol scattering coefficient: A comparative analysis between urban and suburban sites at winter in Beijing, Particuology, 7, 52-60, ISSN 1674-2001, doi:10.1016/j.partic.2008.11.009.

Phanikumar, D. V., K. N. Kumar, K. K. Shukla, H. Joshi, M. Venkat Ratnam, M. Naja, and K. Reddy (2014), Signatures of Rossby wave modulations in aerosol optical depth over the central Himalayan region, Ann. Geophys., 32, 175-180, doi:10.5194/angeo-32-175-2014.

Porter, John N., M. Miller, C. Pietras, and C. Motell (2001), Ship-Based Sun Photometer Measurements Using Microtops Sun Photometers. *J. Atm and Oce Tech.* 18, 5, 765-774.

Prasad, A. K., and R. P. Singh (2007), Changes in aerosol parameters during major dust storm events (2001–2005) over the Indo-Gangetic Plains using AERONET and MODIS data, J. Geophys. Res., 112, D09208, doi:10.1029/2006JD007778.

Prospero, J. M., P. Ginoux, O. Torres, S. E. Nicholson, and T. E. Gill (2002), Environmental characterization of global sources of atmospheric soil dust identified with the Nimbus 7 Total ozone Mapping Spectrometer (TOMS) absorbing aerosol product, *Rev. Geophys.*, 40, 1002, doi:10.1029/2000RG000095.

Prospero, J.M. (1979), Mineral and sea salt aerosol concentrations in various ocean regions, *J. Geophys. Res.*, 84, 725-731.

Prospero, J.M. (1999), Long-range transport of mineral dust in the global atmosphere: Impact of African dust on the environment of the southeastern United States, *Proc. Natl. Acad. Sci*., 96, 3396-3403.

Prospero, J.M., et al. (2002), Environmental characterization of global sources of atmospheric soil dust identified with the Nimbus 7 Total Ozone Mapping Spectrometer (TOMS) absorbing aerosol product, *Reviews of Geophysics*, 40(1), 1002 doi: 10.1029/2000RG000095.

Prospero, J.M., R A. Glaccum, and R.T. Nees (1981), Atmospheric transport of soil dust from Africa to South America, *Nature*, 289, 570-572.

Prospero, J.M., R.J. Charlson, B. Mohnen, R.Jaencke, A.C.Delany, J.Mayers, W.Zoller and K.Rahn (1983), The atmospheric aerosol system- An overview, *Rev. Geophys*., 21,1607-1629.

Pruppacher, H.R., and J.D. Klett (1978), Microphysics of clouds and precipitation, D. Reidel publishing company, Holland.

Quinn, P.K., D. J. Coffman, V.N.Kapustin, T.S.Bates, and D. S. Covert (1998), Aerosol optical properties in the marine boundary layer during ACE 1 and the underlying chemical and physical aerosol properties, *J. Geophys. Res*., 103, 16457-16563.

Quinn, P.K., V.N. Kapustin, T.S. Bates, and D.S. Covert (1996), Chemical and optical properties of marine boundary layer aerosol particles of the mid-Pacific in relation to sources and meteorological transport, *J. Geophys. Res*., 101, 6931-6951.

Rahn, K.A., D.H. Lowenthal (1984), Elemental tracers of distant regional pollution aerosols, *Science*, 223, pp. 132–139.

Raina, V. K. and C. V. Sangewar (2007), Siachen Glacier of Karakoram Mountains, Ladakh – Its Secular Retreat, *Jour. Geol. Society of India,* 70, 11–16, Bangalore.

Ramachandran S., A. Jayaraman (2003), Spectral aerosol optical depths over Bay of Bengal and Chennai: II—sources, anthropogenic influence and

model estimates, *Atmospheric Environment,* Volume 37, Issue 14, May 2003, Pages 1951-1962, ISSN 1352-2310, doi:10.1016/S1352-2310(03)00084-0.

Ramachandran, S. (2005), Aerosol radiative forcing over Bay of Bengal and Chennai: Comparison with maritime, continental, and urban aerosol models, J. Geophys. Res., 110, D21206, doi:10.1029/2005JD005861.

Ramachandran, S., and S. Kedia (2010), Black carbon aerosols over an urban region: Radiative forcing and climate impact, *J. Geophys. Res.*, 115, D10202. doi:10.1029/2009JD013560. Ramanathan, V., and G. Carmichael (2008), Global and regional climate changes due to black carbon, *Nature Geoscience*, 1 (4), 221-227. doi:10.1038/ngeo156.

Ramachandran, S., R. Rengarajan, A., Jayaraman, M.M. Sarin, S.K. Das, (2006), Aerosol radiative forcing during clear, hazy, and foggy conditions over a continental polluted location in north India. *J. Geophys. Res.* 111.

Ramachandran, S., S. Kedia, R. Srivastava (2012), Aerosol optical depth trends over different regions of India, *Atmospheric Environment*, Volume 49, March 2012, Pages 338-347, ISSN 1352-2310, doi:10.1016/j.atmosenv.2011.11.017.

Ramanathan, N., M. Lukac, T. Ahmed, A. Kar, P.S. Praveen, T. Honles, I. Leong, I.H. Rehman, J.J. Schauer, V. Ramanathan, (2011), A cellphone based system for large-scale monitoring of black carbon, *Atmos. Environ.* 45, 4481–4487.

Ramanathan, V. et al. (2001), Indian ocean experiment: an integrated analysis of the climate forcing and effects of the great Indo–Asian haze. *J. Geophys. Res.* 106, 28,371–28,398.

Ramanathan, V., and P. J. Crutzen (2003), New directions: Atmospheric brown “clouds,”, Atmos. Environ., **37**(28),4033–4035.

Ramanathan, V., Li, F., Ramana, M. V., at al. (2007), Atmospheric brown clouds: Hemispherical and regional variations in long-range transport, absorption, and radiative forcing, *J. Geophys. Res.*, 112, D22S21, doi:10.1029/2006JD008124.

Ramanathan, V., M. V. Ramana, G. Roberts, D. Kim, C. Corrigan, C. Chung, and D. Winker (2007) Warming trends in Asia amplified by brown cloud solar absorption, Nature, 448, 575–578, doi:10. 1038/nature06019.

Ramanathan, V., P. J. Crutzen, J. Lelieveld, et al. (2001), Indian Ocean experiment: An integrated analysis of the climate forcing and effects of the great Indo-Asian haze, *Geophys. Res.*, 106(D22), 28371-28398, doi: 10.1029/2001JD900133.

Ramanathan, V., P.J. Crutzen, J.T. Kiehl, and D. Rosenfeld (2001), Aerosols, climate, and the hydrological cycle, *Science*, 294, 2119-2124.

Ramanathan, V., Y. Feng (2009), Air pollution, greenhouse gases and climate change: Global and regional perspectives, *Atmospheric Environment*, 43, 1, Pages 37-50, doi:10.1016/j.atmosenv.2008.09.063.

Rastogi, N., and M. M., Sarin (2005), Chemical characteristics of individual rain events from a semi-arid region in India: three-year study, *Atmos. Environ.*, 39:3313–3323.

Ravishankara, A. R. (1997), Heterogeneous and multiphase chemistry in the troposphere, Science, 276, 1058–1065.

Reddy, B. S. K. (2012), Potential source regions contributing to seasonal variations of black carbon aerosols over Anantapur in Southeast India, *Aerosol Air Qual. Res.*, 12, 145–161. doi:10.4209/aaqr.2011.10.0159.

Reddy, K., D.V. Phanikumar, H. Joshi, Y. N. Ahammed, M. Naja (2015), Effect of diurnal variation OF aerosols on surface reaching solar radiation, Journal of Atmospheric and Solar-Terrestrial Physics, ISSN 1364-6826, doi:10.1016/j.jastp.2015.04.011.

Reddy, M. S., and C. Venkataraman (1999), Direct radiative forcing from anthropogenic carbonaceous aerosols over India, *Current Science*, 76, 1005-1011.

Remer, L., Y.J. Kaufman, D. Tanré, S. Mattoo, D.A. Chu, J. Martins, R.-R. Li, C. Ichoku, R.C. Levy, R.G. Kleidman, T.F. Eck, E. Vermote, B.N.

Holben (2005), The MODIS aerosol algorithm, products, and validation. *J. Atmos. Sci.*, 62 (4), 947–973.

Ren, J., Z. Jing, J. Pu, and X. Qin (2006), Glaciers variations and climate change in the central Himalaya over the past few decades, *Ann. Glaciol.*, 43, 218–222.

Robock, A. (2000), Volcanic eruptions and climate, *Rev. Geophys*., 38, 191-219.

Rodhe, H., and J Grandell (1981), Estimates of characteristic times for precipitation scavenging, *Atmospheric Science Journal*, 38, pp. 370–386

Rosenfeld, D. et al. (2008), Flood or drought: how do aerosols affect precipitation? *Science* 321, 1309–1313.

Russell, P.B., P.V. Hobbs, and L.L. Stowe (1999), Aerosol properties and radiative effects in the United States East Coast haze plume: An overview of Tropospheric Aerosol Radiative Forcing Observational Experiment (TARFOX), *J. Geophys. Res*., 104, 2213-2222.

Sagar, R., B. Kumar, U. C. Dumka, K. K. Moorthy, and P. Pant (2004), Characteristics of aerosol optical depths over Manora Peak: A high altitude station in the central Himalayas, *J. Geophys. Res.,* 109, D06207, doi:10.1029/2003JD003954.

Safai, P. D., et al. (2007), Seasonal variation of black carbon aerosols over a tropical urban city of Pune, India, *Atmos. Environ.*, 41, 2699-2709. doi:10.1016/j.atmosenv.2006.11.044.

Safai, P.D., M.P. Raju, P.S.P. Rao, G. Pandithurai (2014), Characterization of carbonaceous aerosols over the urban tropical location and a new approach to evaluate their climatic importance, *Atmospheric Environment*, Volume 92, August 2014, Pages 493-500, ISSN 1352-2310, doi:10.1016/j.atmosenv.2014.04.055.

Salve, P. R., T. Gobre, H. Lohkare, R. J. Krupadam, A. Bansiwal, D. S. Ramteke, and S. R. Wate (2011), Source identification and variation in

the chemical composition of rainwater at coastal and industrial areas of India, *J. Atmos. Chem.*, 68:183–198.

Samset, B. H., et al. (2014), Modeled black carbon radiative forcing and atmospheric lifetime in AeroCom Phase II constrained by aircraft observations, *Atmos. Chem. Phys. Discuss.*, 14, 20083-20115. doi:10.5194/acpd-14-20083-2014.

Sarangi, T., M. Naja, N. Ojha, R. Kumar, S. Lal, S. Venkataramani, A. Kumar, R. Sagar, and H. C. Chandola (2014), First simultaneous measurements of ozone, CO, and NOy at a high-altitude regional representative site in the central Himalayas, *J. Geophys. Res. Atmos.*, 119, 1592–1611. doi:10.1002/2013JD020631.

Satheesh S. K., and V. Ramanathan (2000), Large differences in the tropical aerosol forcing at the top of the atmosphere and Earth's surface, *Nature*, 405, 60–63. doi:10.1038/35011039.

Satheesh, S. K., and K. K. Moorthy (2005), Radiative effects of natural aerosols: A review, *Atmos. Environ.* **39**, 2089–2110.

Satheesh, S. K., et al. (2008) Climate implications of large warming by elevated aerosol over India, *Geophys. Res. Lett.*, 35, L19809. doi:10.1029/2008GL034944.

Satheesh, S. K., K. K. Moorthy, S. S. Babu, V. Vinoj, V. S. Nair, S. N. Beegum, C. B. S. Dutt, D. P. Alappattu, and P. K. Kunhikrishnan (2009), Vertical structure and horizontal gradients of aerosol extinction coefficients over coastal India inferred from airborne lidar measurements during the Integrated Campaign for Aerosol, Gases and Radiation Budget (ICARB) field campaign, *J. Geophys. Res.*, 114, D05204, doi:10.1029/2008JD011033.

Satheesh, S. K., K. Krishna Moorthy, S. Suresh Babu, V. Vinoj and C.B.S. Dutt (2008), Climate implications of large warming by elevated aerosol over India, 1008, *Geophysical Research Letters*, Vol. 35, 1-6.

Satheesh, S. K., V. Ramanathan., X. L. Jones, J. M. Lobert, I. A. Podogorny, J. M. Prospero, B. N. Holben, and N. G. Leob. (1999), A Model for the natural and anthropogenic aerosols for the tropical Indian ocean

derived from Indian ocean Experiment data, *J. Geophys. Res*., 104, D22, 27421-27440.

Satheesh, S. K., V. Vinoj, and K. K. Moorthy (2011), Weekly periodicities of aerosol properties observed at an urban location in India. *Atmos. Res.*, 101, 307–313. doi:10.1016/j.atmosres.2011.03.003.

Satheesh, S. K., V. Vinoj, S. S. Babu, K. K. Moorthy, and V. S. Nair (2009), Vertical distribution of aerosols over the east coast of India inferred from airborne LIDAR measurements, *Ann. Geophys.*, 27, 4157–4169, doi:10.5194/angeo-27-4157-2009.

Satheesh, S. K., V. Ramanathan, B. N. Holben, K. K. Moorthy, N. G. Loeb, H. Maring, J. M. Prospero, and D. Savoie (2002), Chemical, microphysical, and radiative effects of Indian Ocean aerosols, J. Geophys. Res., 107(D23), 4725, doi:10.1029/2002JD002463.

Satheesh, S. K., V. Ramanathan, B. N. Holben, K. K. Moorthy, N. G. Loeb, H. Maring, J. M. Prospero, and D. Savoie (2002), Chemical, microphysical, and radiative effects of Indian Ocean aerosols, J. Geophys. Res., 107(D23), 4725, doi:10.1029/2002JD002463.

Satheesh, S.K., and J. Srinivasan (2002), Enhanced aerosol loading over Arabian Sea during pre-monsoon season: Natural or Anthropogenic?, *Geophys. Res. Lett*., 10.1029/ 2002GL015687.

Satheesh, S. K., K. Krishna Moorthy, Y. J. Kaufman, T. Takemura (2006), Aerosol optical depth, physical properties and radiative forcing over the Arabian Sea, *Meteorology and Atmospheric Physics*, 2006, 91, pp 45-62.

Satsangi, G. S., A. Taneja, P. Khare, S. P. Singh, A. Lakhani, K. M. Kumari, and S. S. Srivastava, (1998), Deriving critical loads for the Agra region in India, *Sci. Total Environ.*, 222:119–122

Saxena, P., and L. M. Hildemann (1996), Water soluble organics in atmospheric particles: A critical review of the literature and application of thermodynamics to identify candidate compounds, *J. Atmos. Chem*., 24, 57-109.

Saxena, V. K., J. Anderson, and N.-H. Lin (1995), Changes in Antarctic stratospheric aerosol characteristics due to volcanic eruptions as monitored by the Stratospheric Aerosol and Gas Experiment II satellite, *J. Geophys. Res*., 100, 16735-16751.

Schwartz, S.E. (1996), The whitehouse effect - Shortwave radiative forcing of climate by anthropogenic aerosols: An overview, *J. Aerosol Sci*., **27**, 359-383.

Seibert, P., H. Kromp-Kolb, U. Baltensperger, D.T. Jost, M. Schwikowski, A. Kasper, H. Puxbaum (1994), Trajectory analysis of aerosol measurements at high alpine sites, P.M. Borrell, P. Borrell, T. Cvitaš, W. Seiler (Eds.), *Transport and Transformation of Pollutants in the Troposphere*, Academic Publishing, Den Haag, pp. 689–693.

Seinfeld, J. H., (1986), Atmospheric Chemistry and Physics of Air Pollution, John Wiley and Sons, Inc., New York.

Seinfeld, J. H., et al. (2004), ACE-Asia - Regional climatic and atmospheric chemical effects of Asian dust and pollution, Bull. Am. Meteorol. Soc., 85(3), 367–380.

Seinfeld, J.H., and S.N. Pandis (1998), Atmospheric Chemistry and Physics-from Air Pollution to Climate Change. New York, USA, *Wiley*.

Shah, S., T. Kneip, J. Daisey, (1985), Source apportionment of carbonaceous aerosol in New York City by multiple linear regression, *Journal of Air Pollution Control Association*, 35, pp. 541–544.

Sharma, P., J. C. Kuniyal, K. Chand, R. P. Guleria, P. P. Dhyani, C. Chauhan (2013), Surface ozone concentration and its behaviour with aerosols in the northwestern Himalaya, India, *Atmospheric Environment,* Volume 71, June 2013, Pages 44-53, doi:10.1016/j.atmosenv.2012.12.042.

Sheridan, P.J., W.P. Arnott, J. Ogren et al. (2005), The Reno aerosol optics study: overview and summary of results, *Aerosol Sci. Technol.*, 39, 1–16.

Sikka, D. R., (1997), Desert climate and its dynamics, *Curr. Sci.*, India, 72, 35–46.

Singh, R. P., S. Dey, S. N. Tripathi, and V. Tare (2004), Variability of aerosol parameters over Kanpur, northern India, *J. Geophys. Res.*, 109, D23206, doi: 10.1029/ 2004JD004966.

Skamarock, W. C., et al. (2008), A description of the advanced research WRF version 3, NCAR Tech. Note NCAR/TN-475+STR, *Natl. Cent. for Atmos. Res.*, Boulder, Colo, pp. 125.

Smirnov, A., Y. Villevalde, N. T. O'Neill, A. Royer and A. Tarussov (1995), Aerosol optical depth over the oceans: Analysis in terms of synoptic air mass types, *J. Geophys. Res*., 16, 639–650, 24513

Srivastava, A. K., K. Ram, P. Pant, P. Hegde and H. Joshi (2012), Black carbon aerosols over Manora Peak in the Indian Himalayan foothills: implications for climate forcing, Environ. Res. Lett., 7 014002, doi:10.1088/1748-9326/7/1/014002.

Stephens, G. L., et al. (2002), The CloudSat mission and the A-Train: A new dimension of space-based observations of clouds and precipitation, *Bull. Am. Meteorol. Soc.*, 83, 1771– 1790.

Stephens, S., et al. (2008), Weekly patterns of México City's surface concentrations of CO, NOx, PM10 and O3 during 1986–2007, *Atmos. Chem. Phys.*, 8, 5313-5325. doi:10.5194/acp-8-5313-2008.

Stohl, A. (1996), Trajectory statistics-A new method to establish source-receptor relationships of air pollutants and its application to the transport of particulate sulfate in Europe, *Atmospheric Environment*, 30, 4, 579-587, doi:10.1016/1352-2310(95)00314-2.

Stohl, A. (2006), Characteristics of atmospheric transport into the Arctic troposphere, *J. Geophys. Res*., 111(11) D11306. doi:10.1029/2005JD006888.

Streets, D. G. et al. (2003), An inventory of gaseous and primary aerosol emissions in Asia in the year 2000, *J. Geophys. Res.*, 108, 8809, doi:10.1029/2002JD003093, D21.

Streets, D. G., et al. (2009), Anthropogenic and natural contributions to regional trends in aerosol optical depth, 1980-2006, *J. Geophys. Res.*, 114, D00D18. doi:10.1029/2008JD011624.

Stull, R. B. (1998), An Introduction to Boundary Layer Meteorology, *Kluwer Academic Publishers*, Dordrecht.

Tanre, D., Y. J. Kaufman, M. Herman, and S. Mattoo (1997), Remote sensing of aerosol properties over oceans using the MODIS/ESO spectral radiances, *J. Geophys. Res.*, 102, 16971 – 16988.

Tegen, I., and I. Fung (1994), Modeling of mineral dust in the atmosphere: Sources, transport, and optical thickness, *J. Geophys. Res.*, **99**, 22897-22914.

Tegen, I., and I. Fung (1995), Contribution to the atmospheric mineral aerosol load from land surface modification, *J. Geophys. Res.*, 100, 18707-18726.

Tiwari, S., D.M. Chate, D.S. Bisht, M.K. Srivastava, and B. Padmanabhamurty (2012), Rainwater chemistry in the North Western Himalayan Region, India, *Atmospheric Research*, 104–105, 128-138, doi:10.1016/j.atmosres.2011.09.006.

Tiwari, S., et al. (2013), Diurnal and seasonal variations of black carbon and PM2.5 over New Delhi, India: Influence of meteorology, *Atmos. Res.*, 125–126, 50–62. doi: 10.1016/j.atmosres.2013.01.011.

Tiwari, S., U. C. Kulshrestha, and B. Padmanabhamurty, (2007), Monsoon rain chemistry and source apportionment using receptor modeling in and around National Capital Region [NCR] of Delhi, *India, Atmos. Environ.*, 41, 5595–5604.

Torres, O., et al. (1998), Derivation of aerosol properties from satellite measurements of backscattered ultraviolet radiation: theoretical basis, *J. Geophys. Res.*, 103 (D14), 17099-17110. doi:10.1029/98JD00900.

Tripathi, S.N., S. Dey, V. Tare, S.K. Satheesh, (2005), Aerosol black carbon radiative forcing at an industrial city in northern India. *Geophys. Res. Lett.* 32.

Tyson P.D., M. Garstang, R. Swap, P. Kallberg, and N. Edwards (1996), An air transport climatology for subtropical southern Africa, *Int. J. Climatol.*, 16, 256-291.

Venkataraman, C., A.D. Sagar, G. Habib, N. Lam, K.R. Smith (2010), The Indian national initiative for advanced biomass cookstoves: the benefits of clean combustion. *Energy Sustain. Dev.*, 14, 63–72.

Venkataraman, C., et al. (2005), Residential biofuels in south Asia: Carbonaceous aerosol emissions and climate impacts, *Science*, 307, 1454–1456.

Venkataraman, C., et al. (2006), Emissions from open biomass burning in India: Integrating the inventory approach with high-resolution Moderate Resolution Imaging Spectroradiometer (MODIS) active-fire and land cover data, *Global Biogeochem.Cycles.20*, GB2013. doi:10.1029/2005GB002547.

Venzac, H., K. Sellegri, P. Laj, P. Villani, P. Bonasoni, A. Marinoni, P. Cristofanelli, F. Calzolari, S. Fuzzi, S. Decesari, M.-Cr. Facchini, E. Vuillermoz, G.P. Verza (2008), High Frequency New Particle Formation in the Himalayas, *PNAS*, 105, 41, 15666– 15671.

Venzac, H., K. Sellegri, P. Villani, D. Picard, and P. Laj (2009), Seasonal variation of aerosol size distributions in the free troposphere and residual layer at the puy de Dome station, France, *Atmos. Chem. Phys.*, 9, 1465–1478, doi:10.5194/acp-9-1465-2009.

Vinoj, V., and S. K. Satheesh (2003), Measurements of aerosol optical depth over Arabian Sea during summer monsoon season, *Geophys. Res. Lett*., 30 (5): art. no. 1263.

Wang, J., X.Xia, P. Wang, and S. A. Christopher (2004), Diurnal variability of dust aerosol optical thickness and Angstrom exponent over dust source regions in China, *Geophys. Res. Lett*, 31, L08107, doi:10.1029/2004GL019580.

Wang, P. K., S. N. Grover, and H. R. Pruppacher (1978), On the effect of electric charges on the scavenging of aerosol particles by clouds and small raindrops, *J. Atmos. Sci.*, 35, 1735 – 1743.

Washington, R., M. Todd, N.J. Middleton, A.S. Goudie (2003), Dust-storm source areas determined by the Total Ozone Monitoring Spectrometer and surface observations, *Annals of the Association of American Geographers* 93(2), 297–313.

Weingartner, E., et al. (2003), Absorption of light by soot particles: Determination of the absorption co-efficient by means of Aethalometers, *J. Aerosol Sci.*, 34(10), 1445–1463. doi:10.1016/S0021-8502(03)00359-8.

Whelpdale, D.M., A. Eliassen, J.N. Galloway, H. Dovland, and J.M. Miller (1988), The transatlantic transport of sulfur, *Tellus*, 40B, 1-15.

Wiedinmyer, C., et al. (2011), The Fire Inventory from NCAR (FINN): a high resolution global model to estimate the emissions from open burning, *Geosci. Model Dev.*, 4, 625–641. doi:10.5194/gmd-4 625-2011.

Winchester, J. W., M. Bi (1984), Fine and coarse aerosol composition in an urban setting: A case study in Beijing, China, Atmos. Environ., **18**, 1399–1409.

Winker, D. M., et al. (2009), Overview of the CALIPSO mission and CALIOP data processing algorithms, *J. Atmos. Ocean. Tech.*, 26, 2310–2323. doi:10.1175/2009JTECHA1281.1. 2009.

Winker, D. M., J. Pelon, and M. P. McCormick (2003), The CALIPSO mission: Spaceborne lidar for observation of aerosols and clouds, Proc. SPIE Int. Soc. Opt. Eng., **4893**, 1–11.

Winter, B., and P. Chýlek (1997), Contribution of sea-salt aerosol to the planetary clear-sky albedo, Tellus, Ser. B, **49**,72–79.

Wolf, G. T., (1984), On the nature of nitrate in coarse continental aerosols, *Atmos. Environ.*, 18 (1984), pp. 977–981.

Woodcock, A.H. (1953), Salt nuclei in marine air as a function of altitude and wind force, *J. Meteorol.*, 10, 362-371.

Woodcock, A.H. (1972), Smaller sea-salt particles in oceanic air and bubble behavior in the sea, *J. Geophys. Res*., 77, 5316-5321.

Yasunari, T. J., P. Bonasoni, P. Laj, K. Fujita, E. Vuillermoz, A. Marinoni, P. Cristofanelli, R. Duchi, G. Tartari, and K.-M. Lau (2010). Preliminary estimation of black carbon deposition from Nepal Climate Observatory-Pyramid data and its possible impact on snow albedo changes over Himalayan glaciers during the premonsoon season, *Atmos. Chem. Phys. Discuss.*, 10, 9291–9328, doi:10.5194/acpd-10-9291-2010.

Yoon, S-Chang, and J. Kim (2006), Influences of relative humidity on aerosol optical properties and aerosol radiative forcing during ACE-Asia, *Atmospheric Environment*, Volume 40, Issue 23, Pages 4328-4338, ISSN 1352-2310, doi:10.1016/j.atmosenv.2006.03.036.

Young, S. A. and M. A. Vaughan (2009), The retrieval of profiles of particulate extinction from Cloud Aerosol Lidar Infrared Pathfinder Satellite Observations (CALIPSO) data: Algorithm description, *J. Atmos. Ocean. Tech.*, 26, 1105–1119, doi:10.1175/2008 JTECHA1221.1.

Zege, E.P., A.P. Ivanov, and I.L. Katsev (1991), Image transfer through a scattering medium, Springer- Verlag, New York.